CRANFIELD UNIVERSITY

GIUSEPPE IACOPINO

RELIABILITY ANALYSIS OF MECHANICAL COMPONENTS CONTAINING RANDOM FLAWS

SCHOOL OF APPLIED SCIENCES

PHD THESIS

CRANFIELD UNIVERSITY

SCHOOL OF APPLIED SCIENCES

PhD THESIS

Academic Years 2002-2005

G IACOPINO

Reliability Analysis of Mechanical Components Containing Random Flaws

Supervisor: Prof M T Todinov

October 2006

This thesis is submitted in partial fulfilment of the requirements
for the degree of Doctor of Philosophy

ABSTRACT

The goal of structural reliability is to assure that a structure adequately performs its intended function when operating under specified environmental conditions. The major source of unreliability is the variability that characterizes engineering structures subjected to inherent randomness in material properties, loading and geometrical parameters. A sensible approach to structural reliability must be able to evaluate and control the effects of this variability, quantifying the uncertainties in the design variables and measuring their impact on the strength of the final product.

The objective of this research is to assess the role that uncertainties in material microstructure, in particular concerning the presence of defects such as pores, inclusions and through-thickness cracks, have in the failure of engineering structures. For this purpose, a computational procedure, based on the coupled use of Finite Element Analysis and Monte Carlo simulation, is proposed to evaluate the failure probability of complex mechanical components containing random flaws. The proposed methodology is particularly suited for the structural design of ceramic components, whose strength properties are significantly affected by the presence of microstructural defects.

Material flaws are modelled by a population of volume-embedded micro-cracks characterized by different geometrical features and size distributions. For each population the number of flaws is assumed to follow a homogenous Poisson process and flaws are sampled with a uniform spatial distribution and a random orientation. The interaction of a crack with the stress field produced in the component by the applied load is determined through a mixed-mode fracture criterion. Several solutions have been compared in this respect.

The study conducted clearly shows how the application of a traditional deterministic approach may lead to incorrect conclusions. Due to the stochastic nature of the flaw distribution, failure of a component may not be initiated at the point of highest nominal stress. The whole component volume contributes to the total probability of failure and therefore the entire stress field must be considered. Moreover, the sensitivity analysis carried out indicates that the parameters controlling the failure process are strictly dependent on loading conditions. In particular, a significant difference in behaviour between uniform and non-uniform stress states was identified.

A new failure criterion for brittle materials is also proposed. The criterion is based on the maximum admissible individual probability of failure and is applicable to biaxial stress conditions.

ACKNOWLEDGMENTS

I would like to express my gratitude to Professor Michael Todivon for giving me this opportunity and for his continuous supervision throughout the research work. A special appreciation goes to BP for the financial support which made this work possible.

Thanks also to Dr. G. Allegri for the valuable contribution that several discussions with him gave to this thesis.

I would like to remember and to thank all the people I met in Cranfield, who shared this experience with me and made enjoyable the years spent in the UK, and in particular: Andrea, Giuseppe, Harry, Laura and Maria José.

Another special thank must go to my girlfriend Magali for the constant encouragement and the precious help she gave me during the time spent writing the thesis.

Last but not least I thank my parents, my sister Enza, my cousins Francesca, Daniela and Valeria and all my family and friends in Italy who coped with me being away for so long and whose love and support gave me the strength and determination necessary to bring this work to completion.

TABLE OF CONTENTS

LIST OF FIGURES

LIST OF TABLES

NOTATION

a	crack size
A	crack surface area
A	random crack size
α	crack kink angle
α_0	angle of propagation of a branched crack
B	ratio between principal stresses: (σ_2 / σ_1)
β, θ, ϕ	angular coordinates / crack orientation
B, Θ, Φ	random angular coordinates
c_0	through-thickness crack length
COV	coefficient of variation of a probability distribution function
d_c	characteristic distance defined in the RKR model
ΔP_f	probability of failure of a small element ΔV
ΔV	volume of a small solid element in which the stress state can be considered to be constant
$\hat{e}$	estimator of the standard deviation associated with a Monte Carlo calculation
E	elastic modulus
$\mathsf{E}[\ ]$	expected value of a random variable
$\hat{\mathsf{E}}[\ ]$	estimator of the expected value of a random variable
F_c	individual probability of triggering failure (strength cumulative distribution function of a component containing a single defect)
$F_c^{(n)}$	strength cumulative distribution function of a component containing exactly n defects
F_S	strength cumulative distribution function (probability that a component fails under a load equal or smaller than a specified value)
$g(S)$	strength density distribution of critical flaws

$\mathcal{G}$	strain-energy release rate
$\mathcal{G}_{copl}$	coplanar strain-energy release rate
$\mathcal{G}_{crit}$	critical strain-energy release rate
γ_p	energy per unit area dissipated by local plastic flow
γ_s	material surface energy
$\varphi(x)$	probability of rupture of a single link
K_I, K_{II}, K_{III}	stress intensity factors
$K_I^{(\alpha)}$, $K_{II}^{(\alpha)}$	stress intensity factors of the branched crack
K_{Ic}, K_{IIc}, K_{IIIc}	critical stress intensity factors
$\kappa_{I\text{-}II}$	ratio between the square of the first and second critical stress intensity factors: $\left(K_{Ic}/K_{IIc}\right)^2$
$\kappa_{I\text{-}III}$	ratio between the square of the first and third critical stress intensity factors: $\left(K_{Ic}/K_{IIIc}\right)^2$
l	load
λ	mean number density of a Poisson process / mean number of flaws per unit volume
m	shape parameter of a Weibull distribution
M	bending moment
(m, n, p)	local coordinate system of the crack
n	number of defects/links
$\vec{n}$	unit vector normal to the crack plane
$N(\sigma_{crit})$	density distribution of critical flaws
ν	Poison ratio
$p(x)$	probability density function of a random variable
$p(x_1, \ldots, x_m)$	joint density function of a set of random variables
P_f	probability of failure (probability that a component fails under a load equal or smaller than a specified value)

P_n	probability of having exactly n defects
Π	total potential energy
$[R]$	rotational matrix that transforms the principal coordinate system into the local coordinate system of the crack
S	flaw/component strength
σ	uniaxial stress
σ_{crit}	crack critical stress (stress that causes a crack to propagate catastrophically)
σ_f	local fracture stress
σ_n	normal stress
σ_u	threshold parameter of a Weibull distribution
σ_y	yield stress
σ_{YY}	local tensile stress in the y direction ahead of a crack tip
σ_w	Weibull stress defined in Beremin's model
σ_0	scale parameter of a Weibull distribution
σ_1, σ_2, σ_3	principal stresses
Σ	stress field
[T]	stress tensor in principal axes
$[\widetilde{T}\,]$	stress tensor referred to crack axes
τ_{in}	in-plane shear stress
τ_{out}	out-of-plane shear stress
U	material internal strain energy
U	random variable uniformly distributed in (0, 1)
U_i	sample of a random variable uniformly distributed in (0, 1)
V	component's volume
W_s	work required to create new crack surfaces
x, y, z	Cartesian coordinates
X, Y, Z	random Cartesian coordinates

$\overrightarrow{X}_i$	random sample from a multi-variate probability distribution
ξ	random variable uniformly distributed in (0, 1)
(ξ_1, ξ_2, ξ_3)	principal stress coordinate system
Y	crack shape factor

1 INTRODUCTION

1.1. Structural Reliability

The goal of structural reliability is to assure that a structure will adequately perform its intended task when operating under specified environmental conditions. The manner in which an engineering structure will respond to loading is a function of type and magnitude of the applied load and the structural strength and stiffness. If material properties or design solutions are not suitable for the prescribed task, the response will be unsatisfactory and could result in the ultimate collapse of the structure.

The traditional deterministic design methodology attempts to guarantee reliability through the application of conservative expedients such as the safety factor. This approach is based on the deterministic hypothesis that the variables describing the strength of a structure take on known values about which there is assumed to be no uncertainty. This assumption, however, does not generally hold in reality. As a consequence, the lack of a sound quantitative basis to deal with uncertainties does not allow the safety factor methodology to correctly measure the level of reliability and often results in overly conservative designs. Furthermore, physical parameters that control reliability are not identified, nor their importance evaluated.

The source of unreliability is the variability that characterises engineering structures subjected to inherent randomness in material properties, loading and geometrical parameters. The deterministic design provides no firm basis in order to deal with this variability and therefore is not suitable for a reliability approach.

In order to gain a better understanding of failure conditions and to be able to realistically control the effects that variability has on structural reliability, a different approach, able to quantify the uncertainties in the design variables of complex engineering components, must be adopted [Freudenthal *et al.*, 1966]. Because of the stochastic nature of the quantities controlling the strength of a material or the loads acting on a structure, it appears that reliability analysis can only be performed sensibly by using a probabilistic approach. According to this approach, the term reliability is associated to the probability of failure of a structure at any stage during its life and the study of structural reliability is concerned with the calculation and prediction of this probability. The probability of occurrence of an event such as the structure collapse is a numerical measure of the chance of its occurrence. Thus, the notion of reliability admits the possibility of failure. This principle, however, does not imply a reduction of safety with respect to the conventional deterministic approach in which any risk of failure is

considered inadmissible. The principle only attempts to place the concept of structural safety in the realm of physical reality in which absolute quantities, such as minimum strength values, do not exist and knowledge is not perfect. The *probability of failure* is introduced as the quantitative measure in terms of which the reliability of various parts of a system can be defined, compared, and enhanced. This methodology is the only one that guarantees accurate failure predictions and efficient structural utilization of materials and provides quantitative means for dealing with the variability unavoidably associated with a design.

In the research work presented in this thesis, the probabilistic approach is applied to the study of brittle fracture in ceramic and metallic structures. In this context, the variability in the structural response of a mechanical component is attributed to the presence of random defects in the material microstructure. Failure is represented by the critical condition in which one of these defects propagates catastrophically causing the ultimate fracture of the structure.

1.2. Background

1.2.1. WHY STRUCTURES FAIL

The same structure may fail by different mechanisms according to stress and strain conditions and the environmental setting in which it operates. Low carbon steels, for example, may show a fibrous and shear type of fracture at room temperature, brittle fracture below -80°C., and intergranular creep failure in slow straining at temperatures over 600°C.

The main types of failure for typical engineering materials are [Orowan, 1948]:

(i) *Brittle fracture* (or cleavage fracture). – This failure mode is caused by the rapid propagation of a crack initiated at a microstructural defect or naturally present in the material. After reaching critical conditions, crack extension through the surrounding material occurs very rapidly and usually involves very little plastic deformation. In most cases this is the worst type of failure because it is generally difficult to identify the conditions in which the structure is about to break due to the absence of visible damage before catastrophic failure.

(ii) *Ductile rupture* (by localization of plastic deformation). – Many very ductile metals, particularly in sheet form, suffer rupture in tension by continued

thinning around one section ("necking"). In very high purity materials, the tensile specimen may neck down to a sharp point, resulting in extremely large local plastic strain and nearly 100% reduction in area. The parts above and below the neck finally separate along a sharp edge or in a point.

(iii) *Fibrous and Shear fracture* (cup-and-cone fracture surface). – In ductile materials containing impurities (majority of materials of practical use), fracture occurs after a limited amount of plastic deformation through a mechanism of microvoids nucleation, growth and coalescence. The centre of the fracture surface is perpendicular to the maximum tensile stress and has a dimpled appearance due to the nucleation of voids only at larger inclusions and second phase particles. On the contrary, the outer regions of the fracture surface are oriented at 45° from the tensile axis and have a smoother appearance. The formation of these fracture bands is due the concentration of plastic strain in this direction, caused by the coalescence of the central region voids in a macroscopic flaw, which promotes the nucleation and growth of voids at the smaller and more numerous particles, until total breakage occur. These two failure processes are called fibrous fracture and shear fracture respectively and together originate the cup-and-cone matching surfaces commonly observed in uniaxial tensile tests.

(iv) *Fatigue*. – Material fatigue is a progressive, localized, and permanent structural damage that occurs when a component is subjected to cyclic or fluctuating loads. Although the resulting maximum stress may often be below the ultimate tensile stress, or even the yield stress of the material, a sufficient high number of cycles could still cause ultimate failure.

(v) *Intergranular viscous fracture* (*creep*). – This type of failure occurs only if the temperature is high and the rate of deformation low enough for the grains to slide over one another without considerable intracrystalline deformation. As a consequence of the sliding, cavities open up between the grains and finally fracture occurs.

(vi) *Intergranular brittle fracture*. – In some cases, impurities segregating or accumulating along the grain boundaries in metals lower the cohesion between grains so much that fracture can occur by intergranular separation with little or no plastic deformation even if individual grains are very ductile.

Due to the rapidity of the mechanisms involved in the fracture process and the limited forewarning that characterises catastrophic crack propagation, brittle fracture is probably the most interesting failure mode to be analysed within a reliability

framework, especially when dealing with early life failures. This has been the main motivation that has orientated this research work towards the study of brittle fracture.

1.2.2. DESIGN FOR RELIABILITY

While the understanding of material fracture mechanisms has advanced considerably over the past several decades, it is still necessary to over-design structures so as to maintain safety factors. Moreover, although various statistical models of brittle fracture have been developed in the literature during this period, they have rarely been placed within a reliability framework and exploited through the development of sound design strategies aiming at enhance the reliability of mechanical components.

The traditional approach to structural design and material selection is still based on the comparison of the anticipated design stress with the properties of candidate materials. A material is assumed to be adequate if its strength is greater than the expected applied stress. Such an approach may attempt to guard against brittle fracture by imposing a safety factor on stress, combined with minimum tensile elongation requirements on the material.

This type of approach considerably limits the maximum performances achievable by a component, it does not allow the engineer to have control over the variability that characterises engineering structures and is not adequate to current industry requirements. For this reason, a more accurate design methodology needs to be adopted. The new methodology is centred on the concept of reliability and is able to quantifying the probability of a component failing under specified loading conditions. A reliability-based approach will result not only in improvements in product reliability, but it will also allow one to achieve a higher cost effectiveness of the design process. In fact, if a scientific procedure can be developed for evaluating structural safety, it will be possible to study the relationship between the cost of a structure and its reliability and to have available different sets of design options according to the requirements of the customer.

The use of computer-aided engineering (CAE) solutions and simulation tools, such as finite element analysis, at an early stage of the design process can improve product reliability more inexpensively and in a shorter time than building and testing physical prototypes. For this reason, our interest has been focused on the extension of the standard computational techniques currently available in the literature, which can be employed by structural engineers to assess and enhance a component's reliability.

1.3. Thesis Objectives

The principal aim of this research work is to provide the basis for a new design methodology for mechanical components affected by brittle fracture. The starting point of such approach is to assess the effect that uncertainties in material properties, in particular concerning microstructural aspects, such as the presence of crack-like defects, have on the strength of mechanical components. Through the analysis of the link between material variability and component strength distribution, this work aims at promoting new engineering strategies and criteria for designing more reliable structures.

It is widely acknowledged that a key requirement for the consistency of any reliability model is a detailed knowledge about the probability distribution of the input parameters, in particular of the component strength. It is largely the validity of this input information that determines the degree of realism of the design process and the ability to accurately predict the behaviour and therefore the success of the design. For this reason, this study tries to identify the parameters that have a major effect on the strength distribution of a component subjected to different loading configurations.

This aim has been pursued through the following objectives:

- The development and implementation of a statistical model of brittle fracture for predicting a component's strength variability and computing probability distributions of the fracture stress. The model proposed incorporates recent achievements in the theory of stochastic material behaviour as well as established concepts of linear elastic fracture mechanics. In particular, most of the analyses are conducted via a computational procedure based on the coupled use of Finite Element Analysis and Monte Carlo simulation.

- To perform a sensitivity investigation on the impact that different variables characterising the material microstructure have on the predicted component strength distribution. A parametric study on several loading configurations and component geometries was performed for this purpose.

- To identify parameters which play a key role in promoting brittle fracture and to assess the influence that the stress state has on the attainment of critical failure conditions. This task involved a careful and systematic analysis of the shape of the strength distribution focusing, in particular, on the parameters that affect the slope of the curve.

- To analyse the reliability of complex engineering components and suggest measures that allow the reduction of the failure probability associated with a particular operational setting.

1.4. Thesis Structure

A summary of the content of each chapter is presented as follows:

Chapter-1 delineates the background on which this thesis is intended.

Chapter-2 introduces the topic of brittle fracture, highlighting the statistical nature of this phenomenon. It also reviews the major works conducted in the area of probabilistic fracture mechanics in ceramic and metallic materials and in other closely related fields.

Chapter-3 describes the methodology employed to derive the strength distribution of a component containing randomly distributed flaws and subjected to arbitrary loading conditions. Particular attention is reserved for the discussion on the failure criteria employed to determine critical conditions for crack propagation and for a detailed description of the algorithms implemented to perform the Monte Carlo simulations.

Chapter-4 examines the mechanisms that control brittle fracture in ceramic materials. The effects that material parameters, such as mean and standard deviation of the flaw size distribution, and stress conditions have on the material strength distribution are analysed. A design criterion for components subjected to a plane stress state is proposed.

Chapter-5 is dedicated to the reliability analysis of a ceramic turbine blade. Several loading configurations are considered and the associated component's strength distributions determined. The locations at which failure is most likely to occur are also investigated. Finally, the strength distribution relative to an alternative design solution is derived and compared with the original results.

Chapter-6 investigates the phenomenon of brittle fracture in steel structures. Results similar to those obtained for ceramic materials are discussed.

Chapter-7 summarises the main results and gathers the most important conclusions drawn from the analyses conducted. Some suggestions for future work are also included.

2 LITERATURE REVIEW

2.1. The Cost of Fracture

Fracture is a problem that society has faced for as long as there have been man-made structures. The problem may actually be worse today than in previous centuries because of the increasing technological complexity of our society. For this reason, many resources have been employed in the past and are still allocated in the present to study the causes of fracture and to develop new technologies to guarantee structural integrity. In particular, research nowadays is directed towards the better understanding of fracture mechanisms, the development of more fracture and fatigue resistant materials, the improvement of manufacturing and processing techniques to achieve more uniform materials, the advancement of non-destructive evaluation equipment for both inspection and preventive maintenance.

In spite of these efforts to prevent or anticipate fracture, failures do occur and often with tragic consequences. The total impact of fracture on the economy is a measure of both the costs incurred as direct consequences of failure and the resources expended in the attempt of preventing fracture. The former category includes the total or partial loss of equipment, repair costs, personal human costs in pain, suffering and death, losses in cargo, business costs of delay, environmental damages. Many instances of fracture-related accidents, which have involved to various degrees all the consequences aforementioned, have been experienced in the aircraft, civil and oil industries in the past and recent years.

In addition to the direct consequences of unintended fracture, many resources are expended in applying maintenance and inspection procedures, to assure the safety of equipment, and in the stockpiling of redundant equipment which is stored in anticipation of fracture. Replacement parts or entire units are held in reserve, freezing capital which may be used for other purposes, for little reason other than to ensure the continued performance of an activity or function in the event of a component failure.

The total annual cost of fracture in the United States in 1978 was determined by an economic study [Duga, 1983] to be $99 billion (in 1978 US dollars), about 4.4% of the gross national product. Furthermore, this study estimated that the full application of the technology available at that time could have reduced this amount by $29 billion, and that further fracture mechanics research could reduce this figure by an additional $23 billion. A similar study [Faria, 1990] was conducted in Europe by the European Group on Fracture (EGF). The objectives of this work were to evaluate the economic effects of

failure due to fracture and assess the future potential in cost reduction achievable by the development and application of new design standards. The conclusions of this study, once again, indicated the future research in basic and applied sciences as the primary source of savings for the productive economy that has to deal with fracture.

Four broad research areas were identified as the most promising and pertinent to fracture: (1) understanding of the basic materials properties and the mechanisms of material failure; (2) progress in the effectiveness and accuracy of design methodologies, such as stress analysis and development of specialized fracture-prevention designs; (3) improvement in the knowledge and application of processing and fabrication techniques; (4) advancements in the areas related to inspection, testing and maintenance to allow more sensitive detection of flaws and accurate prediction of fatigue life.

The work presented in this thesis aims at promoting new engineering strategies and criteria to design structures that are more reliable by contributing to the first two research areas indicated above. The interest is focused in particular on understanding and modelling the random factors that determine the mechanical properties of brittle materials and ultimately control their fracture behaviour.

2.2. Brittle Fracture in Ceramics and Metal Alloys

The phenomenon of brittle fracture affects many of the materials currently employed in the most diverse sectors of the industry. The extent to which mechanical components are subjected to this type of failure may depend on the specific application and the environmental conditions in which the component operates, but, in general, the problem of predicting and preventing fracture is one of the main obstacles that a structural engineer faces in assessing and ensuring the reliability of a design.

Two families of materials will be considered in this study. These are ceramics, for their specific properties and recognized potential for future application in new promising designs, and metal alloys, due to their large presence in all major sectors of the industry. Both materials experience brittle fracture as relevant failure mode.

2.2.1. CERAMIC MATERIALS

The beneficial properties of structural ceramics include their high melting temperature, light weight, high hardness and good corrosion and oxidation resistance. These properties provide the potential for the successful application of these materials in

a wide range of highly demanding engineering fields such as the aerospace, automotive and petroleum industries [Barsoum, 1997]. Consequently, research has focused on improving ceramic properties and processing, as well as on establishing a sound design methodology.

Ceramic materials include oxides, carbides, sulphides and intermetallic compounds, which are joined by covalent or ionic bonds. Most ceramics are crystalline, but, unlike metals, the high energy of the atomic bond severely limits dislocation motion. Due to the impossibility of stress redistribution through plastic deformation, ceramics are brittle materials and this undesirable property must be carefully tackled during the design process. The lack of ductility and yielding capability leads to low strain tolerance, low fracture toughness and a large variation in observed fracture strength. When a load is applied, the absence of significant plastic deformation causes large stress concentrations to occur at microscopic flaws, which are unavoidably present as a result of material processing or in-service environmental factors. The observed scatter in component strength is caused by the variable severity of these flaws and by the phenomenon of sudden and catastrophic crack growth that may be initiated by the defects.

Because of the statistical nature of these flaw populations, the size of the stressed material volume affects the strength (this effect is known as the *size effect*). For example, suppose a set of samples with a known geometry experiences a load such that 20 per cent of the specimens break at a stress of *400 MPa* or lower. In this case, there is a 20-percent chance that a flaw of this strength or lower is present in any given specimen. If the specimen geometry is scaled such that the volume is 5 times larger, then for the same loading, there is a $100.0 - (1.0\text{-}0.2)^5 \cdot 100 = 67.2$ percent chance that a flaw of strength *400 MPa* or lower is present in any given specimen. Clearly, by increasing component size, the average strength is reduced because of the increased probability of having a weak flaw. Hence, if a ceramic component design is based on material parameters obtained form smaller size test specimens, then the effects of scaling must be taken into account, otherwise a non-conservative design would result.

Another consequence of the random distribution of flaws is that failure of a complex component may not be initiated at the point of highest nominal stress. A particularly severe flaw may be located at a region of relatively low stress, yet still be the cause of component failure. For this reason, the entire solution of the stress field must be considered in the design assessment process. Clearly, it is not adequate to predict reliability based only on the most highly stressed point [Nemeth *et al*., 1990].

2.2.2. STEEL AND OTHER ALLOYS

The two most common fast failure mechanisms experienced by steel and other metal alloys are ductile failure [Garrison and Moody, 1987], which is the result of nucleation, growth and coalescence of numerous microscopic voids that initiate after a significant amount of plastic deformation, and cleavage fracture, which is due to the rapid propagation of a crack along a particular crystallographic plane. Although both mechanisms lead to the total fracture of a component, they involve different physical phenomena, ductile failure being a strain driven process, while cleavage is a brittle fracture mainly controlled by stress levels. The same material may experience both failure modes depending on loading and temperature conditions, and, in some circumstances, a phase of microvoid coalescence may precede cleavage in the same fracture process. Anyway, the two stages can clearly be distinguished by a careful analysis of the fracture surface, with a characteristic fibrous and dimpled appearance in case of ductile failure, against a multifaceted surface typical of cleavage fracture.

In general, cleavage fracture occurs in the presence of macroscopic defects originated by material processing or working conditions, such as cyclic loading, and when plastic flow is restricted. Face centred cubic (FCC) metals are usually not susceptible to cleavage because there have numerous slip systems at all temperatures. On the other hand, materials with a body centred cubic (BCC) crystal structure fail by cleavage, in particular at low temperatures, because of the limited number of active slip systems.

The physical principles underling the cleavage process in metals are essentially the same as those controlling brittle fracture in ceramic materials and have been extensively studied in the past century [Anderson, 2004].

2.3. Linear Elastic Fracture Mechanics

Brittle fracture has long been recognized as a highly localized phenomenon where fracture initiation is mainly controlled by the incidence of flaws that inherently occur in the material. The fracture mechanics approach has three important variables rather than the usual two of stress and strength. The additional structural variable is the flaw size, while fracture toughness (or equivalently critical strain energy release rate) replaces strength as the relevant material property. Fracture mechanics is therefore a methodology that allows one to quantify the critical combinations of these three variables (applied stress, flaw size and material toughness) and determine the behaviour of the system.

Although classical fracture mechanics does not explicitly deal with the randomness characterising flaw size, position and orientation, it sets the fundamental principles necessary for the further development of more complex statistical models that directly examine the random distribution of defects. Since many of the concepts that constitute the basis of linear elastic fracture mechanics will be extensively applied in the following chapters, some of them are briefly reviewed in the next two sections.

Two approaches to fracture analysis exist, which are equivalent in most circumstances: the energy criterion and the stress intensity approach. Both approaches are discussed hereafter.

2.3.1. THE ENERGY APPROACH

The first quantitative approach to fracture able to explain the discrepancies between the theoretical strength, estimated through calculations based on molecular cohesion considerations, and the actual strength of materials was proposed by Griffith and published in 1920. Studying the bursting strength of cracked spherical bulbs and circular tubes made of glass, Griffith based his theory on a simple energy balance, invoking the "theorem of minimum energy". According to this principle, the equilibrium state of an elastic solid body, deformed by specified surface forces, is such that the potential energy of the whole system is a minimum. Therefore, at the equilibrium position, the rupture of the solid occurs only if the system can pass from the unbroken to the broken condition by a process involving a continuous decrease in potential energy. In the specific case of a crack propagating in an elastic solid, the formation of new surfaces in the interior of such solid during crack propagation would entail an increase in potential energy equal to the product of the material surface energy times the area of the new surfaces. For fracture to occur, this increase in potential energy must be offset by the net reduction in strain energy stored in the solid resulting from an increment of crack growth. Since this model assumes that the work of fracture comes exclusively from the surface energy of the material, the Griffith approach only applies to ideal brittle materials.

Several years later, Irwin [1957] rigorously formulated the energy release rate concept, which is related to Griffith approach, but is more convenient for solving engineering problems. The *energy release rate*, $\mathcal{G}$, is defined as the rate of change in potential energy Π per unit of crack area A, for a linear elastic material, and is a measure of the energy available for an increment of crack extension:

$$\mathcal{G} = -\frac{d\Pi}{dA} \tag{2.1}$$

The quantity $\mathcal{G}$ represents the variation in potential energy, supplied by the internal strain energy and external forces, resulting from a unit increase in crack area. The minus sign in front of the right-hand side of the equation (2.1) is due to the fact that, when the crack propagates, the change in potential energy Π is negative. Hence, the minus is necessary to have an energy release rate that is a positive quantity.

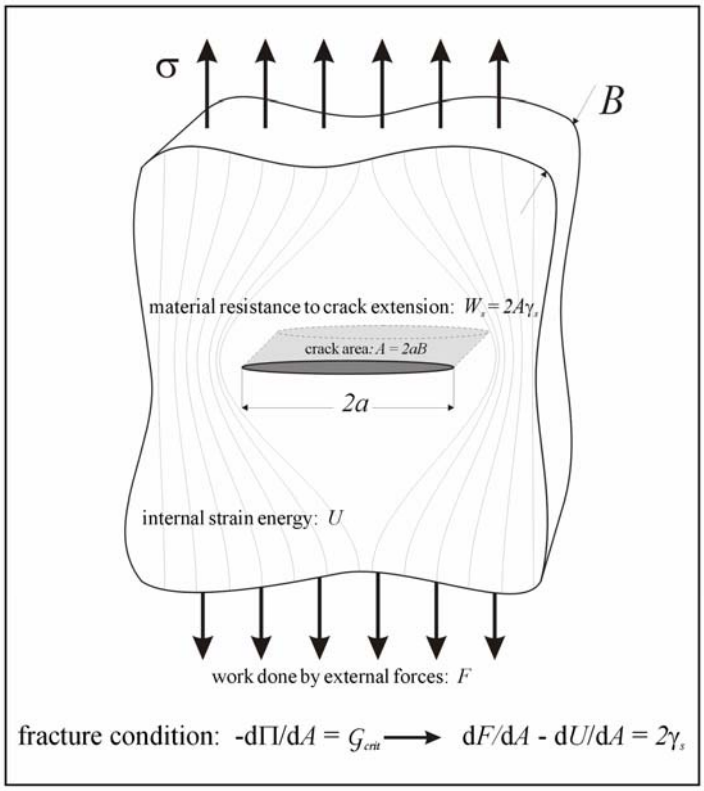

Figure 2.1 Crack energy balance

The energy approach states that crack extension occurs when the energy available for crack growth is sufficient to overcome the resistance of the material. In mathematical terms, at the onset of fracture:

$$\mathcal{G} = \mathcal{G}_c \tag{2.2}$$

where $\mathcal{G}_c$ is the *critical strain energy release rate*, which is a measure of the material's fracture toughness. Indicating with W_s the work required to create the new surfaces of the crack (Figure 2.1), the critical energy release rate can be written as:

$$\mathcal{G}_c = \frac{dW_s}{dA} \tag{2.3}$$

For an ideal brittle solid, the only contribution to the critical energy release rate comes from the material surface energy γ_s. Therefore, considering a unit thickness plate where the extension of a crack with length $2 \cdot a$ results in the formation of a total free surface of $4 \cdot a$, $W_s = 4 \cdot a \cdot \gamma_s$ and $\mathcal{G}_c = 2 \cdot \gamma_s$. The same approach can also be extended

[Felbeck, 1955] to materials that are capable of plastic deformation, such as metals, by taking into account the energy per unit area dissipated by local plastic flow, γ_p, and including this term into the expression of W_s such that $G_c = 2\cdot(\gamma_s+\gamma_p)$. This model, however, can be applied only if nonlinear effects, such as plasticity, are confined to a small region near the crack tip since, in the foregoing definition of G, it was assumed that the global behaviour of the material is elastic.

One of the fundamental assumptions of fracture mechanics is that G_c is independent of the size and geometry of the cracked body and is a material property.

2.3.2. THE STRESS INTENSITY APPROACH

The fundamental cleavage failure mechanism postulates that a microcrack produces stress concentrations of sufficient magnitude so that unstable crack propagation takes place where a local fracture stress exceeds a critical value.

The stress field in proximity of the crack tip in an elastic material subjected to a tensile load perpendicular to the crack plane is completely characterized by a single constant, known as the stress intensity factor, K_I. Each stress component near the crack tip is proportional to this constant, which defines the stress intensification produced by the defect. If one assumes that the material fails locally at some critical combination of stress and strain, then it follows that fracture must occur when the stress intensity factor reaches a critical value, K_{IC}. In practical terms, a failure criterion that predicts fracture when the local tensile stress ahead of the crack tip reaches the critical material resistance, σ_f, is equivalent to requiring that the stress intensity factor K_I relative to the particular load configuration and crack geometry is equal or higher than K_{IC}. Thus, K_{IC} is an alternative measure of the material fracture toughness. For linear elastic materials, the energy and stress intensity approaches to fracture are essentially equivalent.

The stress intensity methodology has been largely applied to the study of the different stress distributions generated ahead of a crack by the action of one of the three loading schemes that a crack can experience. The three so-called fracture modes are shown in Figure (2.2) and consist of Mode I, where the principal load is applied normal to the crack plane, Mode II, corresponding to an in-plane shear loading which tends to slide one crack face with respect to the other and Mode III, which refers to the out-of-plane shear. For each of the fracture modes above, a stress intensity factor (K_I, K_{II} and K_{III} respectively) can be defined and used to describe the stress field in proximity of the cracked area.

The actual value of K depends on the crack/structure geometry, magnitude of the remote stress and obviously fracture mode. Vast amount of literature deals with the problem of determining stress intensity factors and closed-form solutions exist for a number of simple configurations. Stress intensity factors can usually be expressed according to the general formula [Anderson, 2004]:

$$K_{(I,II,III)} = Y \cdot \sigma \cdot \sqrt{\pi \cdot a} \tag{2.4}$$

where σ is the relevant applied stress, a is a characteristic crack dimension and Y is a dimensionless constant that depends on geometry and mode of loading.

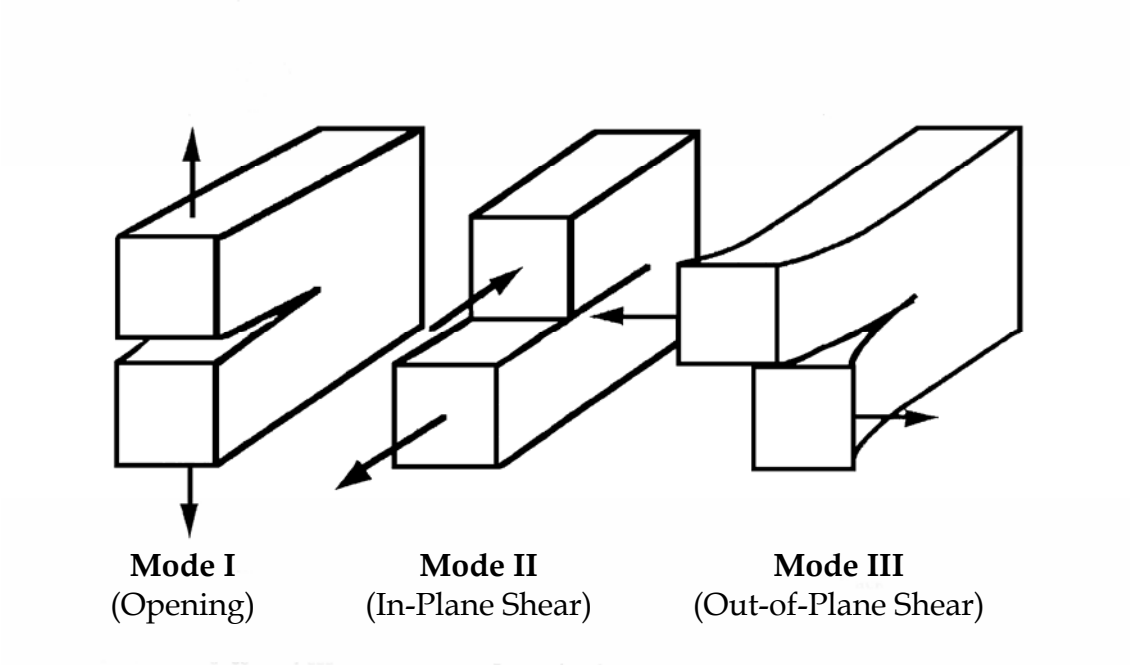

Figure 2.2 Fracture modes

Further work has also been conducted to predict fracture conditions when two or three modes act simultaneously. The solutions for these types of problems are generally obtained by employing energy criteria, since intensity factors relative to different modes are not additive, while energy contributions are. It is possible, however, to convert a stress intensity factor into an energy release rate and vice versa since the two quantities are directly and uniquely related for a linear elastic material [Irwin, 1957]. The main results of these studies will be discussed in the next chapter.

2.4. Statistical Models of Brittle Fracture in Ceramics

While the classical approach to fracture mechanics may resolve the local stresses leading to failure in a large class of problems, it does not take into consideration the statistical behaviour of fracture. Due to inhomogeneity in the local characteristics of the material, such as flaws orientation and size, fracture is of a random nature and therefore should be analysed by statistical methods. The development of suitable models to study the probabilistic aspects of fracture started with the formulation of the "weakest link theory" (WLT), which was successfully applied to explain the scatter in strength inherent to brittle materials subjected to uniform uniaxial tensile stress [Weibull, 1939]. Several statistical models based on the WLT assumptions follow for the analysis of brittle failure of components under multiaxial stress states.

2.4.1. WEAKEST LINK THEORY AND WEIBULL DISTRIBUTION

According to the weakest link theory, a structural component is represented as a chain of n links, each link being associated to a flaw present in the material microstructure. Within this framework, the fracture of a brittle material occurs when the critical stress associated with the weakest flaw is exceeded. In mathematical terms the failure probability (P_f) of a component subjected to a load of magnitude x is given by [Weibull, 1951]:

$$P_f = 1 - \exp\left[-n \cdot \varphi\left(x\right)\right] \tag{2.5}$$

where $\varphi(x)$ is the probability of rupture of a single link. The term $\varphi(x)$ is a function of stress conditions, flaw type and size. Equation (2.5) derives from the simple consideration that, if the survival probability of a single link is $1-\varphi(x)$, the survival probability of the whole chain is $[1-\varphi(\mathrm{x})]^n$, which for small value of $\varphi(x)$ can be expressed as $\exp[-n\cdot\varphi(x)]$.

Using experimental data as the basis for his assumptions, Weibull proposed a power law as the simplest mathematical expression for the function $\varphi(\mathrm{x})$. The result is the well-known empirical Weibull distribution for the failure probability of a structural component under uniform, uniaxial tension:

$$\begin{cases} P_f = 1 - \exp\left[-V\left(\frac{\sigma-\sigma_u}{\sigma_0}\right)^m\right] & \sigma > \sigma_u \\ P_f = 0 & \sigma \le \sigma_u \end{cases} \tag{2.6}$$

where V is the volume of the component, σ the uniaxial tensile stress and m, σ_0 and σ_u are the shape, scale and threshold parameters respectively. The three distribution parameters can be physically interpreted in the following way: σ_u is the minimum value of stress below which the material probability of failure is supposed to be zero, σ_0 is the value of stress in excess to σ_u for which a unit volume specimen has a failure probability of approximately 63%, while m determines the shape of the distribution, with lower values being associated to wider (and therefore more scattered) distributions (Figure 2.3). However, m is not the only parameter controlling the scatter in material strength levels since σ_0 also affects the slope of the strength distribution and therefore the variability associated with it.

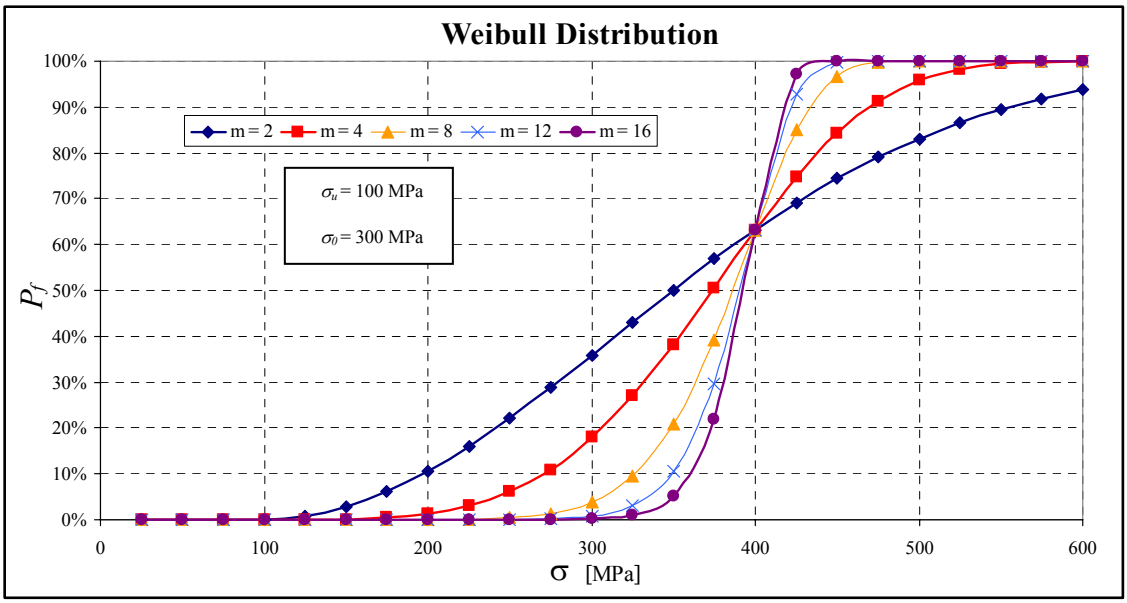

Figure 2.3 Three parameter Weibull distribution for several values of shape parameter, m

Despite its empirical nature, the Weibull approach is able to explain the two most important experimental observations made when testing the strength of brittle materials: the probability of failure increases with load amplitude and with the specimen size. For the analysis of uniaxial stress states, this model is considered the most effective and is probably the most widely employed in the interpretation of experimental results for

uniaxial stress testing configurations such as simple tension and 4-point bending. Several examples of Weibull distributions fitted to strength values of alumina (Al_2O_3) and other ceramic materials exposed to different environmental conditions can be found, among others, in Hoshide [1996].

2.4.2. MULTIAXIAL THEORIES

Extensions to Weibull's theory of brittle fracture have been proposed by several authors in order to include multiaxial and non-uniform loading schemes in the scope of the theory. The main purpose of these studies has been to find a methodology to determine the failure probability of a component under a multiaxial stress distribution by using material parameters that have been estimated through uniaxial stress tests. An interesting review of the most relevant models developed with this intent is presented by Rufin *et al.* [1984].

2.4.2.1. PRINCIPLE OF INDEPENDENT ACTION AND WEIBULL MULTIAXIAL STATISTICS

The simplest and most immediate application of Weibull's formula to a general triaxial stress state is represented by the Principle of Independent Action. According to this model, the survival probability of a isotropic specimen is equal to the product of the survival probabilities calculated for each principal stress applied in turn. The final equation for the probability of failure corresponding to the Weibull/Principle of Independent Action model is (assuming $\sigma_u = 0$):

$$P_f = 1 - \exp\left\{ -\iiint_V \left[\left(\frac{\sigma_1}{\sigma_0} \right)^m + \left(\frac{\sigma_2}{\sigma_0} \right)^m + \left(\frac{\sigma_3}{\sigma_0} \right)^m \right] dV \right\} \tag{2.7}$$

where σ_1, σ_2 and σ_3 are the principal stresses at each point of the structure. This is a very convenient formulation because of its simplicity but, unfortunately, leads to non-conservative estimates of P_f, since the mutual contribution of combined principal stresses to the fracture process is neglected. Despite its limitations, the principle of independent action was extended and applied to the analysis of anisotropic brittle materials by Margetson [1976].

A somehow more sophisticated design methodology for brittle components under arbitrary stress conditions can be found in Dukes [1966]. A comprehensive procedure for the initial phase of material properties characterization (three-parameter Weibull

distribution) and the subsequent stage of component structural design is outlined in his work. To predict material response under multiaxial stress by using statistical parameters obtained from uniaxial tests, this methodology proposes to calculate the probability of failure by averaging the normal component of the stress, σ_n, across all directions of the three-dimensional space. The failure probability of a small sphere characterised by constant values of principal stresses and a volume V is therefore written as:

$$P_f = 1 - \exp\left[-\frac{V}{4\pi} \cdot \iint \left(\frac{\sigma_n - \sigma_u}{\sigma_0} \right)^m \cos\theta \cdot d\theta \cdot d\beta \right] \tag{2.8}$$

where θ is the angle with respect to the *x-y* plane of the principal coordinate system and β is the angle with respect to the *x-z* plane (Figure 2.4), while the constants σ_u, σ_0, m are material parameters obtained from a statistical fitting procedure of uniaxial tensile test results. The normal component that appears in the integral is a function of principal stresses (σ_1, σ_2, σ_3) and the reference direction and is defined by the following relationship [Timoshenko, 1955]:

$$\sigma_n = \sigma_1 \cdot \cos^2\theta \cdot \sin^2\beta + \sigma_2 \cdot \cos^2\theta \cdot \cos^2\beta + \sigma_3 \cdot \sin^2\theta \tag{2.9}$$

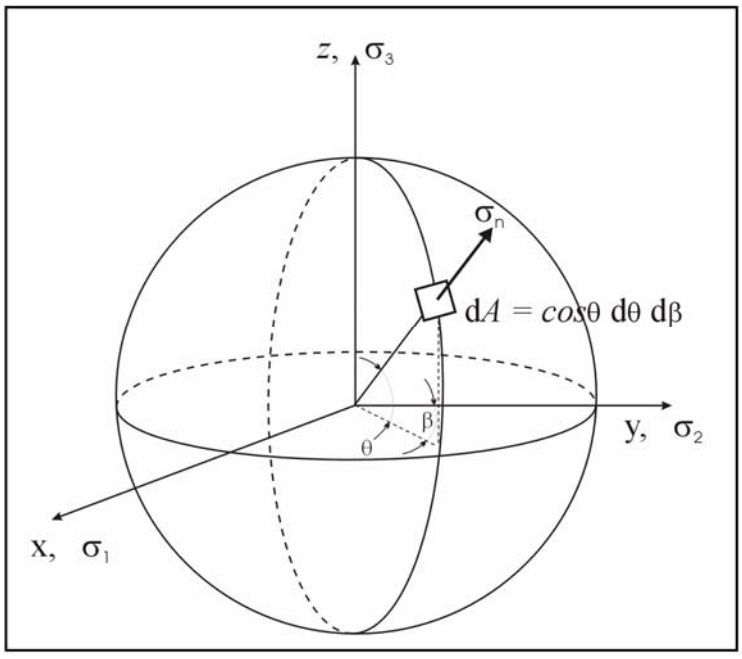

Figure 2.4 Averaging of the normal stress component

Equation (2.8) is applicable only to uniform stress distributions. For non-uniform configurations, the author suggested dividing the structure into a large number of small elements, each subjected to a different but approximately constant stress state, and to combine the contributions of all elements to the total probability of failure through the following expression:

$$P_f = 1 - \prod \left(1 - P_f^{elem}\right) \tag{2.10}$$

Equation (2.10) derives from the weakest link principle, according to which the structure fails if at least one of the constituting elements fails. It is valid under the assumption that fracture of a single element depends uniquely on the stress state within that element and is not affected by the conditions in the surrounding elements (independence assumption).

Although the approach illustrated by Dukes and known in the literature as the multiaxial Weibull theory is intuitively appealing, the idea of the failure probability depending on the spatial average of the normal stress is somewhat arbitrary and lacks a sound physical justification. As observed by other authors [Chao and Shetty, 1990], this methodology does not explicitly take into account the physical characteristics of the strength-controlling flaws and does not establish a formal link between statistical fracture theory and fracture mechanics. Experimental work on the fracture stress of alumina round solid rods under combined tension/torsion loads has also showed how theoretical predictions obtained via this multiaxial theory are not in complete agreement with experimental results [Petrovic and Stout, 1981a/1981b]. Similar conclusions were drawn after an equivalent study on the Weibull failure probability of thin- and thick-walled alumina tubes subjected to various loading configurations [Stout and Petrovic, 1984a/1984b].

2.4.2.2. DENSITY DISTRIBUTION OF CRITICAL FLAWS: BATDORF'S MODEL

Advancements in the statistical theory of brittle fracture were promoted by a new multiaxial model, which, although still based on the weakest link principle, introduced the concept of critical flaw density. According to this approach, the probability of failure is measured by estimating the density function of the number of defects that lead to catastrophic failure under a specified critical stress.

Batdorf and Crose [1974] assumed the material flaws to be microcracks and modelled the mechanical behaviour of a homogeneous isotropic material containing randomly

oriented and uniformly distributed microcracks. In their model, the crack density distribution, $N(\sigma_{cr})$, expressing the number of cracks per unit of volume having a critical stress less than or equal to σ_{cr}, is considered independent from the stress state acting on the structure and therefore is assumed to be a material property. They also hypothesised that fracture depends only on the macroscopic stress normal to the crack plane. Although this assumption neglects the effect that shear stress acting in the in-plane and the out-of-plane directions (corresponding to mode II and mode III fracture types respectively) has on fracture conditions, it has the advantage that allows one to derive an expression for the failure probability without any further knowledge on the actual shape of the cracks. The final equation for determining fracture conditions is obtained by considering the two different contributions to the overall probability of failure:

(i) the probability that a crack with a critical stress smaller than or equal to σ_{cr} will be found in the element volume; this quantity is directly related to the flaw density function, $N(\sigma_{cr})$;

(ii) and the probability that the crack will be oriented in such a way that the actual normal stress, σ_n, acting on the crack plane will be greater than σ_{cr}; this probability is expressed as a fraction of the solid angle $\Omega(\Sigma, \sigma_{cr})$, containing the normals to all orientations for which σ_n is grater than σ_{cr}, and is a function of the stress state Σ and the critical stress considered.

Combining these two contributions, Batdorf and Crose proposed the following expression for the probability of failure ΔP_f of a small element of volume ΔV, subjected to a uniform stress state Σ:

$$\Delta P_f = \Delta V \int_0^{\infty} \left(\frac{\Omega(\Sigma, \sigma_{cr})}{4\pi} \frac{dN}{d\sigma_{cr}} \right) d\sigma_{cr} \tag{2.11}$$

As seen before, the weakest link principle implies that the structure ultimately fractures when one of its constituting elements fails. This means that, rewriting equation (2.10) with the new notation, the overall failure probability can be calculated as:

$$P_f = 1 - \left(1 - \Delta P_f\right)^{\frac{V}{\Delta V}} \tag{2.12}$$

where $V/\Delta V$ represents the number of elements in the component. The total failure probability of a component subjected to a non-uniform stress distribution can therefore be obtained by taking the limit for $\Delta V \rightarrow 0$ of equation (2.12). This operation leads to the final expression:

$$P_f = \int_V dP_f = 1 - \exp\left[-\int_V dV \int_0^{\infty} \left(\frac{\Omega(\Sigma, \sigma_{cr})}{4\pi} \frac{dN}{d\sigma_{cr}} \right) d\sigma_{cr} \right] \tag{2.13}$$

In practical terms, the last integration is often performed numerically by dividing the component in a discrete number of small elements within which the stress state is known and assumed constant. The different contributions to the component probability of failure coming from all elements are then combined together as already seen for Duke's model.

In subsequent publications, Batdorf extended the model to include not only volume-distributed cracks, but also surface cracks typical of glass materials [Batdorf, 1978]. The new analysis assumes that crack planes are normal to the structure's surface, but are otherwise randomly oriented. The results are basically equivalent to those obtained in the treatment of volume embedded flaws. He also proposed several new shear-sensitive fracture criteria to be used within the framework of his theory [Batdorf, 1977]. The application of a different fracture criterion simply implies a modification to the term $\Omega(\Sigma, \sigma_{cr})$ that appears in equation (2.13). The inclusion of the shear stress contribution to the fracture process generally results in a better agreement of theoretical predictions with experimental evidence, but requires further knowledge about the shape of the crack-like defects. The direct comparison of several failure models suggested that the fracture criterion based on the maximum strain energy release rate (which will be discussed in the Chapter-3) is the most accurate.

Applications of Batdorf's model to the reliability analysis of alumina and silicon nitride disks subjected to a biaxial stress state were discussed by Chao and Shetty [1991]. The mathematical expression they employed for the crack density function was, in analogy with Weibull's formulation, of the form: $N(\sigma_{cr}) = k\sigma_c^m$, with k and m being the scale and shape parameters respectively. The possibility of cracks having a preferred orientation rather than being completely random distributed was also investigated in this study, although only the simple case of crack planes normal to the maximum principal stress was considered.

Despite the sophistication and the general assumptions under which this model has been formulated, it suffers some weakness. Specifically, the whole theory is based upon a concept, the critical flaw density function $N(\sigma_{cr})$, that does not seem to have a clear and direct link with the real features of the material microstructure, where number, shape and orientation of the flaws are the tangible quantities that control material mechanical behaviour. The critical flaw density is not a measurable quantity and it does not incorporate the actual number of flaws, but it rather seems a mathematical construct used to obtain an elegant solution to the multiaxial fracture problem.

2.4.2.3. THE ELEMENTAL STRENGTH MODEL

A similar, although mathematically more rigorous, statistical formulation of the fracture process of brittle materials was proposed by Matthews *et al*. [1976]. In deriving the expression for the failure probability of a component subjected to an arbitrary stress distribution, he also employed the idea of a flaw number density function, named $g(S)$ and defined in such a way that the product $g(S)\cdot dS$ expresses the number of flaws per unit volume with strength between S and $S+dS$. If flaws do not interact, the probability of fracture, δP_f, associated with a small element δV at a stress level S_1, equates the probability that a flaw with strength equal or smaller than S_1 exists in the volume δV and is given by:

$$\delta P_f = \left[-\delta V \int_0^{S_1} g(S)\, dS \right] \tag{2.14}$$

The fracture probability of a component of volume V, subjected to a stress S_1, can then be determined from the product of the survival probabilities $(1-\delta P_f)$ of each element into which the volume V has been divided. In the limit $V/\delta V \to \infty$, it is expressed as:

$$P_f(S_1, V) = 1 - \exp\left[-\int_V dV \int_0^{S_1} g(S)\, dS \right] \tag{2.15}$$

Equation (2.15) is essentially equivalent to equation (2.13). However, the disadvantage of this approach compared with the solution proposed by Batdorf is that, since $g(S)$ is not independent of the stress distribution, it cannot be considered as a material property, but must be recalculated every time the stress field in the component

changes. On the other hand, Matthews claimed that the strength of the new equation lies in the fact that, when deriving the expression of $g(S)$ from experimental data, no initial assumptions on its functional form are required. He also proposed a rather complex procedure to estimate the density distribution of surface flaws from fracture stress results in two common testing configurations, 3-point bending and hardness indentation. Subsequently, Evans [1978a] extended this approach by deriving equivalent expressions of $g(S)$ for surface and volume flaws in various specimen geometries and loading schemes frequently used in the uniaxial and biaxial strength testing of ceramics. These studies provided analytical solutions for determining the flaw density function, $g(S)$, by fitting experimental data of fracture stresses, but did not propose a practical methodology for the design of brittle components subjected to arbitrary loading conditions.

Only in a subsequent work [Evans, 1978b], the development of methods for transforming the flaw density function associated with an equitriaxial stress state to that relative to an arbitrarily combination of principal stresses contributed to the applicability of the model to general multiaxial stress configurations. In order to achieve this result, Evans assumed that the flaws controlling material strength properties were penny-shaped cracks and applied a fracture criterion based on the coplanar strain energy release rate to determine critical conditions for crack propagation. Other flaws geometries were also considered in subsequent studies. In particular, the same statistical methodology was employed to analyse the behaviour of microcracks originated at the surface of cylindrical cavities [Evans *et al*., 1979a] and spherical pores [Evans *et al*., 1979b]. A practical application of Evan's approach to a specific component geometry can be fund in Lamon [1983]. In this paper, bending-strength distributions of porcelain cylinders obtained at diverse span lengths are investigated under the assumption of a population of through-thickness cracks.

The term "elemental strength model" was attributed to this multiaxial fracture theory only by a later work [Lamon, 1988]. The expression refers to the idea that the crack-strength density function $g_T(S_T)$, relative to an equitriaxial stress state, is considered as a fundamental material property, uniquely related to the flaw population characterising the material microstructure. The elemental strength function is then transformed into strength distributions in other stress states by employing a suitable fracture criterion and by considering the flaw random orientation and the normal and shear stress components acting on the flaw surface.

The elemental strength model, developed at different stages by Matthews, Evans and Lamon, is a formal variation of Batdorf's approach, but is in substance based on the

same fundamental assumptions. Although in some occasions the superiority of the former model has been claimed [Lamon, 1988], the equivalence of the two methodologies was ultimately demonstrated in two separate studies [Chao, 1990 and Andreasen, 1993]. The author believes that Batdorf's approach offers some advantages in terms of flexibility and ease of application, but, in general, both models are affected by the limitations previously outlined and, in particular, by the lack of a physical parameter directly correlated to the measurable features of the material microstructure, which control the component strength distribution.

2.4.2.4. FURTHER WORK IN THE FIELD OF STATISTICAL BRITTLE FRACTURE

Although a large number of papers in the literature of statistical brittle fracture are dedicated to Batdorf's theory and the elemental strength model, an absolute agreement on the best methodology to be used in the reliability analysis of ceramic materials has not been reached among scientists. On the contrary, research in this field is still extremely active and several alternative approaches have been proposed in the past two decades. Some recent developments include the work of Zimmermann [1999] who formulated a statistical model of brittle fracture based on the interaction between microstructural spherical cavities (pores) and grain size. The model assumes that the length of the most severe microcrack nucleating in proximity of a pore is associated with the size of the grain located around the pore equator.

Other authors proposed some relatively significant modifications to the classical Weibull theory for multiaxial fracture. Quinn [2003] for example, measured Weibull parameters and estimated size effect on the failure probability of unconventional specimen geometries (cylindrical rods). Applicability of Weibull statistic to highly porous materials was investigated by Pernot [1999] and Hoshide [2003]. While the former work confirmed the possibility of applying a Weibull distribution to describe fracture data obtained in flexural tests of a porous glass-ceramic material, the latter research suggested modifying Weibull formulation of the failure probability by multiplying the so-called risk of rupture, i.e. the term in the exponent of equation (2.8), by a factor dependent on porosity.

Attempts to correlated material strength to pore size distribution were made separately by Berdin [1996] and Chao [1992]. In both studies, the probability distribution of the spherical cavities diameter was estimated by means of quantitative image analysis. The relationship between material strength and pore size was established by Berdin through a Weibull type of analysis. In determining the critical stress associated with each flaw size, Berdin assumed that pores behave as penny-

shaped cracks. A multiscale approach was then employed to find an analytical expression for the defect size density that would fit experimental data. The reason why the model is defined as multiscale is that both macroscopic fracture results obtained from mechanical tests and microstructural information related to the observed defect distribution are used in the fitting procedure.

Chao, on the other hand, applied the theory of extreme-value statistics to assess the reliability of sintered silicon nitride specimens subjected to biaxial stress. In this work, annular cracks are assumed to nucleate around the equator of spherical pores. Crack extension (ahead of pore surface) and orientation are fixed, while pore size varies according to an exponential probability law estimated through image analysis techniques. Reasonably good agreement between theory and experiments was observed by the author, who also highlighted the strong dependence of the results on the size of the annular crack relative to the pore and on the associated stress intensity factors.

Another interesting investigation on fracture related issues was conducted by Givli [2006]. He focused the attention on the statistical characteristics of failure location and their relation to strength in brittle materials. A simply one-dimensional component subjected to either a uniform tensile stress or a bending load was considered in this study. The analysis, which was based on the weakest link principle, confirmed that, in materials with random strength, failure does not necessarily initiate at the point of maximum stress. In fact, an element with a lower stress may fail first and, in general, failure location is a random parameter, which is a functional of the whole stress field. A similar type of analysis will be conducted in the following chapters, but on much more complex component geometries and loading configurations.

The proliferation of research papers in the area of statistical brittle fracture, which often propose different, if not contradictory, approaches for the reliability analysis of ceramic components demonstrates how a unified methodology, accepted among most academic researches and industry representatives, has still to be developed. This suggests that there exist concrete opportunities for significantly contributing to the advancement of this field of the applied sciences.

2.4.3. SOFTWARE PACKAGES FOR THE RELIABILITY ANALYSIS OF CERAMIC COMPONENTS

Due to the increasing demand coming from the industry for efficient analysis and simulation tools to be employed at an early stage of the design process, several research institutions have been working at the development of software applications for

determining fast-fracture reliability of ceramic components subjected to complex thermo-mechanical loadings. These tools are generally based on the coupled use of Finite Element Analysis (FEA) and one of the multiaxial fracture theories previously discussed. The standard approach followed in these developments involves a two-stage process in which FEA is first employed to determine the stress field produced in the component by the applied load and then a statistical fracture analysis is performed to estimate component reliability. The statistical failure model is generally incorporated into the finite element method by assuming that each of the elements in which the component is divided is small enough for the stress gradient to be considered negligible. Component integrity is computed by calculating element-by-element reliability and then by determining the component survival probability as the product of the individual element reliabilities.

Several examples of the successful application of such methodology can be found in the literature. NASA developed an integrated software package named CARES (Ceramic Analysis and Reliability Evaluation of Structures) [Nemeth *et al*., 1990], which uses Weibull and Batdorf fracture statistics to predict the reliability of isotropic ceramic components. The computer program operates as a standard finite element post-processing tool, which, after calibrating a set of material parameters, automatically performs component reliability calculations. Material parameters estimation is independent of finite element output and is carried out by fitting experimental data obtained from the fracture of simple components (uniaxial or flexural specimens), to a two-parameter Weibull distribution. A similar computer code was developed in Germany and employed for the reliability analysis of ceramic components for gas turbine applications [Sturmer *et al*. 1991]. The software is known as CERITS and it implements Batdorf's theory for determining the failure probability of structures experiencing multiaxial stress states.

An application of the elemental strength model is represented by the software CERAM [Lamon, 1990]. This computer program is based on the same principles outlined above. It exploits the output of a finite element analysis to compute comparable failure probability distributions obtained by applying Weibull and Evans statistical approaches respectively. Another computer program we came across during our survey is FAILPROB [Wellman, 2002]. In this case, only the normal tensile stress averaging method (Weibull theory) is employed for fast-fracture reliability predictions, but an advance algorithm, developed for the treatment of material interfaces (between a ceramic and a dissimilar material) which can lead to stress singularities, is included in this software.

It is believed that, on the basis of the work conducted in this thesis, an equivalent commercial software package could be developed in the near future, which would benefit from the computationally more efficient approach applied in our investigation and discussed in the next chapters.

2.5. Probabilistic Studies on Cleavage Fracture in Structural Steels

Probabilistic models have also been developed to explore the fracture behaviour of structural steels and to explain the variation in the values of macroscopic fracture toughness, K_{IC}, measured experimentally for different temperatures and microstructures. In these studies, the weakest link concept is applied to the propagation of a sharp macrocrack into the surrounding material in which a statistical distribution of carbide particles is assumed.

2.5.1. CLEAVAGE FRACTURE MECHANISM

The process of cleavage fracture in mild steels has been attributed to the two separate mechanisms of slip-induced cracking (crack nucleation) of carbide particles due to dislocation pile-up, and the subsequent extension of the resultant cracks into the surrounding ferrite matrix (crack propagation). According to this principle, a steel specimen containing a sharp macrocrack fractures when a microcrack, nucleated in a carbide particle in proximity of the (macro) crack-tip, propagates.

Most of the models reviewed in the literature treat crack nucleation as being secondary in importance and assume that the critical step in the fracture process is the propagation of carbide microcracks. One of the first works that orientated research towards this direction was published by McMahon and Cohen in 1965. After a detailed metallographic analysis of specimens under progressively increasing tensile stress, they concluded that cleavage cracks are initiated predominantly by the cracking of iron-carbide particles even when the carbon content is as low as 0.007 per cent. The brittle carbides crack during loading throughout the temperature range of 30°C to -195°C under the influence of the stresses imposed upon them by the plastic deformation of the surrounding ferritic matrix. These microcracks would then propagate in the ferrite grain only if they are large enough to cause a stress concentration able to overcome material resistance. Due to the large number of carbide cracks observed at the moment of fracture, they deduced that one does not have to postulate dislocation-interaction

mechanisms in the ferrite to account for the initiation of cleavage since the process controlling the fracture event is crack propagation.

In a following study Ritchie, Knott and Rice [1973] formulated the so-called RKR model, which postulates that cleavage failure occurs when the local tensile stress ahead of the macro crack tip (σ_{YY}) exceeds the critical value of material resistance, σ_f, over a characteristic distance d_c (Figure 2.5).

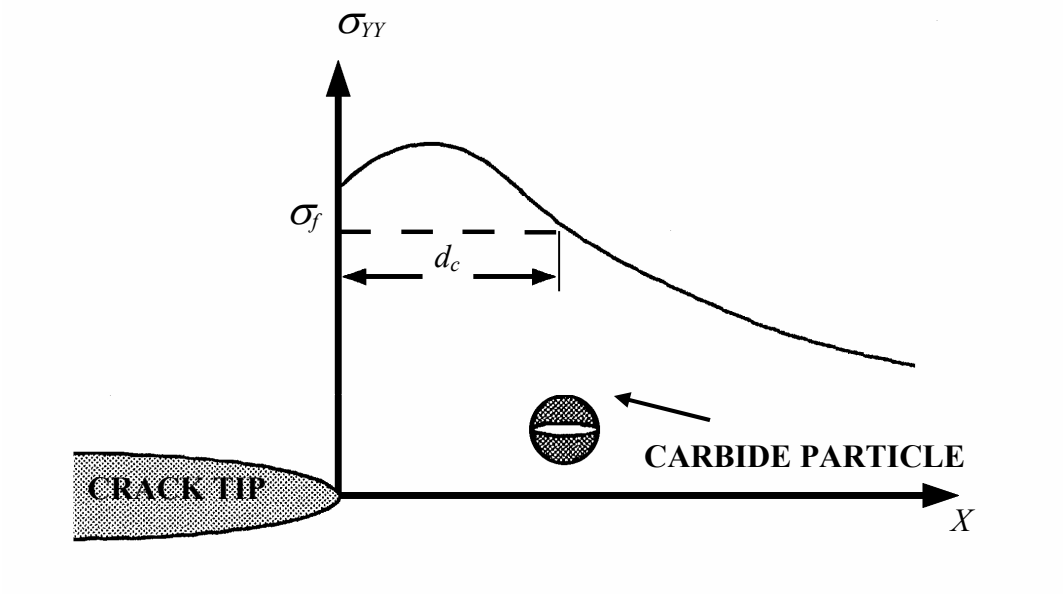

Figure 2.5 Carbide particle ahead of crack tip

Experimental observation on fatigue pre-cracked specimens tested in 3-point bending and direct comparison of nominal fracture stresses with a finite element solution of the stress field ahead of a sharp crack [Hutchinson, 1968] suggested that this characteristic distance is equal, on average, to two grain diameters. Since carbides are generally located on grain boundaries, it was recognised by the authors that this was the length required for the critical stress to reach the first carbide particle (at the first grain boundary) and to propagate the microcrack across the subsequent ferrite grain (second grain boundary). The failure criterion based on a critical value of local tensile stress was adopted from previous investigations [Knott, 1967], which measured a σ_f in the range of *820* to *860 MPa* for mild steels and also suggested that this value was largely independent from loading conditions (temperature and strain rate).

In a subsequent study, however, it was clarified that there is not a clear relationship between critical distance and ferrite grain size valid for any steel chemical composition

and microstructure configuration [Curry and Knott, 1976]. On the other hand, a strong link was identified between average carbide particle size and fracture stress [Curry and Knott, 1978]. The apparent dependence on grain size was simply justified by taking into account the increase in carbides size that is observed when increasing grain size. It was also postulated that, in the analysis of the fracture process, carbide particles can be treated, in first approximation, as Griffith defects (ignoring the dislocation contribution to cleavage initiation). In particular, spherical particles were assumed to act as penny-shaped cracks, while grain boundary carbide films were assimilated to through-thickness cracks (Figure 2.6).

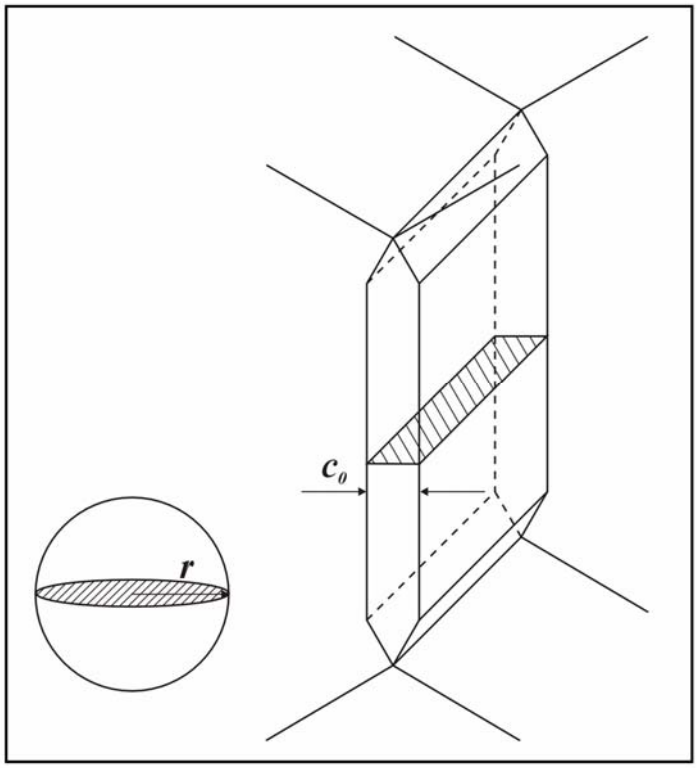

Figure 2.6 Grain boundary carbides

Under these assumptions, the critical conditions for crack propagation in terms of the local fracture stress, σ_f, are:

$$\sigma_f = \left[\frac{\pi \mathrm{E}\left(\gamma_s + \gamma_\mathrm{p}\right)}{2\left(1\text{-}\nu^2\right) r}\right]^{1/2} \qquad \text{penny-shaped}$$

$$\sigma_f = \left[\frac{4 \cdot \mathrm{E}\left(\gamma_s + \gamma_\mathrm{p}\right)}{\pi\left(1\text{-}\nu^2\right) c_0}\right]^{1/2} \qquad \text{through-thickness} \tag{2.16}$$

where γ_s and γ_p are ferrite surface energy and plastic energy dissipated by local yielding to create a unit area of fracture surface respectively. The other material properties are, according to the standard notation, E for the Young's modulus and ν for the Poisson's ratio. The size parameters r and c_0 are particle radius and film thickness for spherical particles and carbide films respectively. For the steel under study, a value of 14 J/m^2 was suggested for ($\gamma_s + \gamma_p$) at a temperature of -150°C.

2.5.2. STATISTICAL CLEAVAGE FRACTURE MODELS

The preliminary considerations discussed above led to the development of one of the first statistical models for cleavage in steels [Curry and Knott, 1979], which gave a probabilistic explanation to the RKR characteristic distance. Experimental evidence and theoretical developments confirmed that, as was previously postulated, for cleavage fracture to occur, the critical stress σ_f must be exceeded not just at a single point ahead of the crack tip, but over a microstructurally-significant (characteristic) distance, whose length depends on the probability that a sufficient large carbide particle is found in this region. The parameter σ_f itself is not treated as a deterministic quantity anymore, but assumes a distribution of values related to the statistical distribution of carbide particle sizes. Employing an image analysis tool, the area number density and the relative frequencies of particle radii was obtained and the corresponding values of σ_f calculated through equation (2.16) by assimilating carbides to penny-shaped cracks. The underlying mathematical model was not very complex since it assumed a simple proportionality relationship between the number of microcracks and the sampled area ahead of the (macro) crack tip. It accounted for the random orientation of cracked particles by merely applying a correction factor (which was also used to scale the proportion of carbides that effectively act as crack nuclei under the local straining conditions).

The basic concepts outlined in Curry's paper were further developed in a subsequent work by Wallin *et al*. [1984]. In this two-dimensional statistical model of brittle fracture, Wallin assumed a population of carbide particles acting as penny-shaped flaws and with a size probability density function of exponential form ahead of a macroscopic crack in both a bainitic and a ferritic carbon steel. He then calculated the failure probabilities relative to progressively increasing stress intensity factors (which in turn were associated with increasing load levels) by applying the weakest link principle. According to this assumption, for a given stress intensity factor $K_{I,i}$, the resulting fracture probability $p_{f,i}$ is given by one minus the product of the survival probabilities of each infinitesimal element of length dX at a distance X from the crack tip. The expected value of material fracture toughness was finally determined through the simple expression: $\mathbb{E}[K_{If}] = \sum[K_{I,i} \cdot (p_{f,i} - p_{f,i-1})]$. As highlighted by the author himself, the main limitations of this approach lie in the two-dimensionality of the model and in the assumption that fracture initiates uniquely along the plane of the macroscopic crack.

A more accurate mathematical formulation of the cleavage fracture process initiated by carbide particles in mild steels with a simple ferrite/grain-boundary-carbide

microstructure was subsequently presented by Lin *et al*. [1986a]. The model proposed recovers some of the concepts previously developed for the analysis of brittle fracture in ceramics. In particular, it is based on the application of the weakest link statistics and it expresses the dependence of critical fracture stress on carbide particle size in terms of a critical flaw density function $g(S)dS$, which is defined as the number of particles per unit volume having strengths between S and $S+dS$ (strength being inversely related to particle size through equation 2.16). Two different solutions of the stress field in proximity of the crack tip were employed in conjunction with this statistical formulation, a linear elastic approximation for materials tested at extremely low temperatures, and an elastic/plastic model [Hutchinson, 1968] for higher temperatures. Carbide particles were again assimilated to penny-shaped cracks, although only a fraction (5%) of the total number was considered "eligible" to act as crack nuclei (this is because not all particles are assumed to nucleate a crack under the action of the local strain). The formula obtained for the calculation of the failure probability (due to unstable propagation of the crack in the weakest particle) is essentially equivalent to equation (2.15), in which the function $g(S)$ is approximated via a three-parameter Weibull distribution.

This model was applied in a following study [Lin *et al*. 1986b] to the analysis of the cleavage process ahead of sharp cracks and rounded notches, e.g. in fatigue pre-cracked and Charpy V-notched specimens respectively. Main objective of the investigation was to identify the point in the region ahead of the stress singularity at which fracture initiation is most probable. The results confirmed that the critical cracking event occurs some distance ahead of the notch or crack tip, consistent with fractographic evidence showing probable initiation sites to be particles located a few grain diameters from a crack tip. Moreover, the differences between sharp cracks and V-notches in terms of the most probable location of the critical fracture event provided an interpretation of the role that stress gradients have in governing microscopic fracture behaviour. For failure ahead of a sharp crack, where stress gradients are large and local stress decreases with progressively increasing distance from the tip, statistical competition exist between the decreasing stresses and an increasing probability of finding a sufficient large particle when moving away from crack tip. In general, crack initiation locations for this type of defect were found at a relative short distance for the crack tip. Conversely, for failure ahead of a rounded notch, where the stress gradients are small, characteristic distances were found to be much larger. To explain the differences in the observed behaviour, it was postulated that the fracture process ahead of a notch is dominated by the larger, lower strength particles. Fracture ahead of the sharp crack on the other hand, is influenced additionally by the more numerous fine particles, as stresses are largest in the

immediate vicinity of the tip. This concept of the relevance of stress gradients in determining material fracture behaviour and strength sensitivity to particle size will be re-examined in the following developments of this thesis.

An alternative, statistical treatment of brittle fracture , based on Weibull statistics and the critical maximum principal stress as a local criterion for cleavage, was developed by Beremin [1983]. He related the critical stress required to propagate a microscopic crack to the length of the crack through the classical Griffith relationship and expressed the probability density function of microcracks having size c_0 with an inverse power law relationship: $P(c_0)\cdot dc_0 = \alpha/c_0^{\beta}\cdot dc_0$, where α is a constant, β defines the shape of the microcrack distribution and $P(c_0)$ indicates the probability of finding a crack with length between c_0 and c_0+dc_0. This relationship simply states that the probability of a crack to have size c_0 decreases with increasing c_0 at a "speed" β. By integrating this expression over the critical length interval ($c_0 > 4E\gamma_p/\pi(1-\nu^2)\sigma^2$, where σ is the maximum principal stress acting on the microcrack), Beremin derived a two-parameter Weibull distribution to describe the cumulative failure probability based on the weakest link statistics:

$$P_f(\sigma_w) = 1 - \exp\left[-\left(\frac{\sigma_w}{\sigma_u}\right)^m\right] \tag{2.17}$$

In this equation σ_u is a constant while σ_w represent the "Weibull stress" defined as he integral of a weighted value of the maximum principal (tensile) stress (σ_1) over the process zone for cleavage fracture (i.e., plastic zone at the crack tip):

$$\sigma_w = \left[\frac{1}{V_0}\int_{V_p} \sigma_1^m \cdot dV\right]^{1/m} \tag{2.18}$$

where V_p is the volume of the cleavage fracture process zone, V_0 is a reference volume and m is a Weibull modulus related to the modulus of the probability density function of microscopic crack sizes in the fracture process zone, β, by the relationship: $m = 2\beta - 2$. A correction to the expression for calculating the Weibull stress was also included for cases in which significant plastic deformation is present at crack tip to take into account the effect plastic strain has in increasing the fracture stress.

Godse and Gurland [1989] proposed one of the few models that incorporate both mechanisms of nucleation and propagation in the prediction of fracture conditions. They translated mathematically the experimentally determined carbide particle size

distribution with a log-normal probability law and assumed that only a fraction of these particles are subject to cracking under the crack-tip stress field. Since crack nucleation is a process associated with plastic deformation, the fraction of pre-cracked particles depend upon the yielding capability of the material and therefore upon temperature. They suggested that at very low temperatures (in the range from -200°C to -140°C), when dislocation motion is very limited due to the lack of atomic vibrational energy, the stress required for crack nucleation is higher than the propagation stress. Under these conditions, the process dominating the fracture event is crack nucleation. On the other hand, at higher temperatures (-100°C to -80°C) the crack propagation mechanism is believed to control fracture conditions. The model seems to fit satisfactorily experimental results, however, some drawbacks can be recognized in the fact that it does not take into account the random orientation of cracked particles and it assumes that only the normal stress acting on the crack plane triggers crack propagation.

More recent works have essentially followed the path outlined by the previous investigations of Curry and Beremin, proposing relative minor modifications to the original models. The two-parameter Weibull distribution employed in Beremin's derivations was "upgraded" to a three-parameter distribution by Gao *et al*. [2005]. Some progresses were made in extending the types of the steel microstructures to which the Weibull approach could be applied. For example, Valiente *et al*. [2005] developed a modified Weibull model to explain the scatter in fracture toughness of steels with a pearlite/ferrite microstructure. Additional propagation criteria for carbide cracks have also been proposed. In particular Wang and Chen, [2001] introduced a dual fracture criterion which includes a critical stress level coupled with a critical strain value.

2.6. A New Equation to Determine the Probability of Failure Initiated by Flaws

A new method for determining the probability of fracture of loaded components with complex shape containing internal flaws has recently been suggested by Todinov [2005a]. The statistical model proposed in this work is based on the classical weakest link principle, but it introduces the new concept of individual failure probability, F_c, as the parameter controlling component reliability.

Todinov assumes a Poisson process as the most appropriate model to simulate the number of flaw occurrences within a component of volume V. The three basic assumptions for the applicability of the Poisson model are [Parzen, 1960]:

(i) the probability of having exactly one defect in an infinitesimal portion ΔV of the total volume V is approximately proportional to ΔV ($P_1(\Delta V) \cong \lambda \cdot \Delta V$);

(ii) the probability of having more than one defect in ΔV is approximately zero ($P_{n\geq 2}(\Delta V) \cong 0$);

(iii) the event of having a defect in a sub-volume ΔV is not affected by the presence of defects in other sub-volumes, but only by the size of ΔV (independency assumption).

The term λ, called mean number density of the process, expresses the proportionality factor between the expected number of flaws and the size of the volume considered. For a homogeneous Poisson process, the mean number density is constant throughout the component's volume, while it is a function of position in the most general case. The probability law of a homogeneous Poisson process establishes that the probability of having exactly n defects in the whole volume V is:

$$P_n(V) = \frac{e^{-\lambda \cdot V}(\lambda \cdot V)^n}{n!} \tag{2.19}$$

By considering the sum of several mutually exclusive events in which failure occurs conditionally on the presence of a specified number of flaws (i.e. failure occurs given that 1 defect is in the component, failure occurs given that 2 defects are in the component, etc.), it is possible to calculate the total probability of failure P_f by applying the total probability theorem:

$$P_f = \sum_{n=0}^{\infty} P_n(V) \cdot F_c^{(n)} \tag{2.20}$$

where $P_n(V)$ is the probability of having n defects in the volume V, while $F_c^{(n)}$ is the probability that a component containing exactly n defects will fail under the specified load. The quantity $F_c^{(n)}$ can in turn be expressed as a function of F_c, which is defined as the conditional individual probability of triggering failure characterising a single flaw, given that the flaw is in the component/structure. In fact, applying the weakest link principle, it is straightforward to derive that (as seen previously but with a different notation) $F_c^{(n)} = 1-(1-F_c)^n$. Combining the last three expressions together and with a few more analytical derivations, Todinov obtained the following equation for the probability of failure of a component containing Poisson distributed random flaws:

$$P_f = 1 - \exp\left(-\lambda V \cdot F_c\right) \tag{2.21}$$

Equation (2.21) is valid not only for a constant stress, but for a loaded component/structure with complex shape for which the stress tensor varies in magnitude and sign from point to point. For different magnitudes of the loading forces, which change the stress field within the component, the conditional individual probability F_c changes too. On the other hand, when comparing the strength distribution of two structures with different volumes but the same stress state, the trends predicted by the model are consistent with the experimental evidence that the failure probability of a brittle component increases when its volume increases.

In the same paper [Todinov, 2005a], a method based on Monte Carlo simulation has been suggested for determining the conditional individual probability of triggering failure F_c characterising a single flaw. The aim of the Monte Carlo simulation is to collect statistical information from all parts of the component/structure volume, locally stressed in different ways, which is necessary to estimate the conditional individual probability F_c. Once F_c has been estimated, it is plugged into equation (2.21) to determine the probability of fracture of the component. The method works irrespective of component's geometry and the type of load.

Equation (2.21) permits one to relate in a simple fashion the conditional individual probability of failure associated with a single flaw to the probability of failure characterising a population of flaws as long as all flaws are assumed to be originated from the same population (in terms of shape, size, location and orientation distributions). However, thanks to the multiplicative properties of the exponential function, equation (2.21) can be easily extended to the case in which several flaw populations are present [Todinov, 2000].

It has also been demonstrated how the classical Weibull distribution could be considered as a special case of equation (2.21) for an appropriate choice of the function F_c [Todinov, 2005b]. Moreover, in a subsequently work [Todinov, 2006], the model was generalised for flaws following a non-homogeneous Poisson process.

The advantage of Todinov's approach compared to the other models reviewed so far lies in the fact that it takes into account the contribution of all flaws to the failure probability and it can be applied to any configuration of applied load and component geometry. The only additional information that is required to solve the problem of determining the strength distribution of theoretically any structure is a reliable and efficient method to estimate the parameter F_c, which, once again, is defined as the

probability of failure given that only a single defect is present in the component's volume:

$$F_c = P_f \,/\, \text{only one defect in the component} \tag{2.22}$$

2.7. Motivations for Further Research

In the present work, the model introduced by Todinov is further developed and detailed for evaluating the individual failure probability, F_c, and the associated strength distribution of components containing crack-like defects and subjected to multiaxial load. The approach proposed is based on a direct simulation procedure, which combines finite element analysis of the stress field acting on the component with a Monte Carlo simulation of defect random parameters, such as size and orientation. This methodology is then applied to the reliability analysis of various component geometries and loading configurations and is employed to perform a parametric study. The aim of the parametric study is to identify the main factors, such as stress state and flaw size variability, that control the fracture strength and to analyse the sensitivity of the failure probability to changes in these variables.

The motivations that are at the origin of this research work are summarized in the following points:

- To demonstrate that equation (2.21) is a valid alternative to existing micro-mechanical models for evaluating the strength distribution of brittle materials. The methodology developed in this work offers significant advantages compare to the best current practice, in terms of computational requirements and ease of application to complex structure geometries and loading configurations.
- To overcome the limitations of the other statistical models of brittle fracture available in the literature. In fact, most of the models reviewed in the previous sections are based on the Weibull distribution and, in particular, on an empirical assumption about the strength distribution of individual flaws. On the other hand, our approach is more fundamental since it uniquely relies upon well-established concepts of fracture mechanics. No a-priori assumptions are made concerning the strength of the flaws and all model input parameters are associated to directly observable physical quantities, which characterise the

material microstructure, such as number density and size of the flaw population.

- To unify the treatment of brittle fracture in ceramic materials and low carbon steels and to show how the same simulation procedure can be applied to both families of materials.
- To apply such methodology to investigate the effect that stress state and material microstructure variability have on component strength distribution.

Concrete applications of the proposed methodology to the reliability analysis of common engineering components, experiencing various loading schemes, are discussed in the following pages. The aim is to evaluate the strength distribution of real mechanical components with complex shape and to investigate the sensitivity of such distribution to variations in material properties and loading conditions.

The results obtained through this analysis allows one to gain a better understanding of the random factors that control material response to fracture and provided helpful suggestions for the design of more reliable mechanical components. It is important to stress at this point that the methodology proposed in this work is thought as an effective design tool, to be used by structural engineers to assess and improve the reliability of their designs, rather than a simple fitting procedure of experimental results as for most of the models encountered so far.

A detailed discussion of the theoretical assumptions and the numerical methods employed in the development of the model is given in the next chapter.

3 METHODOLOGY

3.1. Strength of a Component Containing Random Flaws: Model Formulation

The assessment of the integrity of any flawed mechanical structure requires the development of approaches which can deal not only with simple situations such as uniform uniaxial load, but also with more complex configurations (stress triaxiality, large stress gradients, etc.).

In Chapter-2, we have discussed a general equation to determine the strength of a component containing random flaws under arbitrary loading conditions derived by Todinov in 2005. This equation relates structural strength with the component's volume, V, mean number density of flaws, λ, and the individual probability of failure F_c, defined as the probability of failure given that only a single defect is present in the component. In mathematical terms the equation states that the probability that the component will fail under any configuration of the load is:

$$F_S = 1-\exp\left(-\lambda V \cdot F_c\right) \tag{3.1}$$

While the parameters λ and V can be determined through direct measurements, the quantity F_c must be estimated after further assumptions and theoretical considerations concerning the relevant failure criterion. In particular, a mathematical formulation must be given to the flaw population present in the material and an appropriate failure criterion must be applied to study the interaction between flaw content and the load acting on the structure. In the following pages, a straightforward methodology for determining F_c is presented.

3.1.1. MODEL ASSUMPTIONS

Due to the common statistical nature and the similarities in the mechanisms involved in the fracture process, the same mathematical model will be applied to the reliability analysis of both ceramic materials and low carbon steels. In deriving the equations and the solving algorithms for the calculation of F_c and the associated failure probability of a component subjected to an arbitrary multiaxial load, the following additional basic assumptions will be made:

(i) The only contribution to structural failure comes from the unstable propagation of a crack, initiated at the weakest flaw, which results in the ultimate fracture of the structure.

(ii) The flaw population consists of crack-like defects that nucleate at pores (typically in the case of ceramics) or second-phase content (in particular at carbide particles in low carbon steels). These cracks are naturally present in the material as a result of the manufacturing process or, more generally, of any stress/strain conditions that the material might have undergone before actual loading and are therefore randomly oriented. In the case of steels carbide particle, micro-cracking is driven by the high strain regime characterising the area ahead of a macroscopic stress intensifier.

(iii) Microcracks are assumed to exist and are non-interacting.

(iv) The flaw population is defined in terms of a set of random variables which determine size, location and orientation of the flaw. These random variables will generally be treated as statistically independent.

(v) Microcracks are located in a homogeneous matrix whose mechanical properties are measurable, deterministic and not affected by the presence of the defects.

(vi) Fracture conditions are determined by a local criterion which establishes if a crack in the population is able to propagate into the surrounding material matrix causing component failure.

Under these conditions, the term F_c is a function of several random variables, which describe the properties of the flaw population, such as flaw spatial distribution, orientation and size. If we indicate with X, Y, Z the random coordinates of a point at which a defect is located in an appropriate Cartesian coordinate system, with Θ, B and Φ the angles necessary to completely determine the orientation of the crack in the three-dimensional space and with A the random defect size (single parameter for one-dimensional defects or several parameters for more complex shapes), in the most general case, the properties of the flaw population are defined by the joint probability density function of the form:

$$P\left(x < X < x + dx;\ y < Y < y + dy;\ \ldots\ a < \mathrm{A} < a + da\right) = p_{X,Y,Z,\Theta,\mathrm{B},\Phi,A}\left(x, y, z, \theta, \beta, \phi, a\right) \qquad (3.2)$$

The function $p_{X,Y,Z,\Theta,\mathrm{B},\Phi,A}\left(x, y, z, \theta, \beta, \phi, a\right)$ expresses the probability density that the generic random variable X_i will lie in the interval $x_i < X_i < x_i + dx_i$, x_i being a real number belonging to the variable's sample space. For ceramic materials these variables will

represent the position, orientation and size of a crack nucleated at a pore or inclusion, while in the case of low carbon steels they will indicate the location, orientation and size of a cracked carbide particle in proximity of a macroscopic stress intensification (produced by either a notch or a macrocrack).

If the component (Figure 3.1) is subjected to a specified load, l, the flaws will eventually cause failure depending on the mechanical properties of the surrounding material and in particular, for an elastic and isotropic body, on the value of the *elastic modulus*, E, the *Poisson ratio*, ν, and the *critical strain-energy release rate*, $\mathcal{G}_{crit}$. These parameters, which are necessary to determine the response of the component to the applied load and to describe the material ability to cope with the presence of a defect, are, in accordance with our assumptions, deterministic and uniquely defined.

If the exact position, orientation and size of a crack were known, the strength S, which indicates the maximum load level that the component can withstand before failing, could be written as a deterministic function of crack parameters and material properties:

$$S = S\left(x, y, z, \theta, \beta, \phi, a, E, \nu, \mathcal{G}_{crit}\right) \tag{3.3}$$

Flaw parameters however are random variables and therefore it is not possible to have a deterministic evaluation of S. Expression (3.3), however, can be used within a probabilistic framework in order to determine the cumulative distribution function of the strength (for a single defect) F_c. To do so, the joint probability density function of the random variables on which the strength depends must be integrated along the whole component's volume, in the domain $S \leq l$, for a given value of load l [Parzen, 1960]:

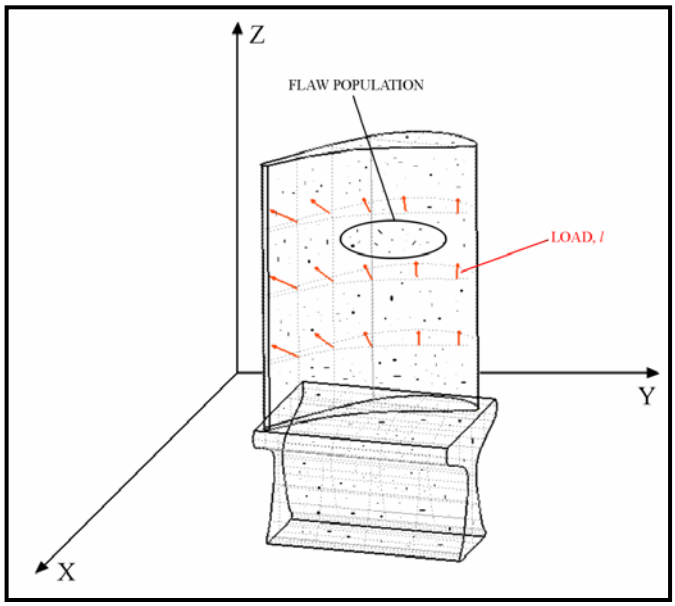

Figure 3.1 Mechanical component containing random flaws

$$F_c = \int\int\ldots\int_{\{(x,y,z,\theta,\beta,\phi,a):S(x,y,z,\theta,\beta,\phi,a)\le l\}} p_{X,Y,Z,\Theta,\mathrm{B},\Phi,A}(x,y,z,\theta,\beta,\phi,a)\,dx\,dy\,dz\,d\theta\,d\beta\,d\phi\,da \quad (3.4)$$

The dependency of the strength on material parameters E, ν and G_{crit} has been omitted in equation (3.4) since these quantities are deterministic and do not change during the integration operation. Equation (3.4) allows one to calculate F_c once the joint probability density function of the flaws population has been determined. Due to the large number of variables involved in the integration of (3.4), a Monte Carlo simulation will be used to perform the calculation. In the specific case of our application, the task is rendered easier by the fact that all random variables are considered to be independent and therefore the joint density function, $p_{X,Y,Z,\Theta,\mathrm{B},\Phi,A}(x,y,z,\theta,\beta,\phi,a)$, can be written simply as a product of the marginal probability densities.

Before discussing the details of the Monte Carlo simulation, an investigation on the influence that a defect, with a given size, position and orientation, has on the component's strength is carried out. The maximum value of load that a component is able to withstand depends on the mechanism by which the stress field generated in the material by the applied load interacts with the defect and by the criterion used to predict fracture.

3.2. Failure Criterion

3.2.1. STRESS CALCULATIONS

The greatest difficulty in establishing the relationship existing between flaw properties (in terms of location, orientation, size) and the maximum admissible load prior to failure derives from the great variety of defect types that may exist in a material at the atomic, micro and macro scale. In order to realistically assess the effect of a flaw population on material mechanical behaviour and strength distribution, flaws have been assumed to be microcracks, whose geometry depends on the particular features of the material under study. This assumption is largely in agreement with the other micro-mechanical models of the fracture process existing in the literature and discussed in the previous chapter.

In order to solve the problem of fracture initiation in the presence of a random population of microcracks, a two-stage approach is proposed here. First, the macroscopic stress field acting on the body is determined assuming that the material

mechanical response is unaffected by the presence of the defects; then, the critical conditions for fracture propagation are determined through the application of a failure criterion that relates crack geometry to critical stress distribution. Considering a component under arbitrarily loading conditions and containing a randomly oriented crack, in the most general configuration, the crack will undergo a mixed-mode fracture mechanism. This means that the crack will simultaneously be subjected to an opening stress normal to the crack plane, an in-plane shear which tends to slide one crack face with respect to the other and an out-of-plane shear. A stress intensity factor is associated with each of the fracture modes (see Chapter-2 for more details).

The stress field $\Sigma(x,y,z)$, acting on a component as the result of a static multiaxial load can be determined under the assumptions of elastic and homogeneous material. The principal stress tensor $[T]$ is calculated at each point of the body through analytical solutions of the theory of elasticity or by a finite element analysis. Once this operation has been completed, the interaction between the stress field and the flaw population is analysed assuming that the macroscopic stress at a certain point of the component is the remote stress acting on the surface of a crack possibly located at that point.

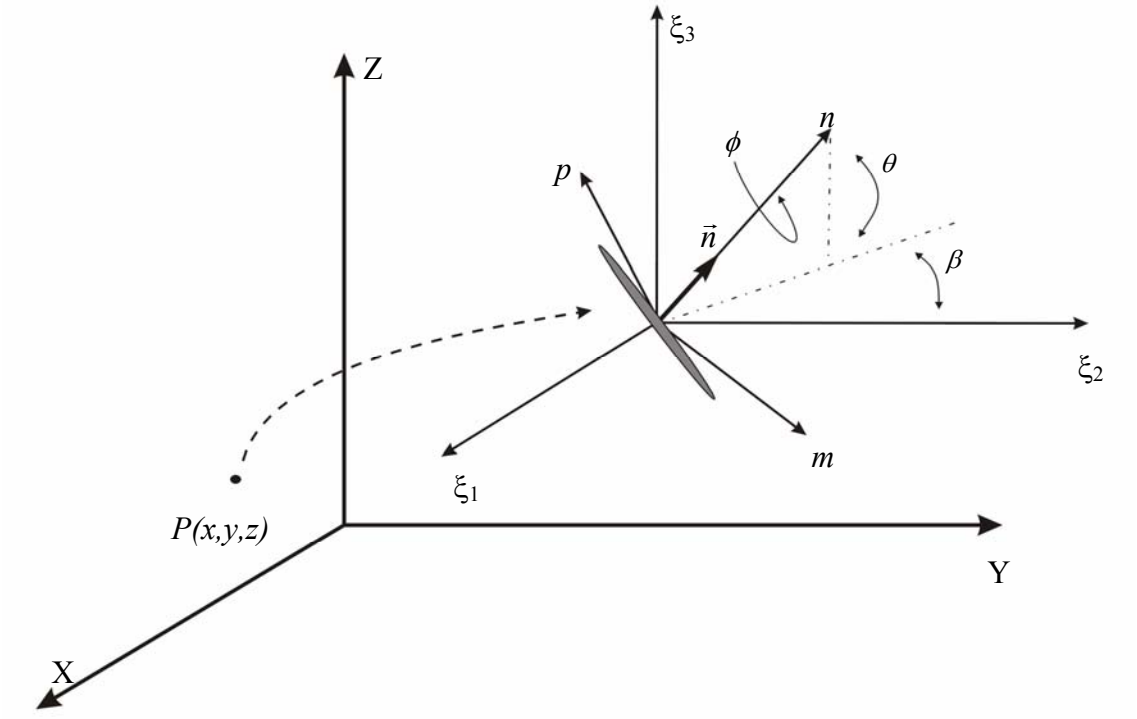

Figure 3.2 Crack orientation relative to principal stress axes

In order to calculate the stress intensity factors relative to a particular configuration and to determine the critical conditions for crack propagation via one of the mixed-

mode fracture criteria that will be discussed in the next section, it is necessary to know the normal and shear components of the stress acting on the crack plane. For this purpose, it is convenient to transform the principal stress tensor [T] at crack location, $P(x, y, z)$, into a stress tensor [$\widetilde{T}$] corresponding to the local coordinate system of the crack. The rotational matrix [R] that transforms the principal coordinate system (ξ_1, ξ_2, ξ_3) into the crack solid system (m, n, p) is:

$$[R] = \begin{bmatrix} \cos\beta\cos\phi - \sin\beta\sin\vartheta\sin\phi & -\sin\beta\cos\vartheta & \cos\beta\sin\phi + \sin\beta\sin\vartheta\cos\phi \\ \sin\beta\cos\phi + \cos\beta\sin\vartheta\sin\phi & \cos\beta\cos\vartheta & \sin\beta\sin\phi - \cos\beta\sin\vartheta\cos\phi \\ -\cos\vartheta\sin\phi & \sin\vartheta & \cos\vartheta\cos\phi \end{bmatrix} \tag{3.5}$$

where β and θ identify the vector $\vec{n}$ normal to the crack plane while ϕ gives the final orientation of the crack on its own plane (Figure 3.2). Three angles (β, θ and ϕ) are necessary to completely determine the orientation of the crack. In some particular cases, such as a penny-shaped crack, due to the polar symmetry, only two angles (β and θ) are sufficient to describe its orientation relative to the principal stress coordinate system. For this configuration the rotational matrix [R] assumes a simpler form in which the terms containing $\sin\phi$ disappear and the factor $\cos\phi$ becomes unity.

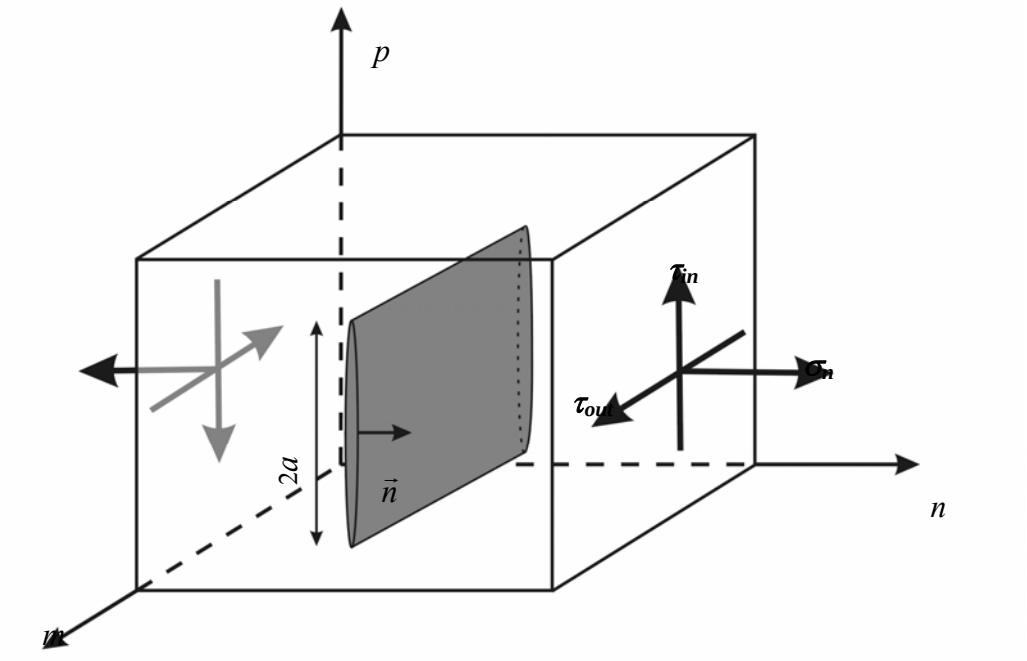

Figure 3.3 Crack local stress conditions

If we now indicate with $[R]^T$ the transpose of the rotational matrix $[R]$, the stress tensor referred to crack axes can then be obtained by matrixes multiplication as:

$$\left[\tilde{T}\right] = \left[R\right]^T \cdot \left[T\right] \cdot \left[R\right] \tag{3.6}$$

Knowing $[\widetilde{T}]$, the values of stress acting on the crack surface, i.e. the out-of-plane shear τ_{out}, the normal stress σ_n and the in-plane shear τ_{in} are simply given by the first, second and third component of the middle column of the tensor $[\widetilde{T}]$ respectively (Figure 3.3).

3.2.2. CRACK GEOMETRY

Besides the three components of the remote applied stress, crack geometry also determines the magnitude of the stress intensity factors and consequently affects fracture conditions. Two relatively simple configurations, for which analytical solutions of the stress intensity factors have been derived under the assumption of linear elastic material, have found extensive application in the development of statistical models of brittle fracture. These are the through-thickness (or Griffith) crack and the penny-shaped crack. As discussed in the previous chapter, the former type of defect has been employed in the analysis of fracture initiation mechanisms in ferritic steels. In these materials, through-thickness cracks nucleate in carbide films, located at grain boundaries, due to plastic deformation. On the other hand, penny-shaped cracks are usually employed to approximate defects that develop in spheroidized steels at grain boundary carbide particles and in ceramic brittle materials, where the presence of a large number of voids and inclusions formed during the manufacturing process is often associated with the nucleation of approximately circular cracks.

Indicating with $2a$ the length (or the diameter in the case of a penny-shaped crack) of a crack remotely subjected to a stress field defined by $[\widetilde{T}]$, the stress intensity factors for a through-thickness crack [Paris, 1965] and a penny-shaped crack [Kassir, 1966] are summarised in Table (3.1).

Griffith sharp cracks and penny-shaped cracks generally represent the two opposite extremes of all possible geometries that actually arise in practical situations. The ratio between the stress intensity factors of the two configurations for all three fracture modes is approximately (if we assume $\nu << 1$) $\pi/2 = 1.571$. It is therefore sensible to define a shape factor Y, whose possible values are in the range [1, 1.571], and employ this

parameter to express the stress intensity factors of any geometry in between the two extreme cases:

$$K_{(I,II,III)} = Y \cdot \frac{2}{\pi} \sigma \cdot \sqrt{\pi \cdot a} \tag{3.7}$$

where σ is the stress component relative to the fracture mode under consideration and a is the crack length. A Y value of 1.571 is associated with a through-thickness crack while values close to unity indicate circular cracks.

THROUGH CRACK	PENNY-SHAPED CRACK
$K_I = \sigma_n \sqrt{\pi a}$	$K_I = \frac{2}{\pi} \cdot \sigma_n \sqrt{\pi a}$
$K_{II} = \tau_{in} \sqrt{\pi a}$	$K_{II} = \frac{4}{\pi(2-\nu)} \cdot \tau_{in} \sqrt{\pi a}$
$K_{III} = \tau_{out} \sqrt{\pi a}$	$K_{III} = \frac{4(1-\nu)}{\pi(2-\nu)} \cdot \tau_{out} \sqrt{\pi a}$

Table 3.1 Stress intensity factors for through-thickness and penny-shaped cracks

More complex crack geometries have been considered by some other authors, especially in studies concerning ceramic materials, where the nucleation of microcracks is often related to the presence of a large number of pores [Evans *et al.*, 1979a and 1979b]. In these materials, the most appropriate flaw model is believed to be that of a crack originated at the surface of a spherical cavity. Three geometries are generally considered in this regard. These are an annular crack around a pore surface, a semi-circular crack and a circular crack located in proximity of a pore (Figure 3.4). Comparative investigations showed that the most critical configuration is represented by the annular crack, also referred as the circumferential crack [Zimmermann 1998b]. For this reason and to maintain a conservative perspective, we will focus our attention on this geometry.

Expressions for the stress intensity factors for this type of defect are relatively complex and often rely on numerical solutions of the local stress field obtained by the superposition of the pore and the crack stress intensifications [Zimmermann 1998a]. The results available show that stress intensity factors can still be expressed in the

general form given by equation (3.7). In the case of a annular crack around the pore equator, the shape factor Y is a function of the crack/pore relative geometry, and in particular of the ratio between pore radius r and peripheral crack extension c, while the crack length a, which has to be plugged into the equation, is in fact given by the sum of these two quantities [Chao and Shetty, 1992].

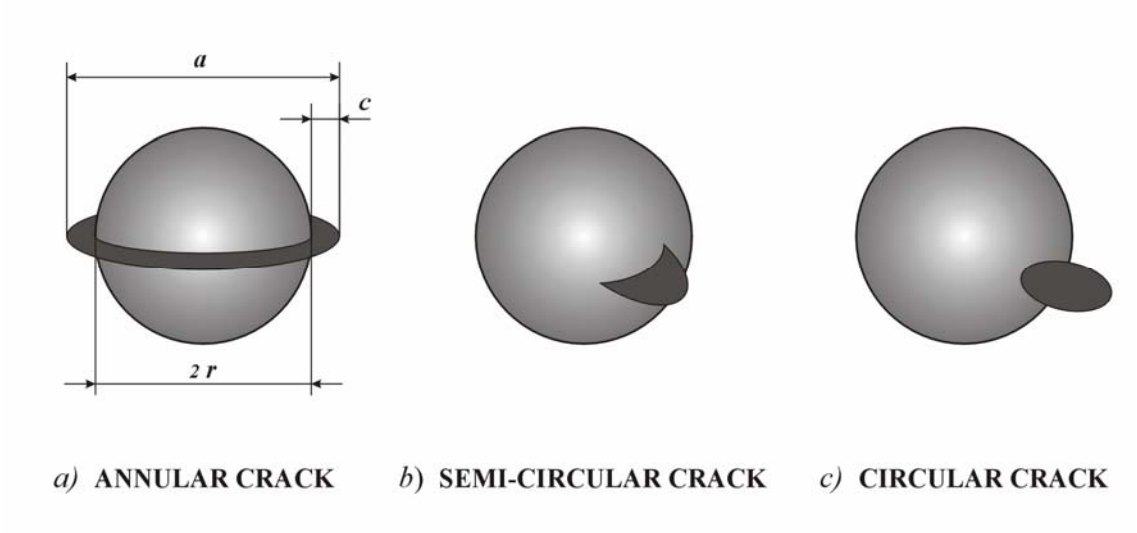

Figure 3.4 Crack geometries in proximity of a spherical cavity

In order to be able to handle all possible configurations, such as peripheral cracks originated on pore surfaces or penny-shape cracks nucleating at inclusions or second phase content, equation (3.7) will be employed in our analysis as a general expression to calculate stress intensity factors. The approach used in this respect will be the following. Crack length distribution will be estimated by pore size in the case of ceramic materials (the peripheral crack extension c will be assumed to be infinitesimal) and by carbide particle diameter for low carbon steels. On the other hand, the shape parameter Y, will be determined by comparing experimental results of material fracture stresses (more precisely the probability distribution of fracture stress) with model predictions. Furthermore, since the cracks considered in this discussion and in our subsequent investigations are normally developed during the component's manufacturing process due to residual stresses, thermal loading and material processing, crack orientation is independent of the in-service applied load and is assumed to have a random distribution.

Once all the parameters describing crack geometry and stress conditions are known, a fracture criterion must be applied in order to determine whether the crack propagates catastrophically under the given remote stress.

3.2.3. MIXED-MODE FRACTURE CRITERIA

Strength-controlling flaws in load-bearing structures, in general, are inclined at random orientations to applied principal stresses. Any design analysis that aims to calculate safe loads for ceramic or metallic structures in the presence of crack-like flaws must explicitly consider the influence of flaw orientation and multiaxial stress on flaw instability. There are several theories that deal with the problem of mixed-mode fracture. The most relevant are discussed in the next three sections.

3.2.3.1. THE COPLANAR ENERGY RELEASE RATE

The coplanar energy release rate criterion is based on the assumption that a planar crack propagates along its initial plane and remains planar. Under these hypotheses, indicating the three stress-intensity factors corresponding to the three loading modes with K_I, K_{II} and K_{III} respectively, the coplanar strain-energy release rate for plane strain configuration is [Paris, 1965]:

$$\mathcal{G}_{copl} = \frac{\left(1-\nu^2\right)K_I^2}{E} + \frac{\left(1-\nu^2\right)K_{II}^2}{E} + \frac{\left(1+\nu\right)K_{III}^2}{E} \tag{3.8}$$

Fracture occurs when the value of $\mathcal{G}_{copl}$ exceeds the critical value for the material, $\mathcal{G}_{crit}$. Despite its simplicity and the fact that it can be considered only a first approximation of the actual mixed-mode fracture behaviour, this relationship has found interesting applications in the statistical analysis of brittle fracture [Evans, 1978].

3.2.3.2. THE MAXIMUM ENERGY RELEASE RATE

In the presence of multiaxial stress it is more likely that the crack will change its direction of propagation, following the path that results in a minimum of the total energy of the system. In these circumstances, the crack would in general form a kink at angle α from the original crack plane (Figure 3.5).

The angle α can be determined under the assumption that the crack extends in the direction that maximizes the strain-energy release rate (driving force to propagation). The angle that satisfies this condition (indicated in the text as α_0) will be the angle of actual propagation. In order to determine the strain-energy release rate of a branched crack, the process of propagation is assumed to be comprised of a first initiation phase, during which the crack deviates of the angle α, and a second phase of actual growth.

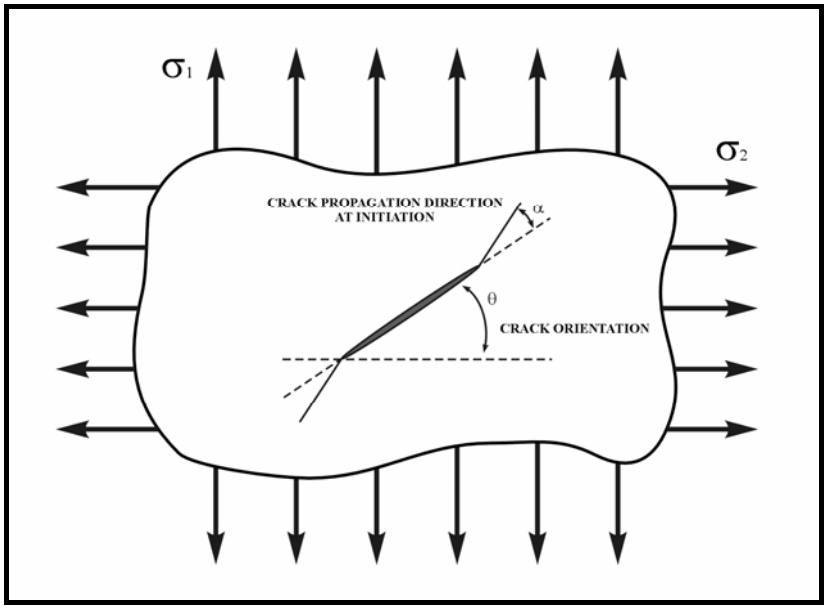

Figure 3.5 Mixed-mode fracture

If initiation takes place at a generic angle α the crack propagation will continue along this plane of the branch-crack. Therefore equation (3.8) can still be used to calculate the value of the strain-energy release of the growing crack, but in its expression the nominal values of stress intensity factors of the plane crack K_I, K_{II}, K_{III}, must be substituted by the stress intensity factors of the branched crack $K_I^{(\alpha)}$, $K_{II}^{(\alpha)}$, $K_{III}^{(\alpha)}$ respectively, calculated at the initiation angle α. The strain-energy release rate is now a function, not only of the crack dimension and remote stress conditions, but also of the angle α:

$$\mathcal{G}^{(\alpha)} = \frac{\left(1-\nu^2\right)K^{(\alpha)2}_{I}}{E} + \frac{\left(1-\nu^2\right)K^{(\alpha)2}_{II}}{E} + \frac{\left(1+\nu\right)K^{(\alpha)2}_{III}}{E} \tag{3.9}$$

To obtain values for this energy release rate, the stress intensity factors for the branched crack are necessary and this, in general, involves the solution of a complicated boundary problem. However, since we are concerned only with the initiation of fracture, we can follow the approach proposed by Nuismer [1975], who found a solution to the problem by assuming that, at initiation, the length of the kink is infinitesimal. As the extension of the kink approaches zero, the stress field at the tip of the branch-crack must be equal to the stress field at the tip of the original crack before the crack propagation. Equating the circumferential and shear components of the local stress at the tip of the plain crack to the normal and shear stress at the tip of the infinitesimal kink

respectively, the stress intensity factors (for the first two modes) of the branched crack at initiation can be written as:

$$K_I^{(\alpha)} = \frac{\cos(\alpha/2)}{2}\left[K_I\left(1+\cos\alpha\right) - 3K_{II}\sin\alpha\right]$$
$$K_{II}^{(\alpha)} = \frac{\cos(\alpha/2)}{2}\left[K_I\sin\alpha + K_{II}\left(3\cos\alpha - 1\right)\right] \tag{3.10}$$

The maximum strain-energy release criterion establishes that the crack propagates along the direction α_0 that maximizes the value of $\mathcal{G}^{(\alpha)}$ determined in the way described above, and only if this value exceeds the critical value of the material, $\mathcal{G}_{crit}$. Considering the first two loading modes as the predominant modes, the direction of propagation at crack initiation is obtained from the solution of equation:

$$\frac{\partial \mathcal{G}^{(\alpha)}}{\partial\alpha} = \frac{\partial}{\partial\alpha}\left[\frac{\left(1-\nu^2\right)K_I^{(\alpha)2}}{E} + \frac{\left(1-\nu^2\right)K_{II}^{(\alpha)2}}{E}\right] = 0 \tag{3.11}$$

Using expressions (3.10) for the stress intensity factors of the branched crack, the angle α_0 that satisfies equation (3.11), resulting in the maximum value of the strain-energy release rate, turns out to be the angle for which $K_{II}(\alpha)$=0 and $K_I(\alpha)$ is maximum. Solution for the case shown in Figure (3.5) are presented in Figure (3.6), where B=σ_2/σ_1.

The negative values of the propagation angle α_0 are due to the fact that the crack will tend to deviate towards the direction normal to the maximum stress σ_1, unless the angular distance between this direction and the crack plane is too big. In any case however, the angle of propagation α_0 is not exactly perpendicular to the maximum stress σ_1 (condition shown by the dotted line in Figure 3.6), causing the branch crack to be subjected to both normal and shear stress.

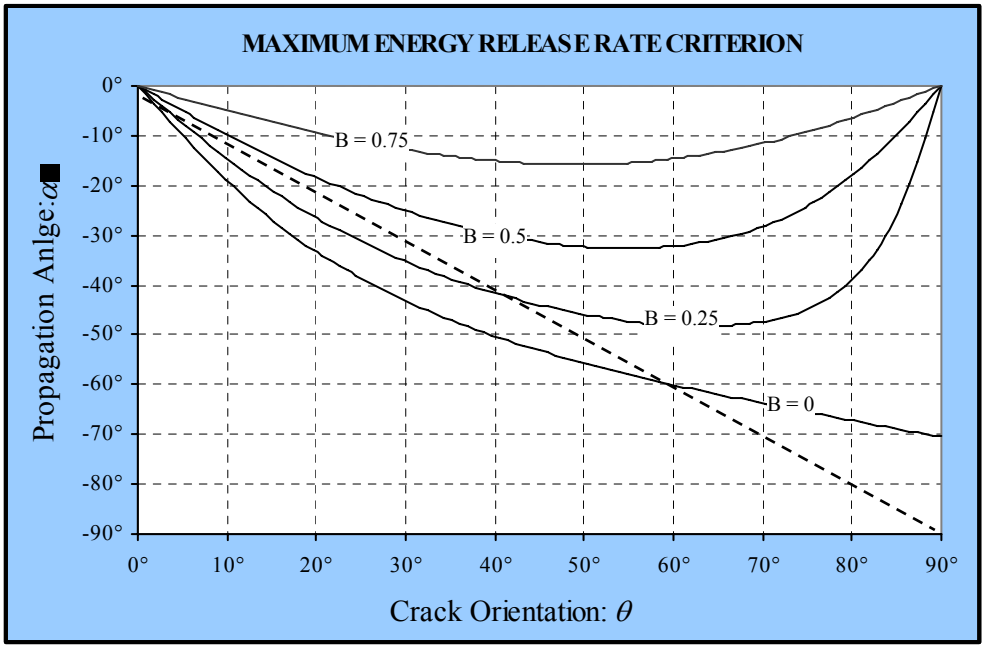

Figure 3.6 Maximum strain energy release rate fracture criterion

3.2.3.3. EMPIRICAL MIXED-MODE FRACTURE CRITERION

Numerous experimental works have been conducted to tackle the problem of mixed-mode fracture. Most of the results obtained in theses studies have shown that, in ceramic materials, the fracture toughness varies with the fracture mode. By comparing critical stresses measured in various testing configurations, the pure mode-II fracture toughness for ceramics, K_{IIc}, has been found to vary between $O.7 \cdot K_{Ic}$ and $2 \cdot K_{Ic}$ [Tikare and Choi, 1993].

Although the maximum strain energy release rate described above is theoretically the most appealing mixed-mode fracture criterion, since it directly derives from the concepts developed by Griffith and Irwin at the origin of fracture mechanics, it fails to predict fracture conditions when the material resistance to crack propagation is not the same for all failure modes. For this reason, several authors have preferred an alternative criterion for the analysis of mixed-mode fracture situations, based on the following empirical relationship [Ikeda and Igaki, 1984]:

$$\left(\frac{K_I}{K_{Ic}}\right)^2 + \left(\frac{K_{II}}{K_{IIc}}\right)^2 + \left(\frac{K_{III}}{K_{IIIc}}\right)^2 = 1 \qquad (3.12)$$

The empirical equation (3.12), unlike the maximum strain energy criterion, does not allow one to predict the direction of crack propagation, but provides greater flexibility in determining the stress conditions promoting critical crack extension and has been proven to be in very good agreement with experimental results. With simple algebraic operations, equation (3.12) can be rewritten as:

$$K_I^{\,2} + \kappa_{I-II} \cdot K_{II}^{\,2} + \kappa_{I-III} \cdot K_{III}^{\,2} \;=\; K_{Ic}^{\,2} \;=\; \frac{G_{crit} \cdot E}{\left(1-\nu^2\right)} \tag{3.13}$$

where $\kappa_{I\text{-}II}$ and $\kappa_{I\text{-}III}$ are the ratios $\left(K_{Ic}/K_{IIc}\right)^2$ and $\left(K_{Ic}/K_{IIIc}\right)^2$ respectively. In this form, the empirical mixed-mode fracture criterion can be readily employed in the Monte Carlo simulation procedure after setting the values of the critical strain energy release rate and the ratios between critical stress intensity factors. Typical values for the parameters $\kappa_{I\text{-}II}$ and $\kappa_{I\text{-}III}$ can be found in the literature. For alumina, experimental investigations suggested a $\sqrt{\kappa_{I\text{-}II}}$ equal to *2.02* [Singh and Shelly, 1989] and a $\sqrt{\kappa_{I\text{-}III}}$ of *2.3* [Suresh and Tschegg, 1987]. These values will generally be assumed in the numerical simulations presented in the following chapters.

For the sake of completeness, it is important to mention that alternative multiaxial fracture criteria, which were developed in the course of the endless research for a unified and consistent model of mixed-mode fracture, exist in the literature. Among these, there are the maximum tangential stress [Erdogan and Sih, 1963] and the minimum strain energy density [Sih, 1974]. These theories were not considered in the present work since they are less fundamental than the maximum strain energy release rate criterion (as recognized by Sih himself) and provide predictions of critical fracture conditions that generally compare less favourably to experimental results than the empirical mixed-mode criterion.

3.3. The Monte Carlo Method

3.3.1. OVERVIEW

The Monte Carlo method is a computer-based statistical sampling approach for solving numerical problems, such as multidimensional integrals, and simulating stochastic processes. It is based on the analogy between probability and volume. According to this concept, the intuitive notion of probability associated with the

occurrence of a random event can be equated to the volume, or measure, of the event relative to that of a universe of possible outcomes. Monte Carlo uses this idea in reverse, calculating the volume of a set by interpreting the volume as probability. This means sampling randomly from a universe of possible outcomes and taking the fraction of random draws that fall in a given set as an estimate of the set's volume. The law of large numbers ensures that this estimate converges to the correct value as the number of draws increases, while the central limit theorem provides further information about the magnitude of the error in the estimate for a finite number of random draws.

Consider the problem of estimating the integral of a function *f* over the unit interval:

$$\alpha = \int_0^1 f(x)dx \tag{3.14}$$

This integral may be represented as an expectation $\mathsf{E}[f(U)]$, with U uniformly distributed between 0 and 1. Suppose there is a mechanism for drawing points U_1, U_2… independently and uniformly from (0, 1). Evaluating the function *f* at *n* of these random points and averaging the results produces the Monte Carlo estimate:

$$\hat{\alpha} = \hat{\mathsf{E}}\left[f(x)\right] = \frac{1}{n}\sum_{i=1}^{n} f(U_i) \tag{3.15}$$

If *f* is indeed integrable over (0, 1) then, by the strong law of large numbers, $\hat{\alpha} \to \alpha$ with probability 1 as $n \to \infty$.

The answer obtained is therefore statistical in nature and subjected to the law of probability. However the accuracy of the calculation can be easily determined. In fact, if *f* is square integrable, the quantity σ_e^2 can be expressed as:

$$\sigma_e^2 = \int_0^1 \left[f(x)-\alpha\right]^2 dx \tag{3.16}$$

According to the central limit theorem the error $(\hat{\alpha}-\alpha)$ in the Monte Carlo estimate is approximately normally distributed with zero mean and standard deviation $\sigma_e/\sqrt{n}$, the quality of this approximation improving with increasing *n*. The parameter σ_e would typically be unknown in a setting in which α is unknown, but it can be estimated using the sample standard deviation:

$$\hat{\sigma}_e = \sqrt{\frac{1}{n-1}\cdot\sum_{i=1}^{n}\left[f(U_i)-\hat{\alpha}\right]^2} \tag{3.17}$$

Thus, from the function values $f(U_1),\ldots f(U_n)$ not only an estimate of the integral α can be obtained, but also a measure of the error in this estimate.

The form of the standard error $\sigma_e/\sqrt{n}$ is a central feature of the Monte Carlo method [Glasserman, 2003]. Cutting this error in half requires increasing the number of points by a factor of four; adding one decimal place of precision requires 100 times as many points. These are tangible expressions of the square-root convergence rate implied by the $\sqrt{n}$ in the denominator of the standard error.

In contrast, the error associated with an alternative numerical integration method such as the simple trapezoidal rule is $O(n^{-2})$, at least for twice continuously differentiable f. Monte Carlo is generally not a competitive method for calculating one-dimensional integrals. The value of Monte Carlo lies in the fact that it is not restricted to integrals over the unit interval. Indeed, the steps outlined above extend to the estimation of integrals over the real space $\mathcal{R}^d$ for all dimensions d. Of course, when we change dimensions we change f and σ_e, but the standard error will still have the form $\sigma_e/\sqrt{n}$ for a Monte Carlo estimate based on n draws. In particular, the $O(n^{-1/2})$ convergence rate holds for all d. In contrast, the error of a trapezoidal rule in d dimensions is $O(n^{-2/d})$ for twice continuously differentiable integrands; this degradation in convergence rate with increasing dimensions is characteristic of all deterministic integration methods. Thus, Monte Carlo methods are attractive in evaluating integrals in high dimensions.

3.3.2. APPLICATION OF THE MONTE CARLO METHOD TO DETERMINE STRENGTH DISTRIBUTIONS

The expectation value of any function $f(x_1, x_2,\ldots x_m)$ of a set of m random variables X_1 $X_2,\ldots, X_m$, characterized by a joint probability density function $p(x_1, x_2, \ldots, x_m)$, is defined by:

$$\mathsf{E}\left[f(X_1,X_2,\ldots,X_m)\right] = \int_{-\infty}^{\infty}\int_{-\infty}^{\infty}\ldots\int_{-\infty}^{\infty} f(x_1,x_2,\ldots,x_m)\cdot p(x_1,x_2,\ldots,x_m)\,dx_1dx_2\ldots dx_m \tag{3.18}$$

This expression allows us to interpret any integral of the form shown on the right-hand side of the equation (3.18) as an expectation value. Therefore, making use of the

law of large numbers as discussed in the previous section, the integral can be estimated by:

$$\hat{\mathrm{E}}\left[f\left(X_1, X_2, ..., X_m\right)\right] = \frac{1}{n}\sum_{i=1}^{n} f(X_1^{(i)}, X_2^{(i)}, ..., X_m^{(i)}) = \frac{1}{n}\sum_{i=1}^{n} f(\overrightarrow{X}_i) \tag{3.19}$$

where $\overrightarrow{X}_i = \left\{X_1^{(i)}, X_2^{(i)}, \ ..., X_m^{(i)}\right\}$ is a random variate ***sampled from the probability density function*** $p(x_1, x_2, \ldots, x_m)$.

This formulation is particularly convenient for performing the calculation in equation (3.4), which gives the individual probability of triggering failure (i.e. the strength cumulative distribution function of a component containing a single flaw), F_c, and involves the integration of a large number of variables. Using the notation employed so far, F_c can be written as:

$$F_c = \int_{-\infty}^{\infty} ... \int_{-\infty}^{\infty} f\left(x, y, z, \theta, \beta, \phi, a\right) \cdot p_{X,Y,Z,\Theta,\mathrm{B},\Phi,A}\left(x, y, z, \theta, \beta, \phi, a\right) dx\ dy\ dz\ d\theta\ d\beta\ d\phi\ da$$

$$\text{where} \quad f\left(x, y, z, \theta, \beta, \phi, a\right) = \begin{cases} 1, & \text{if } S\left(x, y, z, \theta, \beta, \phi, a, E, \nu, \mathcal{G}_{crit}\right) \le l \\ 0, & \text{if } S\left(x, y, z, \theta, \beta, \phi, a, E, \nu, \mathcal{G}_{crit}\right) > l \end{cases} \tag{3.20}$$

$S(x, y, z, \theta, \beta, \phi, a, E, \nu, \mathcal{G}_{crit})$ is the maximum load that a component, containing a flaw with parameters (x, y, z, θ, β, ϕ, a), can withstand and $p_{X,Y,Z,\Theta,\mathrm{B},\Phi,A}\left(x, y, z, \theta, \beta, \phi, a\right)$ is the joint probability density function characterizing the flaw population. The integral in (3.20) can be solved numerically using equation (3.19), simply by sampling a large number of independent variates from $p_{X,Y,Z,\Theta,\mathrm{B},\Phi,A}\left(x, y, z, \theta, \beta, \phi, a\right)$ and evaluating the function $f(x, y, z, \theta, \beta, \phi, a)$ for all sampled values.

The calculation procedure can be summarized in the following steps:

(i) Select a load level l and determine the resulting stress field in the component.

(ii) Generate a random sample $\overrightarrow{X}_i$ from the probability density function $p_{X,Y,Z,\Theta,\mathrm{B},\Phi,A}\left(x, y, z, \theta, \beta, \phi, a\right)$.

(iii) Calculate the value of strength S for the material under consideration, using the sampled values as defect parameters.

(iv) If the strength S is smaller than the load l, then $f\left(\vec{X}_i\right) = 1$ and the sum Σ is increased. If, on the contrary, $S > l$, $f\left(\vec{X}_i\right) = 0$ and Σ remains unchanged. The procedure is reiterated from (ii) for a new trial.

(v) After an adequate number of iterations (i.e. when the error achieved is lower than a target level), F_c is obtained by dividing the sum Σ by the total number of samples considered.

(vi) An estimate of the error associated with the Monte Carlo calculation is given by:

$$\hat{e} = \sqrt{\frac{1}{n}\cdot\left\{\frac{1}{(n-1)}\sum_{i=1}^{n}\left[f\left(\vec{X}_i\right)\right]^2 - \frac{1}{n\cdot(n-1)}\left(\sum_{i=1}^{n}\left[f\left(\vec{X}_i\right)\right]\right)^2\right\}} \tag{3.21}$$

Once F_c has been computed via the procedure outlined above and the values of flaw mean number density λ and component's volume V measured through direct observation, equation (3.1) can be applied to calculate the total probability of failure. By repeating this operation for several values of load, the whole component strength distribution F_s is obtained.

3.3.2.1. INDEPENDENT RANDOM VARIABLES

A general assumption that can be made for practical applications is to consider the variables describing defect location and geometry as independent. Under these conditions each parameter is not affected by the value assumed by the others and the joint probability density function reduces to the product of the individual density functions:

$$p_{X,Y,Z,\Theta,B,\Phi,A}(x,y,z,\theta,\beta,\phi,a) = p_X(x)\cdot p_Y(y)\cdot p_Z(z)\cdot p_\Theta(\theta)\ldots\cdot p_A(a) \tag{3.22}$$

The sampling process from the joint distribution function is now equivalent to the independent sampling of each variable from the respective probability law. In the course of this study only independent random variables have been considered. In particular, uniform distributions were used to simulate defects coordinates (X, Y, Z) and orientation, in order to emphasize the randomness of the flaw population, while log-

normal distributions were adopted to model defect size. Although independent variables have been assumed in this work, the framework outlined here can be directly extended to cases in which correlation among variables is thought to be significant, as long as the appropriate sampling procedure is employed.

Practical applications of this methodology will be discussed in the next chapters. In the remaining part of this chapter, the techniques used to sample random variables from specific probability density functions will be illustrated.

3.3.3. SAMPLING UNIFORMLY DISTRIBUTED RANDOM NUMBERS

At the core of any Monte Carlo simulation is a sequence of uniformly distributed random numbers used to drive the simulation. A random variable, U, is said to have a uniform distribution between (0, 1) when:

$$P\{U \le u\} = u, \qquad u \in (0,\ 1) \tag{3.23}$$

A source of uniform random numbers is necessary in order to sample other probability distributions and carry out Monte Carlo integrations and simulations. A generator of random numbers is a mechanism for producing a sequence of random variables U_1, U_2, … with the property that:

(i) each U_i is uniformly distributed between 0 and 1;
(ii) the U_i are mutually independent.

Some natural phenomena, such as particles emission from radioactive substances or some particular electronic mechanisms, could be used to generate a sequence of true random numbers. This approach, however, is not practical for two main reasons. Most natural sources of random events do not allow the reproduction of identical sequences of random numbers easily. It is often important to be able to rerun a simulation using exactly the same inputs used previously, in particular for debugging purposes. Furthermore, the rate at which the random numbers are supplied must be very high to allow fast simulations and this may not be always possible using natural random phenomena. Thus for most computational purposes, pseudorandom numbers have been introduced. These apparently random numbers are in reality produced by completely deterministic algorithms and therefore they are not truly random. However, under certain conditions, the sequence of values $\{U_1, U_2, \ldots U_k\}$ satisfy properties (i) and (ii), as can be proven by several statistical tests for independence and uniformity.

The algorithms used to generate random numbers may be executed millions of times in the course of a simulation. Therefore, it is very important that they are efficiently implemented and do not involve excessively complex operations. The simplest and most widely used generator is the so-called linear congruential generator. The general linear congruential generator takes the form:

$$\begin{aligned} x_{i+1} &= (ax_i + c) \mod m \\ U_{i+1} &= x_{i+1}/m \end{aligned} \tag{3.24}$$

where the *multiplier a* and the *modulus m* are integer constants that determine the values generated, given an initial value (*seed*) x_0. The algorithm in this form is sometimes called mixed linear congruential generator to distinguish it from a pure linear congruential generator for which $c = 0$. Marsaglia [1972] has demonstrated that little additional generality is achieved by taking $c \neq 0$. Since a generator with a nonzero c is slower than one without, it is often preferred to use pure linear congruential generators.

Beside speed, another significant characteristic of a random number generator is its period, i.e. the length of the sequence of distinct random values produced by the algorithm before repeating itself. In fact, any generator of the form (3.24) will eventually repeat itself after a finite number of cycles and therefore it is advisable to postpone this event by seeking the longest period possible. For a linear congruential generator the maximum period achievable is m-1, in which case the generator is said to have full period. For pure linear congruential generators the full period can be achieved from any $x_0 \neq 0$ simply by selecting a prime number as modulus m and imposing the following conditions on a:

(i) $(a^{m-1}-1)$ is a multiple of m
(ii) (a^j-1) is not a multiple of m for $j = 1, \ldots, m-2$

A couple of values fulfilling these conditions have been proposed by Park and Miller [1988] and are $a = 16807$ and $m = 2^{31}-1 = 2147483647$. The choice of this modulus has been made considering the fact that this number is the largest integer that can be represented in a 32-bit variable (assuming one bit is used for the sign) and it also happens to be a prime, a Marsenne prime. Using an algorithm proposed by Schrage [1979], which allows one to compute the modulo of the product of two 32-bit integers with a 32-bit constant without using any intermediate variable larger than 32 bits, this generator can be implemented on any machine with a 32-bit architecture uniquely via integer arithmetic, which is often faster than floating point arithmetic. This generator,

which will be subsequently referred as the Park & Miller generator, has been largely used in the course of this work to perform most of the simulations.

Other techniques for generating pseudo-random numbers with longer periods are discussed by Glasserman [2003]. They are mainly based on the combination of several linear congruential generators. Of particular interest is the generator proposed by Ecuyer, which is reported to have a period of approximately 2^{319} and no lattice structure. A computer implementation (in C++) of this generator, together with the classic Park & Miller generator in 32-bits integer arithmetic, is given in the appendix (A.1).

3.3.4. GENERAL SAMPLING METHODS

3.3.4.1. THE INVERSE TRANSFORM

Having established a sensible procedure to generate random variates uniformly distributed in the interval (0, 1), it is now possible to discuss techniques that employ sequences of uniform random numbers to sample from other distributions.

For univariate distributions, the most widely used technique for this purpose is the inverse transform method [Kalos, 1986]. According to this methodology, to sample from a cumulative distribution function (CDF) $F_X(x)$, i.e. to generate a random variable X with the property that $P(X \le x) = F(x)$ for all x, it is sufficient to take:

$$X = F_X^{-1}(U), \quad \text{with } U \sim Unif(0,1) \tag{3.25}$$

This follows from the fact that the cumulative distribution function $F_X(x)$ is always a non-decreasing function of x. It can be easily shown that, taken a random variable Ψ with probability law $F_\Psi(\psi)$, if $Y(\Psi)$ is a non-decreasing function of Ψ, then the distribution function of Y is $F_Y(y) = P(Y \le y) = P(\Psi \le \psi) = F_\Psi(\psi)$ for $y = y(\psi)$. In fact the two variables map into each other and $Y(\Psi) \le y(\psi)$ only if $\Psi \le \psi$. This property holds for the two random variables X and U in (3.25), since they are related by the non-decreasing function $F_X(x)$. Consequently they will both have a CDF $F(u) = u$, which in turn means that $P(X \le x) = P(U \le u) = u$ for $u = F(x)$. Substituting the expression for u in the last equation, we obtain that $P(X \le x) = F(x)$ as required.

The inverse transform is an extremely practical method to generate variates from uniform distributions on intervals (a, b) different from the unit interval (0, 1). A sample

can be obtained by simply multiplying the random number U_i by the length (b–a) and summing a. Another straightforward application of this technique is the generation of samples from exponential distributions. Inverting the analytical expression of the exponential CDF, $F(x) = 1 - e^{-\lambda \cdot x}$, it produces the following sampling equation:

$$X = -\frac{1}{\lambda} \ln(U_i) \tag{3.26}$$

Despite the simplicity and generality of the inverse transform method, it is not particularly suitable for distribution functions that are not analytically invertible, such as normal and log-normal. When dealing with this family of probability distributions, it would be necessary to use approximate expressions of the CDF or to discretize the function and store the values in very large look-up tables in order to apply the inverse transform method. In this case, it is often convenient to resort to other solutions. In particular, in the course of this work, the Box-Muller algorithm [Box and Muller, 1958] has been used to sample crack sizes from log-normal distributions. Details on this algorithm can be found in the literature, while a computer implementation has been included in the sampling functions library in appendix (A.3).

3.3.4.2. RANDOM CRACK LOCATIONS

Besides crack size, three other random variables that appear in the integral (3.4) are the Cartesian coordinates (X, Y, Z) identifying crack location. For completely random flaw populations, each coordinate is assumed to be independent from the others and uniformly distributed within the component's volume. For simple geometries, such as a beam with rectangular cross section, each variable can be individually sampled from a uniform distribution in the interval (a_i, b_i), equal to the length of the component in the direction considered (Figure 3.7).

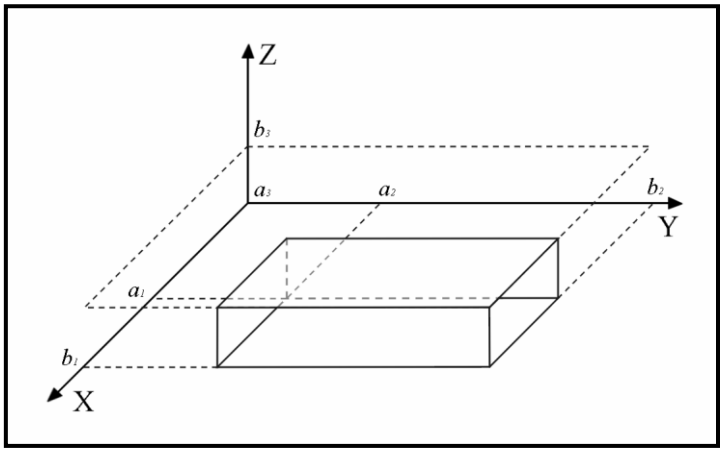

Figure 3.7 Simple component geometry

When dealing with more complex and irregular shapes, for which the interval (a_i, b_i) is not constant throughout the component, the direct sampling approach must be

coupled with rejection techniques. This implies that the whole component's volume is included within a regular parallelepiped, which is used as initial sampling space. Each coordinate is generated individually within the parallelepiped as described above. If the crack location resulting from this sampling process actually falls in the component's volume, the simulation can move on to the next step. If, on the contrary, the point generated is outside this area, the sampling process must be repeated until a valid location is found.

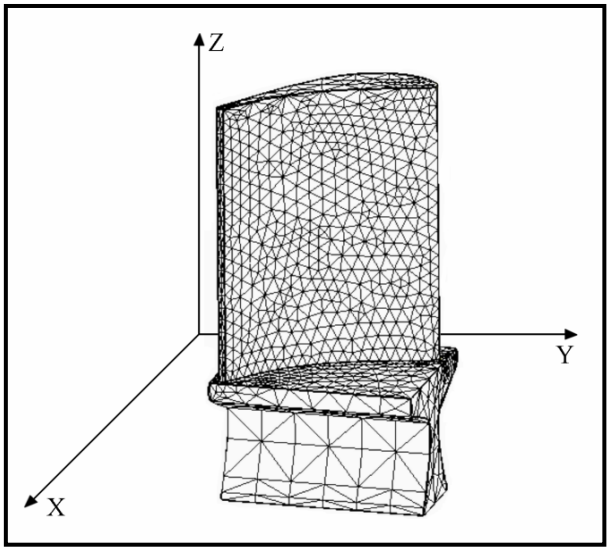

Figure 3.8 FEA representation of component geometry

Although the rejection method guarantees that the resulting distribution of defects in the component is uniform, it may require a large number of iterations before a suitable sample is obtained. In particular, the average number of iterations per valid sample is proportional to the ratio between the parallelepiped's and the component's volume. For particularly irregular shapes, this ratio may be significantly large, resulting in a slow sampling process and consequently in a time consuming simulation. An alternative method, which can be used in conjunction with a finite element analysis of the stress field, is to divide the component in a large number of elements, small enough for the stress state to be consider constant within each element (Figure 3.8). Crack locations can then be sampled randomly by simply selecting one of the elements with a probability proportional to the ratio between its volume the total component's volume. Each location within the element is then equivalent since all point are subjected to the same stress. Another advantage of this approach is that, once a crack location (i.e. an element) has been determined, the stress tensor relative to the element can be directly imported from the finite element solution. In our calculations, the direct sampling of crack coordinates was employed when dealing with simple loading configurations such as a rectangular bar subjected to uniaxial or biaxial tension. For more complex situations, in which a finite element analysis was required to determined the stress state produced in the component by the applied load, the more efficient procedure of element index sampling was preferred.

3.3.4.3. RANDOM CRACK ORIENTATION

Three angles are required to uniquely define the orientation of any object in the three dimensional space. As shown in Figure (3.2), in the case of a crack, two angles, β and θ, are necessary to describe the orientation of the plane on which the crack lies, while the third angle ϕ gives the final orientation of the crack on this plane. In order to simulate a completely random flaw distribution, in which every direction has the same probability to occur, the angles β, θ and ϕ must be sampled from the appropriate distribution function.

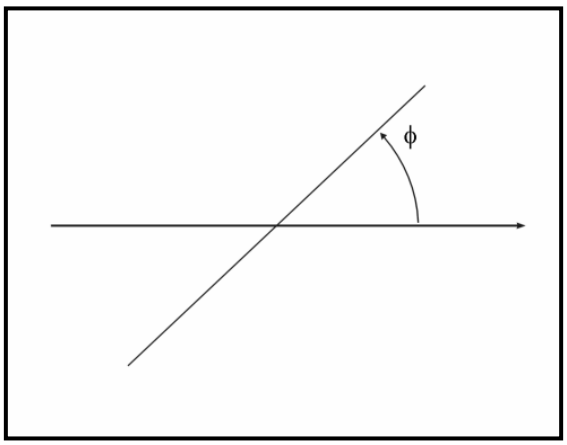

Figure 3.9 Single random angle generation

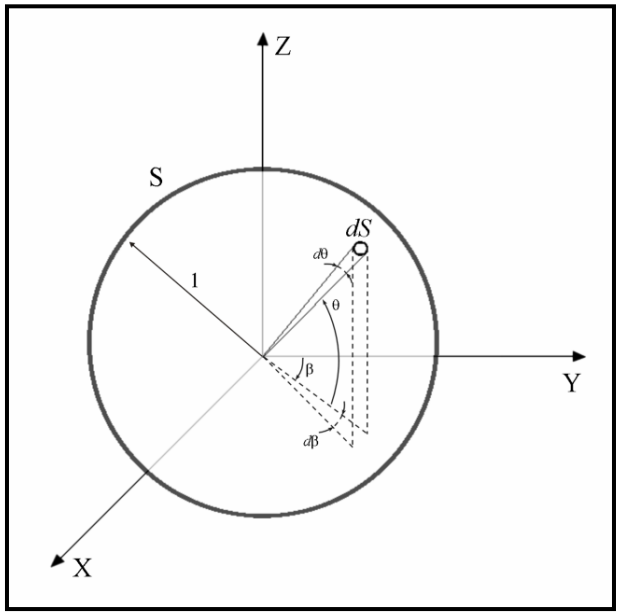

Figure 3.10 Uniform random orientation

Since ϕ simply represents the random angle between a segment and a reference direction on a plane (Figure 3.9) it can be directly sampled from a uniform distribution in $(0, \pi)$. On the other hand, when considering β and θ the situation is more complicated and it can not be assumed *a priori* that they can be sampled from uniform distributions before some careful analytical considerations.

In general, the orientation of a plane in the space is uniquely determined by the direction of the vector normal to it. Assuming that the normal vector has unit length, the problem of a plane randomly oriented is equivalent to a random distribution of points (representing the tip of a vector) on the surface of a sphere with unit radius. The laws of probability state that, for this distribution to be uniform, the probability that a point belongs to the infinitesimal area dS must be proportional to the ratio of the area to the

total surface *S*. Since the area *dS* can be written as $dS = 1 \cdot d\theta \cdot \cos\theta d\beta$ (Figure 3.10), it follows that:

$$P\left(\beta \le \mathrm{B} \le \beta + d\beta;\ \theta \le \Theta \le \theta + d\theta\right) = \frac{1 \cdot d\theta \cdot \cos\theta d\beta}{4\pi} \tag{3.27}$$

where 4π is total area o the sphere. Being B and Θ two independent random variables, it is possible to split their probability density functions as:

$$\begin{cases} p_{\mathrm{B}}(\beta) = \dfrac{d\beta}{2\pi} \\ p_{\Theta}(\theta) = \dfrac{\cos\theta d\theta}{2} \end{cases} \tag{3.28}$$

Both functions have an integral equal to unity over the variable sample spaces ([0, 2π] for B and [$-\pi/2$, $+\pi/2$] for Θ) as required.

It results that B can be sampled from a uniform distribution in (0, 2π), while the sampling function for Θ can be determined through the inverse transform method. Integrating $p_{\Theta}\left(\tilde{\theta}\right)$ from $-\pi/2$ to θ and inverting the cumulative distribution function obtained in this way, we finally get:

$$F(\theta) = \int_{-\frac{\pi}{2}}^{\theta} \frac{\cos\tilde{\theta}}{2} d\tilde{\theta} = \frac{1}{2}\left(1 + \sin\theta\right) \quad \Rightarrow \quad \sin\theta = 2\xi - 1 \tag{3.29}$$

with ξ uniformly distributed in (0, 1). This expression allows the sampling of $\sin\theta$, which can be used directly in equation (3.6).

3.3.4.4. SIMULATING A POISSON PROCESS

It has already been pointed out how the Poisson process is, in general, the most appropriate model to simulate the number of flaws present in a component. Equation (3.1), which has been derived under this assumption, allows us to obtain the total probability of failure by simply estimating the term F_c, without the need to simulate the actual Poisson process that controls the number of flaw occurrences. However, when a map of fracture initiation sites is required, for example in the attempt to determine the

most probable point at which failure occurs, it might be necessary to generate samples from a Poisson probability law.

The easiest way to perform this operation is to exploit the property of Poisson processes according to which the distance between two consecutive events follows an exponential probability distribution [Parzen, 1960]. When dealing with a three-dimensional problem, such as in our case, this property can be applied to volumes rather than distances. In practical terms, this means that to obtain a sample from a Poisson probability law it is sufficient to iteratively generate variates from an exponential distribution using equation (3.26), each variate indicating the volume associated with a flaw, and add them up until the total sum is strictly greater than the component's volume. This condition is equivalent to stating that the last flaw generated falls outside the domain of interest and therefore the number of flaws in the sample is equal to the number of exponential variates generated minus one.

3.3.5. VARIANCE REDUCTION TECHNIQUES

In estimating the function F_c it will often be necessary to determine the probability of occurrence of some rare events, especially in the lower range of the load which refers to the lower tail of the strength distribution. When dealing with a component subjected to a pronounced stress gradient for example, fracture will be triggered only by the small fraction of large defects that fall in the highly stressed region, and the probability of this condition to be satisfied will obviously be small. In the presence of such rare events it may become very time consuming (in terms of computational time) and in general difficult to obtain accurate estimates of the probability of failure through Monte Carlo simulation. For this reason, in many circumstances it might be necessary to apply some sort of variance reduction techniques to improve the convergence (i.e. reduce the estimate error) of the simulation. Among all the techniques available in the literature, one that has shown very good results in our specific application is importance sampling.

3.3.5.1. IMPORTANCE SAMPLING

Importance sampling attempts to reduce the variance of the Monte Carlo estimate by changing the probability law from which samples are generated. The purpose of this operation is to give more weight to "important" outcomes that under the real probability measure would receive very little relevance during the simulation process.

To clarify this idea, consider the problem expressed in (3.18) of estimating

$$\mathsf{E}\left[f\left(X_1, X_2, ..., X_m\right)\right] = \int_{-\infty}^{\infty}\int_{-\infty}^{\infty}...\int_{-\infty}^{\infty} f\left(x_1, x_2, ..., x_m\right)\cdot p\left(x_1, x_2, ..., x_m\right) dx_1 dx_2 ... dx_m$$

where $(X_1, X_2, \ldots, X_m) = \vec{X}$ is a random element in R^m with probability density $p(\vec{x})$ and $f(\vec{x})$ is a function in R^m whose expected value must be calculated. Let $h(\vec{x})$ be any other probability density on R^m satisfying:

$$p\left(x_1, x_2, ..., x_m\right) > 0 \quad \Rightarrow \quad h\left(x_1, x_2, ..., x_m\right) > 0 \tag{3.30}$$

Then we can alternatively represent $\mathsf{E}\left[f\left(X_1, X_2, ..., X_m\right)\right]$ as Glasserman [2003]:

$$\mathsf{E}\left[f\left(\vec{X}\right)\right] = \int_{-\infty}^{\infty}\int_{-\infty}^{\infty}...\int_{-\infty}^{\infty} f\left(\vec{x}\right)\cdot\frac{p\left(\vec{x}\right)}{h\left(\vec{x}\right)}\cdot h\left(\vec{x}\right) dx_1 dx_2 ... dx_m \tag{3.31}$$

This integral can be interpreted as expectation of the function $f\left(\vec{x}\right)\cdot\frac{p\left(\vec{x}\right)}{h\left(\vec{x}\right)}$ with respect to the probability density $h(\vec{x})$, and can be estimated, following the same methodology described above, by:

$$\hat{\mathsf{E}}\left[f\left(\vec{X}\right)\cdot\frac{p\left(\vec{X}\right)}{h\left(\vec{X}\right)}\right] = \frac{1}{n}\sum_{i=1}^{n} f(X_1^{(i)},..,X_m^{(i)})\cdot\frac{p(X_1^{(i)},..,X_m^{(i)})}{h(X_1^{(i)},..,X_m^{(i)})} = \frac{1}{n}\sum_{i=1}^{n} f(\vec{X}_i)\cdot\frac{p(\vec{X}_i)}{h(\vec{X}_i)} \tag{3.32}$$

where $\vec{X}_i = \left\{X_1^{(i)}, X_2^{(i)}, \ ..., X_m^{(i)}\right\}$ is a random variate ***sampled from the probability density function*** $h(x_1, x_2, \ldots, x_m)$.

The value obtained from (3.32) is an unbiased estimator of the expectation (3.18) and the variance of this estimator might be larger or smaller than the variance of the original estimator (3.16) depending on the choice of $h(\vec{x})$. For a proper selection of the density function $h(\vec{x})$, however, a significant reduction in the estimate error can be achieved.

In our specific application, the importance sampling method was applied to the generation of crack size samples from a log-normal probability law. In fact, it was observed that by generating variates from a distribution with a higher mean and the same COV (coefficient of variation defined as the standard-deviation divided by the

mean) as the original density function, better estimate of the quantity F_c (and therefore of the failure probability) were obtained. Concrete examples of the procedure followed will be given in the next chapter.

4 INVESTIGATION ON THE BRITTLE FRACTURE OF CERAMIC MATERIALS

4.1. Scope

This chapter proposes a detailed study on the influence that various parameters related to the features of material microstructure and loading conditions have on the probability of brittle fracture in ceramic components. The main focus of this initial investigation is the fracture behaviour of rather simple component geometries and loading schemes for which analytical solutions of the stress field exist in the literature. A parametric study is then performed by varying characteristic material parameters such as flaw mean number density, mean and variance of the flaw size distribution, and evaluating the changes in the failure probability predicted by the model.

The discussion starts with a comparison between experimental data available in the literature for the same material considered in our analysis and predictions obtained by the model. A best fitting procedure between experimental and theoretical results is performed in order to calibrate the model and estimate the only non-measurable input parameter, i.e. the flaw shape factor Y. Component strength distributions are then analysed for uniaxial loading conditions, such as simple tension and 3-point bending, and the differences in material fracture behaviour between uniform and non-uniform stress states are considered. In particular, the effect that the presence of a stress gradient has on the failure probability is investigated. The sensitivity of component's strength to changes in the parameters characterising the flaws population will be examined as well as the relationships existing between material response and uniaxial stress distribution.

Subsequently, the study proceeds with the analysis of biaxial and triaxial stress states and the construction of a failure probability diagram which defines critical stress conditions in the presence of multiaxial load. This diagram can be used as a design criterion aiming at limiting the maximum probability of failure due to brittle fracture.

The identification of critical conditions for unstable crack propagation in simple geometries is an essential step to comprehend the mechanisms that control the fracture process. The knowledge and understanding gathered in the parametric analysis can then be applied to the study of more complex configurations, such as real engineering components under multi-axial load, in which the factors initially examined independently act simultaneously. A practical application of this methodology will be

presented in the next chapter, where the failure probability of a ceramic turbine blade is investigated.

However, before proceeding with the presentation and discussion of the results collected in this study, one last issue needs to be addressed. We have already explained how the origin of ceramics brittleness lies in the inevitable presence of defects in the material microstructure, but we have not illustrated a practical method to estimate the number and the size of these defects. In the next section a quantitative approach to image analysis is described and applied for this purpose.

4.2. Material Properties Characterisation

It is an explicit objective of this work to directly link the observed component strength distribution with the features of the material microstructure. Most of the input parameters necessary to the simulation procedure proposed in this work and described in Chapter-3 are related to the microstructural characteristics of the material under consideration and, in particular, to flaw content. This section shows how parameters such as defect mean number density, mean and standard deviation of the flaw size, can be determined by direct observation and examination of ceramic microstructures, indicating with this term the structure level of the matter from approximately *0.1* to *100* μm (between the wavelength of visible light and the resolution limit of naked eye). As anticipated in Chapter-3, defects in ceramic materials will be assimilated to annular crack located around spherical pores and the associated flaw size will be considered, in first approximation, equal to the pore diameter.

4.2.1. FLAW SIZE DISTRIBUTION INFERENCE BY DIGITAL IMAGE ANALYSIS

A rather comprehensive treatise on the technical aspects of quantitative image analysis is given by Chinn [2003]. The first step in performing a quantitative analysis on a material specimen is to obtain a high definition image (usually in black-and-white) of the material microstructure through the means of a digital camera connected to a microscope. A black-and-white digital image consists of an array of pixels (picture elements) that have x-y coordinates and a grey level. Generally there are 256 grey levels that are associated with each pixel, from zero (all black) to 255 (all while). Knowing the resolution of the image in *dpi* (dots per inch) and the magnification factor, *mf*, given by

the microscope, the dimension in real units of each pixel can be calculated through the simple equation:

$$pixel\ size = \frac{1}{res \cdot mf} \tag{4.1}$$

Figure (4.1) shows a microstructural sample of tape-cast alumina (Al_2O_3) with a magnification *mf = 120* and a resolution of *300 dpi*. The dark spots on the brighter background represent pore sections in the ceramic matrix. In these conditions the average pixel size in both directions x, y is of *0.706 μm*, corresponding to a pixel area of *0.5* μm^2.

The sample examined was obtained by digitally scanning a hard copy picture of alumina microstructure published in the literature [Chinn 2003]. Due to the limitations on the accuracy achievable through this procedure, which in turn depends on the resolution of the original picture (300 *dpi* as previously stated), the minimum pore size detectable by the image analysis is of about 1.6 *μm*, corresponding to the area covered by four pixels. Smaller defects were not considered in the analysis, since the noise present in the picture would have negatively affected the accuracy of the measurement. It must be said that the limitations existing in the technique employed to obtain a digital sample of alumina microstructure do have an effect on the flaw size distribution resulting from the analysis. However, this is believed not to invalidate the results obtained on the component's failure probability since the noise is mainly associated with the lower bound of the distribution, whilst are the larger defects that are most critical and ultimately control the fracture conditions.

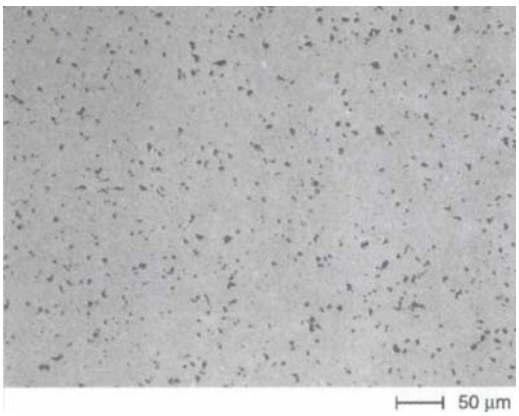

Figure 4.1 Alumina microstructure sample obtained from Chinn [2003]

Figure 4.2 Alumina microstructure image after inverting pixel grey level

Figure 4.3 Alumina microstructure obtained after image processing

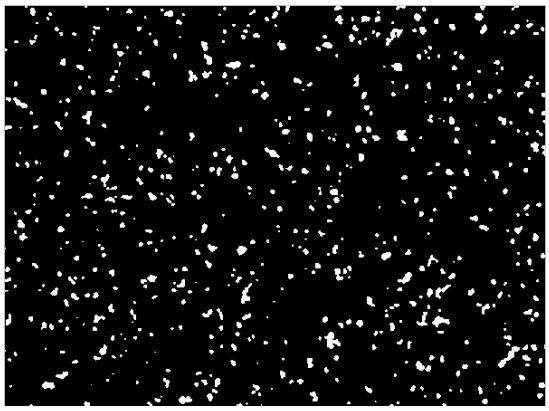

Figure 4.4 Binarized image of alumina microstructure

Using a commercial photo-editing software, the image visualization properties have been improved by inverting pixel grey levels (in Figure 4.2 voids are brighter than the material matrix) and by removing the artefacts present in the photo background (Figure 4.3). The image has then been binarized, i.e. converted to a binary image where only two colour levels (0 for black and 1 for white) are attributed to each pixel (Figure 4.4). This operation is performed by choosing a global threshold value for the original grey levels using the Otsu's method [Otsu, 1979]. All pixels with a grey level above the threshold value become white, while all the remaining are black.

Once these operations have been completed, the material porosity (pores volume fraction) can be estimated simply by counting the number of white pixels in Figure (4.4) and calculating the ratio with the total number of pixels composing the image. For the specimen under consideration, the porosity was measured at *5.54%.* A rather more complex procedure, which involves an algorithm to determine the connectivity properties of white pixels, is required for the estimation of the other microstructural characteristics such as defects number and average size. An image analysis tool provided by the software package *Matlab* was employed for this purpose. The algorithm implemented in the software tool assumes that two pixels are connected, and therefore part of the same object (a defect in this case), if their edges or corners touch. During the image analysis, all white pixels are labelled with an index indicating the object to which they belong. The area of a given pore section can then be estimated by counting the number of pixels labelled with the index relative to the pore under consideration.

Knowing the pore section area, there are several ways to define the average defect size depending on the pore shape. In this work an *equivalent diameter* (defined as the

diameter of a circle having the same area of the pore section) has generally been used. The results obtained in the analysis are shown in Table (4.1).

MATERIAL MICROSTRUCTURE PROPERTIES (2-D SECTION)	
Porosity	5.6171%
Number of Defect Sections	317 / mm^2
Defect Section Area *Mean*	$8.3 \cdot 10^{-11}$ m^2
Defect Section Area *Std-Deviation*	$7.6 \cdot 10^{-11}$ m^2
Defect Section Diameter *Mean*	$9.4 \cdot 10^{-6}$ m
Defect Section Diameter *Std-Deviation*	$4.2 \cdot 10^{-6}$ m

Table 4.1 Summary of two-dimensional defect section properties computed via image analysis of the alumina microstructure sample shown in Figure (4.1)

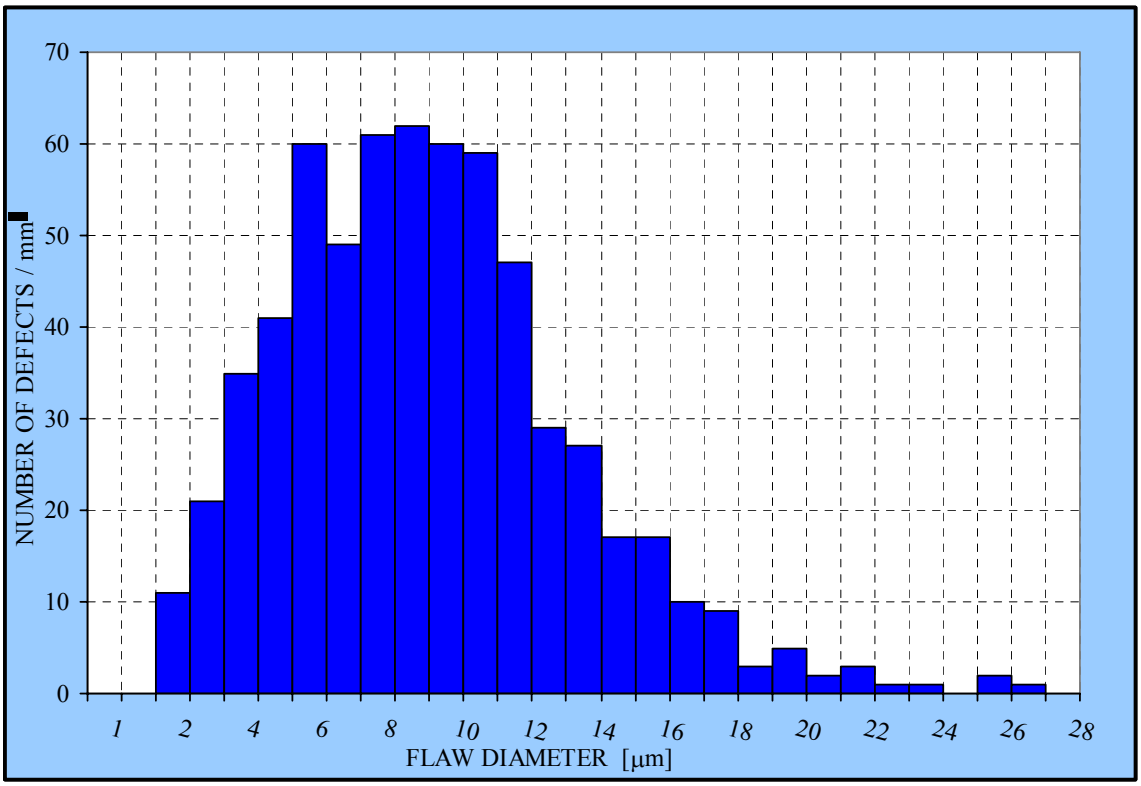

Figure 4.5 Diameters histogram of two-dimensional defect sections computed via image analysis of the alumina microstructure sample shown in Figure (4.1)

The histogram of defect size frequencies was also constructed assuming intervals of section diameter of *0.5 μm* (Figure 4.5). Only pore sections with an equivalent diameter greater than *1.6 μm* (corresponding to 4 pixels) were considered in the analysis due to the limitations imposed by the resolution and magnification of the original image. The values shown in the chart express the number of pores per square millimetre found in a specimen section for each size interval.

4.2.2. STEREOLOGICAL CONSIDERATIONS

The flaw distribution obtained in the previous analysis and shown in Figure (4.5) pertains to objects measured in a two-dimensional (2-D) cross section sampled from a three-dimensional (3-D) material specimen.

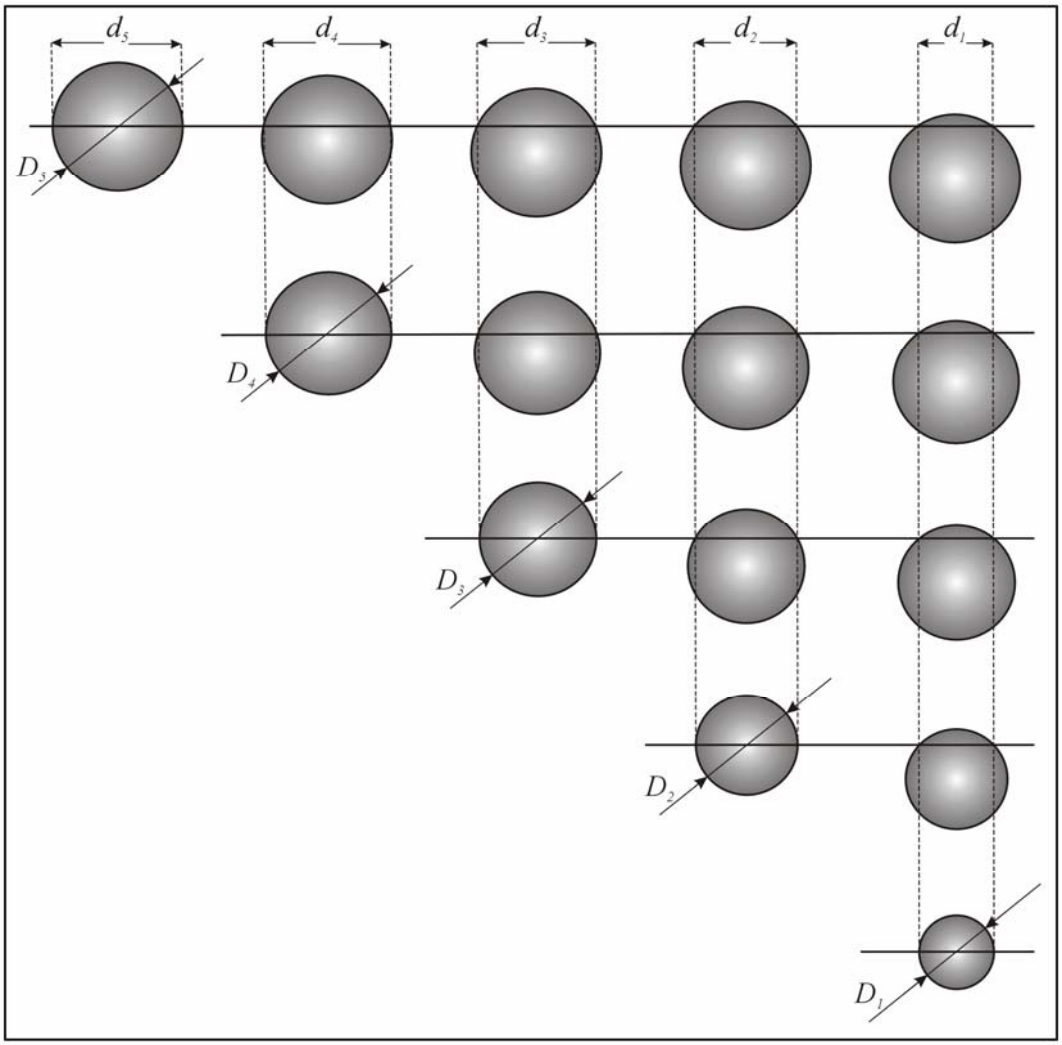

Figure 4.6 Contribution of 3-D particles to 2-D section diameters

The cross section cuts through the 3-D structure randomly and the area (and therefore the equivalent diameters) of the pore sections observed on the 2-D surface depends on the point at which the sampling plane crosses the pores. Since the probability that an object is cut along the section of maximum area is small, the measurement of two-dimensional sections of pores or other types of particles produces size distributions which generally underestimate the actual size of the particles. For this reason, the measurements performed through the image analysis of a specimen cross section cannot be immediately used as input of the Monte Carlo simulation, but must be further manipulated.

Stereology is the discipline that studies the properties of three-dimensional structures and objects based on two-dimensional views of them. Within the field of stereology, several analytical methods have been developed for converting distributions of particle sections measured in 2-D into the corresponding 3-D size distributions. Generally, most of these methods depend on simplifying assumptions on the shape of the objects under investigation. In particular, the Schwarzt-Saltykov method [DeHoff, 1968], which we will be employing in our analysis, assumes that all particles are spherical and their size is uniquely defined by their diameter.

The basic principle at the origin of this (and other) methodology is that the total number of sections with a certain diameter consists of the sum of the separate contributions to this section size from spheres of the same size and all larger sizes (Figure 4.6). Dividing all measured sections into a discrete number of size groups each characterised by an equivalent diameter d_i and indicating with $N_A^{tot}(i)$ the total number of sections per unit area with diameter d_i ($N_A^{tot}(i)$ is the quantity measured through image analysis), it is possible to write:

$$N_A^{tot}(i) = N_A(i,1) + N_A(i,2) + \ldots + N_A(i,j) + \ldots N_A(i,n) \tag{4.2}$$

where $N_A(i, j)$ represents the number of sections per unit area of diameter d_i obtained from spheres with diameter D_j.

The relationship existing between $N_A(i, j)$ and the number of sphere with diameter D_j per unit volume, $N_V(j)$, can be determined by probabilistic considerations. In fact, if $p_{i,j}$ is the probability of a plane intersecting a sphere of diameter D_j so as to yield sections of size d_i, then:

$$N_A(i,j) = p_{i,j} \cdot D_j \cdot N_V(j) \tag{4.3}$$

Note that $p_{i,j}$ is a conditional probability given that the plane actually intersects the sphere, while the probability of intersecting the sphere at any point is equal to D_j (in the unit volume). Combining these last two expressions and considering all size groups for i and j, the problem is reduced to the following system of linear equations:

$$[P]\cdot\left\{\overrightarrow{N_V}\right\}=\left\{\overrightarrow{N_A^{tot}}\right\} \tag{4.4}$$

where $[P]$ is the matrix of coefficients given by $p_{i,j}\cdot D_j$, $\left\{\overrightarrow{N_V}\right\}$ is the vector of unknown number of particles per unit volume for each size interval and $\left\{\overrightarrow{N_A^{tot}}\right\}$ is the vector of measured number of sections. The solution of the system is made simple by the fact that $[P]$ is an upper triangular matrix since for $i > j$, $p_{i,j}$ is equal to zero (a sphere with a diameter D_j cannot generate sections of diameter $d_i > D_j$).

The only issue still to be resolved is the determination of the probabilities $p_{i,j}$. In general, if a sphere of diameter D_j is intersected between distances h_i and $h_{(i-1)}$ from the centre, circular sections with diameters between d_i and $d_{(i-1)}$ will result (Figure 4.7). The probability of intersection of a random plane between h_i and $h_{(i-1)}$ is equal to the thickness h of the circular slice divided by the particle radius. This probability is exactly $p_{i,j}$:

$$p_{i,j}=\frac{h}{D_j/2}=\frac{2\left(h_{i-1}-h_i\right)}{D_j} \tag{4.5}$$

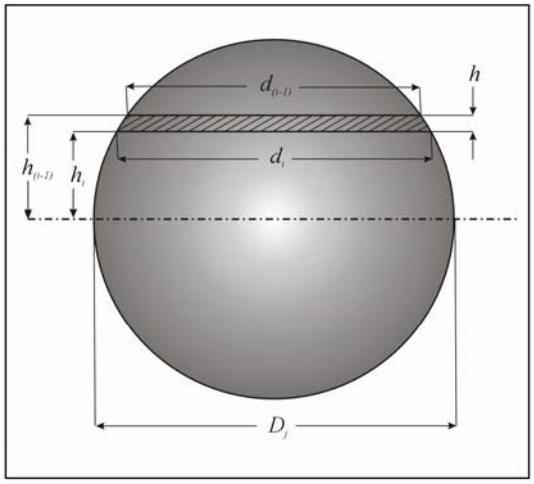

Figure 4.7 Particle/Section diameter relationship

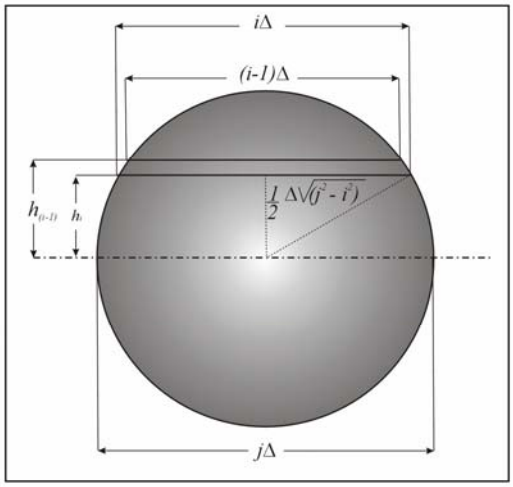

Figure 4.8 Saltykov's representation of particle/section diameter relationship

Saltykov suggested expressing all particle and section diameters in terms of a factor Δ, defined as the ratio between the maximum section diameter observed and the number of size groups considered. D_j would therefore be equal to $j \cdot \Delta$ and d_i to $i \cdot \Delta$. Since the three quantities D_j, d_i and h_i, are related by the geometrical relationship $h_i = \frac{1}{2}\sqrt{D_j^2 - d_i^2}$, all probabilities can be derived from equation (4.5) uniquely as a function of the indices i and j (Figure 4.8):

$$p_{i,j} = \frac{1}{j} \cdot \left[\sqrt{j^2 - (i-1)^2} - \sqrt{\left(j^2 - i^2\right)} \right] \tag{4.6}$$

By substitution of these coefficients into equation (4.4), a well defined linear system is obtained which can be solved by standard methods. The results obtained by applying this methodology to image analysis raw data are summarised in Table (4.2) in terms of pore density, mean and standard deviation of pore diameters and visually illustrated in Figure (4.6) as histogram of 3-D defect diameters.

MATERIAL MICROSTRUCTURE PROPERTIES (3-D ELEMENT)	
Number of Defects	28,533 / mm^3
Defect Diameter *Mean*	$10.6 \cdot 10^{-6}$ m
Defect Diameter *Std-Deviation*	$3.8 \cdot 10^{-6}$ m

Table 4.2 Summary of three-dimensional defect properties computed via image analysis of the alumina microstructure sample shown in Figure (4.1)

The trend shown in Figure (4.9) suggests that the defect size distribution can be mathematically represented by a log-normal probability density function. The best fit for such function is displayed in Figure (4.10), whose parameters are $\mu = -5.29196$ and $\sigma = 0.36014$ (the mean and the standard deviation of log(X) respectively). This probability law will be considered as the size distribution characterising the material flaw population and used as a reference in the subsequent analyses.

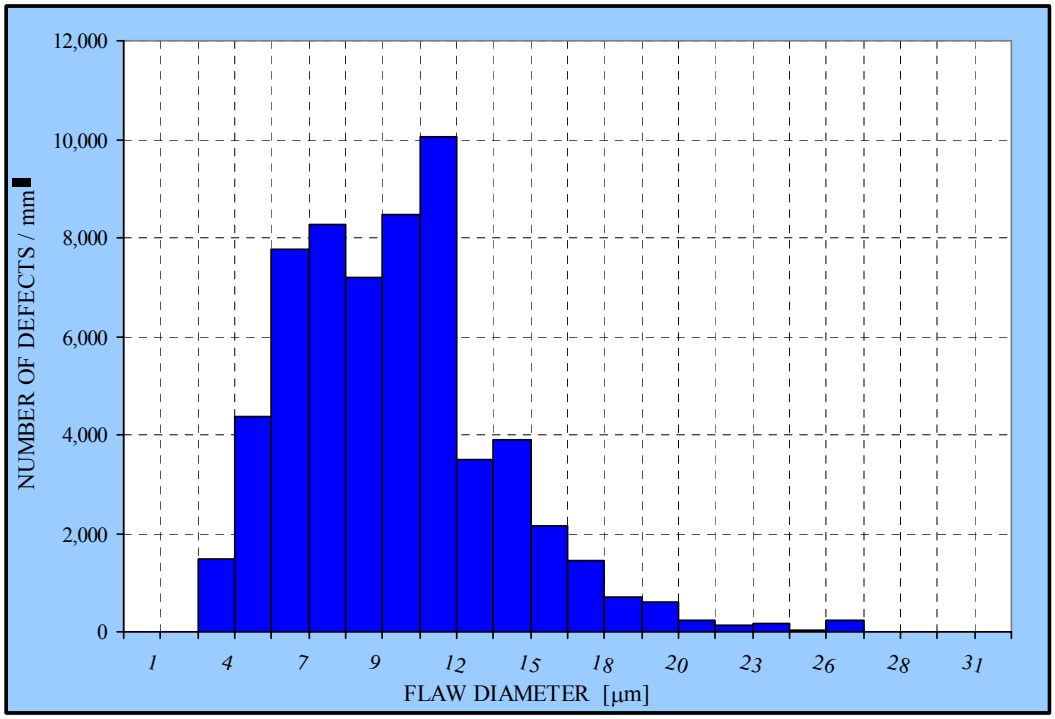

Figure 4.9 Diameters histogram of three-dimensional defects computed via image analysis of the alumina microstructure sample shown in Figure (4.1)

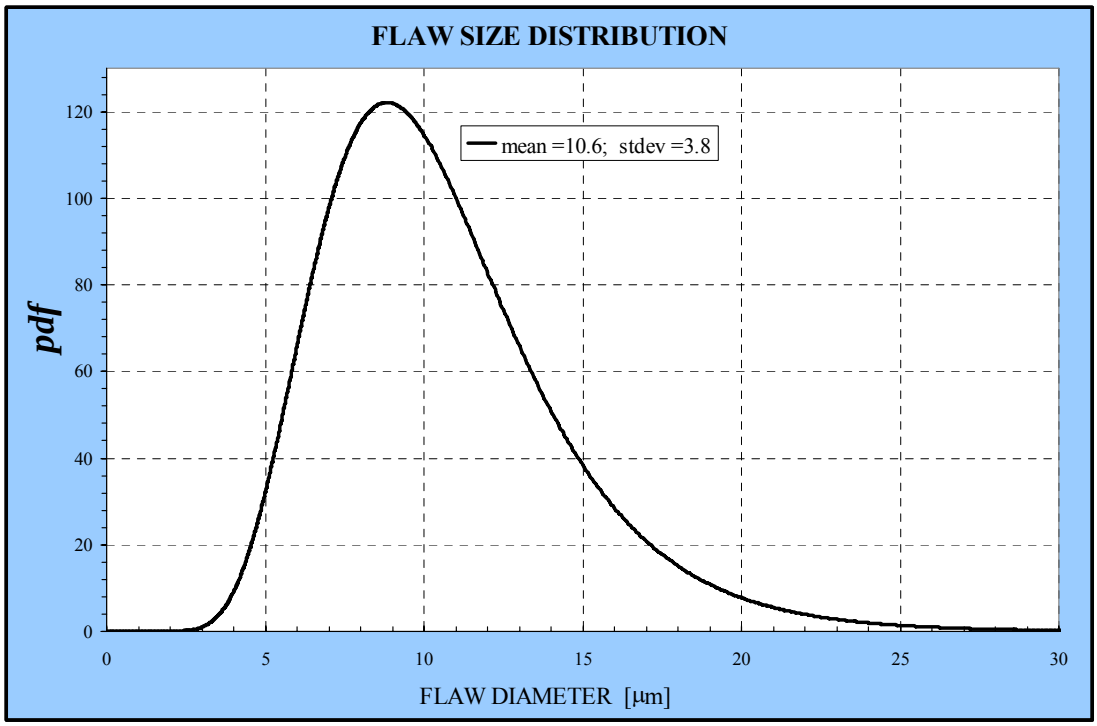

Figure 4.10 Alumina flaw size distribution (of the microstructure sample shown in Figure 4.1) modelled through a log-normal probability density function

4.2.3. OTHER MATERIAL MECHANICAL PROPERTIES

It is probably useful at this stage to discuss in more detail some of the issues concerning the other material properties, such as elastic modulus E and critical energy release rate, $\mathcal{G}_{crit}$, which determine the mechanical response of a structure to loading and fracture initiation. As stated in Chapter-3, these parameters are considered as deterministic throughout our analysis. They are assumed to be unaffected by the presence of defects and measurable by standard material testing techniques. In determining the value of $\mathcal{G}_{crit}$ it is also important to take into consideration the fact that we are dealing with microscopic cracks, whose size is of the same order of magnitude, if not smaller, than the average grain size.

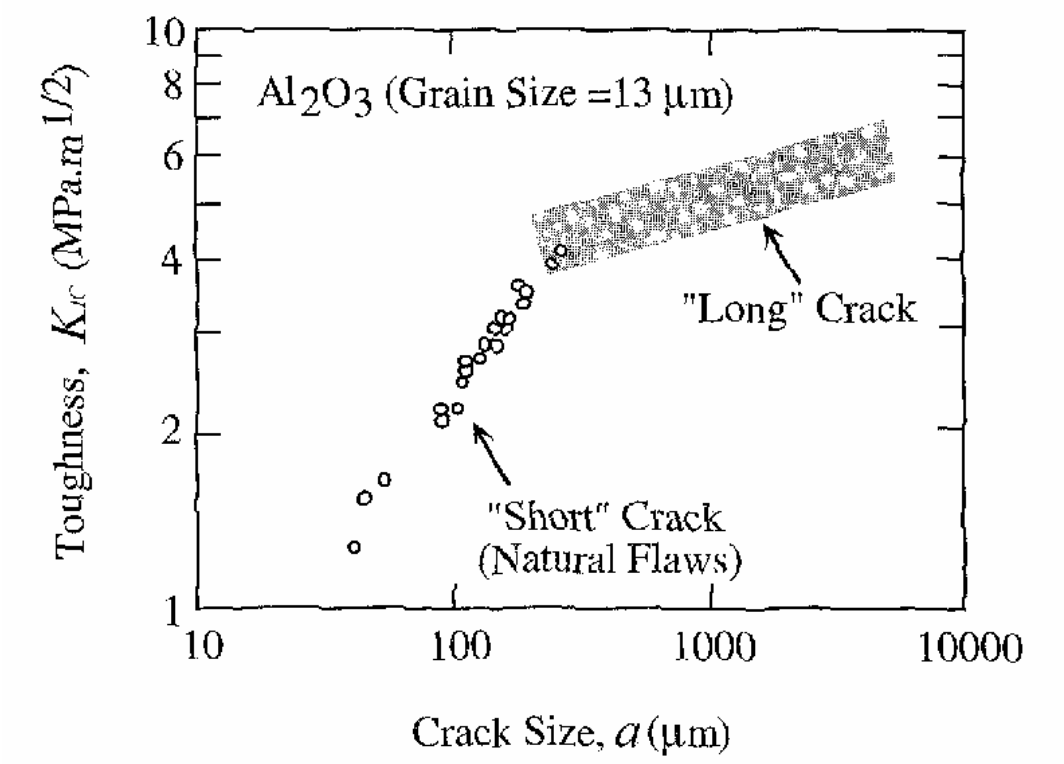

Figure 4.11 Alumina fracture toughness relative to long and short cracks

It is a well established concept in the literature of fracture mechanics the difference in behaviour between “long cracks” and “short cracks” (also called natural flaws) defined in terms of their dimensions relative to the average grain size. In polycrystalline ceramics if flaw sizes are of the same order of magnitude as grain sizes (short crack), the material resistance to crack growth should be that of a single crystal, which is generally lower than that measured by classical fracture mechanics techniques for

macroscopic cracks. In fact, the toughness of the material surrounding a single large grain is significantly higher than the grain itself, due to the presence of grain boundaries and changes in crystal orientation, which make crack propagation energetically more demanding. This distinction in toughness properties is shown in Figure (4.11) [ASTM, 1989]. As a short crack grows, it encompasses more and more grains, leading to fracture toughness values which approach the experimental level of a macroscopic crack. However, the fracture toughness that governs failure is usually assumed to be that of a single grain, since no examples of crack arrest at a grain boundary have been observed once a critical propagation velocity has been reached [Cranmer & Richerson, 1998].

Based upon this evidence, we will assume that the material toughness pertinent to our analysis is that relative to "short cracks" and that, once fracture initiates at a microscopic flaw, it propagates catastrophically leading to global failure of the structure. As suggested by Figure (4.11) an average value of $2.00\ MPa\cdot\sqrt{m}$ was assumed for the K_{IC} of alumina and a corresponding value of $12.32\ J/m^2$ for $\mathcal{G}_{crit}$.

It is generally difficult to obtain accurate values of the critical strain energy release of a material, since environmental conditions, non homogeneity of the material sample examined and differences in testing procedures might affect the result of the measurement. To take into account and cope with potential errors in the assumed value of $\mathcal{G}_{crit}$, a fitting procedure of experimental fracture stress was developed within the statistical framework of our model. As it will be discussed in a subsequent section (4.3.1), this procedure allows to estimate the model parameter Y (flaw shape factor) by comparing simulation results and experimental data. By a best-fit iterative process this parameter is adjusted to match the experimental values of the fracture stress, automatically offsetting differences between the assumed $\mathcal{G}_{crit}$ and the real value characterising the material microstructure.

All relevant material mechanical properties are summarised in Table (4.3).

MATERIAL MECHANICAL PROPERTIES (BULK)	
Modulus of Elasticity, E	304 GPa
Poisson Ratio, ν	0.24
Fracture Toughness, K_{IC}	2 MPa√m
Critical Strain Energy, $\mathcal{G}_{crit}$	12.32 J/m^2

Table 4.3 Material mechanical properties summary

4.3. Model Validation and Calibration

This section deals with various technical aspects of the methodology proposed in this work to evaluate the failure probability of components containing randomly distributed microcracks. Firstly, model calibration is carried out by fitting Monte Carlo results to experimental data of alumina fracture stresses. Some considerations on the convergence of the numerical algorithm employed to perform calculations are then included, while model sensitivity to the main input parameters is investigated at the end of the section. Unless otherwise stated, the fracture criterion employed in the simulation procedure to determine the critical conditions for crack propagation will be the empirical criterion reviewed in Chapter-3 (equation 3.13). The implications and motivations of this choice will be discussed in more details at the end of this chapter, where the strength of cylindrical rods subjected to a combined tension/torsion load will be investigated.

Before discussing these topics, however, a review of the model implementation and the underlying numerical algorithm (already discussed in Chapter-3) is presented.

4.3.1. MODEL IMPLEMENTATION AND MONTE CARLO ALGORITHM

The information gathered on the flaw size distribution and the other material mechanical properties can be directly applied within the probabilistic framework developed in Capter-3 to model the random nature of the fracture process. The two fundamental equations in this framework are:

- equation (3.1), which allows one to calculate the probability of failure of a component once the component's volume, the average number of flaws and the parameter F_c (the individual probability of triggering fracture) have been determined;

- equation (3.4), which gives the value of F_c after an appropriate probability distribution for each of the random variables involved in the failure process and a suitable fracture criteria have been selected.

As outlined earlier, a simple numerical procedure, based on a Monte Carlo simulation, was employed to solve equation (3.4). The model assumes that all random variables in the calculation are independent.

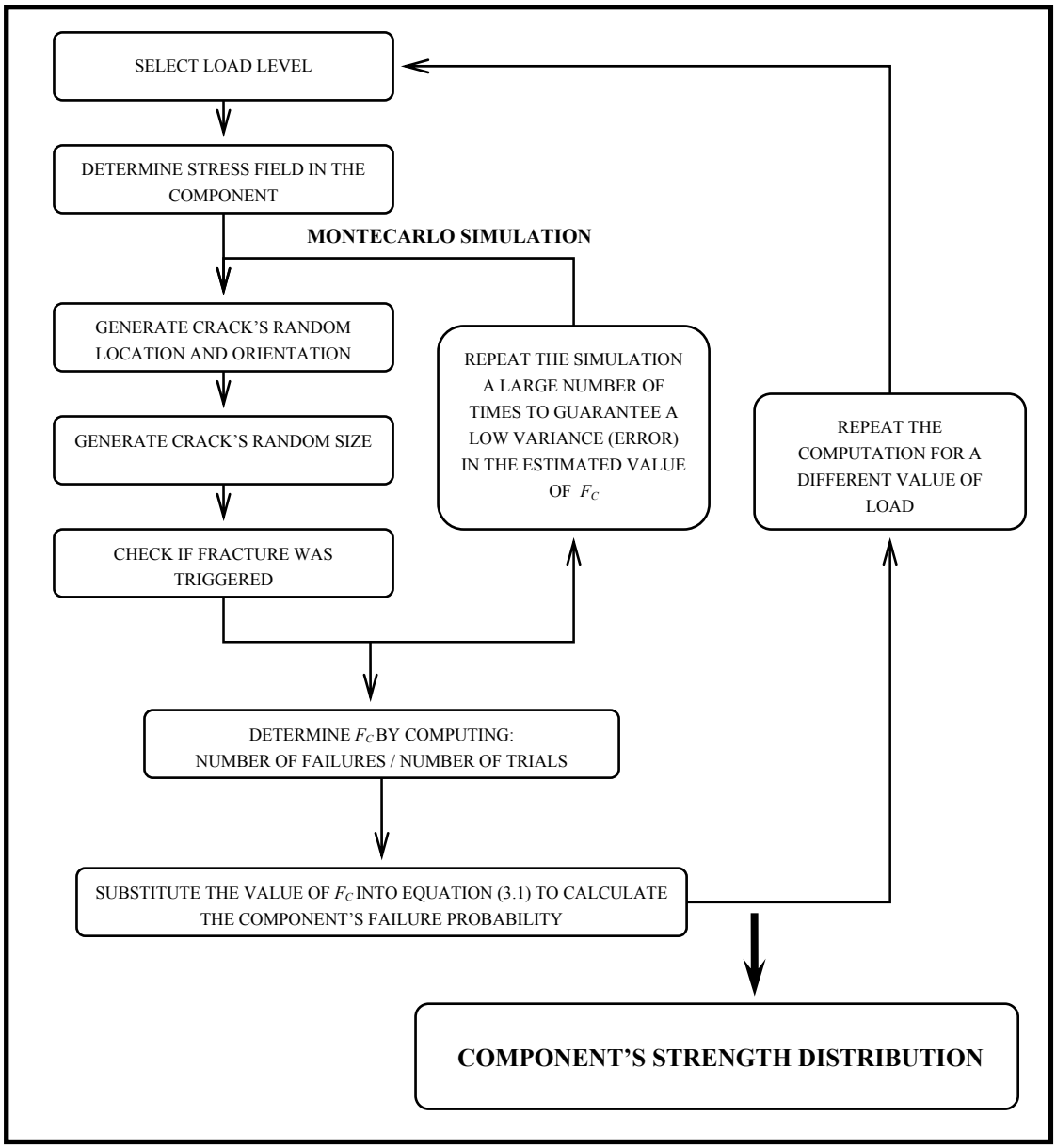

Figure 4.12 Flowchart of the model underlying algorithm

The numerical algorithm implemented to perform the calculations can be summarized in the following steps, schematically represented in Figure (4.12):

(i) select the loading conditions;

(ii) determine the resulting stress field in the component through analytical solutions derived from the theory of elasticity or via Finite Element Analysis;

(iii) generate a random sample for crack coordinates and orientation such that flaws are uniformly distributed and perfectly randomly oriented;

(iv) generate crack random size from the assumed flaw size distribution (Figure 4.10);

(v) check if the set of given conditions of stress state at flaw location, crack orientation and size are severe enough to trigger fracture;

(vi) reiterate the procedure from (iii) and count the number of times failure has occurred; the number of simulations performed should be sufficient to guarantee that the error achieved in the estimated value of F_c is lower than a target level;

(vii) after an adequate number of iterations, F_c is obtained by dividing the number of samples that triggered fracture by the total number of samples considered;

(viii) an estimate of the error associated with the Monte Carlo simulation is calculated through equation (3.21);

(ix) the estimated value of F_c is then substituted into equation (3.1) to determine the component's probability of failure under the specified loading conditions. The calculation must be repeated for several levels of load to generate the whole strength distribution.

4.3.2. MODEL CALIBRATION

Most of the statistical models of brittle fracture developed in the literature thus far rely on the assumption of a single crack geometry in the attempt to predict material fracture behaviour. The configuration usually considered in these studies is either a through-thickness crack or a penny-shaped crack. In the solution proposed here, a single crack geometry is also assumed, which characterises all flaws in the population, but, differently from what was seen before, it is not arbitrarily identified with one of the standardized configurations mentioned above. As discussed in Chapter-2, cracks in ceramic

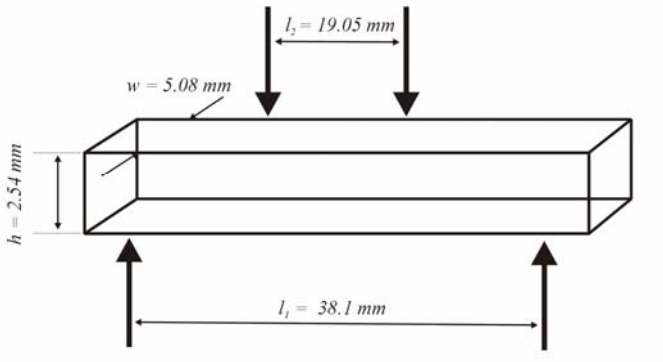

Figure 4.13 4-point bending specimen geometry

materials normally nucleate in proximity of pores or inclusions and the most accurate model representing these conditions is that of an annular crack located around a spherical cavity. In these circumstances, the actual flaw severity depends on the relative size of the pore and the crack and can be defined in terms of a shape factor, *Y*. Although in our model crack length is assumed to be equal, in first approximation, to the associated pore diameter, the actual value of the parameter *Y*, which is employed in the calculation of the stress intensity factors, is estimated directly from experimental data. This value is typically included in the range [1, 1.57], the lower bound being associated with a penny-shaped crack, the least critical configuration, and the upper one with a through-thickness crack.

In order to determine the parameter *Y*, a best-fitting operation between experimental results and model predictions computed for various values of the shape factor was carried out. Fracture stress data for alumina were obtained from an experimental study [Hoshide, 1996] on rectangular specimens tested in 4-point bending. Specimen geometry is displayed in Figure (4.13).

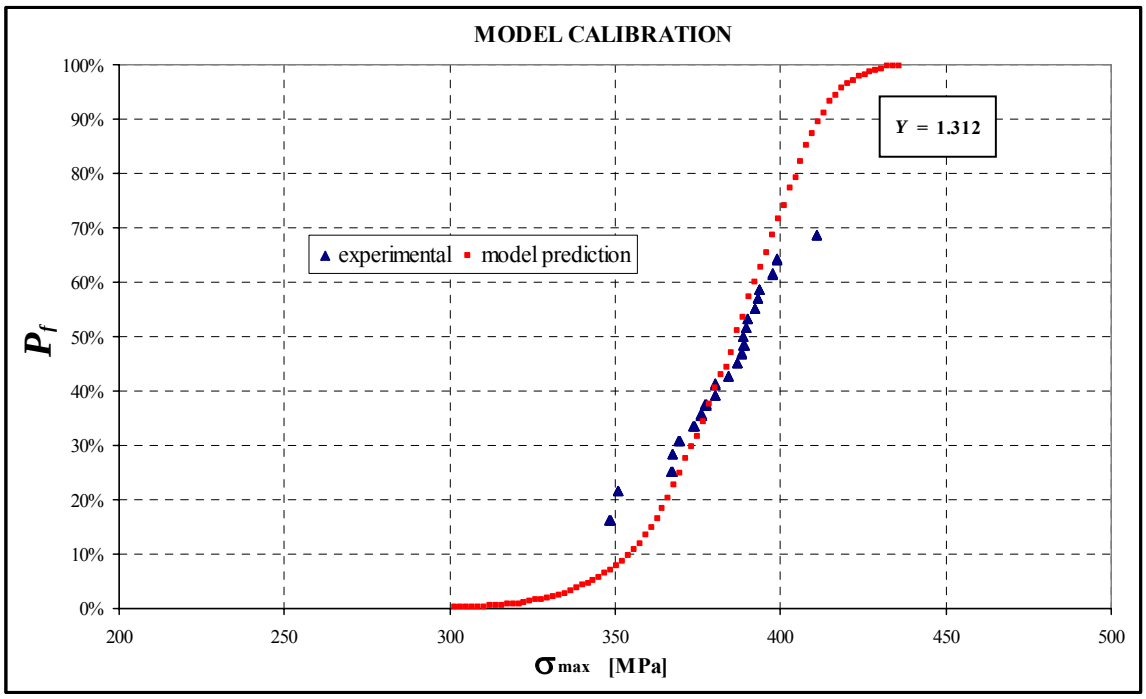

Figure 4.14 Calibration between model predictions and experimental data

The best-fitting curve was found through an iterative procedure which minimised the sum of square distances of experimental data points from the theoretical curve. A simple bracketing method based on the golden section [Press, 1992] was applied on the

estimated value of the shape factor to guarantee convergence. The Monte Carlo predictions obtained for $Y = 1.312$ gave very satisfactory results. These are shown in Figure (4.14) in terms of the maximum stress, σ_{max}, experienced at the edge of the specimen and the corresponding failure probability, P_f. A crack shape factor of *1.312* indicates that the overall behaviour of the flaw population is more critical than that of a population of penny-shaped cracks with the same size distribution.

4.3.3. MONTE CARLO SIMULATION CONVERGENCE

The convergence of a Monte Carlo simulation to the unbiased expectation of a function of several random variables is controlled, according to the law of large numbers, by the number of samples used in the simulation. As discussed in Chapter-3, a convergence rate proportional to the square root of the total number of sample points, which characterises a brute force Monte Carlo simulation, might not be adequate when dealing with the lower tail of the strength distribution, where, for a given load, the probability of failure triggered by a critical flaw is generally very low. For this reason, an importance sampling procedure was suggested to reduce the error in the estimated value of the failure probability. A comparison between the results obtained through a brute force and an importance sampling simulation is shown in Figure (4.15).

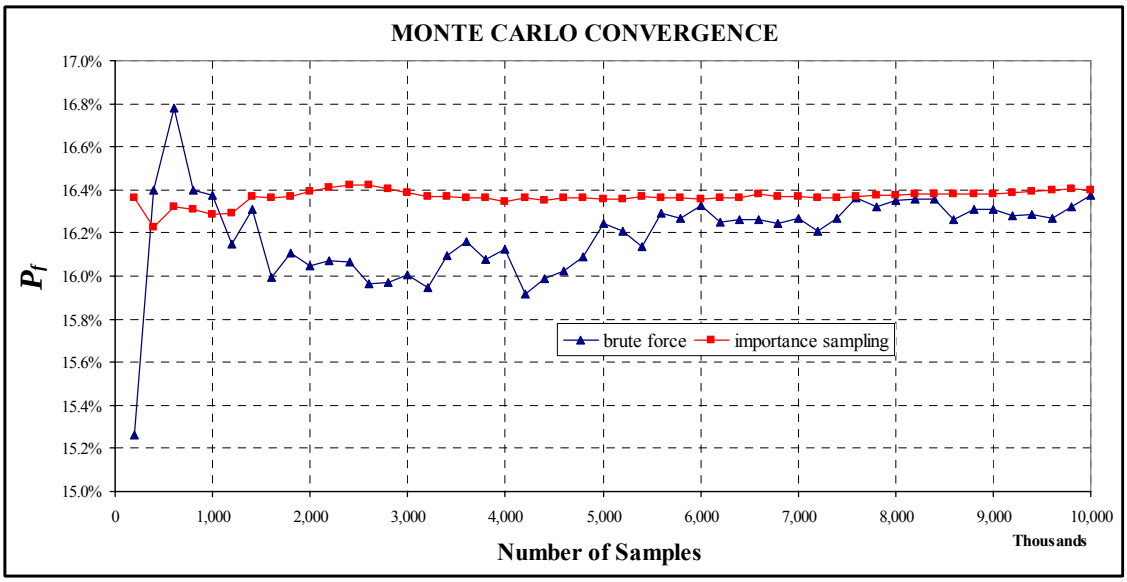

Figure 4.15 Convergence of brute force vs. importance sampling Monte Carlo simulation

The loading configuration considered is a simple case of uniaxial tension at a constant stress of *300 MPa* on the same component illustrated above. Importance sampling was implemented by selecting, for the generation of random crack sizes, a log-normal density function with a higher mean (generally two or three times larger) and the same COV as the original flaw size distribution (Figure 4.10). The value returned at each trial of the simulation was then multiplied by the ratio of the two probability density functions as described in Chapter-3.

As directly observable from Figure (4.16), several millions of samples were required to achieve a reasonably narrow confidence interval in the case of brute force Monte Carlo, while one/two million simulations were sufficient for a satisfactory estimate of the failure probability by using importance sampling techniques. In particular, for one million samples, the relative error in the estimated value of P_f, calculated via equation (3.18), was 5.33% for the former and 0.77% for the latter simulation method.

The correctness of the actual implementation of the algorithm employed to generate random crack coordinates and orientations was also assessed in the following way. Since the spatial distribution of flaws and their orientation are assumed to be completely random, the same results should be obtained when analysing the fracture strength of a rectangular bar subjected to simple tension in the three directions x, y and z respectively.

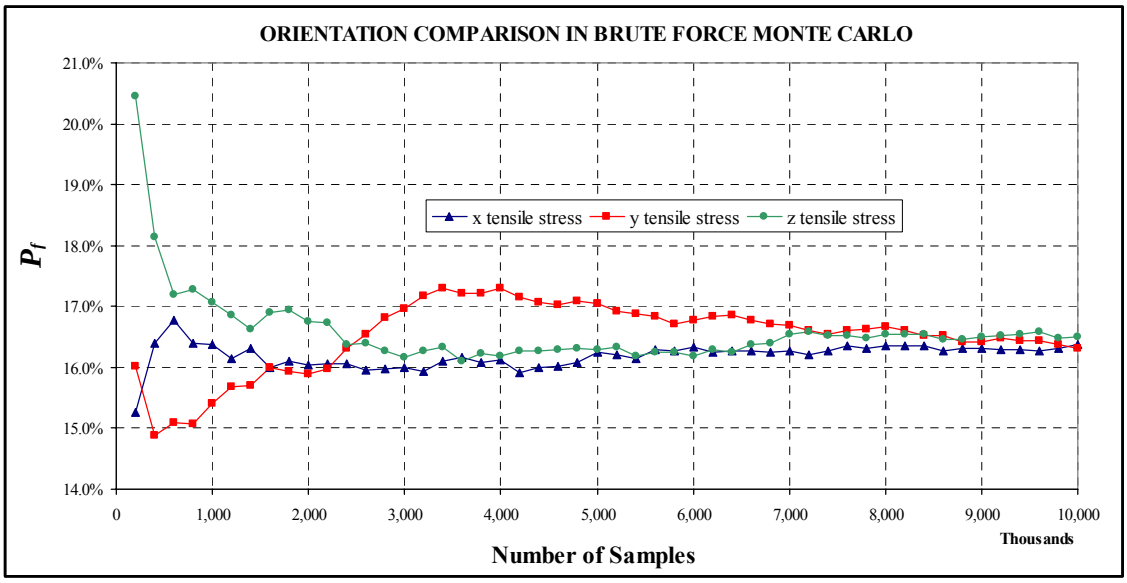

Figure 4.16 Brute force Monte Carlo convergence for different tensile stress orientations

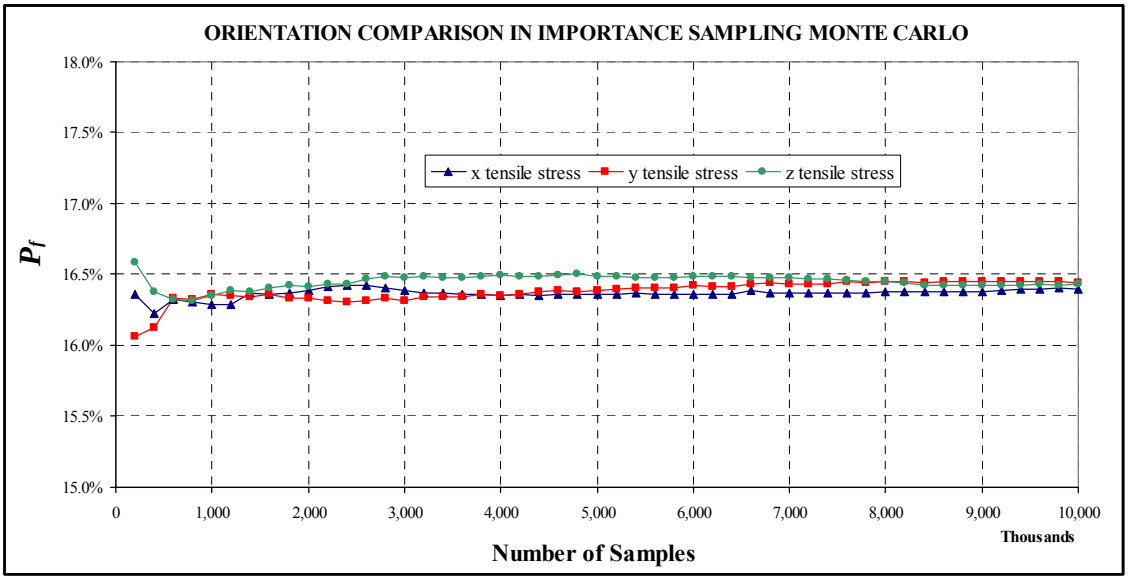

Figure 4.17 Importance sampling Monte Carlo convergence for different tensile stress orientations

Both simulation procedures, brute force and importance sampling, predicted the same value of P_f for all three axial stress configurations (within the limits of the simulation numerical precision). This result was considered as good evidence that the sampling algorithm of random orientations had been implemented correctly. However, between nine and ten million samples were required by the brute force simulation to achieve convergence (Figure 4.16) against a couple of millions needed in the case of importance sampling (Figure 4.17). It is clear from these considerations how the implementation of an importance sampling algorithm might be beneficial in terms of computational time requirements and simulation accuracy. Most of the results that will be presented in the next sections have been obtained by exploiting this simulation technique.

4.3.3.1. MODEL SENSITIVITY TO FLAW MEAN NUMBER DENSITY AND SHAPE FACTOR

An interesting study carried out during the validation phase, was the analysis of model sensitivity to some of the main input parameters. This investigation was conducted by direct comparison of several simulation results obtained for different input data sets. In particular, model response to changes in the value of flaw mean number density, λ, was examined. The sensitivity exhibited by the model was generally low as can be directly observed from Figure (4.18), where the theoretical curve of material strength undergoes relative small shifts for rather significant perturbations of the parameter λ.

This behaviour can be easily explained by considering the first derivative of equation (3.1), employed to determine the failure probability of the component (a rectangular bar subjected to 4-point bending):

$$\frac{dF_S}{d\lambda} = V \cdot F_c \cdot \exp\left(-\lambda V \cdot F_c\right) \tag{4.7}$$

The sensitivity of the strength F_S to changes in λ, expressed by this derivative, is, in first approximation, proportional to the component's volume V and the probability F_c. For the majority of the loading conditions considered, the term F_c is very small and this results in low values of the derivative (4.7).

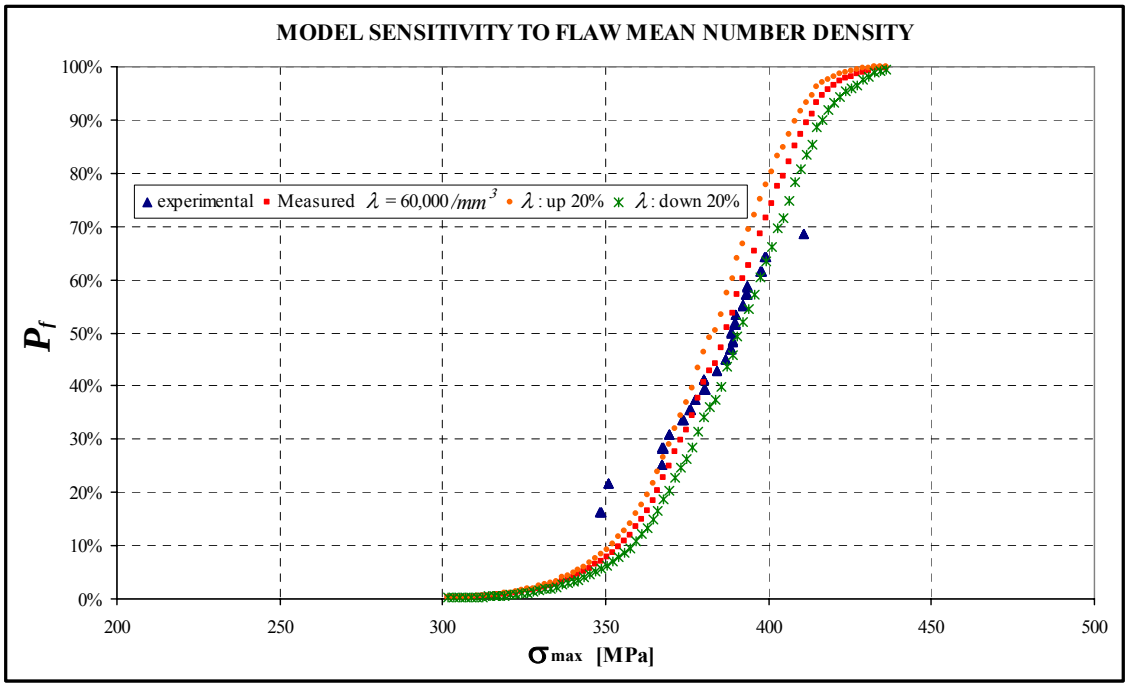

Figure 4.18 Model sensitivity to changes in flaw mean number density

The same type of analysis was also conducted for the flaw shape parameter Y, giving, in certain terms, more interesting insights into the mechanisms involved in the fracture process. The results obtained for variations in Y of ±1% are shown if Figure (4.19). Model sensitivity to changes in flaw shape seems rather high, although it must be taken into consideration that the possible range of variation of Y is relatively small. This investigation, however, suggests how important crack geometry is in determining critical fracture conditions. This detail was often neglected by the previous statistical

models of brittle fracture, which generally assumed an a-priori crack geometry for their derivations. The benefit of using a numerical approach is that crack geometry, as well as the criterion employed to determine critical conditions for crack propagation, can be easily modified according to necessity.

Although the absolute value of the failure probability is rather strongly affected by the flaw shape factor, the trends in fracture behaviour outlined in the next few sections are of general validity and normally independent from the choice of the parameter *Y*. In particular, the analysis conducted on the influence that flaw size parameters and stress state have on the component strength distribution gave exactly the same results for different values of *Y*.

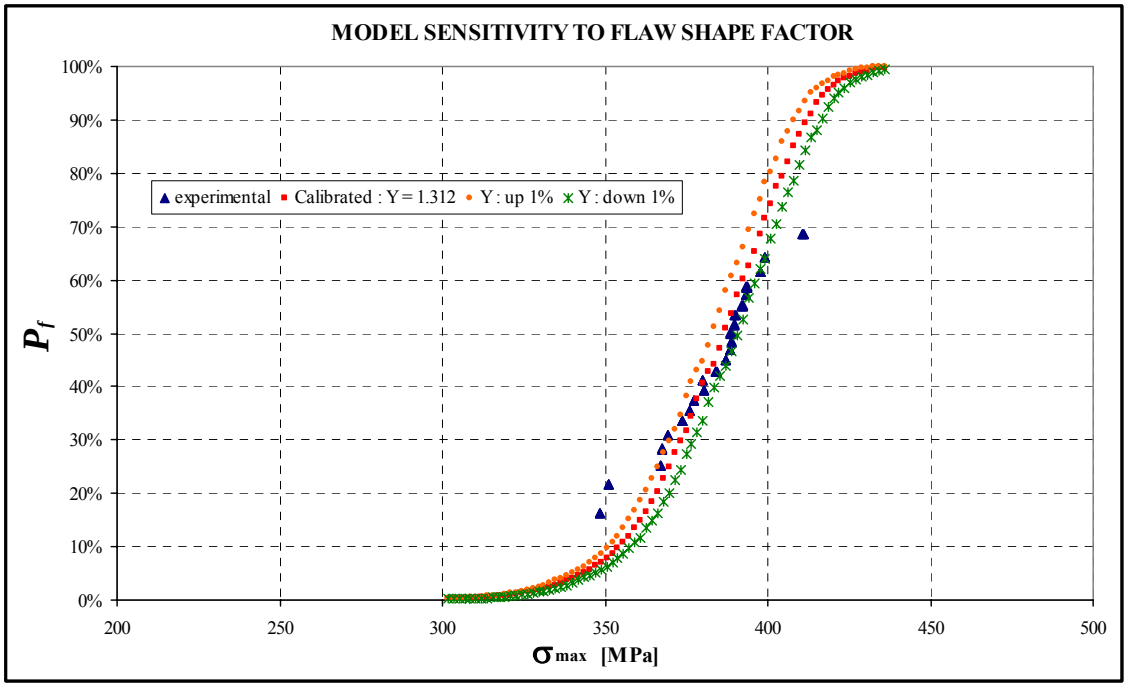

Figure 4.19 Model sensitivity to changes in crack shape factor

4.4. Fracture Strength of Components Subjected to Uniaxial Loading

Once all model input parameters relative to the material microstructure have been estimated, the simulation procedure outlined in Chapter-3 can be employed to determine the probability of failure triggered by brittle facture of any component subjected to arbitrary loading conditions (as long as the stress distribution produced by the applied load is known).

The simplest geometry considered in this preliminary analysis of fracture strength distributions is a rectangular bar subjected to a centred tensile force. In this case, the only principal stress predicted by the Saint-Venant theory of the elastic body is parallel to the direction of the applied load and its value equates the ratio between the force and the bar cross section area. The resulting stress distribution is uniform, with every point subjected to identical stress conditions.

Other loading configurations considered are 3-point and 4-point bending on the same type of component. In both cases the principal stress is, again, normal to the component cross section (ignoring the effect of the shear which, in slim components, is small compared to the normal stress), but it varies along the *z* and *y* axes (Figure 4.20).

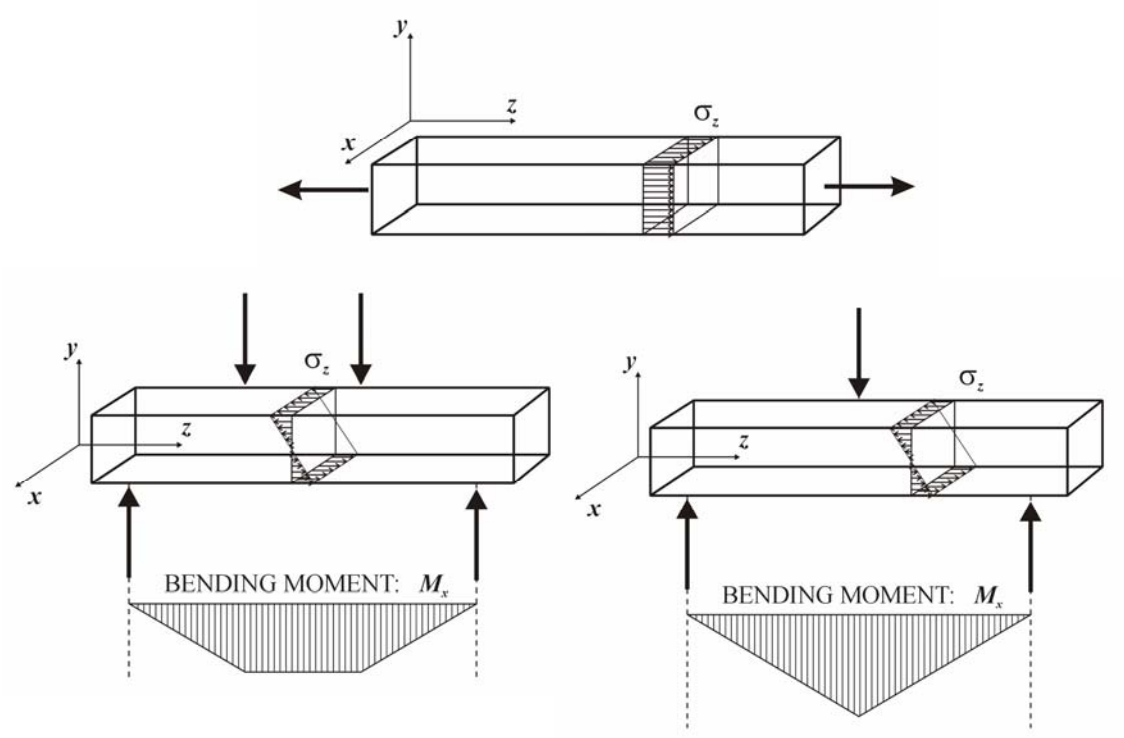

Figure 4.20 Loading configurations

If the load applied in bending is scaled in such a way that the maximum stress, σ_{max}, experienced at the edge of the component is the same in both configurations and equal to the stress acting in simple tension, a classical failure criterion, based on the maximum principal stress, would predict the same failure conditions for all the three loading schemes. However, Figure (4.21) clearly shows that the strength distribution predicted via our probabilistic approach varies significantly from one case to another. The reason for this behaviour lies in what is generally known as the *size effect*. This term here does not simply indicate that the probability of failure increases by increasing component's

volume (actually the three bars have all the same volume), but, most importantly, that it depends on the size of the area on which a given stress operates.

In particular, looking at our examples, this principle translates into a higher P_f for the component subjected to simple tension, since, in this configuration, the maximum tensile stress acts on the entire component's volume. On the other hand, for the case of 4-point bending, the stress distribution is characterised by a gradient in the z direction, due to the variation of the bending moment M_x, and in the y direction as a result of the bending moment itself. The size of the area on which the maximum normal stress acts is therefore much smaller than for the uniform case, while half of the component is effectively under compression, resulting in a lower probability of failure. This condition is even more pronounced for the 3-point bending configuration, where the maximum stress is nominally reached only at a single point and the strength distribution further moves towards higher values of stress. If a design criterion based on a maximum acceptable level of failure probability was employed, three different values of maximum admissible stress would be recommended.

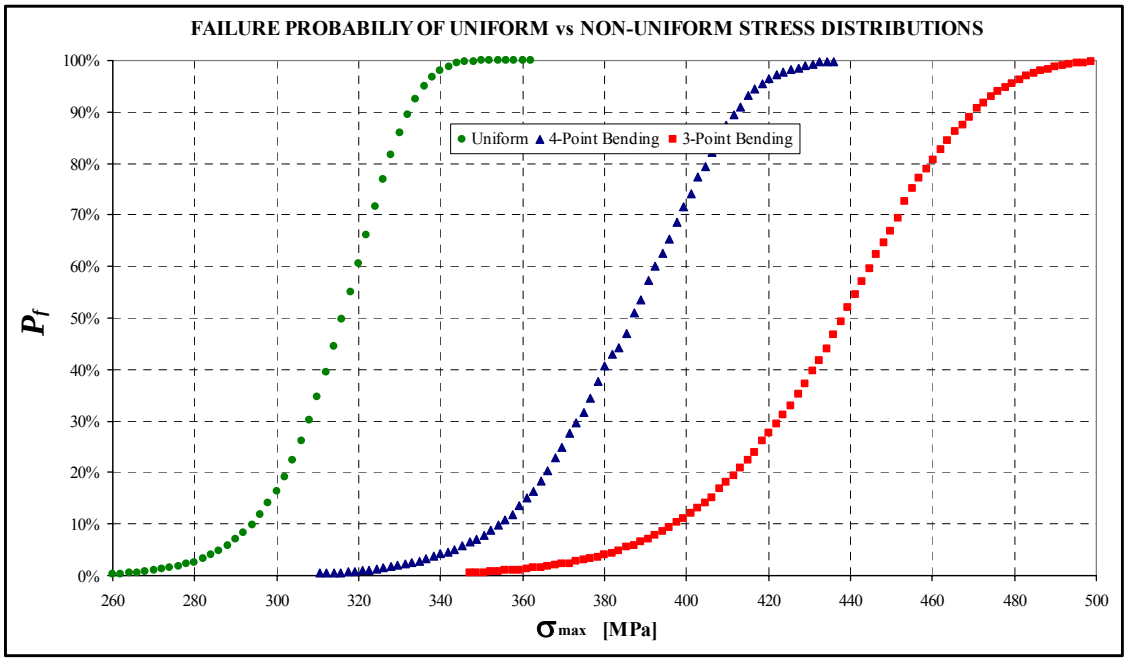

Figure 4.21 Strength comparison between uniform and non-uniform stress states

By moving from a uniform to a more localised stress state, not only the strength distribution shifts towards higher values of maximum stress, but also the slope of the curve varies. What was observed in the simulation results (Figure 4.21) is that a uniform

stress throughout the component produces a steeper trend of the failure probability, while the presence of a stress gradient entails a decrease in the slope of the strength distribution. The slope of a probability distribution is generally associated with the scatter of the correlated random variable, with flatter curves being affected by a higher variability. This means that if the range of variation of fracture strength must be expressed with a given confidence interval (for instance, if the maximum and minimum values of strength are required with a confidence interval of 95%), a wider stress range would result for a component subjected to 3-point bending than one under uniform tensile stress. This behaviour is a direct consequence of the statistical nature of the fracture mechanism. Since, in the presence of a stress gradient, the zone affected by high stress levels is relatively small, there is more uncertainty in the event that a sufficiently large defect will be located in this area.

4.4.1. STRENGTH SENSITIVITY TO FLAW POPULATION PARAMETERS

The properties of the flaw population characterising a particular material are generally described in terms of the average defect size, expressed by the mean of the size distribution, and by the statistical dispersion of all possible values of crack length around the average level, indicated by the coefficient of variation (COV, defined as the ratio between distribution standard deviation and mean). The use of COV is preferred to the standard deviation since it gives information about the variability of defect sizes irrespectively of the distribution mean. On the contrary, the standard deviation is an absolute quantity whose impact on material strength properties is identifiable only if compared with the average flaw size. For example, a standard deviation of 5 μm would have a very different effect on strength variability depending on whether the mean crack size is 10 or 100 μm, while a COV of 0.5 would immediately give a clear indication on the width of the distribution independently on the average crack length.

Since the aim of this study is to identify the main variables that control the fracture mechanisms and the associated failure probabilities in a stressed component containing random flaws, it is interesting to analyse how the material strength distribution is affected by changes in the main flaw population parameters. As it will be demonstrated in the next few paragraphs, the material strength sensitivity to variations in the parameters characterising the crack size distribution (mean and standard deviation) observed for different loading configurations is not uniquely defined, but it also depends on the stress state to which the material is subjected.

Variations in strength distribution were first evaluated for a uniform stress configuration. As it is shown in figure (4.22), an increase in mean flaw size (at constant COV) causes a decrease in component strength. The same behaviour was observed for an increase in COV (at constant mean flaw size). However, for the same percentage change, the increase in mean defect size has generally a smaller impact on the probability of failure than the change in COV. The same type of investigation was conducted for a non-uniform stress state produced by 3-point bending (Figure 4.23). As expected, a strength reduction resulted from an increase in both mean crack length and distribution COV. However the sensitivity to variations in average defect size is higher than the sensitivity to changes in COV, a situation that is the exact opposite of what was observed for uniform stress distributions. The reason for this behaviour is that, in the case of uniform stress, it is the largest flaw that triggers failure since all locations at which a defect may appear are essentially equivalent. On the other hand, in the presence of a stress gradient, only a small number of microcracks located in the highly stressed region are likely to promote failure. In the former configuration it is therefore the width (determined by the COV) of the flaw size distribution that controls the probability of fracture, while in the latter case it is the middle value of the distribution, which defines the size of the most numerous defects, that plays the dominant role.

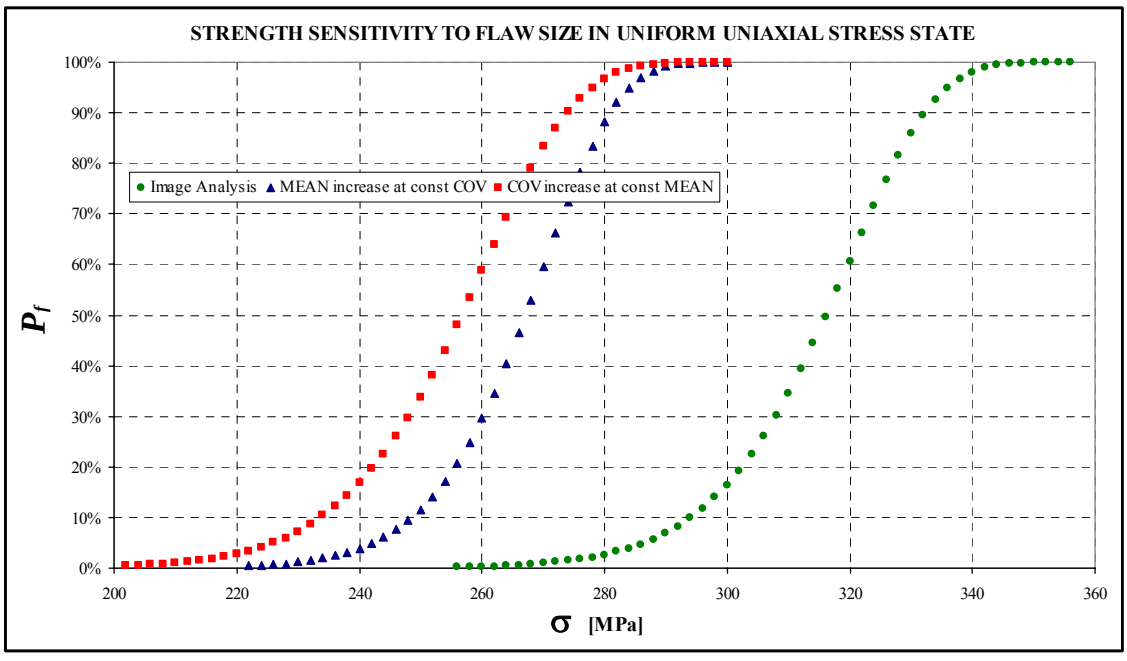

Figure 4.22 Strength sensitivity to flaw size distribution parameters in uniform stress state

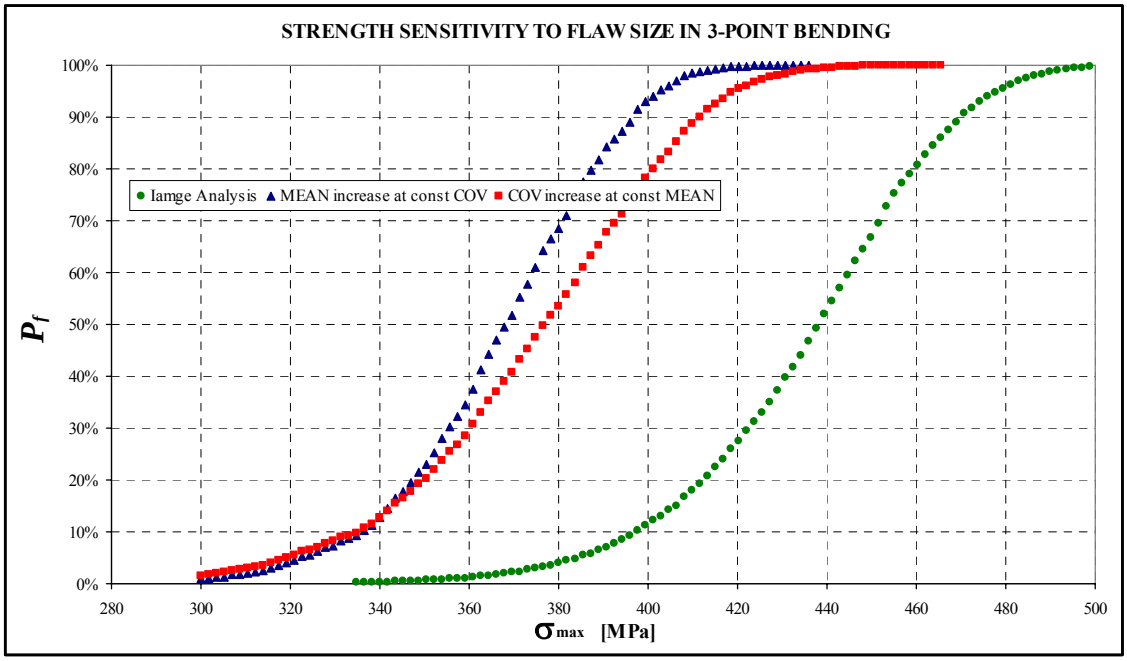

Figure 4.23 Strength sensitivity to flaw size distribution parameters in presence of a stress gradient

This behaviour deduced through a direct simulation procedure is in agreement with experimental observation (see Chapter-2 and Lin *et al.* 1986b) according to which failure is usually initiated at the largest defect under relatively uniform stress conditions, while it is triggered by smaller flaws in the presence of a significant stress gradient. The length of the largest crack is obviously controlled by the COV of the size distribution, while the finer flaws are those in the average size range.

4.5. Fracture Strength of Components Subjected to Multiaxial Load

The loading schemes considered in the previous investigations are characterised by a predominantly uniaxial stress field, which is uniform in the case of simple tension, while varies along the component in 3-point and 4-point bending. Uniaxial stress distributions are very useful in theoretical and experimental studies, allowing direct comparison between theoretical predictions and experimental results, but are less relevant for design purposes since real structural ceramic components are normally subjected to multiaxial stress states in actual operating conditions. This section, therefore, deals with multiaxial load configurations, in which at least two non-zero principal stresses act on the component and contribute to failure.

4.5.1. CYLINDRICAL RODS UNDER COMBINED TENSION/TORSION

Several experimental studies have been conducted in the past on the strength of alumina components, in particular cylindrical rods and thin-walled tubes, subjected to a combined tension/torsion load. The stress state resulting from these loading conditions in a cylindrical specimen is biaxial, with the principal stresses given by:

$$\begin{aligned} \sigma_1 &= \frac{\sigma_z}{2} + \left(\frac{\sigma_z}{4} + \tau_z \right)^2 \\ \sigma_2 &= \frac{\sigma_z}{2} - \left(\frac{\sigma_z}{4} + \tau_z \right)^2 \end{aligned} \tag{4.8}$$

where σ_1 is the maximum principal stress, σ_2 the minimum principal stress, σ_z the axial stress and τ_z the torsional shear stress. The axial stress is $\sigma_z = 4 \cdot L / \pi D_s^2$, where L is the axial load and D_s the specimen diameter ($\sigma_z = 4 \cdot L / \pi [D_s^2 - D_{si}^2]$ in the case of thin-walled tubes with internal diameter D_{si}). The shear stress varies along the specimen radius as $\tau_z = 32 \cdot r_s \cdot M_t / \pi D_s^4$, ($\tau_z = 32 \cdot r_s \cdot M_t / \pi [D_s^4 - D_{si}^4]$ for thin-walled tubes) where M_t is the torsional moment and r_s is the radial distance of the point considered from the central axis. At the rod surface $\tau_z = 16\, M_t / \pi D_s^3$. Thus, the maximum principal stress in combined tension/torsion is found at the rod surface. In pure torsion ($\sigma_z = 0$), the stress state is also biaxial with the two principal stresses being equal in absolute value and opposite in sign throughout the component.

Experimental results obtained from fracture tests of cylindrical specimens showed that the average component strength $\overline{\sigma}_s$, expressed as the average value of maximum principal stress σ_1 measured at the onset of fracture, is larger in pure torsion than in simple tension. In particular, the ratio between the two average values of strength was $\overline{\sigma}_s(torsion) / \overline{\sigma}_s(tension)$ = 1.3 for alumina cylindrical rods [Petrovic and Stout, 1981a] and $\overline{\sigma}_s(torsion) / \overline{\sigma}_s(tension)$ = 1.16 for thin-walled tubes of the same material [Stout and Petrovic, 1984a].

A similar type of analysis was conducted here from a modelling perspective by estimating the component strength distribution via the random sampling procedure previously discussed. The same material mechanical properties and flaw population parameters assumed in the study of uniaxial stress configurations were considered for combined tension/torsion conditions. The average value of strength was calculated

directly from the component strength distribution, F_s, by solving numerically the following integral:

$$\overline{\sigma}_S = \int \frac{dF_s}{d\sigma} \cdot \sigma \cdot d\sigma \tag{4.9}$$

The first objective of this study was to evaluate the theoretical strength of alumina components, subjected to a tensile/torsional load, by applying different fracture criteria in the Monte Carlo algorithm used to perform the calculations, and compare it with the experimental data available in the literature. The fracture criterion that gave the best results (closest to the experimental measurements) was then identified and selected for all other parametric studies. The outcome of such analysis confirmed that the empirical fracture criterion (equation 3.13 with parameters $\sqrt{\kappa_{I\text{-}II}}$ and $\sqrt{\kappa_{I\text{-}III}}$ equal to *2.02* and *2.3* respectively) was the most accurate in matching the strength ratios measured by Petrovic and Stout [1981a, 1984a]. In particular, the simulations conducted on cylindrical rods showed that the application of one of the other fracture criteria reviewed in Chapter-3 (the coplanar and the maximum strain energy release rate) would result in an opposite behaviour to that observed experimentally. The reason for this discrepancy is that fracture criteria based on the coplanar, or the maximum, energy release rate, overestimate flaw sensitivity to the shear stress, resulting in an average torsional strength which is lower than the tensile strength.

Besides uniaxial tension and pure torsion, other three loading configurations were considered. These are characterised by a combined tension/torsion load, defined in terms of the ratio between the maximum shear stress, τ_z, and the axial stress, σ_z, measured at the rod surface. In particular, stress ratios, τ_z/σ_z, of *0.5*, *1.0* and *4.0* were assumed in the course of this investigation. The strength distributions observed for each of these loading schemes are showed in figure (4.24). In the charts, the *x* axis represents the maximum principal stress, σ_1, (calculated via equation 4.9) and the *y* axis is the estimated probability of failure, P_f. As already mentioned, the component is a cylindrical rod with a diameter of *6.35 mm* and an axial length of *76.20 mm*. Note that in the case of cylindrical rods, the component's volume is larger than the volume of the rectangular bar considered in the previous analysis. This results in a strength distribution for uniaxial tensile load which differs from that previously measured. However, the values of failure probability relative to cylindrical rods are consistent with those estimated for rectangular bars and can be directly compared via equation (3.1). In fact, the associated values of individual failure probability, F_c, are the same for both

components under uniaxial tension. The differences in the probability of failure are attributable only to the difference in the expected number of defects.

The average values of strength and the ratios between average tensile strength and combined tension/torsion strength calculated from the strength distributions above are given in table (4.4) for each of the loading schemes considered. The predicted ratio $\overline{\sigma}_s\,(torsion)/\overline{\sigma}_s\,(tension) = 1.234$ is in good agreement with the value of *1.3* measured experimentally.

AVERAGE STRENGTH VALUES OF CYLINDRICAL RODS UNDER COMBINED TENSION/TORSION LOAD					
	TENSION	$\tau_z = 0.5\cdot\sigma_z$	$\tau_z = 1.0\cdot\sigma_z$	$\tau_z = 4.0\cdot\sigma_z$	PURE TORSION
Average Strength, $\overline{\sigma}_s$ [MPa]	295.9	307.5	322.3	336.1	365.0
Ratio $\overline{\sigma}_s$ / $\overline{\sigma}_s\,(tension)$	1	1.039	1.0891	1.136	1.234

Table 4.4 Average strength values of alumina cylindrical rods under combined tension/torsion load

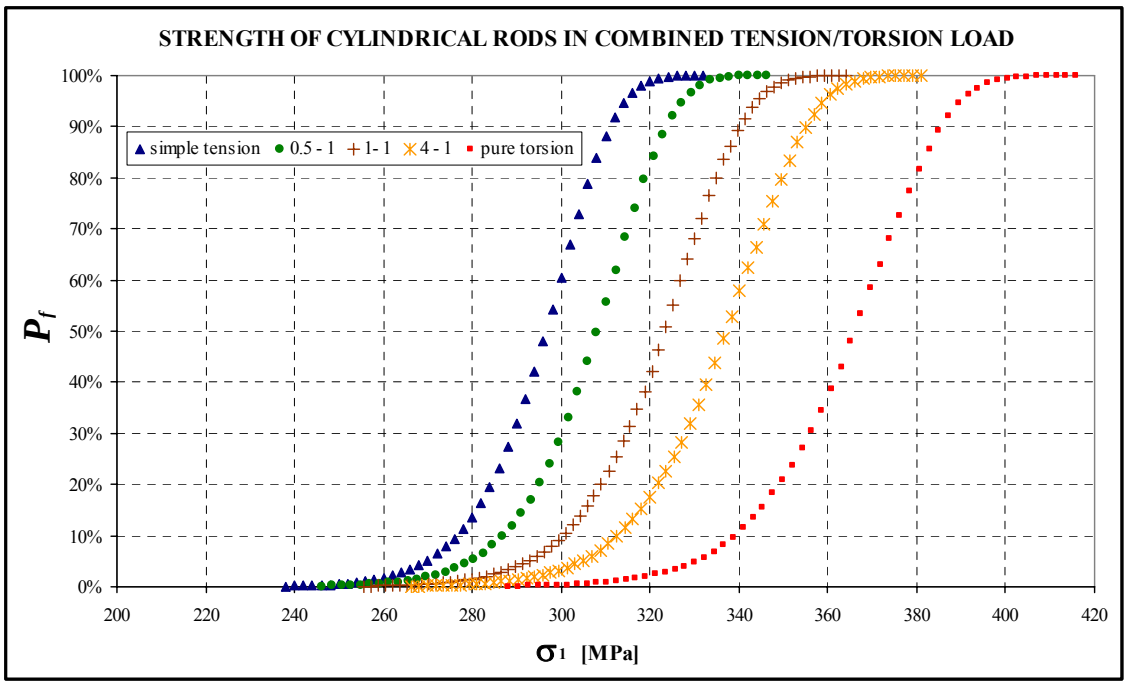

Figure 4.24 Strength distributions of cylindrical rods under combined tension/torsion load

Another interesting feature highlighted by the parametric study is the dependency of the ratio $\overline{\sigma}_s(torsion)/\overline{\sigma}_s(tension)$ on the parameters characterising the flaw size distribution. As Figure (4.25) shows, the ratio between the average tensile strength and the torsional strength is practically insensitive to changes in the flaw mean size. On the other hand, an approximately linear dependence on the COV of the flaw size distribution was observed. This behaviour can be explained via a similar argument employed in section 4.4.1 to justify the variation in strength sensitivity to flaw size parameters in the case of a uniaxial stress state.

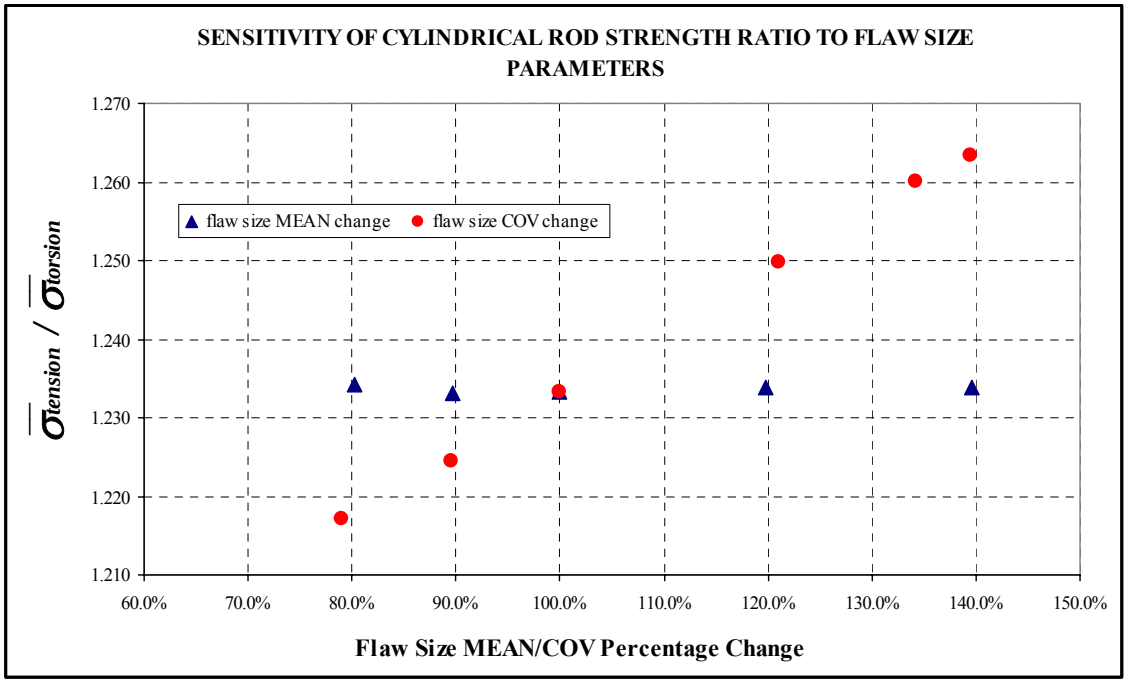

Figure 4.25 Strength ratios for various values of mean flaw size and COV of the flaw size distribution

The model estimated values of failure probability were also in agreement with the experimental observation that the average strength, expressed in terms of the maximum principal stress, of thin-walled cylindrical tubes is higher in torsion than in tension. For this type of component however, the difference in average strength between the two loading configurations is much smaller than for cylindrical rods since in thin-walled tubes all flaws are at a large radial distance from the central axis and therefore are subjected to a high shear stress when loaded in torsion.

On the other hand, in the case of a cylindrical rod subjected to a pure torsional load, most of the microcracks located in proximity of the central axis experience relative low

stress levels and therefore do not contribute (or contribute very little) to the total failure probability. When loaded in tension on the contrary, all flaws experience the same stress conditions and therefore are characterised by the same probability of triggering fracture. In particular, for a specified level of maximum principal stress σ_1, measured on the component's outer surface, the value of individual failure probability, F_c, is lower in cylindrical rods than in thin-walled tubes under torsion, while it is the same and maximum for both geometries under simple tension. The strength ratio obtained for thin-walled tubes was $\overline{\sigma}_s(torsion)/\overline{\sigma}_s(tension) = 1.147$, which was again in good agreement with the experimental value of *1.16*.

4.5.2. EQUIBIAXIAL AND EQUITRIAXIAL STRESS STATES

The effect of multiaxial stress states on material strength distribution was evaluated here by considering uniform equibiaxial and equitriaxial stress states and by comparing fracture probabilities obtained for these loading conditions with those relative to a uniaxial load. As expected, stress triaxiality results in an increase of the failure probability (Figure 4.26).

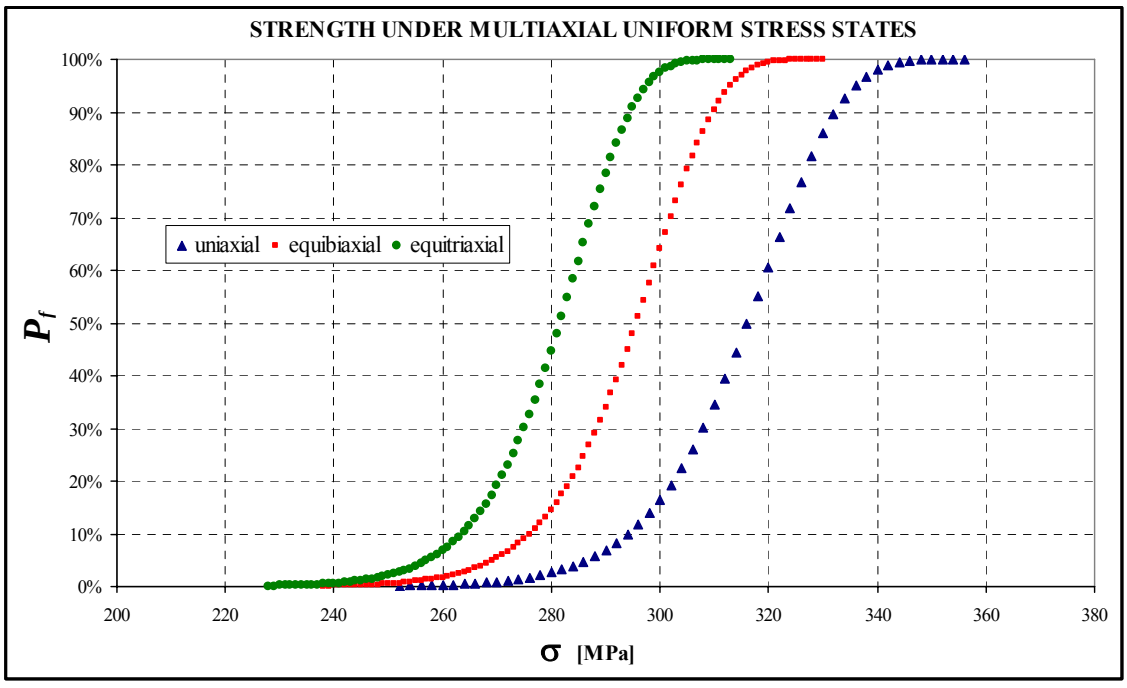

Figure 4.26 Effect of multiaxial stress states on the strength distribution

The simplest explanation for this behaviour is that under an hydrostatic stress state all crack orientations are essentially equivalent and the only contribution to strength variability comes from the random distribution of crack sizes. On the contrary, in other loading configurations, some orientations may be less critical than others and, therefore, not all large cracks are likely to trigger fracture. This condition not only results in an increase of the failure probability for an equitriaxial stress state, but also in a reduction in the scatter of the predicted strength values. This reduction in variability is, once again, confirmed by the increase in the slope of the strength distribution.

A more extensive analysis was conducted for loading conditions in plain stress, for which one of the principal stresses is equal to zero. All possible combinations of the non-zero principal stresses, indicated with σ_1 and σ_2, were considered and the entire failure probability surface was built under the assumption of stress uniformity. Figure (4.27) shows a three-dimensional plot of such surface.

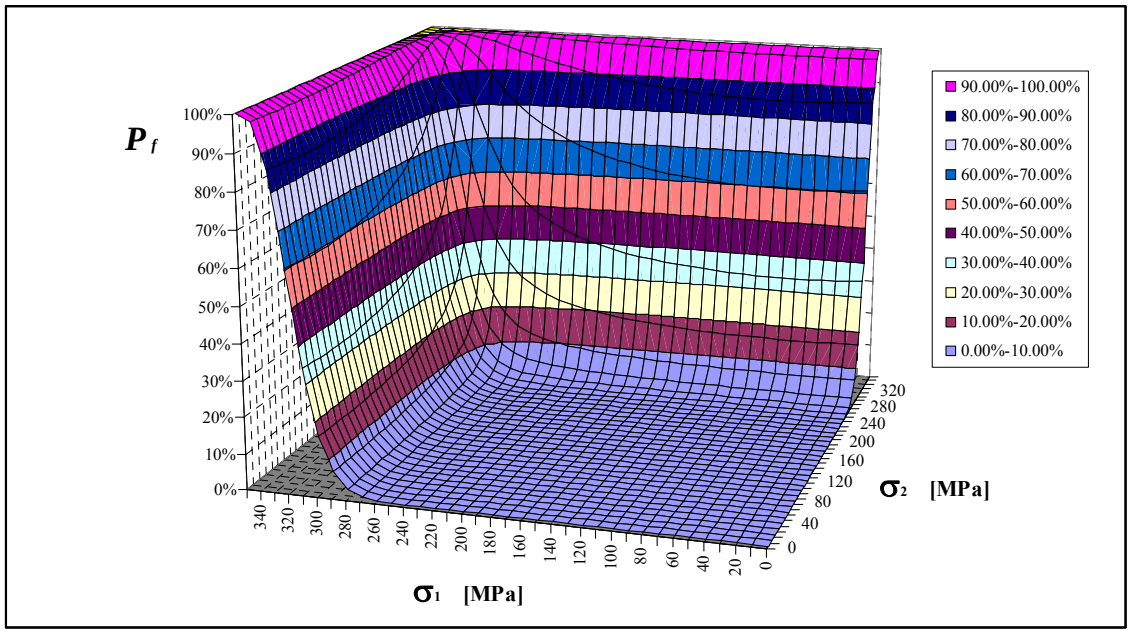

Figure 4.27 Strength distribution surface under plain stress loading

What was observed in the evaluation of critical fracture conditions is that the effect of stress biaxiality on the failure probability is rather limited for small values of the parameter *B,* defined as the ratio between the minimum and the maximum principal stress:

$$B = \frac{\sigma_2}{\sigma_1} \quad \text{for} \quad \sigma_2 \le \sigma_1 \tag{4.10}$$

In particular, when B is smaller than *0.5*, the relative change in the failure probability between the uniaxial and the biaxial case observed for a fixed level of the maximum principal stress σ_1 is less than 5%. On the other hand, for values above the threshold of *0.5*, shifts in the biaxial strength distribution are rather significant, as it is also shown by the red curve in Figure (4.26) for which B is maximum and equal to unity.

4.5.3. A NEW FAILURE CRITERION UNDER PLANE STRESS CONDITIONS

Equation (3.1) provides a direct relationship between global failure probability and the three input parameters characterizing component and material properties and i.e. component's volume, mean flaw number density and individual probability of failure F_c (which in turn depends on material microstructural features and stress conditions). In particular, if a prescribed level of reliability (equal to one minus the failure probability) must be achieved for a component whose volume and material defect number density are known, the value of F_c is uniquely defined by equation (3.1). The analysis conducted in the next few pages can then be used as a design criterion aiming at guaranteeing a prescribed level of reliability for a component subjected to a plane stress state.

For a material with a specified flaw size distribution and a known crack shape factor (estimated by fitting experimental data of specimen fracture stresses to model predictions), the maximum admissible stress diagram for plain stress loading conditions can be built through the simulation procedure described above (Figure 4.28). The diagram assigns a single value of F_c for each combination of the two principal stresses σ_1 and σ_2. All curves were obtained by considering the surface of individual failure probabilities associated with Figure (4.27) and by taking several horizontal sections of such surface for increasing values of F_c.

When assessing a potential design of a component subjected to a uniform biaxial stress state and characterised by a reliability target level R_t, the design will be considered satisfactory if the values of the principal stresses σ_1 and σ_2 fall within the region delimited by the curve in Figure (4.28) and associated with the maximum admissible level of F_c. The relationship between the reliability target level and the maximum individual failure probability can be obtained by simply inverting equation (3.1):

$$F_c = -\frac{\log(R_t)}{V\lambda} \tag{4.11}$$

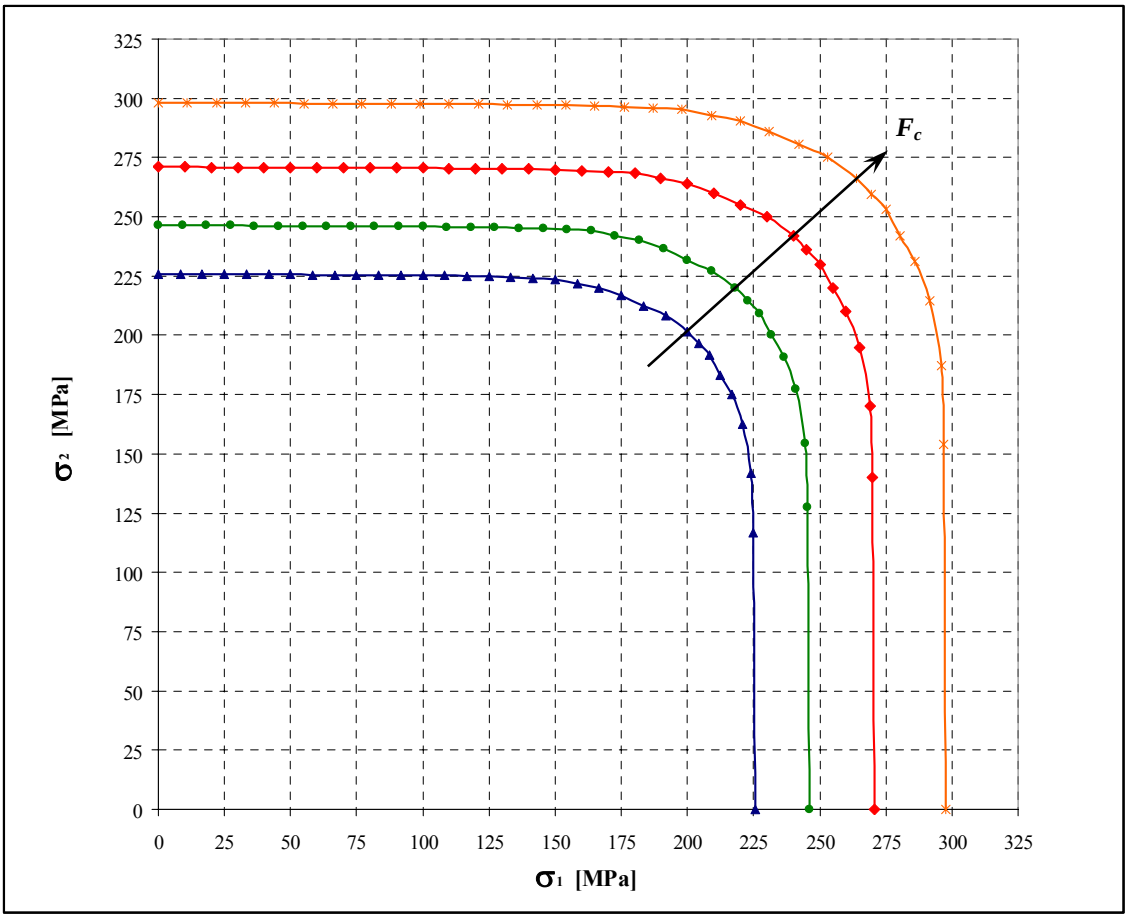

Figure 4.28 Design curves of maximum admissible stress in plain stress loading

A similar approach can also be applied to non-uniform biaxial stress configurations by simply dividing the whole component into a set of small elements within which the stress state can be assumed constant and known. The failure probability of each element subjected to the principal stresses σ_1 and σ_2 can be calculated via equation (3.1) by using values of F_c extrapolated from Figure (4.28). The design under assessment is then considered satisfactory under a structural perspective if the product of the reliabilities of all elements (equal to one minus the failure probability) is greater than the prescribed reliability target level R_t:

$$\prod_i^n \left(1 - P_f^{(i)}\right) \geq R_t \tag{4.12}$$

It is believed that, if a similar analysis is carried out on a large number of materials of engineering interest and equivalent failure probability diagrams are produced for them, the methodology proposed in this work could become a useful tool in the structural design of ceramic mechanical components.

5 RELIABILITY ANALYSIS OF COMPLEX MECHANICAL COMPONENTS

The previous chapter was dedicated to a parametric study on the fracture resistance of components characterised by simple geometries and loading conditions. The main objective of this study was to identify the parameters that control the fracture mechanisms and the strength distribution of a material containing a random population of microstructural flaws. This chapter, on the other hand, deals with the reliability analysis of a real engineering component with a complex shape and subjected to a non-uniform multiaxial stress state. Since ceramic materials are recognized to have a great potential in high temperature applications, especially in aggressive environments, the component chosen for this investigation is a turbine blade.

The superior wear and corrosion resistance of ceramics, together with their creep strength, offer substantial advantages compared to traditional metal alloy designs and, in several cases, offset the shortcomings deriving from their inherent brittleness. Gas turbine engines represent one of the applications in which the use of ceramic components could entail significant improvements in system performances, besides implying substantial reduction in turbine weight. The interest of the aerospace community towards ceramics started more than three decades ago [Burte and Acurlo, 1980]. Since then, there have been several attempts to demonstrate the applicability of such materials to turbine engine components. Among others, it is important to mention the work by Wallace *et al.* [1980], who performed a Weibull analysis on the reliability of a silicon nitride turbine blade, together with extensive experimental testing on the feasibility of this type of design.

The replacement of standard metal alloys with ceramic materials in turbine blade manufacturing could allow a substantial increase in the maximum temperature achievable in the engine thermodynamic cycle resulting in higher efficiencies [Jeal, 1988]. However, the exploitation of these materials in such a strength demanding application will be possible only if an adequate methodology for the structural design of ceramic components is developed. The present work aims at setting the principles of such methodology, showing its direct application to the reliability analysis of a complex structure subjected to arbitrary loading configurations.

The approach proposed in this work is based on the coupled use of Finite Element Analysis (FEA) and the probabilistic framework developed in the previous chapters. In particular, FEA is employed to determine the stress distribution produced in the component by the applied load. As stated in Chapter-3, the global material mechanical

response is assumed not to be affected by the presence of microstructural defects. This means that the stress field throughout the component can be determined independently from the flaw population by employing standard techniques derived from the theory of elasticity.

The stress distribution obtained by FEA can then be used within a Monte Carlo simulation to deal with the stochastic nature of the failure event and to assess the local conditions for critical fracture initiation. The final results are expressed in terms of the failure probability of the structure, quantity that represents the likelihood of a large defect to be located within a highly stressed region and to be oriented in such a way to satisfy the chosen criterion for catastrophic crack propagation.

5.1. Component Geometry and Loading Conditions

The geometry of the component considered in this analysis is shown in Figure (5.1).

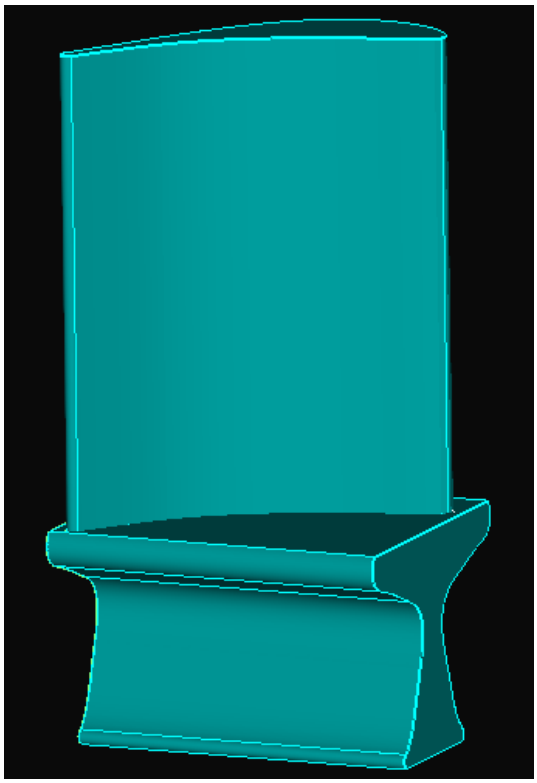

Figure 5.1 Turbine blade geometry

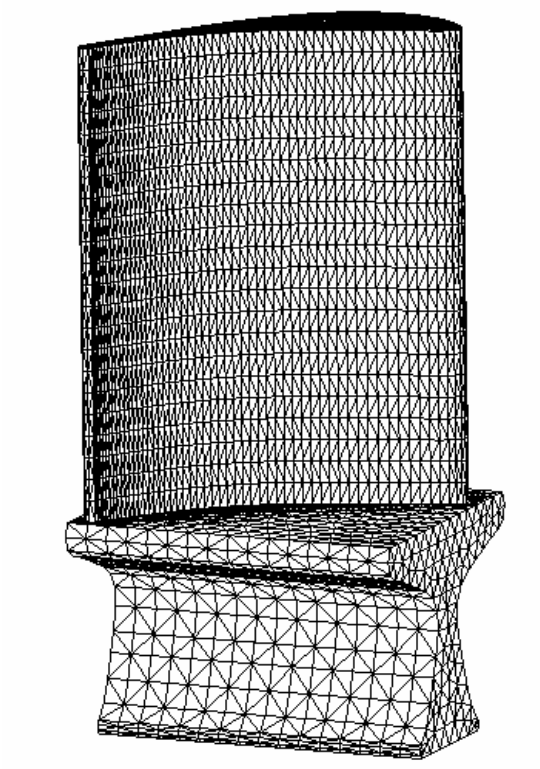

Figure 5.2 Turbine blade finite element mesh

The blade airfoil profile was obtained by Fottner [1990] as a series of *x*-*y* coordinates of the representative points of the blade cross-section. The other relevant geometrical features are the cord length, blade height and distance of the blade root from the centre of the turbine disk to which it is connected. These were assumed equal to *30 mm*, *40 mm* and *167 mm* respectively. The material considered for this study is the same examined in the previous chapter (sintered alumina). In particular, the material microstructure is characterised by the flaw size distribution previously measured through image analysis techniques and the principal material mechanical properties are those given in table (4.3).

The two main sources of stress experienced by a turbine blade during service are the centrifugal force, produced by the high rotational speed, and the bending moment generated by the pressure difference of the gases flowing on the two sides of the blade (the pressure side and the suction side respectively) [Hsiung *et al*., 1988]. In order to study the structural response of the component to different types of load, three loading conditions were considered in just as many simulations. First, the effects of centrifugal force and pressure difference were analysed separately in order to determine the individual contribution of each load to the failure event and to highlight the differences between the two configurations. Then, the overall component strength distribution, relative to loading conditions similar to those experienced by the turbine blade during real operation (when i.e. centrifugal force and bending moment act simultaneously), was examined. In all cases the stress field was determined through a linear elastic Finite Element Analysis on a uniform mesh of approximately 22,000 tetrahedrical elements (Figure 5.2). The stress state computed within each element was assumed to be uniform.

Examples of the stress distributions obtained for different load magnitudes and expressed in terms of the maximum principal stress are shown in Figure (5.3), (5.4) and (5.5). In particular, Figure (5.3) displays the stress fields on the blade pressure side computed for rotational speeds of *360 rev/s* (on the left-hand side) and *460 rev/s* (on the right-hand side). The two distributions appear very similar, with values of the maximum principal stress that increase from the tip to the root of the blade and are almost uniform on each cross-section (especially away from the blade root). For a given section height then, stress levels are obviously greater for higher rotational speeds.

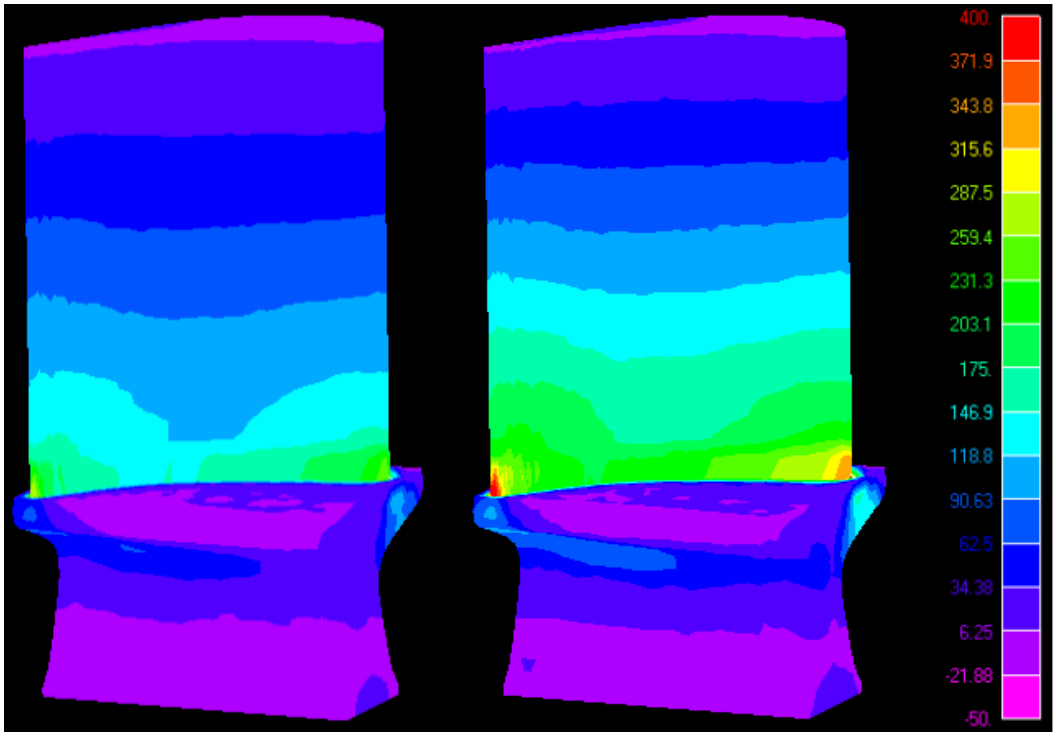

Figure 5.3 Stress distributions produced by the centrifugal force for rotational speeds of 360 rev/s(left) and 460 rev/s (right)

On the other hand, Figures (5.4) and (5.5) show the maximum principal stress on both sides of the blade produced by pressure differences of *1 MPa* and *1.5 MPa* respectively (and zero rotational speed). For simplicity, the pressure distribution was assumed to be uniform across the blade surfaces. This approximation is believed not to limit the validity of the results obtained in our investigation. In fact, the conclusions drawn from the analysis of a uniform pressure are generally valid for non-uniform pressure distributions as well. Also note that the pressure levels selected for the FEA calculations are significantly higher than the values normally associated with actual turbine operating conditions. This choice was made in order to be able to individually assess the effect that this type of load has on the component strength distribution.

In all loading configurations examined, the highest stress was found at the blade root, in proximity of the trailing edge, where the joint with the support acts as a stress intensification feature (similar results were obtained in other finite element calculations of a turbine blade subjected to thermo-mechanical loading [McLeod *et al.*, 1980]). The main difference between the stress field produced by the centrifugal force and that relative to a pressure difference is that in the former case most of the component is under tension, while in the latter configuration large volumes are subjected to a compressive load. This condition has a direct effect on the measured failure probability.

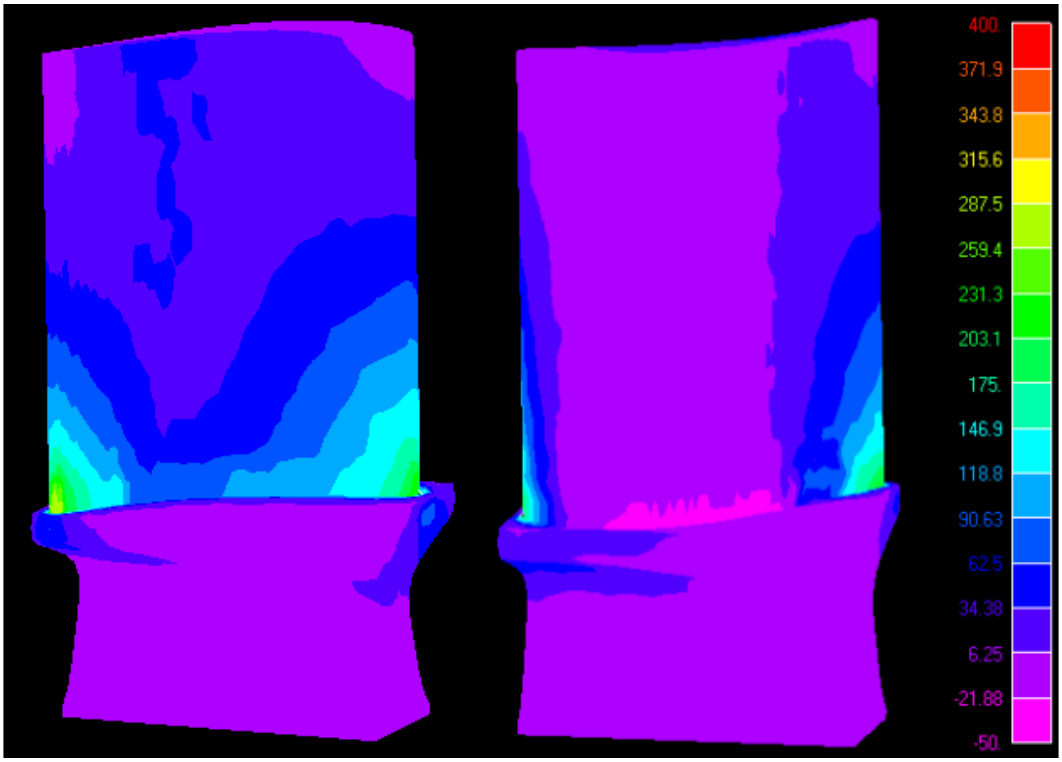

Figure 5.4 Stress field produced by a pressure difference of 1.0 MPa

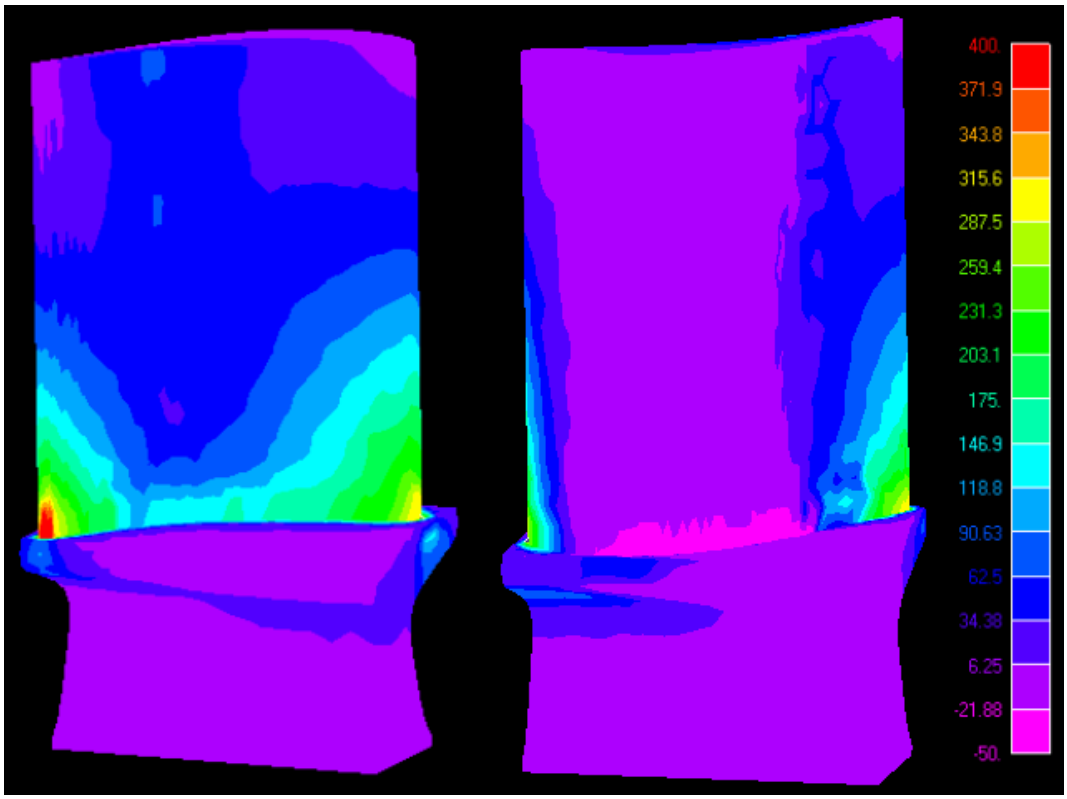

Figure 5.5 Stress field produced by a pressure difference of 1.5 MPa

5.2. Analysis of Component Strength Distribution

In order to determine the component strength distribution relative to a centrifugal load, several finite element analyses were performed for rotational speeds varying in the range 300-600 *rev/s*. The stress values obtained by FEA calculations were then used as input of the Monte Carlo simulation. The properties of the material microstructure considered in this study (in terms of flaw size distribution and average number of flaws) are those previously measured through image analysis techniques and summarised in tables (4.2) and (4.3).

By sampling random defects across the component volume, the individual failure probability F_c was estimated. This value was then substituted into equation (3.1) to determine the final strength distribution of the structure. The results obtained are shown in Figure (5.6) in terms of the cumulative distribution function, *CDF*, which gives the probability P_f that the component fails at a rotational speed equal or smaller than the value specified on the *x* axis. No failure events were observed below *380 rev/s*, while for higher speeds the probability of failure progressively increases.

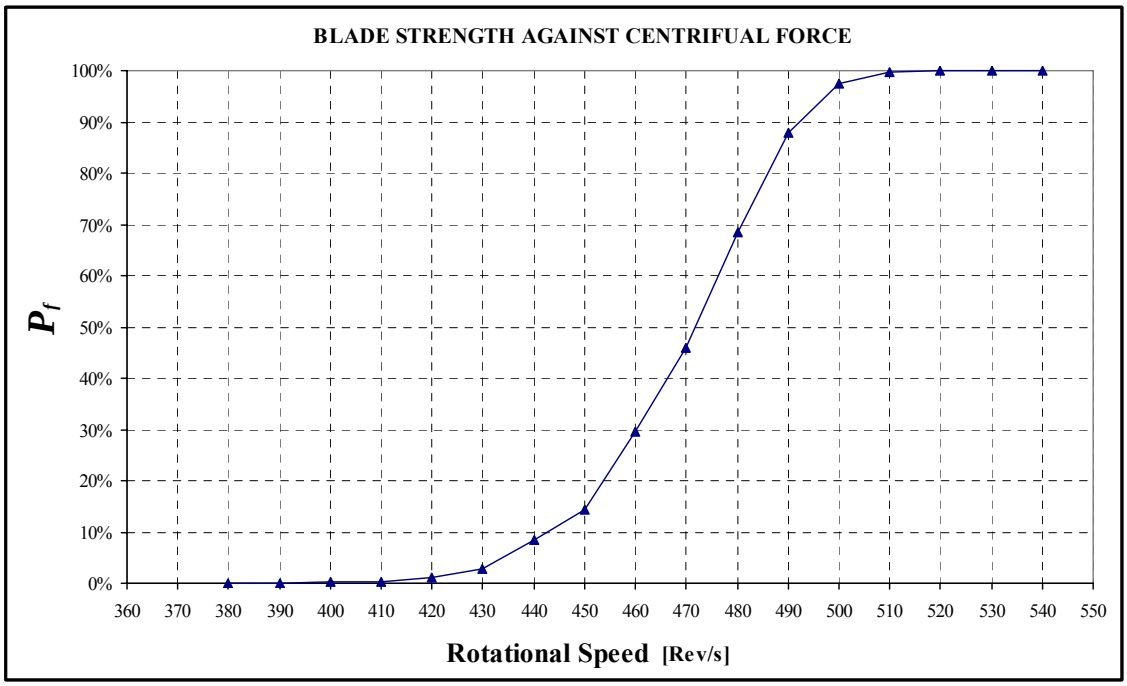

Figure 5.6 Strength distribution of a turbine blade containing a flaw population with size distribution given in Figure (4.10) and subjected to a centrifugal load

The effect that variations in the flaw size parameters have on the component strength distribution was also examined. Figure (5.7) illustrates the trend of the failure probability obtained when the mean of the crack size distribution is increased by 20% for a constant value of COV (red curve) and, conversely, when the distribution COV changes at a constant mean (green curve). Higher values of flaw average size or COV are associated with higher probabilities of finding large defects in the material microstructure and therefore cause the component strength distribution to shift towards lower levels of load (and consequently lower rotational speeds). Overall, the larger variations in failure probability were produced by changing the mean value of the flaw size distribution. Only along the lower tail of the strength distribution, i.e. in the range of interest for reliable designs, an opposite trend was observed. As discussed in Chapter-4, the greater sensitivity of the strength distribution to changes in the average flaw size compare to variations in COV is typical of non-uniform stress fields.

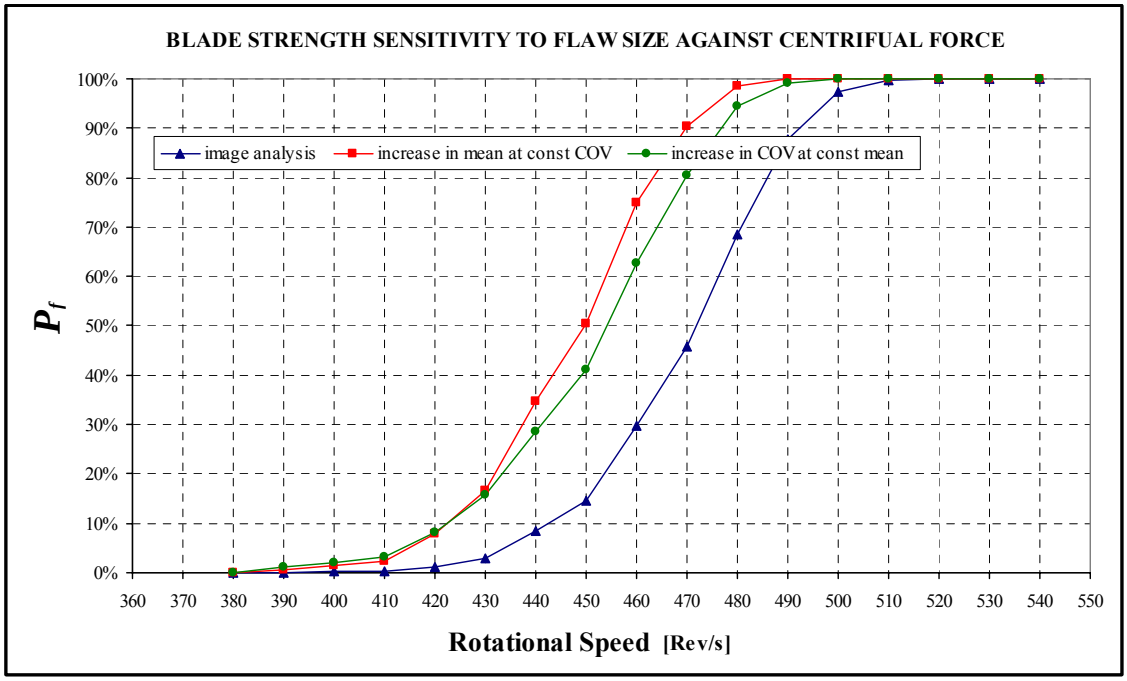

Figure 5.7 Sensitivity of the blade strength distribution relative to a centrifugal load to changes in flaw size parameters

The same type of analysis was conducted for the second source of structural load. The stress states produced in the component by pressure differences ranging from *1.0* to *2.5 MPa* were computed through several finite element analyses and imported into the Monte Carlo engine. As in the previous case, the Monte Carlo simulation was based on

a total of 1 million samples. This, in conjunction with the application of importance sampling techniques, allowed to achieve an estimated relative error on the individual failure probability F_c smaller than 5% (for a two standard deviation confidence level). The resulting strength distribution is given in Figure (5.8). Under the sole action of the pressure load, failures were observed only for pressures higher than about *1.2 MPa*.

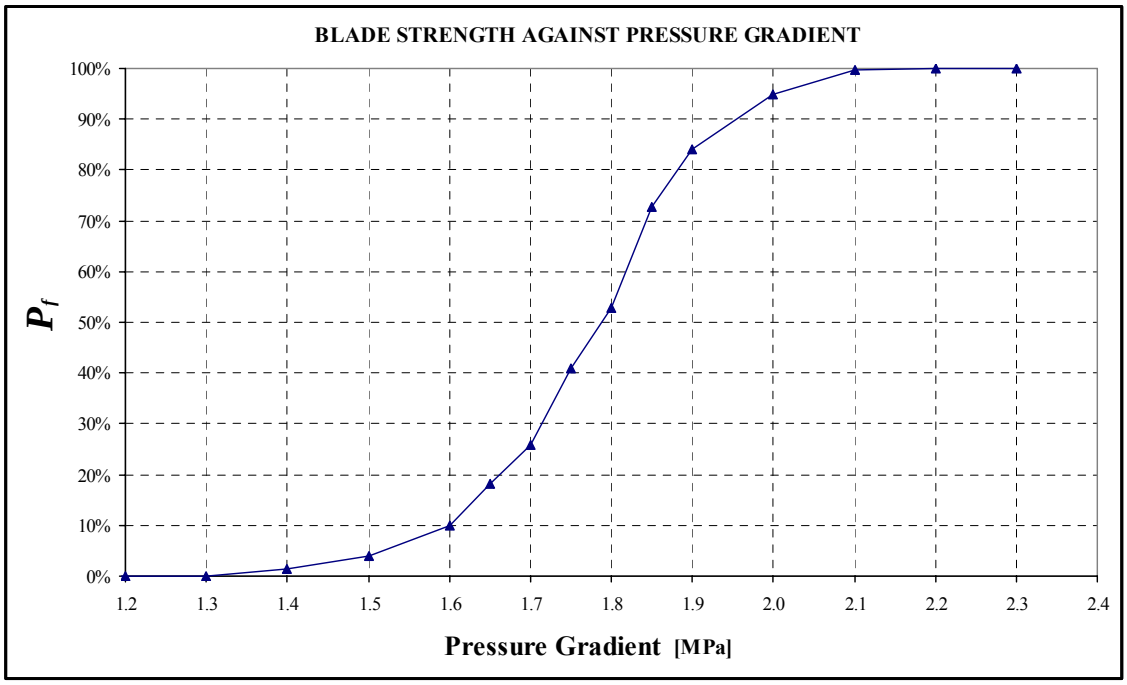

Figure 5.8 Strength distribution of a turbine blade containing a flaw population with size distribution given in Figure (4.10) and subjected to a pressure load

The effect of flaw size parameters on the failure probability was analysed also in the case of a pressure load. Figure (5.9) illustrates how, for all configurations examined, a variation in the average crack size has a larger impact on the blade strength distribution than an equivalent increase in the crack length COV. None of the two loading schemes produce a uniform stress distribution, but, in general, the stress field relative to a pressure load is characterised by steeper stress gradients and therefore is less affected by increases in crack size variability than a centrifugal load. An explanation for this behaviour was given in section 4.4.1.

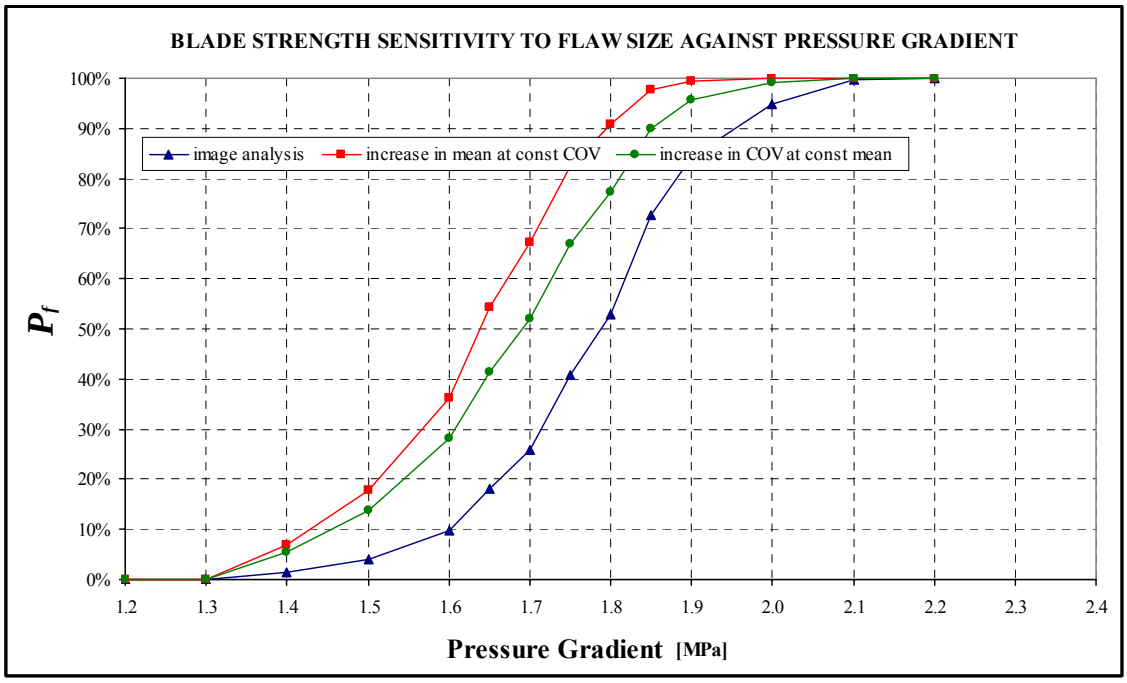

Figure 5.9 Sensitivity of the blade strength distribution relative to a pressure load to changes in flaw size parameters

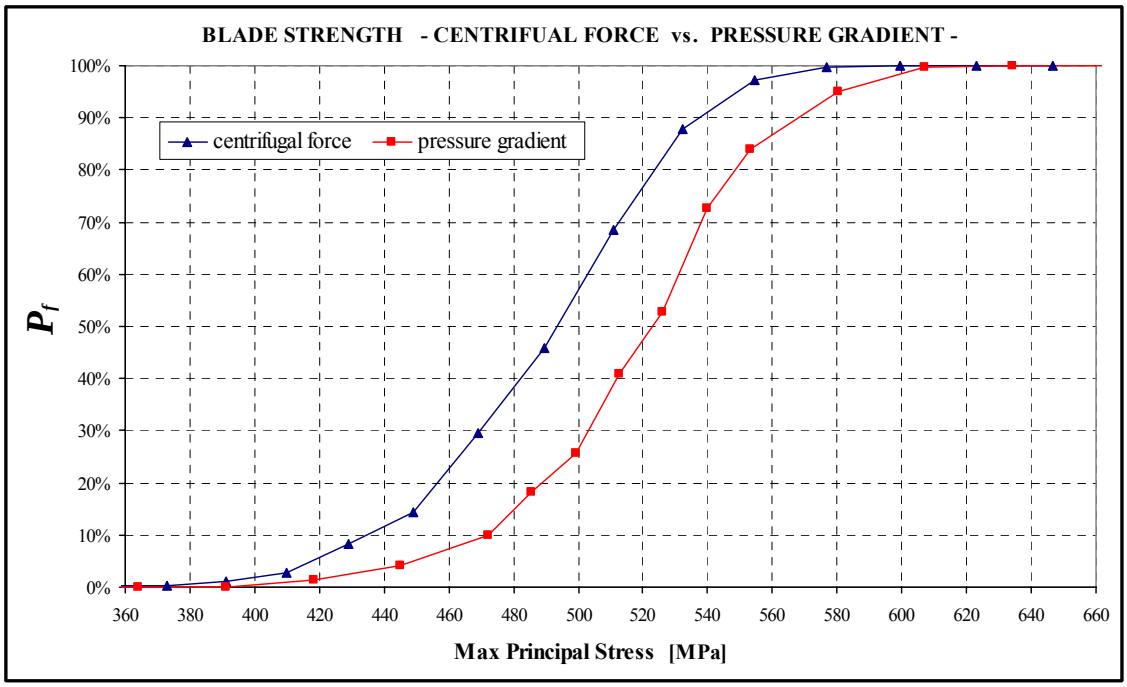

Figure 5.10 Comparison between the blade strength distribution relative to a centrifugal load and that associated with a pressure load

The trend followed by the probability of failure is significantly influenced by the type of load acting on the component. A traditional design methodology, based on the maximum principal stress, would clearly predict the same failure probability for two different loads resulting in the same maximum normal stress. However, as Figure (5.10) clearly highlights, this is not true when considering the failure probability relative to centrifugal force and pressure load. If two loading conditions characterized by the same value of maximum principal stress are considered, the failure probability associated with the centrifugal force is substantially higher than that relative to the pressure load. This is mainly due to the fact that the bending moment produced by a pressure gradient puts part of the component under tension, increasing the maximum principal stress, and part under compression. Compression is less critical in terms of crack initiation and therefore results in a lower probability of failure (it is necessary to point out that the load arising from the gas pressure difference is an alternating force and, for this reason, it can give origin to dynamic effects, which have not been covered in the present study).

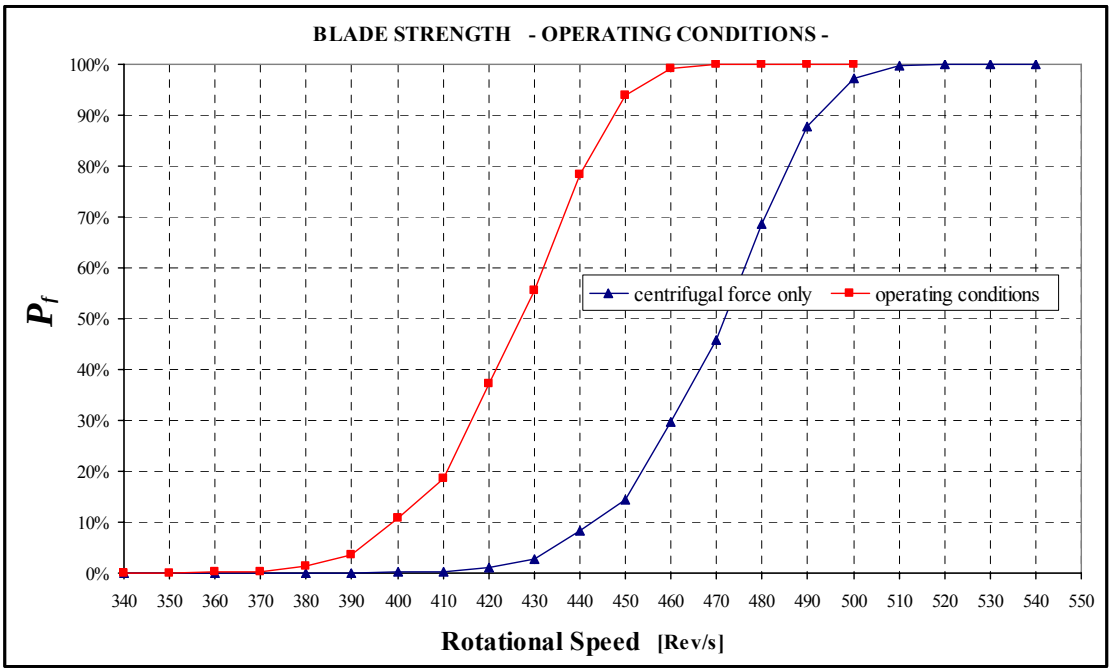

Figure 5.11 Strength distribution of a turbine blade containing a flaw population with size distribution given in Figure (4.10) under general operating conditions

Finally, the failure probability associated with the combined action of centrifugal force and pressure difference was analysed. The values of pressure assumed in these calculations were closer to those experienced during actual operation of the turbine blade. The gas velocity distribution along the blade profile was known from

experimental data [Fottner, 1990]. An average value of pressure acting on each side of the blade was calculated for different velocity of the inlet flow and assumed constant along the whole blade length. The speed of the inlet flow was then assumed to be proportional to the square of the rotational speed. This procedure allowed the author to calculate an average value of pressure difference for each rotational speed. The estimated pressure difference started at *0.14 MPa* for a rotational speed of *340 rev/s* and went up to *0.3 MPa at 500 rev/s.* The overall blade probability of failure is presented in Figure (5.11) as a function of the disk rotational speed. The global blade behaviour is compared with the failure probability resulting exclusively from the action of the centrifugal force. The combined effect of centrifugal force and pressure difference obviously results in higher failure probabilities for each fixed value of rotational speed.

5.2.1. MOST PROBABLE FAILURE LOCATIONS

The analysis presented in this chapter is essential for accurate prediction of brittle failure initiated in components containing random flaws and subjected to complex stress states. The approach proposed in this work can also be used to identify the regions in the component that are more likely to fracture.

Figure (5.12) for example, shows the different locations of fracture initiation recorded during the Monte Carlo simulation at a rotational speed of *400 rev/s*. A higher density of crack locations initiating fracture indicates a higher failure probability of that part of the component. Critical conditions are not always encountered at the point of maximum stress, but are also found in a region where a lower stress is spread over a large volume. In particular, in the present case, although the highest stress was found at the blade trailing edge, a substantial contribution to the failure probability appears also to come from the turbine leading edge, where the stress is smaller but is associated with a larger volume. Traditional design methodologies do not take into consideration this contribution to the probability of failure.

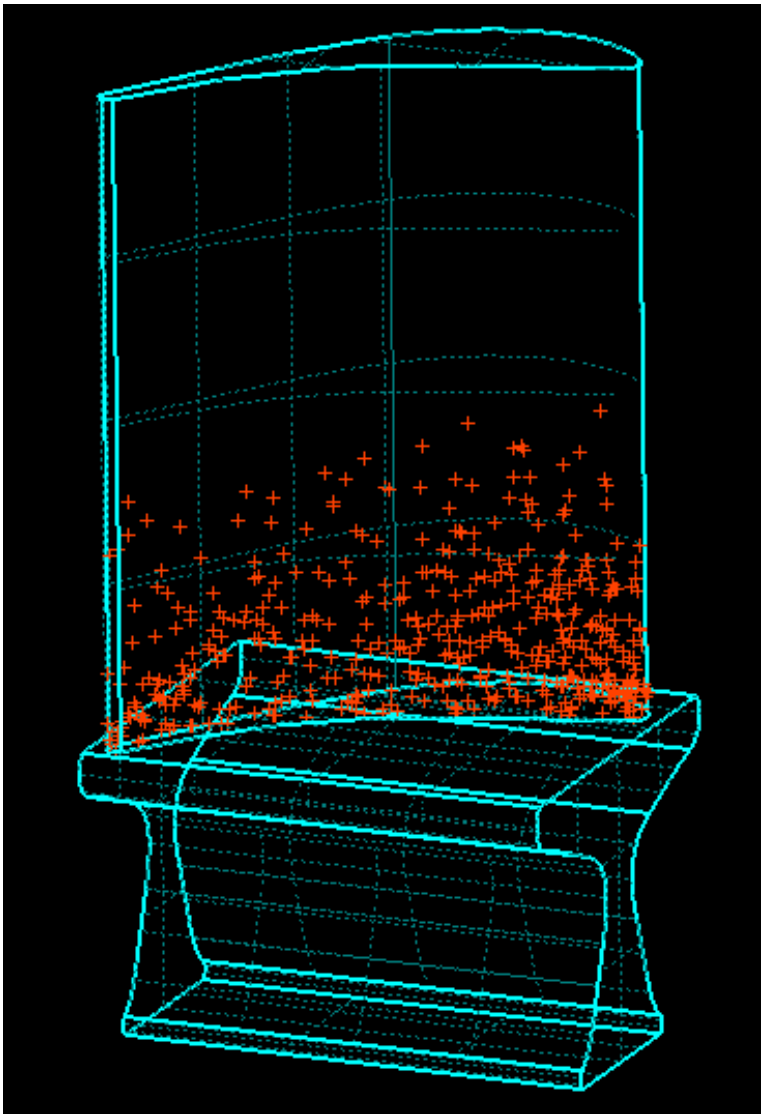

Figure 5.12 Failure locations

This condition of a large part of the component contributing to the overall probability of failure becomes even more pronounced when the crack size COV increases. As Figure (5.13) shows, by increasing this parameter by 20%, failure initiation sites progressively spread throughout the bulk of the component. In these circumstances, larger flaws may be located in the upper part of the blade and be critical even under the lower stresses characterising this area.

The opposite effect is encountered when the variability of the defect size, described by the log-normal distribution, is reduced. By reducing the COV by one fifth of its initial value, only zones characterised by a high stress substantially contribute to the total probability of failure (Figure 5.14).

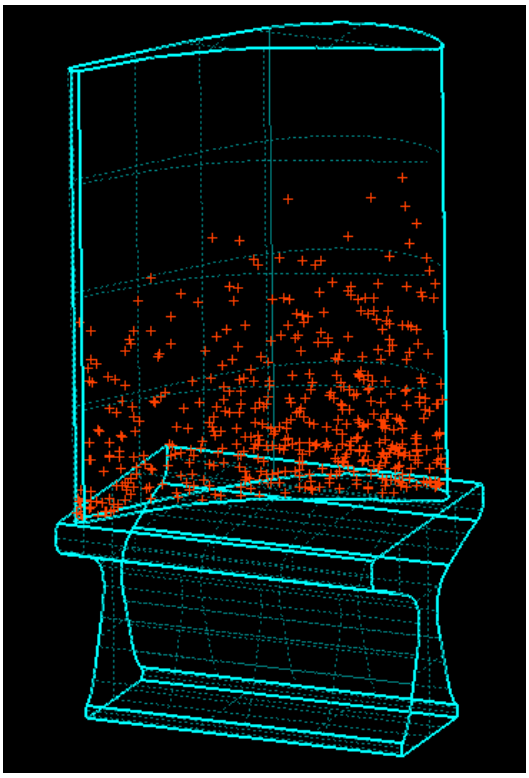

Figure 5.13 Failure locations for higher values of COV

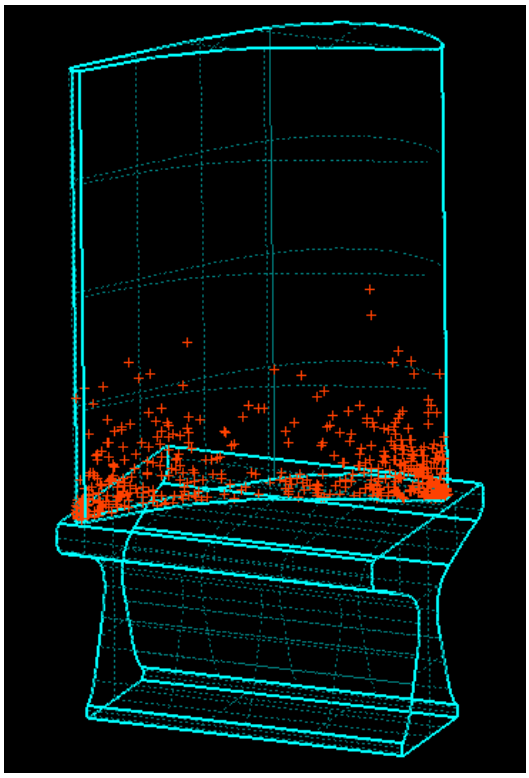

Figure 5.14 Failure locations for lower values of COV

The present methodology not only allows one to adequately predict the reliability on demand of a highly complex component, but can also be used to analyse how the component's strength distribution responds to a variation in design parameters and material properties. A reduction of the flaw average size obviously produces significant enhancement in component's strength. If a strict quality control is applied to monitor material properties especially in the most critical regions of the component (trailing and leading edges in the case of a turbine blade), substantial reliability improvements can be achieved. Alternative approaches can be employed depending on the type of load to which a component is subjected. For relatively uniform stress states, the maximum scatter of the crack length should be kept under control, while, for stress fields characterised by steep gradients, the average defect size is the most significant parameter and should be closely monitored. Also, depending on the magnitude of the flaw size COV, variable portion of the component volume should be subjected to careful scrutiny.

5.3. Design Modifications

The final section of this chapter illustrates how the Monte Carlo approach developed in this work can be employed to identify opportune design modifications, whose implementation could result in significant improvements in a component's reliability, and to quantify the actual changes that such modifications produce on the probability of failure.

A rather common design solution that is often used in turbine blade manufacturing, in order to optimise material usage and improve structure performances, is the tapering of the blade along its height. This configuration allows a reduction in the component's mass and consequently the magnitude of the centrifugal force to which the blade is subjected. By following this strategy, despite the slight increase in rotational speed that would be required to obtain the same power output as from a straight blade (due to the reduction in the lifting surface area) sections in proximity of the blade root, which are the most critical from a structural perspective, experience a substantial decrease in maximum axial stress.

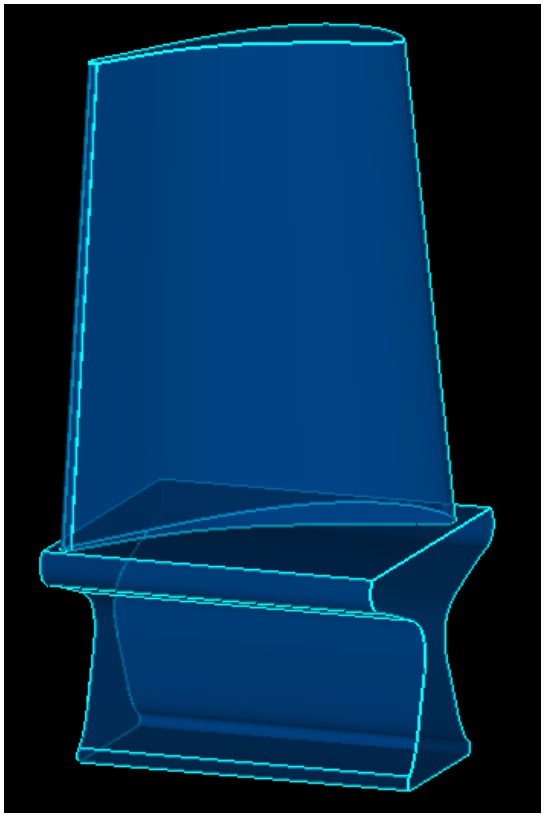

Figure 5.15 Tapered blade geometry

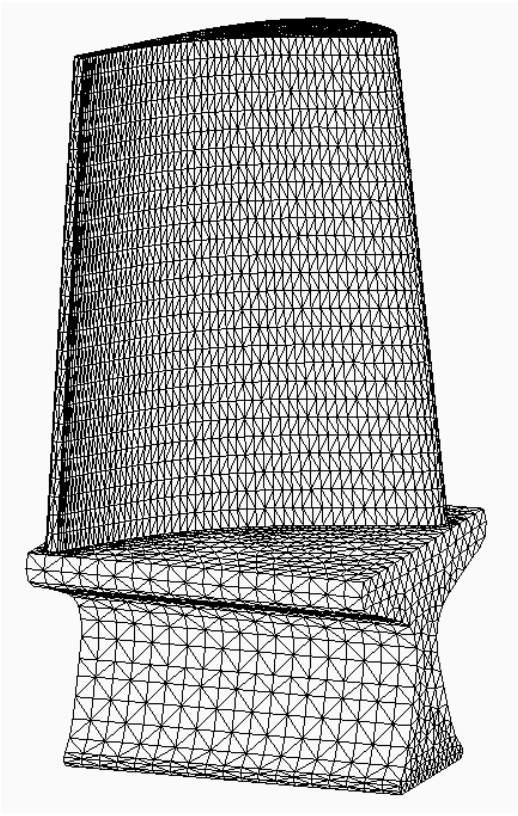

Figure 5.16 Tapered blade finite element mesh

Component's geometry was therefore modified with the intent of assessing the improvement in reliability resulting from blade tapering. The new geometry is shown in Figure (5.15), together with the corresponding finite element mesh, composed of 28,353 tetrahedrical elements, employed in FEA calculations (Figure 5.16). The reduction in blade cross-section area is linear from root to tip and reaches a maximum value of 20% at the blade tip.

Several solutions of the stress field were computed for a wider range of rotational speeds (from *340 rev/s* to *640 rev/s*) than that considered for the original design. The results obtained for two representative cases characterized by rotational speeds of *360 rev/s* (left-hand side) and *460 rev/s* (right-hand side) are shown in Figure (5.17). The reduction in maximum principal stress is clearly visible when comparing Figure (5.17) with Figure (5.3), where the stress distributions relative to the same rotational speeds were displayed for a straight blade.

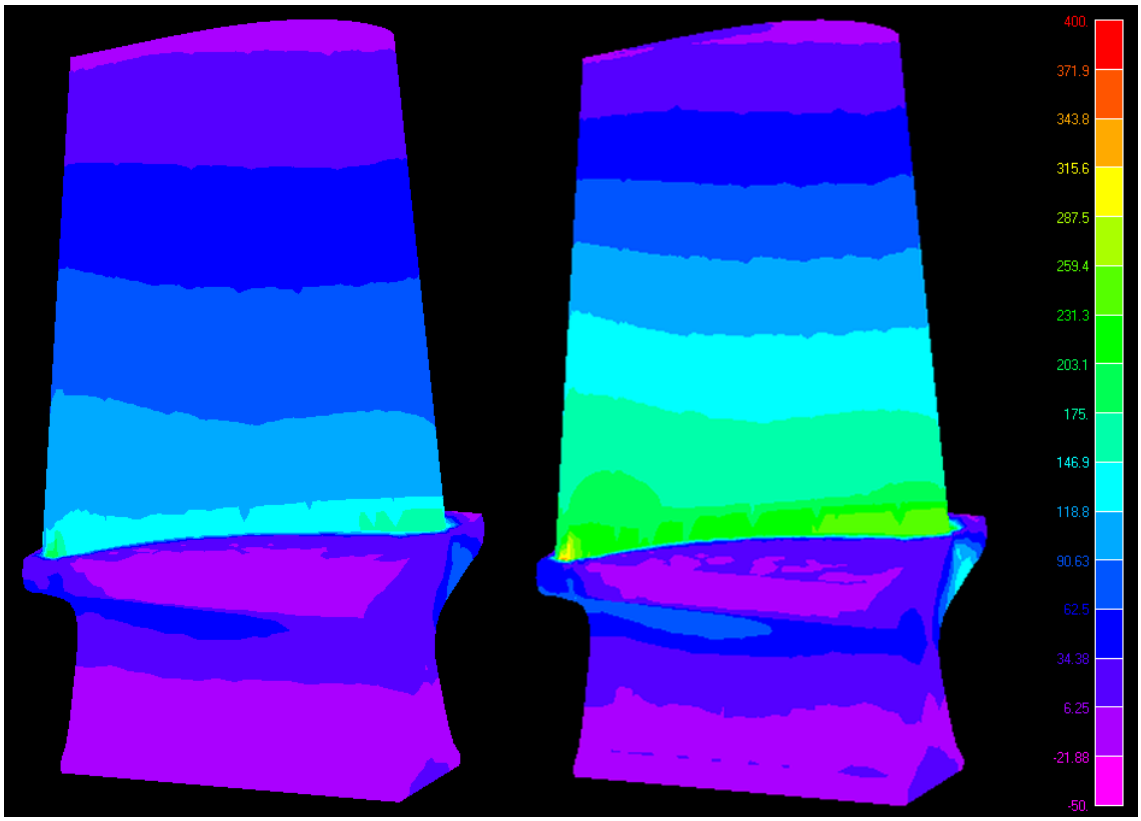

Figure 5.17 Stress distributions in tapered turbine blade for rotational speeds of 360 rev/s and 460 rev/s

When considering the centrifugal force as the only load to which the blade is subjected, the significant reduction in stress levels experienced throughout the component volume has a direct beneficial effect on the strength distribution of the tapered turbine blade (Figure 5.18). In fact, for the same level of reliability, the increase in maximum admissible rotational speed that was estimated via the Monte Carlo simulation is of about 20%.

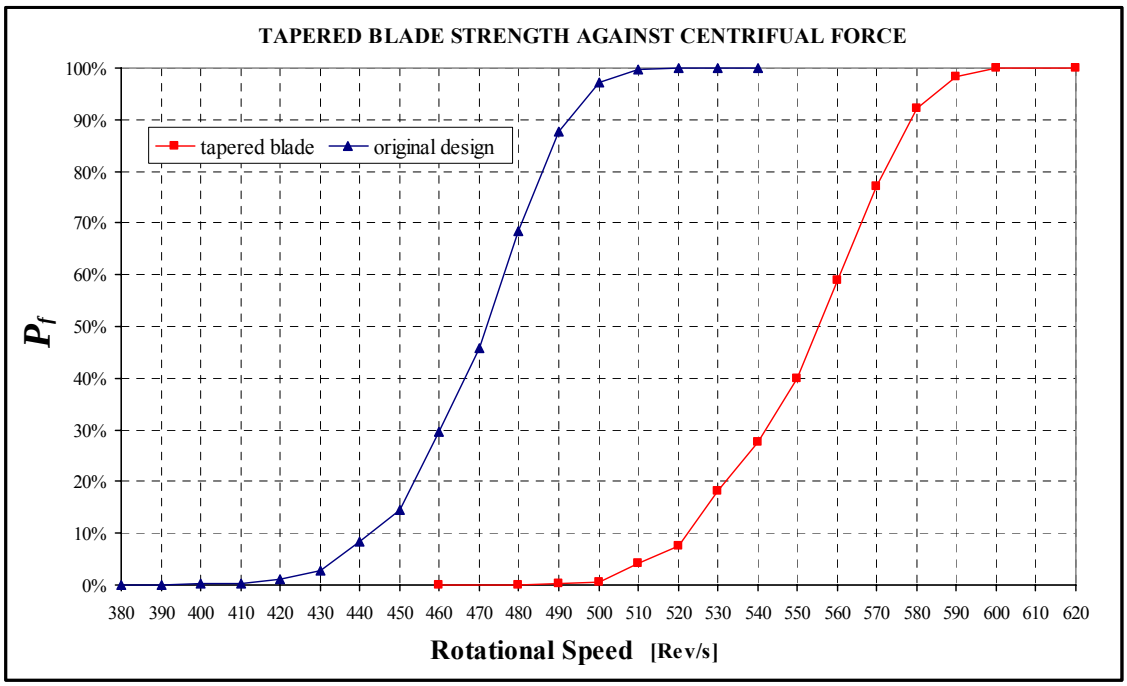

Figure 5.18 Tapered blade strength distribution relative to a centrifugal load

On the other hand, the opposite behaviour was observed when analysing the response to a pressure load. The reduction in area of a tapered blade entails smaller moments of inertia of the cross-sections and therefore results in higher values of stress when the component is subjected to a bending moment. In particular, while the stress experienced in proximity of the blade root is not affected by tapering, moving towards the blade tip cross-sections are progressively characterised by lower values of the moment of inertia and therefore experience higher stress levels. Since the whole component volume contributes to the total failure probability, blade tapering has a negative effect on the estimated probability of failure relative to a pressure load (Figure 5.19).

In general, the predominant effect resulting from blade tapering is the reduction in stress due to the centrifugal force. The strength distribution under the combined action of the centrifugal and the pressure load moves towards higher values of rotational speed (Figure 5.20). In particular, for the same probability of failure of about 0.5%, the

maximum admissible rotational speed changes from *370 rev/s* for a straight blade to *400 rev/s* in the case of a tapered blade.

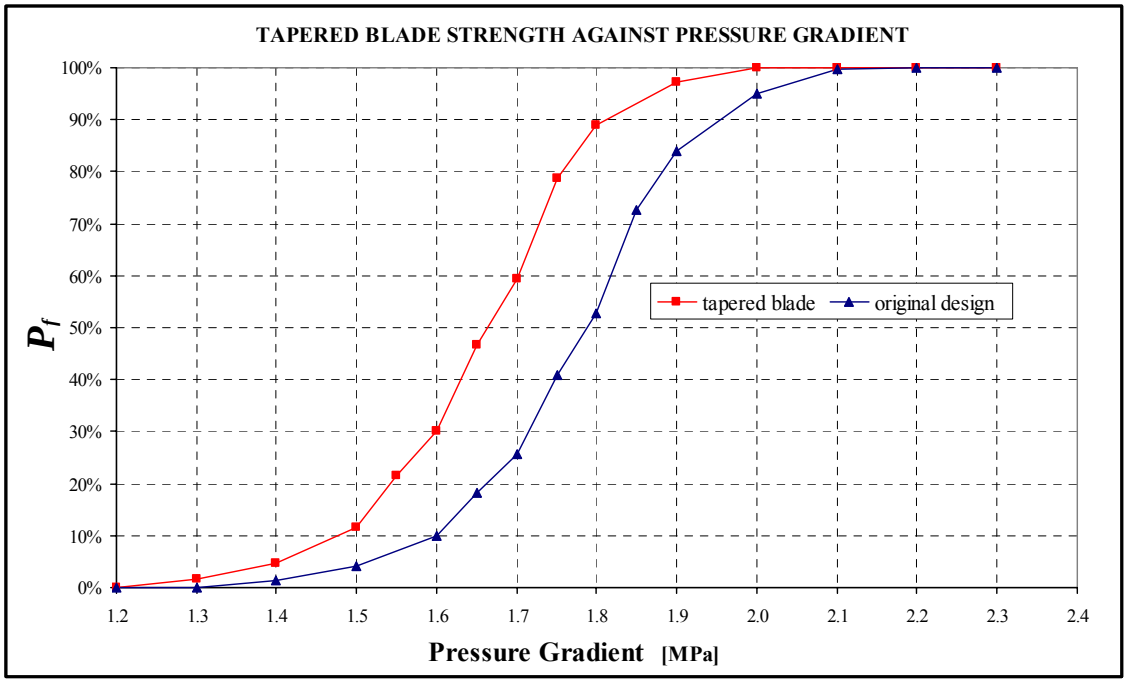

Figure 5.19 Tapered blade strength distribution relative to a pressure load

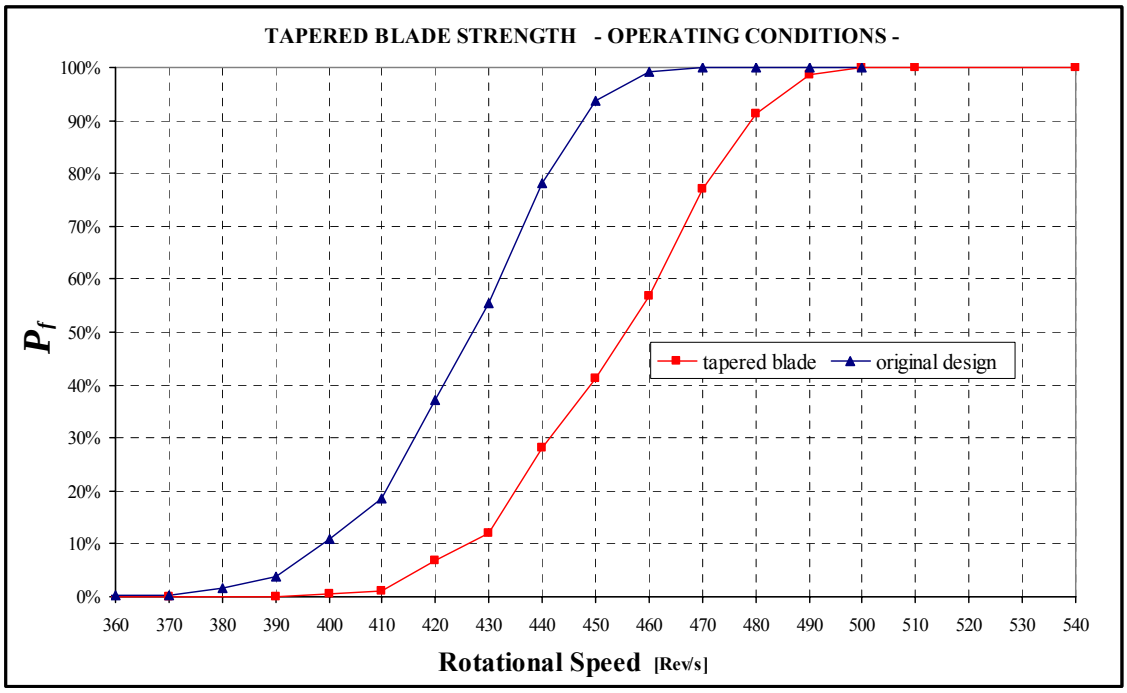

Figure 5.20 Tapered blade strength distribution relative to operating conditions (combined action of centrifugal and pressure load)

6 PROBABILISTIC STUDY OF CLEAVAGE IN STEEL STRUCTURES

The most accredited model of cleavage fracture in steel structures is the so-called RKR model [Ritchie, Knott and Rice,1973]. It postulates that cleavage fracture in mild steels occurs (principally at low temperatures) when the local tensile stress ahead of a sharp crack exceeds the critical value of material resistance over a characteristic distance. A subsequent study [Curry and Knott, 1979] gave a probabilistic explanation of the RKR characteristic distance, by assuming that a statistical distribution of carbide particles exists ahead of the crack tip. The size of the area in which high stress levels must develop for brittle failure to occur depends on the probability that a sufficient large carbide particle is found in this region.

The approach mentioned above is extended in this work by applying the probabilistic framework, based on the weakest link concept, developed in the previous chapters. Monte Carlo simulation is employed to sample the material ahead of the crack tip and gather information about the likelihood of a sufficient large carbide particle to be located in this area. The statistical properties of the carbide population and, in particular, the mean number density and the size distribution of particles, can be obtained by image analysis.

The carbide films and particles, usually located at the grain boundaries, are readily cracked by slip bands in the ferrite matrix since the carbide has a low effective surface energy and is brittle. The critical step in cleavage may then become the propagation of the carbide crack into the more plastic ferrite [Petch, 1986]. As already attempted in other studies, this means that carbide particles can be effectively assimilated to microcracks, whose number and size properties can be directly derived from the originating population. In the case considered here however, microcracks are characterised by a shape factor that generally differs from that of a penny-shaped or a through-thickness crack, which were usually assumed in the past.

In the next sections of this chapter the effectiveness of this methodology will be supported by several practical applications. Firstly, the variability in fracture toughness of a mild steel will be investigated and the points at which fracture is more probable to initiate identified. Then, the strength distribution of a typical steel component will be evaluated.

6.1. Model Calibration

6.1.1. MATERIAL PARAMETERS

The material considered in this study is a mild carbon steel, AISI 1008, whose main mechanical properties [Walsh, 2000] are summarized in Table (6.1). Values for the yield stress, σ_y, and the effective surface energy at -150ºC were obtained by Lin *et al.* [1986a]. As discussed in Chapter-2, the effective surface energy is calculated by adding the material surface energy γ_s to the energy dissipated by local plastic flow γ_p. The sum of these two quantities gives the total energy per unit area that is required by the crack to propagate and create new free surfaces. The effective surface energy is immediately related to the critical strain energy release rate, $\mathcal{G}_{crit}$, by the simple expression: $\mathcal{G}_{crit} = 2\cdot(\gamma_s+\gamma_p) = 46\ J/m^2$.

The statistical distribution of carbide particle sizes was also estimated by Lin *et al.* [1986a] through an image analyser. A plot of the relative frequencies measured for each size interval is given in Figure (6.1). The estimated average particle size is $2.5\ \mu m$ while the standard deviation is $1.7\ \mu m$. In order to use this experimental observation into the Monte Carlo engine, the empirical histogram shown in Figure (6.1) was fitted with a log-normal probability distribution with parameters $\mu = -6.1815$ and $\sigma = 0.6165$ (the mean and the standard deviation of $\log(X)$ respectively). This analytical function was employed to sample the size of randomly located and oriented microcracks ahead of the macrocrack tip.

MECHANICAL PROPERTIES OF CARBON STEEL: AISI 1008	
Modulus of Elasticity, E	210 GPa
Shear Modulus	82 GPa
Poisson Ratio, ν	0.27
Yield Strength (at -150ºC), σ_y	520 MPa
Density	7871 Kg/m^3
Effective Surface Energy : $\gamma_p+\gamma_s$	23 J/m^2

Table 6.1 Mechanical properties of mild steel: AISI 1008

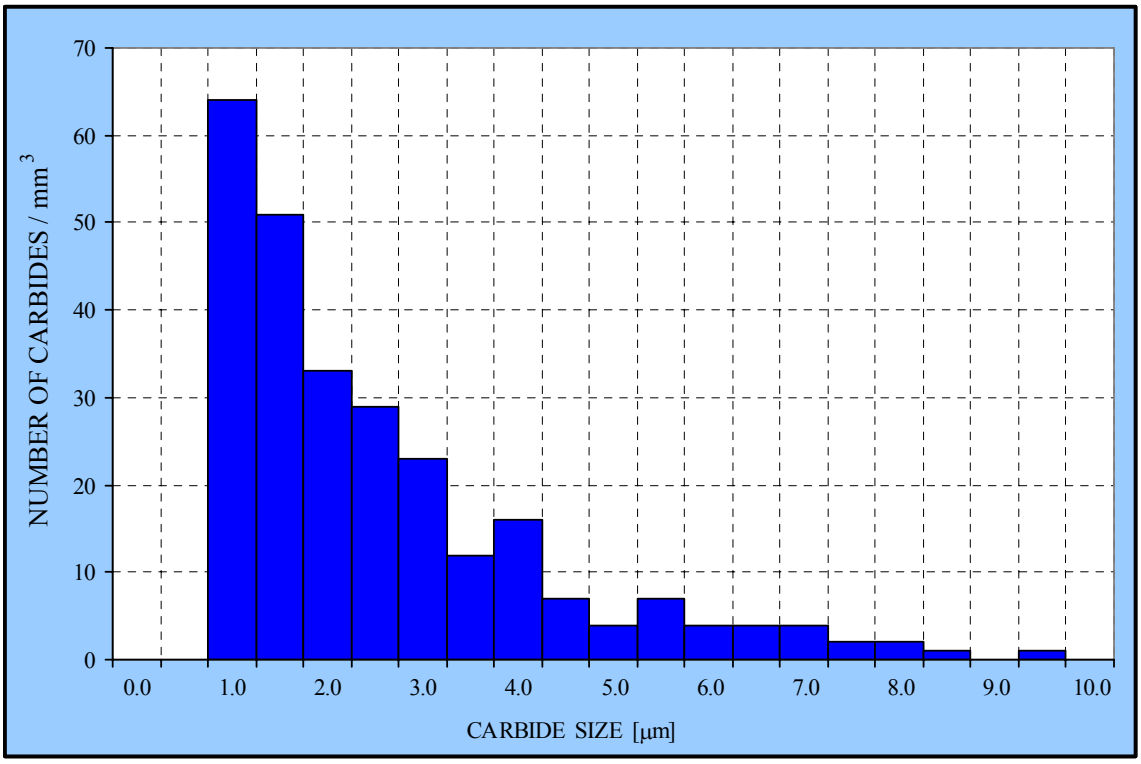

Figure 6.1 Size distribution of carbides measured with an image analyser in AISI 1008 mild steel [Lin et al. 1986a]

6.1.2. SPECIMEN GEOMETRY

The expected value of material fracture toughness was computed by simulating fracture conditions on a typical single edge notched bend test-piece (Figure 6.2). A fatigue macrocrack with a length of *12 mm* was assumed to pre-exist in the component. The geometry considered corresponds to a ratio between initial crack length and specimen width of $a_0/W = 0.6$. Fracture toughness values relative to this configuration were computed by the following formula [Ritchie *et al.*,1973]:

$$K_{IC} = \frac{Y \cdot M}{B \cdot \left(W - \tilde{a}_0\right)^{3/2}} \tag{6.1}$$

where M is the applied bending moment at failure, W and B are the specimen width and thickness respectively, Y is a calibration parameter that for $a_0/W \geq 0.6$ can be assumed equal to 4 and $\tilde{a}_0$ is the effective crack length which incorporates the effect of plasticity. In particular $\tilde{a}_0 = a_0 + r_y$, where r_y is the plastic radius given by:

$$r_y = \frac{1}{6\pi}\left(K_I / \sigma_y\right)^2 \tag{6.2}$$

For the geometry considered the bending moment M is given by $M = 1/2 \cdot l \cdot W$, where l is the fracture load.

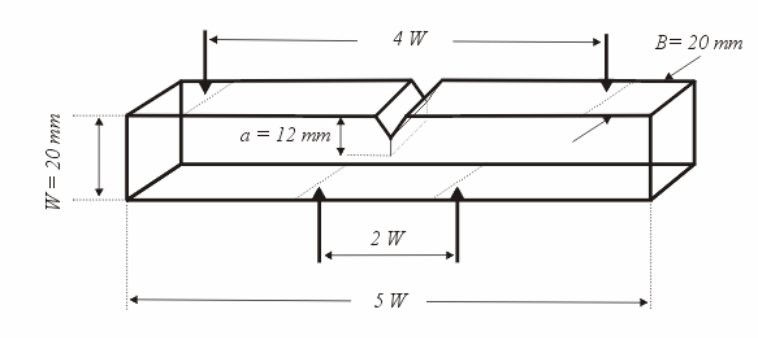

Figure 6.2 Single edge notched bend test-piece

The stress analysis ahead of the crack tip was performed through an elastic/plastic model which was already used by other authors in similar analyses [Curry and Knott, 1976]. This solution of the stress field gives the stress intensification (the ratio of maximum tensile stress to uniaxial yield stress) at a point x ahead of the crack tip as a function of the dimensionless quantity $x/(K/\sigma_y)^2$. These values were derived directly from the reference given above. The local stress obtained in this way was employed to establish if a carbide particle, randomly generated ahead of the crack tip, initiates failure. Due to its random orientation, the crack is subjected to a mixed-mode type of failure. Most of the analyses conducted in the past have applied a simple maximum normal stress criterion to determine critical conditions for crack propagation. In this study, the empirical mixed-mode fracture criterion previously discussed is employed.

6.1.3. FRACTURE TOUGHNESS RESULTS

Several levels of load were considered in the analysis and the corresponding values of fracture toughness were calculated via equation (6.1). For each load, the fraction of configurations resulting in a failure was computed and assumed as an estimate of the probability of failure. The average value of fracture toughness was then determined via numerical integration of this probability distribution. A value of *28.1 MPa·√m* was obtained, which compares reasonably well with the value of about *30 MPa·√m* measured experimentally by Lin *et al.* [1986b]. The full probability distribution of the fracture toughness is given in Figure (6.3) in terms of both cumulative distribution, *CDF*, and density function, *pdf*. The standard deviation associated with this distribution

is of *2.9 MPa·√m*. These estimates were obtained by assuming a crack shape factor, *Y*, equal to *1.27*.

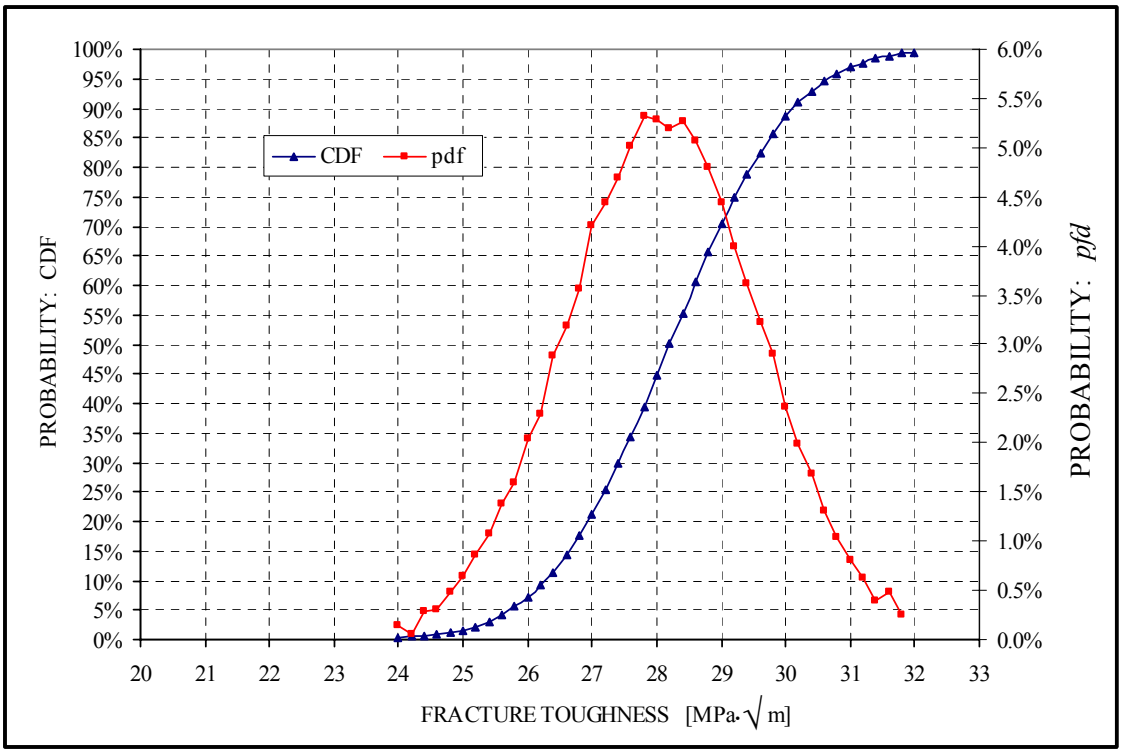

Figure 6.3 Fracture toughness distribution computed via Monte Carlo simulation

6.1.4. FRACTURE INITIATION LOCATIONS

Together with the average value of fracture toughness, the model allows one to determine the most probable point for fracture to initiate. As explained in Chapter-3, when failure locations are investigated via Monte Carlo simulation, equation (3.1) cannot be employed. On the contrary, a full simulation of the total number of flaws (modelled via a Poisson process) must be performed. This is to be able to identify the most critical cracked carbide particle among all those that could possibly trigger fracture. Sampling a single defect would allow one to compute the failure probability of the component (first by getting F_c and then plugging it into equation 3.1), but would not give information about the point at which failure is more likely to occur.

The histogram of the failures found for a 1,000 sample Monte Carlo simulation is shown in Figure (6.4). The average distance of the fracture initiation point from the crack tip was estimated to be *146.5 μm*.

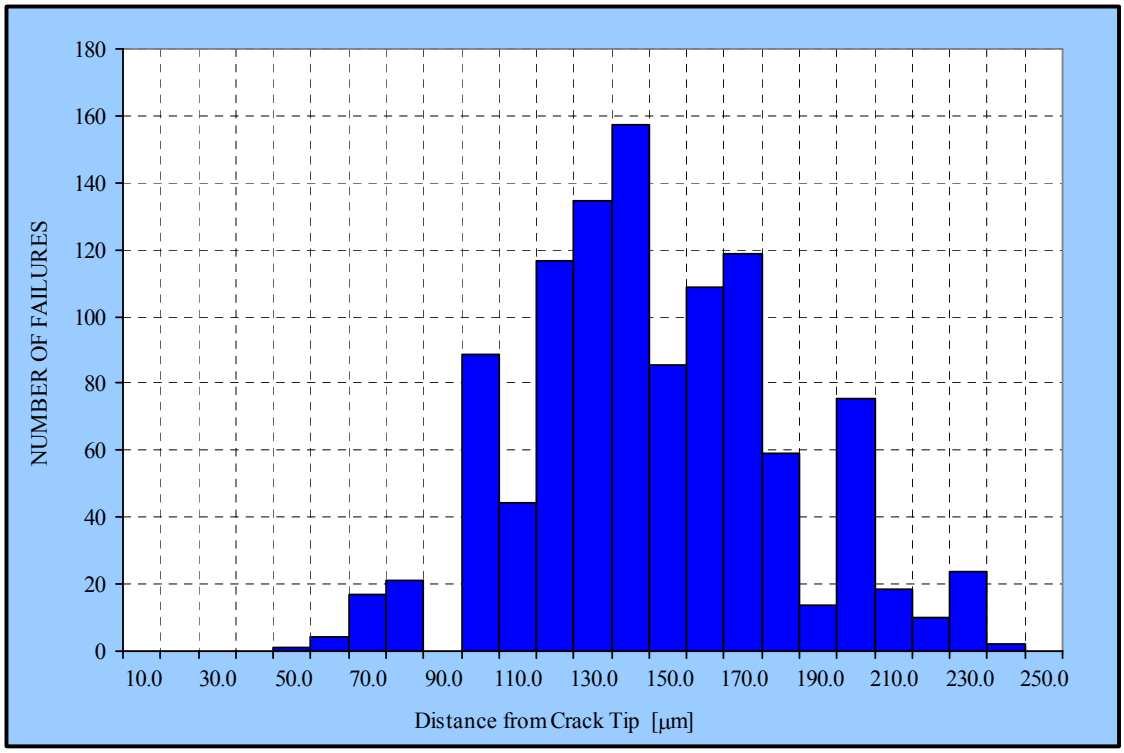

Figure 6.4 Fracture initiation locations estimated by Monte Carlo simulation

6.2. Strength Distribution of Notched Components

In engineering structures and components, notches are difficult to avoid and some notch-like geometries are necessary for structure design. Notches produce stress intensifications as well as elastic and plastic constraints, which typically result in triaxial stress states (plane strain conditions). All these factors promote cleavage fracture. The design methodology of components operating at low temperatures and presenting geometrical features which may lead to brittle fracture must reflect the statistical nature of the cleavage process. As previously discussed, brittle failure can initiate in proximity of a stress intensification feature (such as a crack or a notch), particularly when material yielding capability is limited by mechanical constraints or environmental conditions. Under these circumstances, in the case of steels, the population of microcracks nucleating at grain boundary carbide particles can cause global failure. A brief example of a component, in which the presence of severe stress intensification features considerably affects its strength properties, is presented in the next sections.

6.2.1. COMPONENT GEOMETRY AND LOADING CONDITIONS

The component considered in this analysis is a typical steel shaft for power transmission. Component's geometry is shown in Figure (6.5). The picture also shows the way the shaft is attached to its supports. The shoulders to which bearings are connected present a notch-like geometry to allow the change in shaft diameter. These parts of the component act as stress intensification features and, as it will be shortly clear, are liable to brittle fracture.

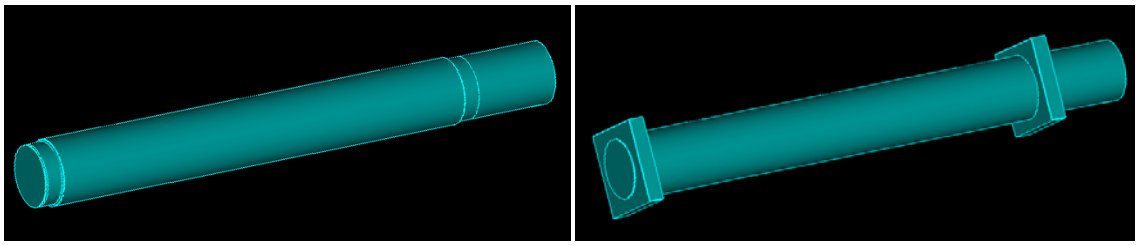

Figure 6.5 Shaft geometry (left) and displacement constraints represented by the contact surfaces between bearings and shaft shoulders (right)

A single loading condition was considered in the present investigation. This is represented by a uniform transversal force acting on one side of the lateral surface of the shaft (along the y direction). The bending moment M_x produced by this load varies from a minimum value at the central section of the shaft to a maximum at the extremities, where the constraints due to the bearings are applied. The stress in a cross section mainly comprises a normal stress in the axial direction z, together with a shear stress τ_{zy} due to the transversal force. The finite element method was used once again for the stress analysis of the body. The component was divided into a large number of tetrahedral elements whose displacement interpolation function prescribes a constant stress within each element. The displacement boundary conditions of the model were defined through contact surfaces between the bearings, assumed to be fixed in the space, and the shaft, along the shaft shoulders. This type of constrain represents a Herzian contact between the two solids (bearing-shaft) and prevents the two bodies from breaking into each other, while allows them to move apart. An axial rotation constraint was also applied to one end of the shaft to simulate the power transmission to the user.

The typical distribution of the Von Mises stress resulting from the application of a total load of *350KN*, is shown in Figure (6.6). Clearly, the most stressed regions are in proximity of the bearing connections.

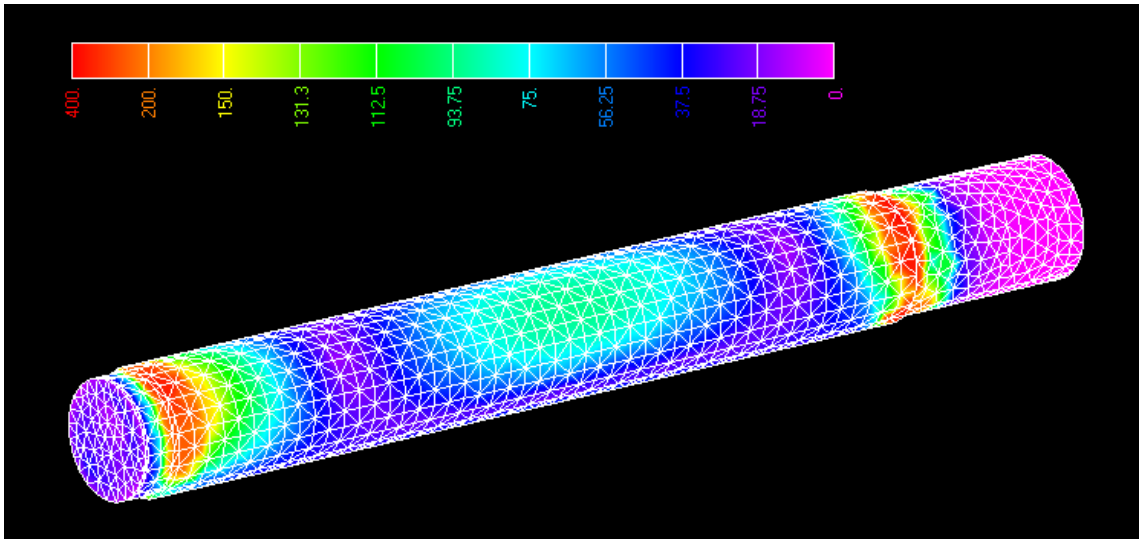

Figure 6.6 Von Mises stress distribution in a steel shaft subjected to transversal load

During the Monte Carlo simulation, the elements of the FEA mesh are randomly selected with a probability proportional to their volume. At each trial, the element selected identifies the location of the random defect and the stress experienced at this point is the stress remotely acting on the crack.

6.2.2. COMPUTATION OF THE STRENGTH DISTRIBUTION

Several finite element analyses were conducted for a transversal load varying in the range *200 – 500 kN*. A Monte Carlo simulation was then run for each of these loading conditions. Material properties are the same as those considered in the previous investigation. In particular, crack size was assumed to follow the log-normal distribution previously determined. The component strength distribution (Figure 6.7) was therefore determined for three different values of the crack shape factor, *Y*.

As seen before, the critical locations characterized by a high probability of triggering brittle fracture can be identified by the simulation procedure. Figure (6.8) shows the relative frequency of failures occurring in each element during the random generation of defects for the loading conditions considered in Figure (6.6). The spatial location of these elements in the component structure is displayed in Figure (6.9). Only a very small number of elements contribute to failure. This is a direct consequence of the high concentration of stresses that characterises this type of component.

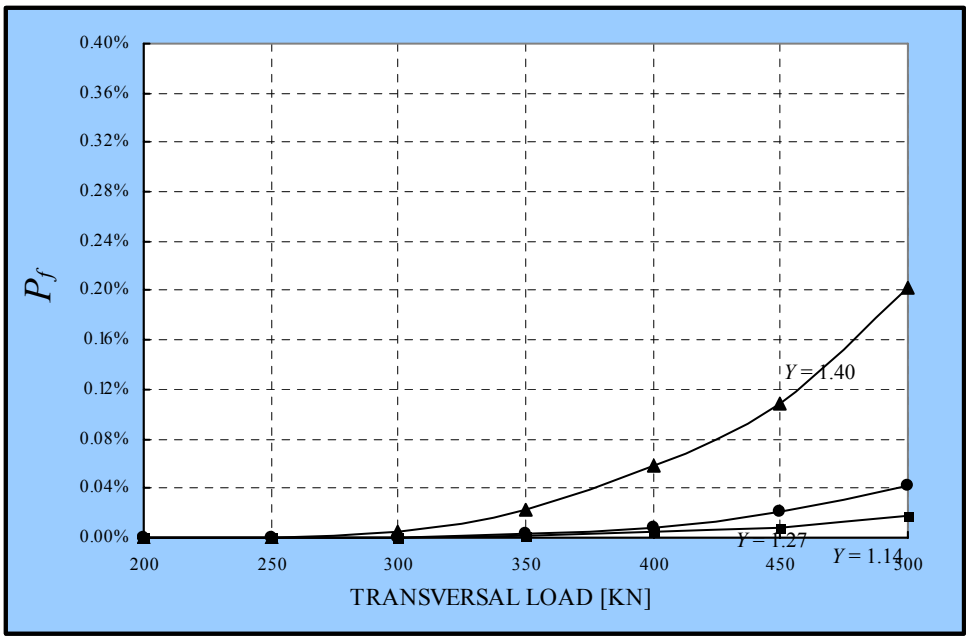

Figure 6.7 Strength distribution of a steel shaft for different values of crack shape factor

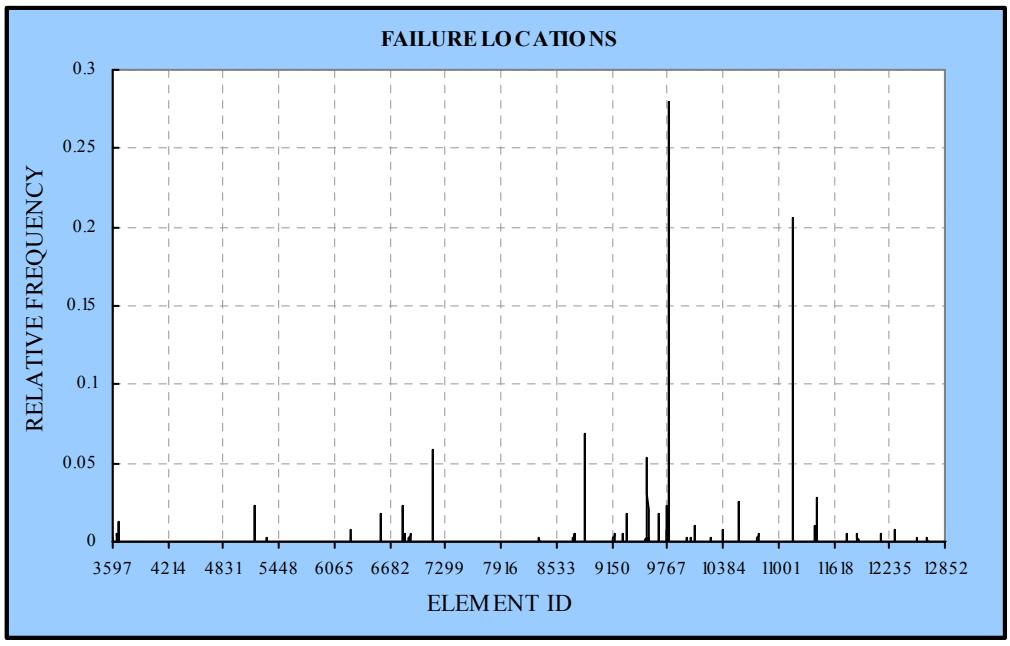

Figure 6.8 Failure locations expressed in terms of FEA element IDs

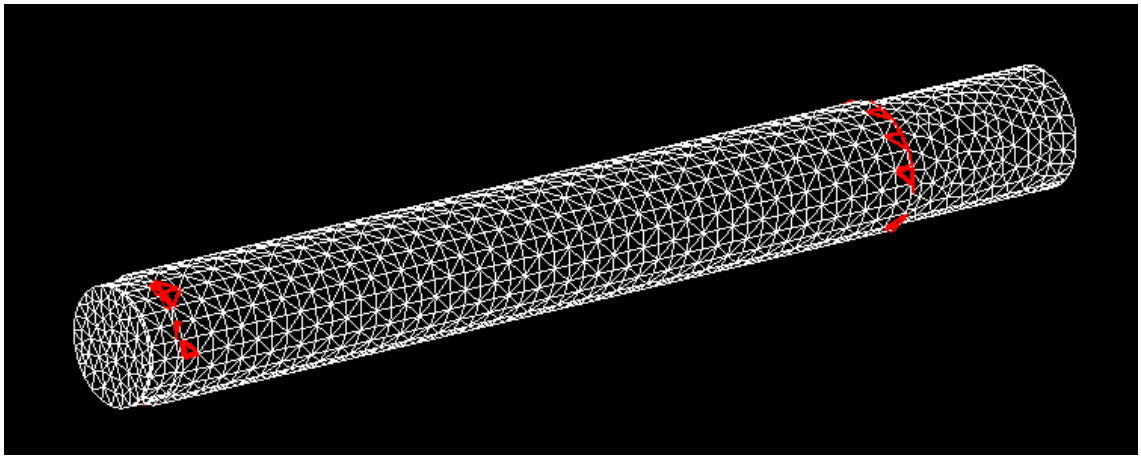

Figure 6.9 Failure locations is a steel shaft subjected to transversal load

7 CONCLUSIONS AND SUGGESTIONS FOR FURTHER WORK

7.1. Conclusions

A computer-simulation based model has been developed for determining the probability of failure initiated by random defects and applied to study the strength properties of brittle materials and components. The methodology proposed in this work can be employed by structural engineers as an effective tool to assess the reliability of brittle components, to estimate fracture strength sensitivity to changes in the main material properties and loading parameters, to identify weak spots in the component structure and to design out or modify appropriately geometrical features that are at the origin of high probabilities of failure.

Three basic steps are necessary for a full evaluation of the failure probability of a mechanical component subjected to specified loading conditions. These are:

1. The determination of material microstructural features. In particular, the mean number density and the size distribution of volume-embedded defects must be estimated. In Chapter-4, it was shown how image analysis techniques can be used for this purpose. The other material mechanical properties, such as elastic modulus and critical strain energy release rate, are assumed to be deterministic and can be found in the literature or measured by standard testing methods. A value for the flaw shape factor is not arbitrary selected among those most generally used (associated with a penny-shaped or a through-thickness crack for example), but evaluated through the calibration of the model against available experimental data of fracture stresses.

2. To compute the entire stress field produced in the component by the applied load. This operation can be performed by using analytical formula derived from the theory of elasticity, if the geometry considered is simple enough for such solutions to be applicable, or via finite element analysis for more complex configurations.

3. To import the stress analysis results into the Monte Carlo engine and run the simulation. The combined use of statistical sampling techniques with an appropriate fracture criterion allows one to estimate the individual probability of triggering fracture, F_c, which represents the failure probability given that a single defect is

present in the component. This parameter can then be substituted into equation (3.1) to calculate the total failure probability of the component.

The results obtained from the application of the proposed methodology to a series of key studies have suggested the following conclusions:

- The traditional design approach based on the maximum admissible level of the highest principal stress, or of any other equivalent stress obtained as a combination of the three principal stresses, fails to predict failure conditions for brittle materials and does not guarantee component's reliability, unless very large safety factors are applied. The limitations existing in the current methodology can be overcome by the application of a probabilistic approach which expresses component's strength as a quantity related to the probability of failure under specified loading conditions.

- The probabilistic model of brittle fracture developed in this work can be calibrated very satisfactorily to experimental data of fracture stresses by choosing an appropriate value of the crack shape factor. This parameter in used to calculate the stress intensity factors associated with all cracks belonging to the random flaw population characterising the microstructure of the material under consideration.

- Significant differences in the strength properties measured for the same component under different loading conditions (simple tension vs. 3-point bending) are attributable to what is generally known as the size effect. This term does not simply indicate that the probability of failure increases when increasing component's volume, but, most importantly, refers to the dependence of the strength distribution on the size of the area on which a given stress operates.

- Differences in the sensitivity of the strength distribution to changes in the material microstructure parameters were observed for different loading conditions. In particular, the failure probability of a component subjected to a uniform stress state is characterised by high sensitivities to variations in the COV of the crack size distribution. On the other hand, in the presence of stress gradients, the main parameter in controlling component strength properties is the average defect size.

- The application of the empirical mixed-mode fracture criterion (equation 3.13) within the Monte Carlo framework gave the best results in terms of torsional

strength. In particular, the ratio between average tensile strength and average torsional strength obtained by applying this fracture criterion was the closest to the value measured experimentally. Although this approach for predicting critical conditions for fracture initiation does not provide information about the direction of crack propagation, it is generally applicable to any crack geometry and resulted to be the most accurate in modelling crack sensitivity to the shear stress.

- The ratio between the average tensile strength and the torsional strength is practically insensitive to changes in the flaw mean size. On the other hand, an approximately linear dependence on the COV of the flaw size distribution was observed.

- The effects of stress biaxiality on failure probability are rather small for low values of the ratio between the two principal stresses $B = \sigma_2/\sigma_1$, with $\sigma_1 > \sigma_2$. In particular, when B is smaller than 0.5, the relative change in the failure probability between the uniaxial and the biaxial case observed for a fixed level of the maximum principal stress, σ_1, is less than 5%. On the other hand, for values of B above the threshold of 0.5, shifts in the biaxial strength distribution are significant and directed towards lower levels of maximum stress.

- A new failure criterion for brittle components subjected to plane stress states was proposed. The criterion is based on the maximum admissible individual probability of failure and can be applied to guarantee a target level of reliability once the defect mean number density of the material employed and the component's volume are known.

- Studying the behaviour of a ceramic turbine blade, the differences in the response to the stresses originated by blade rotation and gas pressure gradient have been analysed. The proposed approach has been used to assess critical physical parameters that affect the probability of fracture. It was also demonstrated how appropriate modifications of the component geometrical features can entail substantial improvements in terms of structural reliability.

- The results obtained from the reliability analysis of a ceramic turbine blade indicate that a significant contribution to the total probability of failure comes from a large part of the component and not only from the region of maximum stress. For this reason, it is not adequate to predict reliability based only on the most highly

stressed point, but the entire solution of the stress field must be considered in the design assessment process. The size of the volume involved in promoting failure depends on the loading conditions and the defect size variability.

- A probabilistic approach based on equation (3.1) and Monte Carlo simulation was also successfully applied to model fracture toughness variability of mild steels at low temperatures. Fracture behaviour was assumed to be controlled by a statistical population of carbide particles assimilated to volume-embedded microcracks. The stress intensification generated in proximity of a macrocrack or a notch-like geometry interacts with this flaw population until catastrophic failure is triggered by the most critical particle. The average distance from the crack tip at which fracture initiates was investigated. The strength distribution of a steel shaft subjected to a transversal load was also analysed under the same assumptions.

7.2. Suggestions for Further Work

The analysis conducted in this work has allowed the author to gain interesting insights into the fracture behaviour of brittle materials and a better understanding of the effect that random factors have on the strength properties of brittle structures. At same time however, it has highlighted the necessity for further research and offered ideas for future investigations.

The first issue that needs to be addressed concerns the mixed-mode fracture criterion employed to determine critical conditions for crack propagation. Although the empirical criterion (equation 3.13) provided satisfactory results in predicting the torsional strength of alumina cylindrical rods, its validity to general stressing conditions has still to be rigorously proved. Based on experimental evidence, it has been argued that different expressions should be employed to identify the critical combination of stresses that promotes failure, depending on the stress state analysed. In particular, a mixed-mode fracture criterion of general validity has not been developed yet. In this respect, the advantage of using a simulation based model, compared to analytical formulations, is that it allows to easily employ a different fracture criterion into the Monte Carlo algorithm without affecting other elements of the model. The most suitable criterion can then be chosen depending on personal experience and the specifics of the application.

The next step in extending the methodology proposed here would be to consider the contribution to the fracture process coming from surface flaws. In our analysis we have been concerned exclusively with volume-embedded defects. However, in some cases,

fracture is initiated at superficial defects such as scratches or corrosion induced cracks. The approach based on the combined use of equation (3.1), FEA and Monte Carlo simulation is generally applicable to any type of defect as long as the correct formulation of the stress intensity factors and the fracture criterion is employed. The probability of failure induced by superficial defects can be estimated by simply sampling random cracks across the whole component surface and checking whether they undergo unstable propagation. The resulting individual probability of failure F_c is then plugged into a equation (3.1) where the component's volume is replaced by its surface and the defect mean number density is expressed per unit area.

Multi-factor models, where two or more parameters defining crack geometry are simultaneously simulated, could also be of some interest. This approach would obviously require a much deeper knowledge of the material microstructure, but could provide a deeper understanding on how random variables control the fracture event. The difficulties in implementing such strategy mainly lie in the fact that fracture conditions under arbitrary triaxial stress states cannot be easily determined for complex crack geometries.

Finally, the methodology developed in the course of this work could be extended in the near future to include the time dimension of reliability. Fast fracture is concerned with the reliability on-demand of a structure, but it does not allow one to make predictions on the component's expected life. Time dependent reliability models would need to deal with stable crack propagation and answer to the question of if and how material properties deteriorate after several loading cycles.

REFERENCES

Anderson T. L. (2004). *Fracture Mechanics: Fundamentals and Applications*. 3rd edition, Taylor & Francis, London.

Andreasen J. H. (1993). Statistics of Brittle Failure in Multiaxial Stress States. *Journal of The American Ceramic Society,* Vol. 76, No. 11, 2933-2935.

ASTM (1989). *Annual Book of ASTM Standards*, American Society for Testing and Materials, Vol. 03.01, Philadelphia, USA, 480-504.

Barsoum M. W. (1997). *Fundamental of Ceramics*, McGraw-Hill, New York.

Batdorf S. B. and Crose J. G. (1974). A Statistical Theory for the Fracture of Brittle Structures Subjected to Nonuniform Polyaxial Stresses. *Journal of Applied Mechanics*, Vol. 41, 459-464.

Batdorf S. B. (1977). *Fundamentals of the Statistical Theory of Fracture*. In: Proceeding of the International Symposium on Fracture Mechanics of Ceramics, July 27-29, Pennsylvania State University, Vol. 3, 1-30.

Batdorf S. B. and Heinisch H. L. (1978). Fracture Statistics of Brittle Materials with Surface Cracks. *Engineering Fracture Mechanics*, Vol. 10, 831-841.

Berdin C., Cailletaud G. and Jeulin D. (1996). Brittle Failure Prediction of Ceramics Using a Multiscale Approach. *Journal of the American Ceramic Society*, Vol. 79, No. 11, 2825-2832.

Beremin F. M. (1983). A Local Criterion for Cleavage Fracture of a Nuclear Pressure Vessel Steel. *Metallurgical Transaction A*, Vol. 14A, 2277-2287.

Box G. E. and Muller M. E. (1958). A note on the generation of random normal deviates. *Annals of Mathematical Statistics,* Vol. 29, No. 2, 610-611.

Burte H. M. and Acurlo J. (1980). *The Potential for Ceramics in Aerospace Turbine Engines*. AGARD Report No. CP-276, Neuilly Sur Seine, France.

Chao L. Y. and Shetty D. K. (1990). Equivalence of Physically Based Statistical Fracture Theories for Reliability Analysis of Ceramics in Multiaxial Loading. *Journal of the American Ceramic Society*, Vol. 73, No. 7, 1917-1921.

Chao L. Y. and Shetty D. K. (1991). Reliability Analysis of Structural Ceramics Subjected to Biaxial Flexure. *Journal of the American Ceramic Society*, Vol. 74, No. 2, 333-344.

Chao L. Y. and Shetty D. K. (1992). Extreme-Value Statistics Analysis of Fracture Strengths of a Sintered Silicon Nitride Failing from Pores. *Journal of the American Ceramic Society*, Vol. 75, No. 8, 2116-2124.

Chinn R. E. (2003). *Ceramography*. John Wiley & Sons, New York.

Cranmer D. C. and Richerson D. W. (1998). *Mechanical Testing Methodology for Ceramic Design and Reliability*, Marcel Dekker INC., New York, 1-7.

Curry D. A. and Knott J. F. (1976). The Relationship Between Fracture Toughness and Microstructure in the Cleavage Fracture of Mild Steel. *Metal Science*, Vol. 10, 1-6.

Curry D. A. and Knott J. F. (1978). Effects of Microstructure on Cleavage Fracture Stress in Steel. *Metal Science*, Vol. 12, 511-514.

Curry D. A. and Knott J. F. (1979). Effect of Microstructure on Cleavage Fracture Toughness of Quenched and Tempered Steels. *Metal Science*, Vol. 15, 341-345.

DeHoff R. T. and Rhines F. N. (1968). *Quantitative Microscopy*, McGraw-Hill, New York.

Duga J. J. et al. (1983). *Economic Effects of Fracture in the Us, Part 2*: A Report to Nbs by Battelle Columbus Laboratories, Final Report.

Dukes W. H. (1966). *Handbook of Brittle Material Design Technology*, AGARD, Paris.

Erodogan F. and Sih G. C. (1963). On the Crack Extension in Plates Under Plane Loading and Transverse Shear. *Transaction of ASME, Journal of Basic Engineering*, Vol. 85, No. 4, 519-527.

Evans A. G. (1978a). Evaluation of a Fundamental Approach for the Statistical Analysis of Fracture. *Journal of the American Ceramic Society*, Vol. 61, 156-160.

Evans A. G. (1978b). A General Approach for the Statistical Analysis of Multiaxial Fracture. *Journal of the American Ceramic Society*, Vol. 61, 302-308.

Evans A. G. Biswas D. R. and Fulrath R. M. (1979a). Some Effects of Cavities on the Fracture of Ceramics: I, Cylindrical Cavities. *Journal of the American Ceramic Society*, Vol. 62, No. 1-2, 95-100.

Evans A. G. Biswas D. R. and Fulrath R. M. (1979b). Some Effects of Cavities on the Fracture of Ceramics: II, Spherical Cavities. *Journal of the American Ceramic Society*, Vol. 62, No. 1-2, 101-106.

Faira L. (1990). Economic Effects of Fracture. *Forensic Engineering*, Vol. 2, No. 1-2, 25-28.

Felbeck D. K. Orowan E. (1955). Experiments on Brittle Fracture of Steel Plates. *Welding Journal, Research Supplement*, Vol. 34, No. 11, 570-575.

Fottner, L. (1990). *Test cases for computation of internal flows in aero engine components*. , AGARD Report No. AR-275, Neuilly Sur Seine, France.

Freudenthal A. (1956). *Safety and the Probability of Structural Failure*. Transactions of the American Society of Civil Engineers, Paper No. 2843.

Freudenthal A., Garrelts J. and Shinozuka M. (1966). The Analysis of Structural Safety. *Journal of the Structural Division of the American Society of Civil Engineers,* Vol. 92, 267-325.

Gao X., Zhang G. and Srivatsan T. S. (2005). Prediction of Cleavage Fracture in Ferritic Steels: A Modified Weibull Stress Model. *Materials Science and Engineering A*, Vol. 394, 210–219.

Garrison W. M. and Moody N. M. (1987). Ductile Fracture. *Journal of Physics and Chemistry of Solids*, Vol.48, No. 11, 1035-1074.

Givli S. and Altus E. (2006). Relation Between Stochastic Failure Location and Strength in Brittle Materials. *Transactions of the ASME*, Vol. 73, 698-701.

Glasserman P. (2003). *Monte Carlo Methods in Financial Engineering*, Stochastic Modelling and Applied Probability (Vol. 53), Springer, New York.

Godse R. and Gurland J. (1989). A Statistical Model for Low Temperature Cleavage Fracture in Mild Steels. *Acta Metallurgica*, Vol. 37, No. 2, 541-548.

Griffith A. A. (1920). The Phenomena of Rupture and Flow in Solids. *Philosophical Transactions, Series A*, Vol. 221, 163-198.

Hoshide T. (1996). Strength Characteristics of Structural Ceramics. *Material Science Research International*, Vol. 2, No. 4, 220-228.

Hoshide T. and Abe J. (2003). A Statistical Approach to Strength Evaluation Incorporating Porosity Effect for Porous Ceramics. *Fatigue & Fracture of Engineering Materials & Structures*, Vol. 26, No. 5, 383-389.

Hsiung H. C., Dunn A. J., Woodling D. R. and Loh D. L. (1988). *Stress Analysis and Life Prediction of Gas Turbine Blade*, AIAA Paper 88-3218.

Hutchinson J. W. (1968). Singular Behaviour at the End of a Tensile Crack in a Hardening Material. *Journal of the Mechanics and Physics of Solids*, Vol. 16, No. 1, 13-31.

Ikeda K. and Igaki H. (1984). Fracture Criterion for Alumina Ceramics Subjected to Triaxial Stresses. *Journal of the American Ceramic Society*, Vol. 67, No. 8, 538-544.

Irwin G. R. (1957). Analysis of Stresses and Strains Near the End of a Crack Traversing a Plate. *Journal f Applied Mechanics*, Vol. 24, 361-364.

Jeal B. (1988). Moving Towards the Non-Metallic Aero Engine. *Metallurgia*, Vol. 55, No. 8, 371-374.

Kalos M. H. and Whitlock P. A. (1986). *Monte Carlo Methods*, John Wiley & Sons, New York.

Kassir M. K. and Sih G. C. (1966). Three-Dimensional Stress Distribution Around an Elliptical Crack Under Arbitrary Loadings. *Journal of Applied Mechanics*, Vol. 33, No. 3, 601-611.

Knott J. F. (1967). On Stress Intensifications in Specimens of Charpy Geometry Prior to General Yield. *Journal of the Mechanics and Physics of Solids*, Vol. 15, No. 2, 97-103.

Lamon J. and Evans A. G. (1983). Statistical Analysis of Bending Strengths for Brittle Solids: A Multiaxial Fracture Problem. *Journal of the American Ceramic Society*, Vol. 66, No. 3, 177-182.

Lamon J. (1988). Statistical Approaches to Failure for Ceramic Reliability Assessment. *Journal of the American Ceramic Society.* Vol. 71, No. 2, 106-112.

Lamon J. (1990). Ceramics Reliability: Statistical Analysis of Multiaxial Failure Using the Weibull Approach and the Multiaxial Elemental Strength Model. *Journal of the American Ceramic Society.* Vol. 73, No. 8, 2204-2212.

Lin T., Evans A. G. and Ritchie R. O. (1986a). A Statistical Model of Brittle Fracture by Transgranular Cleavage. *Journal of the Mechanics and Physics of Solids,* Vol. 34, No. 5, 477-497.

Lin T., Evans A. G. and Ritchie R. O. (1986b). A Statistical Analysis of Cleavage Fracture Ahead of Sharp Cracks and Rounded Notches. *Acta Metallurgica,* Vol. 34, No. 11, 2205-2216.

Margetson J. (1976). *A Statistical Theory of Brittle Fracture for an Anisotropic Structure Subject to a Multi-Axial Stress State*, AIAA Paper 76-632.

Marsaglia G. (1968). Random Numbers Fall Mainly in the Planes. *Proceedings of the National Academy of Sciences*, Vol. 61, 25-28.

Marsaglia G. (1972). *The Structure of Linear Congruential Generators*. In: Applications of Number Theory to Numerical Analysis, S.K. Zaremba, Academic Press, New York, 249-286.

Matthews J. R., McClintock F. A. and Shack W. J. (1976). Statistical Determination of Surface Flaw Density in Brittle Materials. *Journal of The American Ceramic Society*, Vol. 59, No. 7-8, 304-308.

McLeod S. A., Walker B. H. and Mendelson M. I. (1980). *Development of an Integral Ceramic Blade-Metal Disk with Circumferential Blade Attachment*. AGARD Report No. CP-276, Neuilly Sur Seine, France.

McMahon C. J. and Cohen J. M. (1965). Initiation of Cleavage in Polycrystalline Iron. *Acta Metallurgica*, Vol. 13, No. 6, 591-604.

Nemeth N. N., Manderscheid J. M. and Gyekenyesi (1990). *Ceramic Analysis and Reliability Evaluation of Structures (CARES).* NASA Technical Paper 2916.

Nuismer R. J. (1975). An Energy Release Rate Criterion for Mixed Mode Fracture. *International Journal of Fracture*, Vol. 11, No. 2, 245-250.

Orowan E. (1948). Fracture and Strength of Solids. *Reports on Progress in Physics*, Vol. 12, 185-232.

Otsu N. (1979). A Threshold Selection Method from Gray-Level Histograms. *IEEE Transactions on Systems, Man, and Cybernetics*, Vol. 9, No. 1, 62-66.

Paris P. C. and Sih G. C. (1965). *Stress Analysis of Cracks*. In: Fracture Toughness Testing and Its Application, American Society for Testing and Materials, Annual Meeting, 67th, Chicago, 21-26 June 1964.

Park S. K. and Miller K. W. (1988). Random Number Generators: Good Ones Are Hard to Find. *Communications of the ACM*, Vol. 32, 1192-1201.

Parzen E. (1960). *Modern Probability Theory and Its Applications*, John Wiley & Sons, New York.

Pernot F., Etienne P., Boschet F. and Datas L. (1999). Weibull Parameters and the Tensile Strength of Porous Phosphate Glass-Ceramics. *Journal of the American Ceramic Society*, Vol. 82, No. 3, 641-648.

Petch N. J. (1986). The Influence of Grain Boundary Carbide and Grain Size on the Cleavage Strength and Impact Transition Temperature of Steel. *Acta Metallurgica*, Vol. 34, No. 7, 1387-1393.

Petrovic J. J. and Stout M. G. (1981a). Fracture of Al_2O_3 in Combined Tension/Torsion: I, Experiments. *Journal of the American Ceramic Society*, Vol. 64, No.11, 656-660.

Petrovic J. J. and Stout M. G. (1981b). Fracture of Al_2O_3 in Combined Tension/Torsion: II, Weibull Theory. *Journal of the American Ceramic Society*, Vol. 64, No.11, 661-666.

Press W. H., Teukolsky S. A., Vetterling W. T. and Flannery B. P.(1992). *Numerical Recipes in C, The Art of Scientific Computing*, 2nd edition, Cambridge University Press, Cambridge.

Quinn G. D. (2003). Weibull Effective Volumes and Surfaces for Cylindrical Rods Loaded in Flexure. *Journal of the American Ceramic Society*, Vol. 86, No. 3, 475-479.

Ritchie R. O., Knott J. F. and Rice J. R. (1973). On the Relationship Between Critical Tensile Stress and Fracture Toughness in Mild Steel. *Journal of the Mechanics and Physics of Solids* , Vol. 21, 395-410.

Rufin A. C., Samos D. R. and Bollard R. J. H. (1984). Statistical Failure Prediction Models for Brittle Materials. *AIAA Journal*, Vol. 22, No. 1, 135-140.

Sih G. C. (1974). Strain-Energy-Density Factor Applied to Mixed Mode Crack Problems. *International Journal of Fracture*, Vol. 10, 305-321.

Singh D. and Shelly D. K. (1989). Fracture Toughness of Polycrystalline Ceramics in Combined Mode I and Mode II Loading. *Journal of the American Ceramic Society*, Vol. 72, No. 1, 78-84.

Schrage L. (1979). A more portable FORTRAN random number generator. *ACM Transactions on Mathematical Software*, Vol. 5, 132–138.

Stout M. G. and Petrovic J. J. (1984a). Multiaxial Loading Fracture of Al_2O_3 Tubes: I, Experiments. *Journal of the American Ceramic Society*, Vol. 67, No.1, 14-18.

Stout M. G. and Petrovic J. J. (1984b). Multiaxial Loading Fracture of Al_2O_3 Tubes: II, Weibull Theory and Analysis. *Journal of the American Ceramic Society*, Vol. 67, No.1, 18-23.

Sturmer G., Fundus M., Schulz A. and Witting S. (1991). Design of Ceramic Gas Turbine Components. *Journal of Engineering for Gas Turbines and Power*, Vol. 113, No 4, 621-627.

Suresh S. and Tschegg E. K. (1987). Combined Mode I-Mode III Fracture of Fatigue-Precracked Alumina. *Journal of the American Ceramic Society,* Vol. 70, No. 10, 726-733.

Tikare V., Choi S. R. (1993). Combined Mode I and Mode II Fracture of Monolithic Ceramics. *Journal of the American Ceramic Society*, Vol. 76, No. 9, 2265-2272.

Timoshenko S. P. (1955). *Strength of materials*. 3rd edition, Van Nostrand, Berlin.

Todinov M. T. (2000). Probability of Fracture Initiated by Defects. *Materials Science and Engineering A*, Vol. 276, No.1, 39-47.

Todinov M. T. (2005a). Limiting the Probability of Failure for Components Containing Flaws. *Computational Material Science*, Vol. 32, 156-166.

Todinov M. T. (2005b). *An Equation and a Fast Algorithm for Determining the Probability of Failure of Loaded Components Containing Flaws*. In: Proceedings of the ICOSSAR-2005 Conference, Rome, 20-23 June 2005.

Todinov M. T. (2006). Equations and a Fast Algorithm for Determining the Probability of Failure Initiated by Flaws. *International Journal of Solids and Structures*, Vol. 43, 5182-5195.

Valiente A., Ruiz J. and Elices (2005). A probabilistic model for the pearlite-induced cleavage of a plain carbon structural steel. *Engineering Fracture Mechanics*, Vol. 72, 709–728.

Wallace F. B., Harper J. E., Dins C. R., Richerson D. W. and Kington H. L. (1980). *Silicon Nitride Turbine Blade Development*. AGARD Report No. CP-276, Neuilly Sur Seine, France.

Wallin K., Saario T. and Törrönen K. (1984). Statistical Model for Carbide Induced Brittle Fracture in Steel. *Metal Science*, Vol. 18, 13-16.

Walsh R.A. (2000). *Electromechanical Design Handbook*, 3rd Edition, McGraw Hill, New York.

Wang G. Z. and Chen J. H. (2001). A Statistical Model for Cleavage Fracture in Notched Specimens of C-Mn Steel. *Fatigue and Fracture of Engineering Materials and Structures*, Vol. 24, No. 7, 451-459.

Weibull W. (1939). *A statistical Theory of the Strength of Material*. In: Ingeniors Vetenskap Akademiens, Handlinger, Stockholm, Sweden, 1939, No. 151, 1-45.

Weibull W. (1951). A statistical Distribution of Wide Applicability. *Journal of Applied Mechanics*, Vol. 18, 293-297.

Wellman G. W. (2002). *FAILPROB--A Computer Program to Compute the Probability of Failure of a Brittle Component*. Sandia Report, No. SAND2002-0409.

Zimmermann A., Hoffman M., Flinn B. D., Bordia R. K., Chuang T., Fuller E. R. and Rödel J. (1998a). Fracture of Alumina with Controlled Pores. *Journal of the American Ceramic Society*, Vol. 81, No. 9, 2449-2457.

Zimmermann A. and Rödel J. (1998b). Generalized Orowan-Petch Plot for Brittle Fracture. *Journal of the American Ceramic Society*, Vol. 81, No. 10, 2527-2532.

Zimmermann A. and Rödel J. (1999). Fracture Statistics Based on Pore/Grain-Size Interaction. *Journal of the American Ceramic Society*, Vol. 82, No. 8, 2279-2281.

APPENDICES

A.1. Random Number Generator Classes in C++

```
// Random_Sampling.h file
//***** CLASSES TO SAMPLE RANDOM VARIATES FROM SEVERAL PROBABILITY DISTRIBUTIONS **************

        //  (C) 2004 Giuseppe Iacopino
        //  PhD Student
        //  Cranfield University, SIMS
        //  Reliability Engineering and Risk Management Centre

#ifndef SAMPLING_FUNCTIONS_H
#define SAMPLING_FUNCTIONS_H
#define PI 3.141592653589
#define SQRTPI 2.506628274631
#define IA 16807
#define IM 2147483647
#define AM (1.0/IM)
#define IQ 127773
#define IR 2836
#define NTAB 32
#define NDIV (1+(IM-1)/NTAB)
#define EPS 1.2e-7
#define RNMX (1.0-EPS)
#include <math.h>
#include<vector>


//*************************************************************************************************************
//********************** THIS CLASS ALLOWS TO GENERATE UNIFORM VARIATES IN (0,1) ********************
//*************************************************************************************************************
class Random_Generator
        {
        private:
                const long int  m, m1,  m2;
                const long int a12, a13, a21, a23, q12, q13, q21, q23, r12, r13, r21, r23;
                const double Invmp1;
                static long int seed;
                static long int x10, x11, x12, x20, x21, x22;

        public:

                // CONSTRUCTOR OF THE CLASS "Random_Generator": DEFINES THE CONSTANTS IN THE GENERATOR
                // AND THE INITIAL SEED
                Random_Generator(long int initial_seed) : m(2147483647), m1(2147483647),  m2(2145483479), a12(63308),
                                                        a13(-183326), a21(86098), a23(-539608), q12(33921), q13(11714), q21(24919),
                                                q23(3976), r12(12979), r13(2883), r21(7417), r23(2071), Invmp1(4.656612873077393e-10)

                        {
                        seed = initial_seed;
                        x10 = -initial_seed;
                        x11 = (int) (1033007.0*(1712.0*x10 - ((double)m)*((int)(1712.0*x10/m))) -
                                ((double)m)*((int)(1033007.0*(1712.0*x10 - ((double)m)*((int)(1712.0*x10/m)))/m)));
                        x12 = (int) (1033007.0*(1712.0*x11 - ((double)m)*((int)(1712.0*x11/m))) -
                                ((double)m)*((int)(1033007.0*(1712.0*x11 - ((double)m)*((int)(1712.0*x11/m)))/m)));
                        x20 = (int) (1033007.0*(1712.0*x12 - ((double)m)*((int)(1712.0*x12/m))) -
                                ((double)m)*((int)(1033007.0*(1712.0*x12 - ((double)m)*((int)(1712.0*x12/m)))/m)));
                        x21 = (int) (1033007.0*(1712.0*x20 - ((double)m)*((int)(1712.0*x20/m))) -
                                ((double)m)*((int)(1033007.0*(1712.0*x20 - ((double)m)*((int)(1712.0*x20/m)))/m)));
                        x22 = (int) (1033007.0*(1712.0*x21 - ((double)m)*((int)(1712.0*x21/m))) -
                                 ((double)m)*((int)(1033007.0*(1712.0*x21 - ((double)m)*((int)(1712.0*x21/m)))/m)));
                        }


// MEBMBER FUNCTION TO UPDATE THE INITIAL SEED OF THE GENERATOR
                        void set_new_seed(long int new_seed)
                        {
```

```
                seed = new_seed;
                x10 = -new_seed;
                x11 = (int) (1033007.0*(1712.0*x10 - ((double)m)*((int)(1712.0*x10/m))) -
                        ((double)m)*((int)(1033007.0*(1712.0*x10 - ((double)m)*((int)(1712.0*x10/m)))/m)));
                x12 = (int) (1033007.0*(1712.0*x11 - ((double)m)*((int)(1712.0*x11/m))) -
                        ((double)m)*((int)(1033007.0*(1712.0*x11 - ((double)m)*((int)(1712.0*x11/m)))/m)));
                x20 = (int) (1033007.0*(1712.0*x12 - ((double)m)*((int)(1712.0*x12/m))) -
                        ((double)m)*((int)(1033007.0*(1712.0*x12 - ((double)m)*((int)(1712.0*x12/m)))/m)));
                x21 = (int) (1033007.0*(1712.0*x20 - ((double)m)*((int)(1712.0*x20/m))) -
                        ((double)m)*((int)(1033007.0*(1712.0*x20 - ((double)m)*((int)(1712.0*x20/m)))/m)));
                x22 = (int) (1033007.0*(1712.0*x21 - ((double)m)*((int)(1712.0*x21/m))) -
                         ((double)m)*((int)(1033007.0*(1712.0*x21 - ((double)m)*((int)(1712.0*x21/m))))/m)));
                }

                // "real_random()" AND "real_random_ecuyer()" ARE TWO MEMBER FUNCTIONS THAT RETURN
                // VARIATES UNIFORMLY DISTRIBUTED IN (0,1)
                double real_random(), real_random_ecuyer();

                double display_seed() {return seed;}

        };

//*** INITIALISE STATIC MEMBERS **********
long Random_Generator::seed = 0;
long Random_Generator::x10  = 0;
long Random_Generator::x11  = 0;
long Random_Generator::x12  = 0;
long Random_Generator::x20  = 0;
long Random_Generator::x21  = 0;
long Random_Generator::x22  = 0;


//******* MEMBER FUNCTION TO GENERATE UNIFORM RANDOM NUMBERS IN (0,1) ********
//******* ACCORDING TO PARK &  MILLER GENERATOR **********************************
//* FROM: NUMERICAL RECIPES IN C, P. TEUKOLSKY et al., CAMBRIDGE UNIVERSITY PRESS, 1992
        double Random_Generator:: real_random()
        {
                int j;
                long k;
                static long iy=0;
                static std::vector<long int> iv(NTAB);
                double temp;
                 if (seed <= 0 || !iy)                          //INITIALIZE
                        {
                        if (- seed < 1) seed=1;                 //BE SURE TO PREVENT SEED = 0
                         else seed = -seed;
                        for (j=NTAB+7;j>=0;j--)                 //LOAD THE SHUFFLEE TABLE (AFTER 8 WARM-UPS)
                                {
                                k=seed/IQ;
                                seed=IA*(seed-k*IQ)-IR*k;
                                if (seed < 0) seed += IM;
                                if (j < NTAB) iv[j] = seed;
                                }
                        iy=iv[0];
                        }

                k=seed/IQ;                                      //START HERE WHEN NOT INITIALIZING
                seed=IA*(seed-k*IQ)-IR*k;
                if (seed < 0) seed += IM;
                j=iy/NDIV;                                      //WILL BE IN THE RANGE 0 TO NTAB-1
                iy=iv[j];                               //OUTPUT PREVIOUSLY STORED VALUE AND REFILL THE SHUFFLE TABLE
                iv[j] = seed;
                if ((temp=AM*iy) > RNMX) return RNMX;       //BECAUSE USERS DON'T EXPECT ENDPOINT VALUES
                else return temp;
                }

//******* MEMBER FUNCTION TO GENERATE UNIFORM RANDOM NUMBERS IN (0,1) *********
//******* ACCORDING TO ECUYER GENERATOR ***************************************
        double Random_Generator:: real_random_ecuyer()
                {
                long int h, p12, p13, p21, p23;

                h=x10/q13; p13= -a13*(x10-h*q13)-h*r13;
```

```
        h=x11/q12; p12= a12*(x11-h*q12)-h*r12;
        if(p13<0) p13=p13+m1; if(p12<0) p12=p12+m1;
        x10=x11; x11=x12; x12= p12-p13; if(x12<0) x12=x12+m1;

        h=x20/q23; p23= -a23*(x20-h*q23)-h*r23;
        h=x22/q21; p21= a21*(x22-h*q21)-h*r21;
        if(p23<0) p23=p23+m2; if(p21<0) p21=p21+m2;
        x20=x21; x21=x22; x22= p21-p23; if(x22<0) x22=x22+m2;

        if(x12<x22) return (double)(x12-x22+m1)*Invmp1; else return (double)(x12-x22)*Invmp1;
        }

//*************************************************************************************************
//*************************************************************************************************
```

```
//*************************************************************************************************
//************* THIS CLASS ALLOWS TO GENERATE RANDOM UNIVARIATES ACCORDING TO NORMAL *********
//************* LOGNORMAL AND OTHER DISTRIBUTIONS, USING PARK & MILLER GENERATOR **************
//*************************************************************************************************
class Sampling
	{
	private:
		const double pi;
		const double sqrt_2_pi;
		Random_Generator generator_1;
	public:
		Sampling(long int first_seed);
		void set_new_seed(long int new_seed);
		double Normal_pdf(double, double, double);
		double LogNormal_pdf(double, double, double);
		double Normal_Generator(double, double);
		double LogNormal_Generator(double, double);
		int Poisson_Process(double, double);
	};

//*************** CONSTRUCTOR OF THE CLASS "Sampling": DEFINES THE INITIAL SEEDS **********************
//*************** OF THE RANDOM GENERATORS AND OTHER CONSTANTS ************************************
	Sampling::Sampling(long int first_seed) : generator_1(first_seed), pi(3.14159), sqrt_2_pi(sqrt(2*pi))
							{}

//***** MEBMBER FUNCTION TO UPDATE INITIAL SEEDS OF THE GENERATOR *****
	void Sampling::set_new_seed(long int new_seed)
		{
		generator_1.set_new_seed(new_seed);
		}

//***** MEMBER FUNCTION THAT RETURNS THE PDF OF A NORMAL DISTRIBUTION *****
	double Sampling::Normal_pdf(double x, double mean, double deviation)
		{
		double pdf;
		pdf=(1/(sqrt_2_pi*deviation))*exp(-(pow((x-mean),2)/(2*pow(deviation,2))));
		return pdf;
		}

//***** MEMBER FUNCTION THAT RETURNS THE PDF OF A LOG-NORMAL DISTRIBUTION *****
	double Sampling::LogNormal_pdf(double x, double mu, double sigma)
		{
		double pdf;
		pdf=(1/(sqrt_2_pi*sigma*x))*exp(-(pow((log(x)-mu),2)/(2*pow(sigma,2))));
		return pdf;
		}

//*********** MEMBER FUNCTION TO GENERATE NORMAL VARIATES *****
//* FROM: NUMERICAL RECIPES IN C, P. TEUKOLSKY et al., CAMBRIDGE UNIVERSITY PRESS, 1992
	double Sampling::Normal_Generator(double mean, double deviation)
		{
		static int iset=0;
		static double gset;
		double fac,rsq,v1,v2;
		if (iset == 0 || generator_1.display_seed() < 0)	//WE DON'T HAVE AN EXTRA DEVIATE, OR IT'S FIRST RUN
			{
			do {
				v1=2.0* generator_1.real_random()-1.0;		//PICK TWO UNIFORM NUMBERS
				v2=2.0* generator_1.real_random()-1.0;
				rsq=v1*v1+v2*v2;				//SEE IF THEY ARE IN THE UNIT CIRCLE
				}
			while (rsq >= 1.0 || rsq == 0.0);	//AND IF THEY ARE NOT, TRY AGAIN
			fac=sqrt(-2.0*log(rsq)/rsq);		//MAKE BOX-MULLER TRANSFORMATION TO GET NORMAL
DEVIATES
			gset=v1*fac;
			iset=1;					//SET FLAG.
			return (mean+deviation*v2*fac);
			}
		else						//WE HAVE AN EXTRA DEVIATE HANDY
			{
			iset=0;					//SO UNSET THE FLAG
			return (mean+deviation*gset);		//AND RETURN IT
			}
```

```
        }

//******** MEMBER FUNCTION TO GENERATE LOG-NORMAL VARIATES *****
    double Sampling::LogNormal_Generator(double mu, double sigma)
        {
        double standard;
        double variate;
        standard = Normal_Generator(0.0, 1.0);
        variate = exp(standard*sigma+mu);

        return variate;
        }

//********** MEMBER FUNCTION TO GENERATE THE NUMBER OF OCCURRENCES **************************
//********** OF AN EVENT FOLLOWING A HOMOGENEOUS POISSON PROCESS ********************************
    int Sampling::Poisson_Process(double density, double limit)
        {
        int n=0;
        double x;

        x = -((1/density)*log(generator_1.real_random()));
        while (x<=limit)
            {
            n++;
            x = x - ((1/density)*log(generator_1.real_random()));
            }
        return n;
        }

//*************************************************************************************************
//*************************************************************************************************
```

```
//*****************************************************************************************************
//************* THIS CLASS ALLOWS TO GENERATE RANDOM UNIVARIATES ACCORDING TO NORMAL *********
//************* LOGNORMAL AND OTHER DISTRIBUTIONS, USING ECUYER GENERATOR *********************
//*****************************************************************************************************
class Sampling_Ecuyer
	{
	private:
		const double pi;
		const double sqrt_2_pi;
		Random_Generator generator_ecu1;
	public:
		Sampling_Ecuyer(long int first_seed);
		void set_new_seed(long int new_seed);
		double Normal_pdf(double, double, double);
		double LogNormal_pdf(double, double, double);
		double Normal_Generator(double, double);
		double LogNormal_Generator(double, double);
		int Poisson_Process(double, double);
	};


//*************** CONSTRUCTOR OF THE CLASS "Sampling_Ecuyer": DEFINES THE INITIAL SEEDS ***************
//*************** OF THE RANDOM GENERATORS AND OTHER CONSTANTS ************************************
	Sampling_Ecuyer::Sampling_Ecuyer(long int first_seed) : generator_ecu1(first_seed), pi(3.14159), sqrt_2_pi(sqrt(2*pi))
                                                                {}


//***** MEBMBER FUNCTION TO UPDATE INITIAL SEEDS OF THE GENERATOR *****
	void Sampling_Ecuyer::set_new_seed(long int new_seed)
		{
		generator_ecu1.set_new_seed(new_seed);
		}

//******** MEMBER FUNCTION THAT RETURNS THE PDF OF A NORMAL DISTRIBUTION *****
	double Sampling_Ecuyer::Normal_pdf(double x, double mean, double deviation)
		{
		double pdf;
		pdf=(1/(sqrt_2_pi*deviation))*exp(-(pow((x-mean),2)/(2*pow(deviation,2))));
		return pdf;
		}

//***** MEMBER FUNCTION THAT RETURNS THE PDF OF A LOG-NORMAL DISTRIBUTION *****
	double Sampling_Ecuyer::LogNormal_pdf(double x, double mu, double sigma)
		{
		double pdf;
		pdf=(1/(sqrt_2_pi*sigma*x))*exp(-(pow((log(x)-mu),2)/(2*pow(sigma,2))));
		return pdf;
		}

//*********** MEMBER FUNCTION TO GENERATE NORMAL VARIATES *********************
//* FROM: NUMERICAL RECIPES IN C, P. TEUKOLSKY et al., CAMBRIDGE UNIVERSITY PRESS, 1992
	double Sampling_Ecuyer::Normal_Generator(double mean, double deviation)
		{
		static int iset=0;
		static double gset;
		double fac,rsq,v1,v2;
		if (iset == 0)                                  //WE DON'T HAVE AN EXTRA DEVIATE, OR IT'S FIRST RUN
			{
			do {
				v1=2.0* generator_ecu1.real_random_ecuyer()-1.0;          //PICK TWO UNIFORM NUMBERS
				v2=2.0* generator_ecu1.real_random_ecuyer()-1.0;
				rsq=v1*v1+v2*v2;                                  //SEE IF THEY ARE IN THE UNIT CIRCLE
				}
			while (rsq >= 1.0 || rsq == 0.0);       //AND IF THEY ARE NOT, TRY AGAIN
			fac=sqrt(-2.0*log(rsq)/rsq);            //MAKE BOX-MULLER TRANSFORMATION TO GET NORMAL
DEVIATES
			gset=v1*fac;
			iset=1;                                 //SET FLAG.
			return (mean+deviation*v2*fac);
			}
		else                                            //WE HAVE AN EXTRA DEVIATE HANDY
			{
			iset=0;                                 //SO UNSET THE FLAG
```

```
                return (mean+deviation*gset);          //AND RETURN IT
                }
        }

//********** MEMBER FUNCTION TO GENERATE LOG-NORMAL VARIATES ***************
        double Sampling_Ecuyer::LogNormal_Generator(double mu, double sigma)
                {
                double standard;
                double variate;
                standard = Normal_Generator(0.0, 1.0);
                variate = exp(standard*sigma+mu);

                return variate;
                }

//********** MEMBER FUNCTION TO GENERATE THE NUMBER OF OCCURRENCES ***************************
//********** OF AN EVENT FOLLOWING A HOMOGENEOUS POISSON PROCESS *********************************
        int Sampling_Ecuyer::Poisson_Process(double density, double limit)
                {
                int n=0;
                double x;

                x = -((1/density)*log(generator_ecu1.real_random_ecuyer()));
                while (x<=limit)
                        {
                        n++;
                        x = x - ((1/density)*log(generator_ecu1.real_random_ecuyer()));
                        }
                return n;
                }

//*************************************************************************************************************
//*************************************************************************************************************

#endif
```

A.2. FEA Results Import Classes in C++

```
// FEA_Library.h file
//*********** CLASS TO READ AND PROCESS FEA INPUT AND OUTPUT DATA FROM NASTRAN FILES ***********

	//  (C) 2004 Giuseppe Iacopino
	//  PhD Student
	//  Cranfield University, SIMS
	//  Reliability Engineering and Risk Management Centre

#ifndef FEA_LIBRARY_H
#define FEA_LIBRARY_H
#include <stdio.h>
#include <stdlib.h>
#include <string.h>
#include <math.h>

//*************************************************************************************************************
//************** THIS CLASS REPRESENTS A PLANE IN THE THREE-DIMENSIONAL SPACE *********************
//*************************************************************************************************************
	class Plane
		{
		double temp;
			public:
				int Find_Coefficients();
				double a, b, c, d;
				double x1, y1, z1, x2, y2, z2, x3, y3, z3;
		};

// *** THIS FUNCTION FINDS THE PLANE (of equation aX+bY+cZ+d=0) PASSING THROUGH 3 GIVEN POINTS
// WITH COORDINATES (x1,y1,z1); (x2,y2,z2); (x3,y3,z3)) ***********************************************
	int Plane::Find_Coefficients()
		{
		if(z1==z2)
			{
			temp=z2; z2=z3; z3=temp;
			temp=x2; x2=x3; x3=temp;
			temp=y2; y2=y3; y3=temp;
			}
		if((z1!=z2)&&(((y3-y1)-(y2-y1)*(z3-z1)/(z2-z1))!=0))
			{
			a=1;
			temp=((y3-y1)-(y2-y1)*(z3-z1)/(z2-z1));
			b=((x1-x3)-(x1-x2)*(z3-z1)/(z2-z1))/temp;
			c=((x1-x2)-(y2-y1)*b)/(z2-z1);
			d=(-x1-y1*b-z1*c);
			}
		else
			{
			if(z1==z2)
				{
				a=0; b=0;
				if(((y2-y1)/(x2-x1))!=((y3-y2)/(x3-x2))) {c=1; d=-z1;}
				else
					{
					printf("IMPOSSIBLE TO FIND A PLANE CONTAINING THE THREE POINTS GIVEN\n");
					return 0;                                          // RETURN 0 IF THERE IS A PROBLEM
					}
				}
			else
				{
				a=0; b=1;
				c=(y1-y2)/(z2-z1);
				d=-y1-c*z1;
				}
			}
		return 1;                                                      // RETURN 1 IF EVERYTHING IS OK
		}
//*************************************************************************************************************
//*************************************************************************************************************
```

```
//*************************************************************************************************************
//** THIS CLASS ALLOWS TO READ ALL NECESSARY INFORMATION FROM NASTRAN INPUT AND OUTPUT FILES*
//**** INPUT FILE MUST BE GENERATED WITH THE MESHING AND POST-PROCESSING APPLICATION FEMAP ****
//*************************************************************************************************************
	class Nastran
		{
		Plane normal_plane;

		void input_file_name(void);
		void output_file_name(void);
		int Number_Of_Nodes(void);
		int Number_Of_Elements(void);
		void Read_Input_Data(void);
		void Read_Output_Data(void);
		double Element_Volume(int);
		int *node_ID, *element_ID_input, *element_ID_output;
		double  *node_X, *node_Y, *node_Z;

			public:
				Nastran();
				char nastran_input_file_name[255];
				char nastran_output_file_name[255];
				int number_of_nodes, number_of_elements;
				int *element_ID, *element_node_1, *element_node_2, *element_node_3, *element_node_4;
				double *node_1_X, *node_1_Y, *node_1_Z,*node_2_X, *node_2_Y, *node_2_Z,*node_3_X, *node_3_Y,
					*node_3_Z,*node_4_X, *node_4_Y, *node_4_Z ;
				double *x_max, *x_min, *y_max, *y_min, *z_max, *z_min;
				double *principal_stress_A, *principal_stress_B, *principal_stress_C;
				double *cos_dir_Ax, *cos_dir_Ay, *cos_dir_Az;
				double *cos_dir_Bx, *cos_dir_By, *cos_dir_Bz;
				double *cos_dir_Cx, *cos_dir_Cy, *cos_dir_Cz;
				double *element_volume, *element_volume_fraction, *sum_element_volume_fraction;
				double total_volume, max_x, min_x, max_y, min_y, max_z, min_z;
				void Process_Data();
				~Nastran();
		};

//*** CLASS CONSTRUCTOR ***
	Nastran::Nastran()
		{
		Process_Data();
		}

	//*** FUNCTION TO INPUT THE NAME OF THE NASTRAN INPUT FILE THAT HAS TO BE READ ***
	void Nastran::input_file_name()
		{
		printf("\n\n\nInsert the name of the NASTRAN input file\n");
		gets(nastran_input_file_name);
		}

	//*** FUNCTION TO INPUT THE NAME OF THE NASTRAN OUTPUT FILE THAT HAS TO BE READ ***
	void Nastran::output_file_name()
		{
		printf ("\nInsert the name of the NASTRAN output file\n");
		gets (nastran_output_file_name);
		}

	//*** FUNCTION TO COUNT THE NUMBER OF NODES IN THE FEA MODEL IMPORTED***
	int Nastran::Number_Of_Nodes()
		{
		char sentence_check[255]="GRID";
		int n=0;
		char *pt, buffer[255];

		FILE *f_input;
		f_input=fopen(nastran_input_file_name,"r");
		if(f_input==NULL){	printf("Cannot open the .NAS file!\n\n\n");
					scanf("%*c");
					exit(EXIT_FAILURE);
					}

		while ((pt = fgets(buffer, 255, f_input)) != NULL)
			{
```

```
		if (strncmp(buffer, sentence_check, 4)==0)
			{
			n++;
			}
		}
	fclose(f_input);
	return n;
	}

//*** FUNCTION TO COUNT THE NUMBER OF TETRAHEDRICAL ELEMENTS IN THE FEA MODEL IMPORTED***
int Nastran::Number_Of_Elements()
	{
	int n=0;
	char *pt, buffer[255];
	char sentence_check[255]="CTETRA";

	FILE *f_input;
	f_input=fopen(nastran_input_file_name,"r");
	if(f_input==NULL){	printf("Cannot open the .NAS file!\n\n\n");
				scanf("%*c");
				exit(EXIT_FAILURE);
				}

	while ((pt = fgets(buffer, 255, f_input)) != NULL)
		{
		if (strncmp(buffer, sentence_check, 6)==0)

			{
			n++;
			}
		}
	fclose(f_input);
	return n;
	}

//*** FUNCTION TO READ NODE AND ELEMENT GEOMETRICAL DATA FROM THE FEA MODEL IMPORTED***
// IT READS: node_ID, node_COORDINATES, element_ID, element_nodes ************************************
void Nastran::Read_Input_Data()
	{
	char sentence_check1[255]="GRID";
	char sentence_check2[255]="CTETRA";
	char string_read[255], *pt, bin[255], char_zero[1];
	double zero, data1, data2, data3;
	int data_int_1, data_int_2, data_int_3, data_int_4, data_int_5;

	FILE *f_input;
	f_input=fopen(nastran_input_file_name,"r");
	if(f_input==NULL){	printf("Cannot open the .NAS file!/n");
				scanf("%*c");
				exit(EXIT_FAILURE);
				}

	node_ID = new int[number_of_nodes];
	node_X = new double[number_of_nodes];
	node_Y = new double[number_of_nodes];
	node_Z = new double[number_of_nodes];
	element_ID_input = new int[number_of_elements];
	element_node_1 = new int[number_of_elements];
	element_node_2 = new int[number_of_elements];
	element_node_3 = new int[number_of_elements];
	element_node_4 = new int[number_of_elements];
	while ((pt = fgets(string_read, 255, f_input)) != NULL)
		{
		if (strncmp(string_read, sentence_check1, 4)==0)
			{
			sscanf (string_read,"%s%d%c%c%c%c%c%c%c%c%lf%lf%lf", &bin, &data_int_1, &char_zero, &char_zero,
				&char_zero, &char_zero, &char_zero, &char_zero, &char_zero, &char_zero, &data1, &data2
,&data3);
			*node_ID = data_int_1;
			*node_X = data1;
			*node_Y = data2;
			*node_Z = data3;
			node_ID++;
```

```
                node_X++;
                node_Y++;
                node_Z++;
                }
        if (strncmp(string_read, sentence_check2, 6)==0)
                {
                sscanf (string_read,"%s%d%lf%d%d%d%d", &bin, &data_int_1, &zero, &data_int_2, &data_int_3,
                        &data_int_4, &data_int_5);
                *element_ID_input = data_int_1;
                *element_node_1 = data_int_2;
                *element_node_2 = data_int_3;
                *element_node_3 = data_int_4;
                *element_node_4 = data_int_5;
                element_ID_input++;
                element_node_1++;
                element_node_2++;
                element_node_3++;
                element_node_4++;
                }
        }
    node_ID -= number_of_nodes;
    node_X -= number_of_nodes;
    node_Y -= number_of_nodes;
    node_Z -= number_of_nodes;
    element_ID_input -= number_of_elements;
    element_node_1 -= number_of_elements;
    element_node_2 -= number_of_elements;
    element_node_3 -= number_of_elements;
    element_node_4 -= number_of_elements;
    fclose(f_input);
    }

//*** FUNCTION TO READ TETRAHEDRICAL ELEMENT RESULT DATA FROM THE FEA MODEL IMPORTED***
// IT READS: element_ID, principal_stresses (AT THE CENTRE OF THE ELEMENT), cos_dir (DIRECTORIAL COSINES
//                  OF THE PRINCIPAL AXES) ***************************************************************
void Nastran::Read_Output_Data()
    {
    char sentence_check1[255]="                S T R E S S E S";
    char sentence_check2[255]="  ELEMENT-ID    ";
    char sentence_check3[255]="                      Z";
    char sentence_check4[255]="0GRID CS 10 GP";
    char sentence_check5[255]="0              CENTER  ";
    char  buffer[255], string_read[255], *pt, bin[255];
    int dato_int1;
    double zero, dato1, dato2, dato3, dato4;

    FILE *f_output;
    f_output=fopen(nastran_output_file_name,"r");
    if(f_output==NULL){    printf("Cannot open the .f06 file!/n");
                        scanf("%*c");
                        exit(EXIT_FAILURE);
                        }

    element_ID_output = new int[number_of_elements];

    principal_stress_A = new double[number_of_elements];
    principal_stress_B = new double[number_of_elements];
    principal_stress_C = new double[number_of_elements];

    cos_dir_Ax = new double[number_of_elements];
    cos_dir_Ay = new double[number_of_elements];
    cos_dir_Az = new double[number_of_elements];

    cos_dir_Bx = new double[number_of_elements];
    cos_dir_By = new double[number_of_elements];
    cos_dir_Bz = new double[number_of_elements];

    cos_dir_Cx = new double[number_of_elements];
    cos_dir_Cy = new double[number_of_elements];
    cos_dir_Cz = new double[number_of_elements];

    while ((pt = fgets(buffer, 255, f_output)) != NULL)
        {
```

```
if (strncmp(buffer, sentence_check1, 33)==0)
        {
        pt = fgets(string_read, 255, f_output);
        while (string_read[0]!='1')
                {
                pt = fgets(string_read, 255, f_output);
                if ((strncmp(string_read, sentence_check2, 16)==0)||(strncmp(string_read, sentence_check3, 26)==0))
                        {
                        pt = fgets (string_read, 255,f_output);
                        if ((string_read[22]==sentence_check4[0]) && (string_read[23]==sentence_check4[1]) &&
                            (string_read[24]==sentence_check4[2]) && (string_read[25]==sentence_check4[3]))
                                {
                                sscanf (string_read,"%lf%d",&zero, &dato_int1);
                                *element_ID_output = dato_int1;
                                fgets (string_read, 255,f_output);
                                }
                        if((strncmp(string_read, sentence_check5, 22)==0))
                                {
                                sscanf (string_read,"%lf%s%s%lf%s%lf%s%lf%s%lf%lf%lf",&zero, &bin, &bin, &zero,
                                        &bin, &zero, &bin, &dato1, &bin, &dato2, &dato3 ,&dato4);
                                *principal_stress_A = dato1;
                                *cos_dir_Ax = dato2;
                                *cos_dir_Bx = dato3;
                                *cos_dir_Cx         = dato4;

                                fgets (string_read, 255,f_output);
                                sscanf (string_read,"%s%lf%s%lf%s%lf%s%lf%lf%lf", &bin, &zero, &bin, &zero, &bin,
                                        &dato1, &bin, &dato2, &dato3 ,&dato4);

                                *principal_stress_B = dato1;
                                *cos_dir_Ay = dato2;
                                *cos_dir_By = dato3;
                                *cos_dir_Cy         = dato4;

                                fgets (string_read, 255,f_output);
                                sscanf (string_read,"%s%lf%s%lf%s%lf%s%lf%lf%lf", &bin, &zero, &bin, &zero, &bin,
                                                &dato1, &bin, &dato2, &dato3 ,&dato4);

                                *principal_stress_C = dato1;
                                *cos_dir_Az = dato2;
                                *cos_dir_Bz = dato3;
                                *cos_dir_Cz         = dato4;

                                element_ID_output++;

                                principal_stress_A++;
                                principal_stress_B++;
                                principal_stress_C++;

                                cos_dir_Ax++;
                                cos_dir_Ay++;
                                cos_dir_Az++;

                                cos_dir_Bx++;
                                cos_dir_By++;
                                cos_dir_Bz++;

                                cos_dir_Cx++;
                                cos_dir_Cy++;
                                cos_dir_Cz++;
                                }
                        }
                }
        }

element_ID_output -= number_of_elements;

principal_stress_A -= number_of_elements;
principal_stress_B -= number_of_elements;
principal_stress_C -= number_of_elements;

cos_dir_Ax -= number_of_elements;
```

```
        cos_dir_Ay -= number_of_elements;
        cos_dir_Az -= number_of_elements;

        cos_dir_Bx -= number_of_elements;
        cos_dir_By -= number_of_elements;
        cos_dir_Bz -= number_of_elements;

        cos_dir_Cx -= number_of_elements;
        cos_dir_Cy -= number_of_elements;
        cos_dir_Cz -= number_of_elements;

        fclose(f_output);
        }

//********** FUNCTION TO CALCULATE TETRAHEDRICAL ELEMENT VOLUME ****************
double Nastran::Element_Volume(int k)
        {
        double side_1, side_2, side_3, distance, semiperimeter, area, volume;

        element_ID[k];
        side_1= sqrt(pow((node_2_X[k]-node_3_X[k]),2)+pow((node_2_Y[k]-node_3_Y[k]),2)+pow((node_2_Z[k]-
                        node_3_Z[k]),2));
        side_2= sqrt(pow((node_3_X[k]-node_4_X[k]),2)+pow((node_3_Y[k]-node_4_Y[k]),2)+pow((node_3_Z[k]-
                        node_4_Z[k]),2));
        side_3= sqrt(pow((node_4_X[k]-node_2_X[k]),2)+pow((node_4_Y[k]-node_2_Y[k]),2)+pow((node_4_Z[k]-
                        node_2_Z[k]),2));

        normal_plane.x1 = node_2_X[k];
        normal_plane.y1 = node_2_Y[k];
        normal_plane.z1 = node_2_Z[k];
        normal_plane.x2 = node_3_X[k];
        normal_plane.y2 = node_3_Y[k];
        normal_plane.z2 = node_3_Z[k];
        normal_plane.x3 = node_4_X[k];
        normal_plane.y3 = node_4_Y[k];
        normal_plane.z3 = node_4_Z[k];

        normal_plane.Find_Coefficients();

distance=(fabs(normal_plane.a*node_1_X[k]+normal_plane.b*node_1_Y[k]+normal_plane.c*node_1_Z[k]+normal_plane.d)) /
                sqrt(pow(normal_plane.a,2)+pow(normal_plane.b,2)+pow(normal_plane.c,2));
        semiperimeter= (side_1+side_2+side_3)/2;
        area=sqrt(semiperimeter*(semiperimeter-side_1)*(semiperimeter-side_2)*(semiperimeter-side_3));
        volume=area*distance/3;
        return volume;
        }

//*** FUNCTION TO IMPORT FEA DATA INTO MEMORY: ONLY PUBLIC METHOD ******************
void Nastran::Process_Data()
        {
        int i, j, j1, j2;
        input_file_name();
        output_file_name();
        number_of_nodes = Number_Of_Nodes();
        number_of_elements = Number_Of_Elements();
        Read_Input_Data();
        Read_Output_Data();

        element_ID = new int[number_of_elements];
        node_1_X = new double[number_of_elements];
        node_1_Y = new double[number_of_elements];
        node_1_Z = new double[number_of_elements];
        node_2_X = new double[number_of_elements];
        node_2_Y = new double[number_of_elements];
        node_2_Z = new double[number_of_elements];
        node_3_X = new double[number_of_elements];
        node_3_Y = new double[number_of_elements];
        node_3_Z = new double[number_of_elements];
        node_4_X = new double[number_of_elements];
        node_4_Y = new double[number_of_elements];
        node_4_Z = new double[number_of_elements];
        x_max = new double[number_of_elements];
        x_min = new double[number_of_elements];
```

```
y_max = new double[number_of_elements];
y_min = new double[number_of_elements];
z_max = new double[number_of_elements];
z_min = new double[number_of_elements];
element_volume = new double[number_of_elements];
element_volume_fraction = new double[number_of_elements];
sum_element_volume_fraction = new double[number_of_elements];

for (i=0; i<=number_of_elements-1; i++)                    //SCAN ALL ELEMENTS
        {
        if(element_ID_input[i]==element_ID_output[i])
                {
                element_ID[i]=element_ID_input[i];
                j1=0;
                j2=number_of_nodes-1;
                j=(j1+j2)/2;
                while (node_ID[j]!=element_node_1[i])     // FIND THE INDEX IN THE NODE POINTER (node_ID)
                                                                //OF THE FIRST NODE OF THE ELEMENT SELECTED
                        {
                        if(node_ID[j]<element_node_1[i]) j1=j+1; else j2=j-1;
                        j=(j1+j2)/2;
                        }
                node_1_X[i] = node_X[j];
                node_1_Y[i] = node_Y[j];
                node_1_Z[i] = node_Z[j];

                j1=0;
                j2=number_of_nodes-1;
                j=(j1+j2)/2;
                while (node_ID[j]!=element_node_2[i])     // FIND THE INDEX IN THE NODE POINTER (node_ID)
                                                                //OF THE SECOND NODE OF THE ELEMENT SELECTED
                        {
                        if(node_ID[j]<element_node_2[i]) j1=j+1; else j2=j-1;
                        j=(j1+j2)/2;
                        }
                node_2_X[i] = node_X[j];
                node_2_Y[i] = node_Y[j];
                node_2_Z[i] = node_Z[j];

                j1=0;
                j2=number_of_nodes-1;
                j=(j1+j2)/2;
                while (node_ID[j]!=element_node_3[i])     // FIND THE INDEX IN THE NODE POINTER (node_ID)
                                                                //OF THE THIRD NODE OF THE ELEMENT SELECTED
                        {
                        if(node_ID[j]<element_node_3[i]) j1=j+1; else j2=j-1;
                        j=(j1+j2)/2;
                        }
                node_3_X[i] = node_X[j];
                node_3_Y[i] = node_Y[j];
                node_3_Z[i] = node_Z[j];

                j1=0;
                j2=number_of_nodes-1;
                j=(j1+j2)/2;
                while (node_ID[j]!=element_node_4[i])     // FIND THE INDEX IN THE NODE POINTER (node_ID)
                                                                //OF THE FORTH NODE OF THE ELEMENT SELECTED
                        {
                        if(node_ID[j]<element_node_4[i]) j1=j+1; else j2=j-1;
                        j=(j1+j2)/2;
                        }
                node_4_X[i] = node_X[j];
                node_4_Y[i] = node_Y[j];
                node_4_Z[i] = node_Z[j];

                x_max[i] = node_1_X[i];
                if(node_2_X[i]>=x_max[i]) x_max[i]=node_2_X[i];
                if(node_3_X[i]>=x_max[i]) x_max[i]=node_3_X[i];
                if(node_4_X[i]>=x_max[i]) x_max[i]=node_4_X[i];
                x_min[i] = node_1_X[i];
                if(node_2_X[i]<=x_min[i]) x_min[i]=node_2_X[i];
                if(node_3_X[i]<=x_min[i]) x_min[i]=node_3_X[i];
                if(node_4_X[i]<=x_min[i]) x_min[i]=node_4_X[i];
```

```
                y_max[i] = node_1_Y[i];
                if(node_2_Y[i]>=y_max[i]) y_max[i]=node_2_Y[i];
                if(node_3_Y[i]>=y_max[i]) y_max[i]=node_3_Y[i];
                if(node_4_Y[i]>=y_max[i]) y_max[i]=node_4_Y[i];
                y_min[i] = node_1_Y[i];
                if(node_2_Y[i]<=y_min[i]) y_min[i]=node_2_Y[i];
                if(node_3_Y[i]<=y_min[i]) y_min[i]=node_3_Y[i];
                if(node_4_Y[i]<=y_min[i]) y_min[i]=node_4_Y[i];

                z_max[i] = node_1_Z[i];
                if(node_2_Z[i]>=z_max[i]) z_max[i]=node_2_Z[i];
                if(node_3_Z[i]>=z_max[i]) z_max[i]=node_3_Z[i];
                if(node_4_Z[i]>=z_max[i]) z_max[i]=node_4_Z[i];
                z_min[i] = node_1_Z[i];
                if(node_2_Z[i]<=z_min[i]) z_min[i]=node_2_Z[i];
                if(node_3_Z[i]<=z_min[i]) z_min[i]=node_3_Z[i];
                if(node_4_Z[i]<=z_min[i]) z_min[i]=node_4_Z[i];

                element_volume[i]=Element_Volume(i);
                }

        else {printf("\n A PROBLEM HAS OCCURRED INT HE ELEMENT INDEX\n' index");}
        }

    total_volume=0;
    for (i=0; i<=number_of_elements-1; i++)
        {
        total_volume += element_volume[i];
        }

    for (i=0; i<=number_of_elements-1; i++)
        {
        element_volume_fraction[i]=element_volume[i]/total_volume;
        if(i==0)
            sum_element_volume_fraction[i]=element_volume_fraction[i];
        else
            sum_element_volume_fraction[i]=sum_element_volume_fraction[i-1]+element_volume_fraction[i];
        }

    max_x = 0; min_x = 0; max_y = 0; min_y = 0; max_z = 0; min_z= 0;
    for (i=0; i<=number_of_nodes-1; i++)
        {
        if(node_X[i] > max_x) max_x = node_X[i];
        if(node_X[i] < min_x) min_x = node_X[i];
        if(node_Y[i] > max_y) max_y = node_Y[i];
        if(node_Y[i] < min_y) min_y = node_Y[i];
        if(node_Z[i] > max_z) max_z = node_Z[i];
        if(node_Z[i] < min_z) min_z = node_Z[i];
        }

    delete []element_ID_input;
    delete []element_ID_output;
    delete []node_ID;
    delete []node_X;
    delete []node_Y;
    delete []node_Z;
    }

//*** CLASS DESTRUCTOR ******************
Nastran::~Nastran ()
    {
    delete []cos_dir_Ax;
    delete []cos_dir_Ay;
    delete []cos_dir_Az;
    delete []cos_dir_Bx;
    delete []cos_dir_By;
    delete []cos_dir_Bz;
    delete []cos_dir_Cx;
    delete []cos_dir_Cy;
    delete []cos_dir_Cz;
    delete []element_ID;
    delete []element_node_1;
```

```
            delete []element_node_2;
            delete []element_node_3;
            delete []element_node_4;
            delete []node_1_X;
            delete []node_1_Y;
            delete []node_1_Z;
            delete []node_2_X;
            delete []node_2_Y;
            delete []node_2_Z;
            delete []node_3_X;
            delete []node_3_Y;
            delete []node_3_Z;
            delete []node_4_X;
            delete []node_4_Y;
            delete []node_4_Z;
            delete []principal_stress_A;
            delete []principal_stress_B;
            delete []principal_stress_C;
            delete []x_max;
            delete []x_min;
            delete []y_max;
            delete []y_min;
            delete []z_max;
            delete []z_min;
            delete []element_volume;
            delete []element_volume_fraction;
            delete []sum_element_volume_fraction;
            }
//*************************************************************************************************************
//*************************************************************************************************************

#endif
```

A.3. Random Function Class in C++

```
// Random_Function.h file
//*************************************************************************************************
//** THIS CLASS IS USED AS INPUT OF THE MONTE CARLO ENGINE TO EVALUATE FUNCTION EXPECTATION ****
//********** THE FUNCTION TO BE VALUATED IS IMPLEMENTED IN THE METHOD evaluate() ******************
//*************************************************************************************************

        //  (C) 2004 Giuseppe Iacopino
        //  PhD Student
        //  Cranfield University, SIMS
        //  Reliability Engineering and Risk Management Centre

#ifndef RANDOM_FUNCTION_H
#define RANDOM_FUNCTION_H
#include "Random_Sampling.h "
#include "FEA_Library.h"
#include "Failure_Criteria.h"

#define IMPORTANCE_SAMPLING 1
#define FAILURE_CRITERION 3
#define MAPPING 0
#define TOTAL_SIMULATION 0
#define INDEX_GENERATION 1

//********** ABSTRACT CLASS **********************
class Random_Function
        {
        public:
        virtual double evaluate() = 0;
        virtual ~Random_Function() ;
        };
        Random_Function::~Random_Function(){;}

//*************************************************************************************************
//** THIS CLASS EVALUATES THE STRENGTH OF A MECHANICAL COMPONENT ****
//*************************************************************************************************
class Component_Strength : public Random_Function
        {

        private:
                const double m_mu;                              //FLAW DISTRIBUTION PARAMETERS
                const double m_sigma;

                const double m_imp_mu;                          //PARAMETERS TO BE USED WITH IMPORTANT SAMPLING
                const double m_imp_sigma;

                const double m_crack_density;                       //PARAMETERS TO BE USED IN TOTAL SIMULATION
                const double m_volume;

                const Nastran& component;                       //FEA RESULT OBJECT
                Random_Generator rg1;                           //UNIFORM RANDOM GENERATOR
                Sampling sample;                                //GENERIC RANDOM GENERATOR
                double x_start, x_range, y_start, y_range, z_start, z_range;
                const double pi;

                int Index_Generation();
                void Gen_Coords_rejection(double &x_point, double &y_point, double &z_point);
                int Find_element(const double &x_point, const double &y_point, const double &z_point);
                bool Find_stresses(const double &x_point, const double &y_point, const double &z_point,
                                   double& stress_A, double& stress_B, double& stress_C);
                bool Find_stresses(const int& index, double& stress_A, double& stress_B, double& stress_C);

        public:
                int num_stores, data_stored;
                Component_Strength(double mu, double sigma, double imp_mu, double imp_sigma, long int seed,
                                   double crack_density, int n_stores,  Nastran& component_FEA);
                ~Component_Strength();
                double *stored_x, *stored_y, *stored_z, *stored_teta, *stored_beta, *stored_fi;
                double *stress_A, *stress_B, *stress_C, *stored_lengths;
```

```
        double evaluate();
};

//*** CLASS CONSTRUCTOR ******************
Component_Strength::Component_Strength(double mu, double sigma, double imp_mu, double imp_sigma, long int seed,
                                       double crack_density, int n_stores, Nastran& component_FEA) :
                                       m_mu(mu), m_sigma(sigma), m_imp_mu(imp_mu), m_imp_sigma(imp_sigma),
                                       m_crack_density(crack_density), component(component_FEA),
                                       num_stores(n_stores), m_volume(component_FEA.total_volume),
                                       rg1(seed), sample(seed), pi(3.14159)
                                              {
                                              x_start = component.min_x;
                                              x_range = (component.max_x  - component.min_x);
                                              y_start = component.min_y;
                                              y_range = (component.max_y  - component.min_y);
                                              z_start = component.min_z;
                                              z_range = (component.max_z  - component.min_z);
                                              data_stored = 0;
                                              stored_x = new double[num_stores];
                                              stored_y = new double[num_stores];
                                              stored_z = new double[num_stores];
                                              stored_beta = new double[num_stores];
                                              stored_teta = new double[num_stores];
                                              stored_fi = new double[num_stores];
                                              stress_A = new double[num_stores];
                                              stress_B = new double[num_stores];
                                              stress_C = new double[num_stores];
                                              stored_lengths = new double[num_stores];
                                              }

//*** CLASS DESTRUCTOR ******************
Component_Strength::~Component_Strength()
        {
        delete []stored_x;
        delete []stored_y;
        delete []stored_z;
        delete []stored_teta;
        delete []stored_beta;
        delete []stored_fi;
        delete [] stress_A;
        delete [] stress_B;
        delete [] stress_C;
        delete []stored_lengths;
        }

//*** THIS FUNCTION USES A NASTRAN OBJECT (component) TO FIND THE ELEMENT IN THE FEA MESH TO WHICH
//*** A POINT WITH COORDINATES (x_point, y_point, z_point) BELONGS ***************************************
int Component_Strength::Find_element(const double &x_point, const double &y_point, const double &z_point)
        {
        Plane plane_1, plane_2, plane_3, plane_4;
        int i;
        double check1_tedra, check2_tedra, check3_tedra, check4_tedra, check1_point, check2_point, check3_point, check4_point;
        for (i=0; i<=component.number_of_elements-1; i++)
                {
                if((x_point<=component.x_max[i])&&(x_point>=component.x_min[i]))
                        {
                        if((y_point<=component.y_max[i])&&(y_point>=component.y_min[i]))
                                {
                                if((z_point<=component.z_max[i])&&(z_point>=component.z_min[i]))
                                        {
                                        plane_1.x1 = component.node_2_X[i];
                                        plane_1.y1 = component.node_2_Y[i];
                                        plane_1.z1 = component.node_2_Z[i];
                                        plane_1.x2 = component.node_3_X[i];
                                        plane_1.y2 = component.node_3_Y[i];
                                        plane_1.z2 = component.node_3_Z[i];
                                        plane_1.x3 = component.node_4_X[i];
                                        plane_1.y3 = component.node_4_Y[i];
                                        plane_1.z3 = component.node_4_Z[i];
```

```
                    if(plane_1.Find_Coefficients())                 // FIND THE COEFFICIENT OF A PLANE
PASSING
                                                                    //THROUGH 3 POINTS OF THE
TETRAHEDRON
                        {
                        check1_tedra = plane_1.a*component.node_1_X[i] + plane_1.b*component.node_1_Y[i] +
                                       plane_1.c*component.node_1_Z[i] + plane_1.d;
                        check1_point = plane_1.a*x_point+plane_1.b*y_point+plane_1.c*z_point+plane_1.d;
                        }
                                                                    //IF THERE IS A PROBLEM THE FUNCTION RETURNS
-1
                    else {printf("ERROR IN FINDING MESH ELEMENT\n"); return -1;}

                    if (((check1_tedra<0)&&(check1_point<=0))||((check1_tedra>0)&&(check1_point>=0)))
                        {
                        plane_2.x1 = component.node_3_X[i];
                        plane_2.y1 = component.node_3_Y[i];
                        plane_2.z1 = component.node_3_Z[i];
                        plane_2.x2 = component.node_4_X[i];
                        plane_2.y2 = component.node_4_Y[i];
                        plane_2.z2 = component.node_4_Z[i];
                        plane_2.x3 = component.node_1_X[i];
                        plane_2.y3 = component.node_1_Y[i];
                        plane_2.z3 = component.node_1_Z[i];
                        if(plane_2.Find_Coefficients())             // FIND THE COEFFICIENT OF A PLANE
PASSING
                                                                    //THROUGH 3 POINTS OF THE
TETRAHEDRON
                            {
                            check2_tedra = plane_2.a*component.node_2_X[i] + plane_2.b*component.node_2_Y[i] +
                                           plane_2.c*component.node_2_Z[i] + plane_2.d;
                            check2_point = plane_2.a*x_point+plane_2.b*y_point+plane_2.c*z_point+plane_2.d;
                            }
                                                                    //IF THERE IS A PROBLEM THE FUNCTION RETURNS
-1
                        else {printf("ERROR IN FINDING MESH ELEMENT\n"); return -1;}

                        if (((check2_tedra<0)&&(check2_point<=0))||((check2_tedra>0)&&(check2_point>=0)))
                            {
                            plane_3.x1 = component.node_4_X[i];
                            plane_3.y1 = component.node_4_Y[i];
                            plane_3.z1 = component.node_4_Z[i];
                            plane_3.x2 = component.node_1_X[i];
                            plane_3.y2 = component.node_1_Y[i];
                            plane_3.z2 = component.node_1_Z[i];
                            plane_3.x3 = component.node_2_X[i];
                            plane_3.y3 = component.node_2_Y[i];
                            plane_3.z3 = component.node_2_Z[i];
                            if(plane_3.Find_Coefficients())         // FIND THE COEFFICIENT OF A PLANE
PASSING
                                                                    //THROUGH 3 POINTS OF THE
TETRAHEDRON
                                {
                                check3_tedra = plane_3.a*component.node_3_X[i] +
plane_3.b*component.node_3_Y[i]
                                               + plane_3.c*component.node_3_Z[i] + plane_3.d;
                                check3_point = plane_3.a*x_point+plane_3.b*y_point+plane_3.c*z_point+plane_3.d;
                                }
                                                                    //IF THERE IS A PROBLEM THE FUNCTION RETURNS
-1
                                else {printf("ERROR IN FINDING MESH ELEMENT\n"); return -1;}

                            if (((check3_tedra<0)&&(check3_point<=0))||((check3_tedra>0)&&(check3_point>=0)))
                                {
                                plane_4.x1 = component.node_1_X[i];
                                plane_4.y1 = component.node_1_Y[i];
                                plane_4.z1 = component.node_1_Z[i];
                                plane_4.x2 = component.node_2_X[i];
                                plane_4.y2 = component.node_2_Y[i];
                                plane_4.z2 = component.node_2_Z[i];
                                plane_4.x3 = component.node_3_X[i];
                                plane_4.y3 = component.node_3_Y[i];
                                plane_4.z3 = component.node_3_Z[i];
```

```
                                        if(plane_4.Find_Coefficients())        // FIND THE COEFFICIENT OF A PLANE
PASSING
                                                                               //THROUGH 3 POINTS OF THE
TETRAHEDRON
                                                {
                                                check4_tedra = plane_4.a*component.node_4_X[i] +
                                                               plane_4.b*component.node_4_Y[i] +
                                                               plane_4.c*component.node_4_Z[i] + plane_4.d;
                                                check4_point = plane_4.a*x_point + plane_4.b*y_point + plane_4.c*z_point +
                                                               plane_4.d;
                                                }
                                                               //IF THERE IS A PROBLEM THE FUNCTION RETURNS
-1
                                        else {printf("ERROR IN FINDING MESH ELEMENT\n"); return -1;}

                                        if
(((check4_tedra<0)&&(check4_point<=0))||((check4_tedra>0)&&(check4_point>=0)))
                                        return i;              //IF THE ELEMENT IS FOUND RETURN ITS INDEX
                                        }
                                    }
                                }
                            }
                        }
                    }
                }
        return -2;                             //IF THE ELEMENT HAS NOT BEEN FOUND THE FUNCTION RETURNS
-2
        }


//*** THIS FUNCTION RETURNS THE PRINCIPAL STRESSES AT A POINT OF COORDINATES (x_point, y_point, z_point)
//*** BY USING FEA RESULTS STORED IN A NASTRAN OBJECT (component) ***********************************
bool Component_Strength::Find_stresses(const double &x_point, const double &y_point, const double &z_point,
                                       double& stress_A, double& stress_B, double& stress_C)
        {
        int index = Find_element(x_point, y_point, z_point);
        if(index >= 0)
                {
                stress_A = component.principal_stress_A[index];
                stress_B = component.principal_stress_B[index];
                stress_C = component.principal_stress_C[index];
                return true;
                }
        printf("INCORRECT MESH ELEMENT INDEX\n");
        return false;
        }

//*** OVERLOADED FUNCTION THAT RETURNS THE PRINCIPAL STRESSES RELATIVE TO AN ELEMENT WITH
//*** INDEX (index) BY USING FEA RESULTS STORED IN A NASTRAN OBJECT (component) ******************
bool Component_Strength::Find_stresses(const int& index, double& stress_A, double& stress_B, double& stress_C)
        {
        if(index >= 0)
                {
                stress_A = component.principal_stress_A[index];
                stress_B = component.principal_stress_B[index];
                stress_C = component.principal_stress_C[index];
                return true;
                }
        printf("INCORRECT MESH ELEMENT INDEX\n");
        return false;
        }

//*** THIS FUNCTION GENERATES A RANDOM INDEX POINTING AT AN ELEMENT IN THE FEA MESH ******
//******* THE PROBABILITY OF AN ELEMENT TO BE SELECTED IS PROPORTIONAL TO ITS VOLUME *******
        int Component_Strength::Index_Generation()
                {
                int index;
                int j1, j2;
                double x;

                x=rg1.real_random();
                j1=0;
                j2=component.number_of_elements-1;
```

```
        index=(j1+j2)/2;
        while ((component.sum_element_volume_fraction[index-1]>x)||(component.sum_element_volume_fraction[index]<x))

                {
                if(component.sum_element_volume_fraction[index]<x) j1=index+1; else j2=index-1;
                index=(j1+j2)/2;
                }
        return index;
        }


//*** THIS FUNCTION GENERATES A SET OF RANDOM COORDINATES ************************************
        void Component_Strength::Gen_Coords_rejection(double &x_point, double &y_point, double &z_point)
                {
                x_point=x_start+x_range*rg1.real_random();
                y_point=y_start+y_range*rg1.real_random();
                z_point=z_start+z_range*rg1.real_random();
                }
```

```
//*** THIS FUNCTION GENERATES A RANDOM NUMBER OF CRACKS WITHIN THE COMPONENT VOLUME AND
//*** CHECKS IF ONE OF THE CRACKS TRIGGERS ************************************************************
//*** SEVERAL SIMULATION OPTIONS CAN BE SET UP AT COMPILE TIME *******************************
	double Component_Strength::evaluate()
		{
		double p_stress_A=0.0, p_stress_B=0.0, p_stress_C=0.0;
		double bet, sintet, fi, length;
		int number_of_cracks, cracks=0;
		double value=0.0;
		bool already_counted=false;
		double criticality=0.0;
		bool valid_element=false, map=false;

		// ***SET INDIVIDUAL OR TOTAL SIMULATION **********************************
			#if TOTAL_SIMULATION == 1
				number_of_cracks = sample.Poisson_Process(m_crack_density, m_volume);
			#else
				number_of_cracks = 1;
			#endif
		// ***************************************************************************

		while (cracks<=number_of_cracks)
		{
		 // *** COORDINATES OR ELEMENT INDEX SIMULATION *******************
			#if INDEX_GENERATION == 1
				int element_index = Index_Generation();
				valid_element = Find_stresses(element_index, p_stress_A, p_stress_B, p_stress_C);
			#else
				double x_point, y_point, z_point;
				Gen_Coords_rejection(x_point, y_point, z_point);
				valid_element = Find_stresses(x_point, y_point, z_point,
							p_stress_A, p_stress_B, p_stress_C);
			 #endif
		  // ************************************************************
		if (valid_element)
			{
			cracks++;

		  //*** GENERATE DEFECT ORIENTATION *****
			bet=2*pi*rg1.real_random();
			sintet=2*rg1.real_random()-1;
			fi = pi*rg1.real_random();
		  //*****************************************

		  //***** DEFECT SIZE SIMULATION ***********************************************************
			#if IMPORTANCE_SAMPLING == 1			//IMPORTANCE SAMPLING
				length = sample.LogNormal_Generator(m_imp_mu, m_imp_sigma);			//[mm]
			#else						//STANDARD SIMULATION
				length = sample.LogNormal_Generator(m_mu, m_sigma);			//[mm]
			#endif
		 //*****************************************************************************************

		  //****************** FAILURE CRITERION *********************************
			#if FAILURE_CRITERION == 1
				if(Failure_Maximum_Energy (length, bet, sintet, fi, p_stress_A, p_stress_B, p_stress_C, criticality, map))
			#elif FAILURE_CRITERION == 2
				if(Failure_Coplanar_Energy (length, bet, sintet, fi, p_stress_A, p_stress_B, p_stress_C, criticality, map))
			#elif FAILURE_CRITERION == 3
				if(Failure_Empirical(length, bet, sintet, fi, p_stress_A, p_stress_B, p_stress_C, criticality, map))
			#endif
		   //*********************************************************************
				{
			// ******* RETURN VALUE FOR FAILURE OCCURRED*********
			#if IMPORTANCE_SAMPLING == 1
				if(map)		value = (sample.LogNormal_pdf(length, m_mu, m_sigma)/
						sample.LogNormal_pdf(length, m_imp_mu, m_imp_sigma));
			#else
				if(!already_counted) value = 1;
			#endif
		// ************************************************

		//*** MAPPING ************************************************************
			#if MAPPING == 1
```

```
                        if (data_stored<=(num_stores-1))
                                {
                                if(!already_counted) data_stored++;
                                already_counted = true;                 //TO COUNT THE FAILURE ONLY ONCE

                                if(map)
                                        {
                                        #if INDEX_GENERATION == 1
                                         //******* TO STORE ELEMENT INDEX ***************
                                                stored_x[(int) (data_stored-1)]=element_index;
                                                stored_y[(int) (data_stored-1)]=0.0;
                                                stored_z[(int) (data_stored-1)]=0.0;
                                         //**********************************************
                                        #else
                                         //******* TO STORE COORDINATES *********
                                                stored_x[(int) (data_stored-1)]=x_point;
                                                stored_y[(int) (data_stored-1)]=y_point;
                                                stored_z[(int) (data_stored-1)]=z_point;
                                         //**************************************
                                        #endif

                                        //******* TO STORE ORIENTATIONS *********
                                                stored_beta[(int) (data_stored-1)]=180*bet/pi;
                                                stored_teta[(int) (data_stored-1)]=asin(sintet)*180/pi;
                                                stored_fi[(int) (data_stored-1)]=180*fi/pi;
                                        //***************************************

                                                stored_lengths[(int) (data_stored-1)]=length;           //[mm]
                                                stress_A[(int) (data_stored-1)]=p_stress_A;
                                                stress_B[(int) (data_stored-1)]=p_stress_B;
                                                stress_C[(int) (data_stored-1)]=p_stress_C;
                                                }
                                        }
                                #else
                                        break;
                                #endif
                        //*************************************************************************
                                }
                        }
                }
        return value;
   }
//*************************************************************************************************************
//*************************************************************************************************************

#endif
```

A.4. Monte Carlo Engine in C++

```
//*** THIS FUNCTION RUNS THE MONTE_CARLO SIMULATION
//*** IT RETURNS THE EXPECTED VALUE OF A RANDOM FUNCTION
//*** AS INPUT ARGUMENTS IT REQUIRES THE RANDOM FUNCTION TO BE EVALUATED AND THE ALIAS OF
//*** NUMBER OF TRIALS, CONVERGENCE CHECK AND STANDARD DEVIATION OF THE ESTMATE
#include "Random_Function.h"

double Monte_Carlo_Simulation (Random_Function& function, int &i, double &check, double &deviation)
	{
	double probability_1=0, probability_2=0, probability_3=1;
	double real_count=0, x;
	int j=0;

	deviation=0;
	for (i=1; i<=NUM_TRIALS; i++)
		{
		x = function.evaluate();
		real_count += x;
		deviation += sqr(x);
		if ((i-j)>=INTERVAL_CHECK)
			{

			probability_1 = (double) real_count/i;
			j=i;
			check=fabs(probability_1-probability_2)+fabs(probability_1-probability_3);
			if(probability_1!=0) check = check/probability_1;
			probability_3 = probability_2;
			probability_2 = probability_1;
			}
		}
	i--;
	deviation =  sqrt((deviation/NUM_TRIALS-sqr((double) real_count/NUM_TRIALS))/(NUM_TRIALS-1));
	return (double) real_count/NUM_TRIALS;
	}
//*****************************************************************************************************
//*****************************************************************************************************
```

A.5. Fracture Propagation Criteria in C++

```
// Failure_Criteria.h file
//*************************************************************************************************
//**** THIS CLASS IS A COLLECTION OF FUNCTION FOR DETERMINING CRITICAL CONDITION FOR CRACK ******
//************ PROPAGATION ACCORDING TO SEVERAL MIXED-MODE FRACTURE CRITERIA ******************
//*************************************************************************************************

#ifndef FAILURE_CRITERIA_H
#define FAILURE_CRITERIA_H

// ***  MATERIAL PARAMETERS **********
        const double shp_fact = 0.0;
        const double g_crit = 0.0;
        const double poisson_ratio = 0.0;
        const double elastic_modulus = 0.0;
        const double ratio_KIc_KIIc = 0.0;
        double k_1;
        double k_2;
        double k_3;
        const double pi = 3.14159;
// ***************************** **********


// ****** Template Functions ******************
        template<typename T>
        double sqr(T value)
                {
                return (value*value);
                }
// ****************************************


//*** THIS FUNCTION FINDS THE CRACK PROPAGATION DIRECTION FOR MAXIMUM STRAIN ENERGY CRITERION
        int Find_Cos_Alfa_Zero(double &x1, double&x2)
                {
                double a;
                a=sqr(k_2)/sqr(k_1);
                x1=(3*a+sqrt(8*a+1))/(1+9*a);        //POSITIVE
                x2=(3*a-sqrt(8*a+1))/(1+9*a);        //NEGATIVE
                 return 2;
                }
//*************************************************************************************************


//FAILURE CRITERION 1
//******* MAXIMUM STRAIN-ENERGY RELEASE RATE CRITERION FOR A THROUGH CRACK*****
bool Failure_Maximum_Energy(double length, double bet, double sintet, double fi, double p_stress_A,
                                        double p_stress_B, double p_stress_C, double criticality, bool map)
        {
        double sqrt_length_pi, sinbet, costet, cosbet, sinfi, cosfi;                //CRACK PARAMETERS
        double sinbet_2, cosbet_2, sintet_2, costet_2;
        double sigma_normal, tau_in_plane, tau_out_plane;                        //STRESSES REFFERED TO THE CRACK PLANE
                //DIRECTION OF PROPAGATION
        double alfa_zero1, alfa_zero2, cos_alfa_zero1, cos_alfa_zero2, sin_alfa_zero1, sin_alfa_zero2, k_1_alfa_zero;
        double temp, g_max=0;
        bool failure=false;
        map = false;

 // **** GEOMETRICAL QUANTITIES *******
        sinbet= sin(bet);
        cosbet= cos(bet);
        sinbet_2= sqr(sinbet);
        cosbet_2= sqr(cosbet);
        sintet_2= sqr(sintet);
        costet_2= 1-sintet_2;
        costet=sqrt(costet_2);
        sinfi= sin(fi);
        cosfi=cos(fi);
 // ***********************************
```

```
        sigma_normal = p_stress_A*costet_2*sinbet_2 + p_stress_B*costet_2*cosbet_2 + p_stress_C*sintet_2;
        tau_in_plane = (cosbet*sinfi+sinbet*sintet*cosfi)*(-sinbet)*costet*p_stress_A+(sinbet*sinfi-cosbet*sintet*cosfi)*
                        cosbet*costet*p_stress_B+costet*cosfi*sintet*p_stress_C;
        tau_out_plane = (cosbet*cosfi-sinbet*sintet*sinfi)*(-sinbet)*costet*p_stress_A+(sinbet*cosfi+cosbet*sintet*sinfi)*
                         cosbet*costet*p_stress_B+costet*sintet*(-sinfi)*p_stress_C;

        sqrt_length_pi = sqrt(pi*length/2.0);                           // LENGTH IS TOTAL CRACK EXTENSION: 2a
        k_1 = sigma_normal*sqrt_length_pi;
        k_2 = tau_in_plane*sqrt_length_pi;
        k_3 = tau_out_plane*sqrt_length_pi;

        if (sigma_normal>=0)
                {
                Find_Cos_Alfa_Zero(cos_alfa_zero1, cos_alfa_zero2);         //FIND PROPAGATION ANGLE
                if(k_1*k_2>=0)
                        {
                        sin_alfa_zero1=-sqrt(1-sqr(cos_alfa_zero1));        //PROPAGATION ANGLE 1 with positive cos and negative sin
                        sin_alfa_zero2=sqrt(1-sqr(cos_alfa_zero2));         //PROPAGATION ANGLE 2 with negative cos and positive sin
                        }
                else
                        {
                        sin_alfa_zero1=sqrt(1-sqr(cos_alfa_zero1));         //PROPAGATION ANGLE 1 with positive cos and positive sin
                        sin_alfa_zero2=-sqrt(1-sqr(cos_alfa_zero2));        //PROPAGATION ANGLE 2 with negative cos and negative sin
                        }
                alfa_zero1= atan2(sin_alfa_zero1, cos_alfa_zero1);          //PROPAGATION ANGLE 1
                alfa_zero2= atan2(sin_alfa_zero2, cos_alfa_zero2);          //PROPAGATION ANGLE 2
                k_1_alfa_zero=k_1*(0.75*cos(0.5*alfa_zero1)+0.25*cos(1.5*alfa_zero1))+k_2*(-0.75*(sin(0.5*alfa_zero1)+
                                sin(1.5*alfa_zero1)));              //THE FIRST TWO MODES ARE CONSIDERED PREDOMINANT
                temp=k_1*(0.75*cos(0.5*alfa_zero2)+0.25*cos(1.5*alfa_zero2))+k_2*(-0.75*(sin(0.5*alfa_zero2)+
                                sin(1.5*alfa_zero2)));              //THE FIRST TWO MODES ARE CONSIDERED PREDOMINANT
                if((fabs(temp))>(fabs(k_1_alfa_zero))) k_1_alfa_zero=temp;
                        //ADD MODE 3 INTENSITY-FACTOR UNCHANGED
                g_max=((1-sqr(poisson_ratio))*sqr(k_1_alfa_zero)+(1+poisson_ratio)*sqr(k_3))/elastic_modulus;
                }
        else
                {
                        //IF SIGMA_NORMAL<0, ONLY MODE 2 AND 3 CONTRIBUTE TO FAILURE
                g_max=((1-sqr(poisson_ratio))*sqr(k_2)+(1+poisson_ratio)*sqr(k_3))/elastic_modulus;
                }
        if (g_max>=g_crit)
                {
                failure=true;
                if (g_max-g_crit>criticality) {criticality=g_max-g_crit; map=true;}
                }
        return failure;
        }
//*************************************************************************************************************
//*************************************************************************************************************


// FAILURE CRITERION 2
//** COPLANAR STRAIN-ENERGY RELEASE RATE CRITERION FOR A CRACK WITH A SPECIFIED SHAPE FACTOR **
//THIS FUNCTION CHECKS WHETHER A PENNY-SHAPED CRACK RANDOMLY GENERATED TRIGGERS FAILURE
ACCORDING TO THE COPLANAR ENERGY RELEASE RATE CRITERION.
bool Failure_Coplanar_Energy_Penny(double length, double bet, double sintet, double fi, double p_stress_A,
                                        double p_stress_B, double p_stress_C, double criticality, bool map)
        {

        double sigma_normal, tau_x, tau_z, tau_max, g;                  //STRESSES REFERRED TO THE CRACK PLANE
        double sinbet, cosbet, costet;
        double sinbet_2, cosbet_2, sintet_2, costet_2;
        double sqrt_length_pi;
        bool failure=false;
        map = false;

 // *** GEOMETRICAL QUANTITIES *****
        sinbet= sin(bet);
        cosbet= cos(bet);
        sinbet_2= sqr(sinbet);
        cosbet_2= sqr(cosbet);
        sintet_2= sqr(sintet);
        costet_2= 1-sintet_2;
```

```
        costet=sqrt(costet_2);
 // ********************************

        sigma_normal = p_stress_A*costet_2*sinbet_2 + p_stress_B*costet_2*cosbet_2 + p_stress_C*sintet_2;
        tau_x = -p_stress_A*costet*cosbet*sinbet+p_stress_B*costet*cosbet*sinbet;
        tau_z = -p_stress_A*costet*sintet*sinbet_2-p_stress_B*costet*sintet*cosbet_2+p_stress_C*costet*sintet;
        tau_max= sqrt (sqr(tau_x) + sqr(tau_z));

        sqrt_length_pi = 2*sqrt(length/(2*pi));                         //LENGTH IS TOTAL CRACK EXTENSION: 2a

        k_1 = shp_fact*sigma_normal*sqrt_length_pi;
        k_2 = shp_fact*tau_max*sqrt_length_pi*2/(2-poisson_ratio);
        k_3 = 0.0;

        if (sigma_normal>=0) g = (1-sqr(poisson_ratio))*(sqr(k_1)+sqr(k_2))/elastic_modulus;
        else                 g = (1-sqr(poisson_ratio))*sqr(k_2)/elastic_modulus;

        if (g>=g_crit) {failure=true;}
        if (g-g_crit>criticality) {criticality=g-g_crit; map=true;}
        return failure;
        }
//*************************************************************************************************
//*************************************************************************************************


// FAILURE CRITERION 3
//***** EMPIRICAL FRACTURE CRITERION FOR A CRACK WITH A SPECIFIED SHAPE FACTOR ******************
bool Failure_Empirical(double length, double bet, double sintet, double fi, double p_stress_A,
                       double p_stress_B, double p_stress_C, double criticality, bool map)
        {
        double sigma_normal, tau_x, tau_z, tau_max, g;                  //STRESSES REFERRED TO THE CRACK PLANE
        double sinbet, cosbet, costet;
        double sinbet_2, cosbet_2, sintet_2, costet_2;
        double sqrt_length_pi;
        bool failure=false;
        map = false;

 // *** GEOMETRICAL QUANTITIES *****
        sinbet= sin(bet);
        cosbet= cos(bet);
        sinbet_2= sqr(sinbet);
        cosbet_2= sqr(cosbet);
        sintet_2= sqr(sintet);
        costet_2= 1-sintet_2;
        costet=sqrt(costet_2);
 // ********************************

        sigma_normal = p_stress_A*costet_2*sinbet_2 + p_stress_B*costet_2*cosbet_2 + p_stress_C*sintet_2;
        tau_x = -p_stress_A*costet*cosbet*sinbet+p_stress_B*costet*cosbet*sinbet;
        tau_z = -p_stress_A*costet*sintet*sinbet_2-p_stress_B*costet*sintet*cosbet_2+p_stress_C*costet*sintet;
        tau_max= sqrt (sqr(tau_x) + sqr(tau_z));

        sqrt_length_pi = 2*sqrt(length/(2*pi));                         //LENGTH IS TOTAL CRACK EXTENSION: 2a

        k_1 = shp_fact*sigma_normal*sqrt_length_pi;
        k_2 = shp_fact*tau_max*sqrt_length_pi*2/(2-poisson_ratio);
        k_3 = 0.0;

        if (sigma_normal>=0) g = (1-sqr(poisson_ratio))*(sqr(k_1)+sqr(ratio_KIc_KIIc*k_2))/elastic_modulus;
        else                 g = (1-sqr(poisson_ratio))*sqr(ratio_KIc_KIIc*k_2)/elastic_modulus;

        if (g>=g_crit) {failure=true;}
        if (g-g_crit>criticality) {criticality=g-g_crit; map=true;}
        return failure;
        }
//*************************************************************************************************
//*************************************************************************************************

#endif
```